Epithelial-mesenchymal transition, translocation of Ca^{2+} signalling complexes and regulation of migration in pancreatic cancer cells

Thesis submitted in accordance with the requirements of the University of Liverpool for the degree of Doctor of Philosophy

By

Emmanuel Okeke

January 2015

Dedicated to My Beloved Father

Emmanuel Okeke

Table of Contents

Abstract

The high mortality of pancreatic cancer is predominantly caused by tumour metastasis. The formation of metastases is dependent on the co-ordinated processes of epithelial-mesenchymal transition (EMT), cell migration and invasion. The importance of Ca^{2+} signalling in the formation of metastasis in a number of cancer types has been documented. However, our understanding of the Ca^{2+} signalling components involved in the metastatic dissemination of pancreatic ductal adenocarcinoma (PDAC, specifically PANC-1) is limited. Inositol 1,4,5-trisphosphate receptors (IP_3Rs) and store-operated Ca^{2+} entry (SOCE) channels are the important Ca^{2+} signalling mechanisms in this cell type. IP_3Rs are Ca^{2+}-releasing channels in the endoplasmic reticulum (ER). After Ca^{2+} release via IP_3Rs, restoring of ER Ca^{2+} involves SOCE mediated by STIM1, which activates PM Ca^{2+} channels Orai1 to permit Ca^{2+} influx. This process of Ca^{2+} influx takes place in unique structures – ER-PM junctions. The goal of the present study was to determine and characterise the fate of IP_3Rs and STIM1-competent ER-PM junctions during EMT and the significance of these Ca^{2+} signalling mechanisms for PANC-1 cell migration.

In the present study, I demonstrated that during EMT, PANC-1 cells undergo a dramatic morphological change from apical-basal polarity to front-rear polarity. In cellular monolayers IP_3Rs are juxtaposed to cell-cell contacts and closely co-positioned with markers of the tight and adherens junctions. When individual cells migrate away from their neighbours, IP_3Rs and SOCE-competent ER-PM junctions underwent dramatic redistribution from cell-cell contacts to accumulate preferentially at the leading edge of PANC-1 cells, where they are in close apposition with the components of migratory apparatus (e.g. focal adhesions). I further demonstrated that focal adhesions were closely encompassed by IP_3Rs, creating potholes in excitable medium in which Ca^{2+} released through IP_3Rs affects the remodelling and turnover of focal adhesions, which in turn is necessary for cell migration. Finally, I demonstrated that the migration of PANC-1 cells was suppressed by inhibition of IP_3Rs and SOCE, indicating that these mechanisms are functionally important for migration.

Taken together, I successfully demonstrated that Ca^{2+} signalling complexes concentrate in the leading edge of migrating PANC-1 cells and regulate focal adhesion turnover in order to control cell adhesion dynamics and forward movement of PANC-1 cells.

Acknowledgements

I would like to hugely thank my supervisors: Prof. Alexei Tepikin, Dr Lee Haynes and Prof. Bob Burgoyne. I would like to personally thank Prof. Alexei Tepikin (The Boss) for his never-ending support, assistance, guidance, patience and help throughout the entire period of my PhD study, and for being a father figure to me. Apart from being a supportive supervisor to me, Lee is a good friend and a collaborator who kindly assisted me with the production of awesome constructs and taught me a number of molecular biology techniques.

I would also like to thank my collaborators for their help and support during my PhD study. Prof. Robert Sutton for letting me use the 710 LSM microscope and for his kind advice on experiments. Dr Mohammed Awais for his kind and whole-hearted assistance with the use of the 710 microscope and help with uncaging experiments. Dr David Criddle & Prof. Ian Prior for general experimental advice. Dr Judy Coulson for advice on quantitative RT-PCR. Tony Parker for helping with experimental work.

I would like to thank all the past and present members of Blue block for their help. Dr S. Voronina for her kind advice and support with uncaging experiments on the 510 LSM microscope. Dr M. Chvanov for general advice on experiments. Dr H. Dingsdale and Dr A. Burdyga for showing me the art of immunofluorescence and confocal microscopy amongst other research techniques.

I also like to thank Dayani Rajamanoharan for accommodating me in Red block and for her whole-hearted help with molecular biology techniques.

I would like to show my appreciation for my role models – Tiger Woods and Serena Williams.

I would like to thank my mentors – Breda Roche and Dr Catherine Vial for everything they have done for me. Thanks also to the Wellcome Trust for generously funding and supporting my PhD research study. Also, thank you to all the people that have lent their support to me who I haven't named.

Lastly, I would like to say special thanks to my parents – Emmanuel Okeke & Alice Okeke for trusting in me and for their unconditional support and guidance through good and tough times.

Publication

Some of the work presented in this thesis has been published in the paper below:

Dingsdale H, **Okeke E**, Awais M, Haynes L, Criddle DN, Sutton R, Tepikin AV. Saltatory formation, sliding and dissolution of ER-PM junctions in migrating cancer cells. Biochem J. (2013) 451(1):25-32.

Abbreviations

AOBS – Acousto-optical beam splitter

Arp2/3 – Actin related protein 2/3 complex

ATCC – American Type Culture Collection

AU – Arbitrary unit

BSA – Bovine serum albumin

Ca^{2+} – Calcium

$[Ca^{2+}]_C$ – Cytosolic Ca^{2+} concentration

$[Ca^{2+}]_{ER}$ – Endoplasmic reticulum Ca^{2+} concentration

cAMP – cyclic Adenosine monophosphate

CFP – Cyan fluorescent protein

CICR – Ca^{2+} induced Ca^{2+} release

CPA – Cyclopiazonic acid

CRAC – Ca^{2+} release activated Ca^{2+} channels

DAG – Diacylglycerol

DMEM – Dulbecco's modified eagle medium

DNA – Deoxyribonucleic acid

dSTORM – Direct stochastical optical reconstruction microscopy

ECL – Enhanced Chemiluminescence

EDTA – Ethylenediaminetetraacetic acid

EM – Electron microscopy

ER – Endoplasmic reticulum

FBS – Heat-inactivated foetal bovine serum

FKBP – FK506-binding protein

FRB – Fragment of mTOR that binds FKBP12

GCaMP – Genetically encoded Ca^{2+} indicator

GDP – Guanosine diphosphate

GFP – Green fluorescent protein

GPCRs – G-protein coupled receptors

GSK – GlaxoSmithKline

GTP – Guanosine triphosphate

HEPES – 4-(2-hydroxyethyl)-1-piperazineethanesulphonic acid

HRP – Horseradish peroxidase

IBC – IP_3 binding core

IICR – IP_3-induced Ca^{2+} release

IP_3 – Inositol 1,4,5-trisphosphate

IP_3R – IP_3 receptor

LSM – Laser scanning microscope

MEFs – Murine embryonic fibroblasts

NA – Numerical aperture

PBS – Phosphate buffered saline

PFA – Paraformaldehyde

PI – Phosphatidylinositol

PIP_2 – Phosphatidylinositol (4,5) bisphosphate

PIP_3 – Phosphatidylinositol (3,4,5) trisphosphate

PKC – Protein kinase C

PLC – Phospholipase C

PM – Plasma membrane

PMCA – Plasma membrane Ca^{2+} ATPase pump

PSG – PenStrep Glutamine

RFP – Red fluorescent protein

RNA – Ribonucleic acid

RPM – Revolutions per minute

RT – Room temperature

RTKs – Receptor tyrosine kinases

SD – Suppressor domain

SERCA – Sarco(endo)plasmic reticulum Ca^{2+} ATPase

SOCE – Store-operated Ca^{2+} entry

STIM – Stromal interaction molecule

TG – Thapsigargin

TIRF – Total internal reflection fluorescence

TK – Thymidine kinase

TRP – Transient receptor potential

Xes-B – Xestospongin-B

YFP – Yellow fluorescent protein

Chapter 1: Introduction

Chapter 1: Introduction

1.1 IP_3R-mediated Ca^{2+} responses

1.1.1 Ca^{2+} signalling and ER

Ca^{2+} is a remarkable, versatile and ubiquitous second messenger molecule that controls plethora of biological processes starting from when life begins at fertilisation, all the way through development, and eventually when life is terminated at death (Berridge *et al.*, 1998). Ca^{2+} is able to mediate a vast number of cellular processes because of its enormous versatility as a second messenger, which is orchestrated through its complex spatial and temporal patterning (Berridge *et al.*, 2000). Ca^{2+} fluxes from both internal and external reservoirs are utilised by cells to generate their Ca^{2+} signals (Berridge *et al.*, 2000). External reservoirs are situated in the extracellular environment outside cells, whilst the internal reservoirs are held within the intracellular organelles primarily the endoplasmic reticulum (ER) (Ehrlich & Watras, 1988; Berridge *et al.*, 1998).

The ER is an intracellular organelle that was first described using electron microscopy by Porter and colleagues (Porter *et al.*, 1945). The ER is characterised by a tubular and a membranous network consisting of three morphologically distinct compartments: the nuclear envelope (NE), the rough ER and the smooth ER (Baumann & Walz, 2001; Voeltz *et al.*, 2002). The ER is a heterogeneous compartment with many different functions within its different sub-compartments (Meldolesi & Pozzan, 1998). The ER functions as sites for lipid synthesis, protein synthesis and sorting as well as forming the major intracellular Ca^{2+} reservoir in most cells (Ashby & Tepikin, 2001; Baumann & Walz, 2001; Berridge, 2002). The specialised regions of ER involved in Ca^{2+} handling and signalling are characterised

by the increased density of Ca^{2+} uptake pumps, luminal Ca^{2+} sequestering proteins, and Ca^{2+} release channels (primarily the inositol 1,4,5-trisphosphate receptor (IP_3Rs) and ryanodine receptors (RyRs)) (Berridge *et al.*, 2000; Petersen *et al.*, 2001). The ER lumen holds a substantial amount of $[Ca^{2+}]_{ER}$ of ~400 μM compared to the resting level of cytosolic $[Ca^{2+}]_C$ of ~50-100 nM, and maintaining the steep gradient between the two cellular compartments is essential for efficient Ca^{2+} response signals after receptor stimulation (Foskett *et al.*, 2007; Carrasco & Meyer, 2011). Briefly, stimulation of cell surface receptors for example G-protein coupled receptors (GPCRs) and receptor tyrosine kinases (RTKs) lead to the activation of multiple isoforms of phospholipase C (PLC) enzyme, which in turn catalyses the hydrolysis of phosphatidylinositol 4,5-bisphosphate ($PI(4,5)P_2$) to generate inositol 1,4,5-trisphosphate (IP_3) and diacylglycerol (DAG). IP_3 then subsequently binds IP_3Rs in the ER membrane to mediate intracellular Ca^{2+} release (Berridge *et al.*, 1998; Berridge *et al.*, 2000; Foskett *et al.*, 2007; Carrasco & Meyer, 2011). IP_3R is an important platform for intracellular Ca^{2+} signalling, which is essential for many cellular processes including gene expression, cell proliferation, contraction, secretion, motility and cell death (Patterson *et al.*, 2004; Vermassen *et al.*, 2004; Foskett *et al.*, 2007).

1.1.2 Structure of IP_3Rs

IP_3Rs are intracellular Ca^{2+} release channels localised predominantly in the ER membrane (Foskett *et al.*, 2007). There are three mammalian isoforms of IP_3Rs (IP_3R1, IP_3R2 and IP_3R3), which are encoded by three distinct genes (Furuichi *et al.*, 1994; Taylor *et al.*, 1999; Patterson *et al.*, 2004). Each isoform is a six transmembrane protein with both N- and C- termini projecting into the cytoplasm (Foskett *et al.*, 2007). The three mammalian isoforms share a 60-80% overall

sequence homology (Furuichi *et al.*, 1994; Taylor *et al.*, 1999; Foskett *et al.*, 2007). Functional IP_3Rs are tetrameric complexes that can be present as homo- and/or heterotetramers and with their subunits splice variants contributing to receptor diversity (Joseph *et al.*, 1995; Monkawa *et al.*, 1995; Taylor *et al.*, 1999; Foskett *et al.*, 2007). IP_3R isoforms have a primary sequence of ~2700-2800 amino acids, and they share a similar general structure consisting of N-terminal IP_3 binding core region, a large central modulatory and transducing region (also known as the coupling domain), and a C-terminal channel-forming region (Mignery & Sudhof, 1990; Miyawaki *et al.*, 1991; Bosanac *et al.*, 2004; Foskett *et al.*, 2007; Taylor & Tovey, 2010).

The N-terminal region of IP_3Rs is about 600 amino acids in length and is composed of two key domains, the suppressor domain (SD) which is adjacent to the IP_3-binding core (IBC) (Bosanac *et al.*, 2004). IP_3Rs without the SD region bind IP_3 but fails to open the channel pore (Uchida *et al.*, 2003; Szlufcik *et al.*, 2006). It was also s bhown that IP_3R1 lacking the SD region failed to induce clustering following cell surface receptor-stimulated IP_3 production (Tateishi *et al.*, 2005). Therefore, It has been suggested that the SD is an essential link between IP_3 binding to the IBC and the follow-up conformational changes that lead to pore opening and receptor clustering (Tateishi *et al.*, 2005; Rossi *et al.*, 2009; Taylor & Tovey, 2010). The SD region has also been reported to house interaction sites for proteins that regulate IP_3R activity, and these include calmodulin (Sienaert *et al.*, 2002), Homer (Tu *et al.*, 1998), and phosphorylation sites for several kinases (Vanderheyden *et al.*, 2009). However, the precise location of the SD region within the 3D structure of IP_3Rs is yet to be resolved.

The coupling domain is a large region of ~1600-1700 amino acids in length and it is located between the N-terminal IBC and the C-terminal channel-forming regions (Bosanac *et al.*, 2004; Foskett *et al.*, 2007). This region is the least conserved region amongst the IP_3R isoforms (Tu *et al.*, 2005). This region contains different consensus sequences for numerous target proteins that interact with and modulate the activity of IP_3Rs. For example, phosphorylation sites for protein kinase A/G (PKA/PKG), extracellular-signal regulated kinase (ERK) and cyclin-dependent kinase 1 (CDK1) (Vanderheyden *et al.*, 2009), in addition to two glycine-rich regions that are putative ATP-binding sites (Furuichi *et al.*, 1989; Mignery & Sudhof, 1990; Tu *et al.*, 2005; Vanderheyden *et al.*, 2009) are all found in the coupling domain of IP_3R1. This region also contains additional regulatory interaction sites for AKAP9, Bcl-2 and calmodulin (only in IP_3R1 and IP_3R2) (Yamada *et al.*, 1995; Michikawa *et al.*, 1999).

The C-terminal Ca^{2+} release channel-forming region is composed of six transmembrane domain (TMD), and binding sites for a number of other regulatory and adaptor proteins such as phosphatase PP1A and protein 4.1N, respectively (Vermassen *et al.*, 2004). Similar to ryanodine receptor channel pore, the final pairs of TMD5-6 and the luminal loop that links them in each of the tetrameric subunits form the pore of the IP_3Rs (Ramos-Franco *et al.*, 1999). IP_3Rs have astonishingly large conductance of ~50 pS (Williams *et al.*, 2001; Foskett *et al.*, 2007).

1.1.3 Regulation and gating of IP_3Rs

The regulation of IP_3R activity has been postulated to be an important factor for the spatial and temporal coding of Ca^{2+} signals that control numerous cellular processes. Multiple intracellular mechanisms exist that are known to regulate the activity of IP_3Rs and these include but not limited to the binding of cytoplasmic ligands (IP_3,

free Ca^{2+}, free ATP), post-translational modifications, protein-protein interactions, receptor clustering, tetrametric compositions (homo- and hetero-tetramer) and differential localisation (Bezprozvanny *et al.*, 1991; Bezprozvanny & Ehrlich, 1993; Wojcikiewicz, 1995; Miyakawa *et al.*, 1999; Berridge *et al.*, 2000; Pieper *et al.*, 2001; Patterson *et al.*, 2004; Vermassen *et al.*, 2004; Tateishi *et al.*, 2005; Tu *et al.*, 2005; Foskett *et al.*, 2007; Taylor & Tovey, 2010; Decuypere *et al.*, 2011).

The primary activator of IP_3R-mediated Ca^{2+} release is a soluble second messenger molecule called IP_3 (Berridge, 1983; Ehrlich & Watras, 1988). IP_3 is synthesized from the hydrolysis of ($PI(4,5)P_2$) by the action of PLC upon cell surface receptor activation (for example, GPCRs and/or RTKs) (Berridge, 1983, 1993; Furuichi & Mikoshiba, 1995; Foskett *et al.*, 2007). Mutational analysis provided further support for the current consensus that IP_3 binds to the IP_3-binding core (IBC) at the N-terminal domain of the receptor to stimulate Ca^{2+} release via the channel-forming region of the receptor tetramer (Furuichi & Mikoshiba, 1995; Yoshikawa *et al.*, 1996; Taylor & Tovey, 2010). IP_3R isoforms differ in their affinity for IP_3 – IP_3R2>IP_3R1>IP_3R3 (Miyakawa *et al.*, 1999; Tu *et al.*, 2005). SD within the N-terminal region of IP_3Rs has been suggested to be an important determinant of the differing affinities exhibited by the IP_3R isoforms for IP_3 (IP_3R2>IP_3R1>IP_3R3) (Iwai *et al.*, 2007). In addition to IP_3 being the primary activator ligand, cytosolic free Ca^{2+} has also been shown to regulate the activity of IP_3-induced Ca^{2+} release (IICR) as a co-agonist (Bezprozvanny *et al.*, 1991; Finch *et al.*, 1991; Miyakawa *et al.*, 1999; Foskett *et al.*, 2007; Taylor & Tovey, 2010).

Cytosolic free Ca^{2+} has been shown to have a biphasic effect on IICR (the so-called bell-shaped Ca^{2+} dependence curve) (Bezprozvanny *et al.*, 1991; Finch *et al.*, 1991; Miyakawa *et al.*, 1999). Modest increases in $[Ca^{2+}]_C$ (100-300 nM) enhanced IICR

with maximum channel activity observed at ~200-300 nM, whereas higher concentrations (>300-500 nM) exhibited inhibitory effect on IICR in guinea pig smooth muscles (Iino, 1990), canine cerebellum (Bezprozvanny *et al.*, 1991), mouse cerebellum (Michikawa *et al.*, 1999), rat brain synaptosomes (Finch *et al.*, 1991), and B-cells (Miyakawa *et al.*, 1999). Increased $[Ca^{2+}]_C$ at ≥300 nM also reversibly inhibited IP_3 binding to IP_3Rs (Supattapone *et al.*, 1988; Thrower *et al.*, 1998). Cytosolic free Ca^{2+} has both potentiating and inhibitory effects on IICR and both effects are universally accepted phenomena. There is a universal understanding that the stimulatory or potentiating effect of cytosolic Ca^{2+} on IICR is a result of Ca^{2+} directly interacting with IP_3R after Ca^{2+} release through the receptor (Michikawa *et al.*, 1999; Foskett *et al.*, 2007; Taylor & Tovey, 2010). However, how cytosolic Ca^{2+} confers its inhibitory effect on IICR is still a subject of intense debate. One side of the debate argues that Ca^{2+} inhibition is a result of free Ca^{2+} binding directly to the receptor (Marshall & Taylor, 1994; Thrower *et al.*, 1998), while the other side states that Ca^{2+} inhibition is likely to be mediated by an accessory Ca^{2+}-binding protein(s) (Supattapone *et al.*, 1988; Michikawa *et al.*, 1999). In support of Ca^{2+} acting directly on IP_3R to exercise its inhibitory effect, the proposed model was that there are two distinct Ca^{2+}-binding sites with differing affinities for Ca^{2+} within the IP_3R that are thought to mediate both stimulatory and inhibitory effects of cytosolic Ca^{2+} (Marshall & Taylor, 1994; Striggow & Ehrlich, 1996). Another proposed model was that there is a single Ca^{2+}-binding site that switches from being inhibitory in the absence of IP_3 to stimulatory in the presence of IP_3 (Mak *et al.*, 2003). Finally Ca^{2+} inhibition could be mediated by an accessory Ca^{2+}-binding protein. Supporting evidence in favour of the inhibitory effect of cytosolic Ca^{2+} exerted via an accessory protein(s) on IICR cannot be underestimated. Purified IP_3Rs (IP_3R1) does not exhibit the bell-shaped

dependence of IICR as a function of cytosolic Ca^{2+}, in other words bell-shaped dependence on Ca^{2+} is restricted to microsomal vesicles and crude extract preparations (Supattapone *et al.*, 1988; Bezprozvanny *et al.*, 1991; Finch *et al.*, 1991; Michikawa *et al.*, 1999). In support of these observations, in the presence of high free Ca^{2+} level, even as high as 1.5 mM, IP_3 binding to purified IP_3R1 was unaffected but inhibition was restored in the presence of detergent-solubilized cerebellar membranes (Supattapone *et al.*, 1988). Purified IP_3R1-mediated Ca^{2+} release activity could be stimulated, but not inhibited by high cytosolic Ca^{2+} (Michikawa *et al.*, 1999). Also partially purified IP_3R2 isolated from ventricular cardiac myocytes failed to exhibit the bell-shaped dependence of cytosolic Ca^{2+} (Ramos-Franco *et al.*, 1998). These observations triggered the search for a potential accessory/auxiliary protein(s) that could be responsible for mediating this inhibitory effect.

One potential candidate for this role is calmodulin (CaM), a well-characterised Ca^{2+}-binding protein (Gnegy, 1993). Purified mouse cerebellar IP_3R1 was shown to bind CaM in a Ca^{2+}-dependent manner (Maeda *et al.*, 1991). Yamada et al. (1995) also demonstrated that CaM binds IP_3R1 and IP_3R2 in a Ca^{2+}-dependent manner, whereas IP_3R3 does not bind CaM even in the presence of 1.5 mM Ca^{2+}. The binding sites of CaM have been mapped to the SD region within the N-terminal domain of IP_3R1 (Sienaert *et al.*, 2002) and within residues 1564-1585 and 1558-1596 in the coupling domain of IP_3R1 and IP_3R2, respectively (Yamada *et al.*, 1995). Michikawa et al. (1999) provided exquisite evidence by demonstrating that the addition of CaM restored Ca^{2+} inhibition to purified IP_3R1, which in the absence of CaM was resistant to inhibition at high Ca^{2+} concentration (~200 μM). They also showed that Ca^{2+}-dependent inactivation of the microsomal IP_3R at high free Ca^{2+}

was reversed in the presence of CaM antagonist W-7 (Hidaka *et al.*, 1981) in a dose-dependent manner (Michikawa *et al.*, 1999). Missiaen and colleages also showed that exogenous CaM inhibits IICR in permealised A7r5 cells (Missiaen *et al.*, 1999). It was also shown in DT40 cells, that IICR via IP_3R3 failed to exhibit the biphasic Ca^{2+} dependence (Miyakawa *et al.*, 1999), perhaps because IP_3R3 lacks a CaM binding site (Yamada *et al.*, 1995). In addition, IP_3R3 in RIN-5F cells is activated monotonically with increased cytosolic Ca^{2+} up to 100 μM (Hagar *et al.*, 1998).

Another cofactor involved in the regulation of IP_3R activity is cytosolic ATP (Ehrlich & Watras, 1988; Iino, 1991; Maeda *et al.*, 1991; Bezprozvanny & Ehrlich, 1993; Miyakawa *et al.*, 1999; Tu *et al.*, 2005). It is noteworthy that ATP alone is not sufficient to stimulate IP_3R channel opening but it elicits its potentiating effect in the presence of IP_3 (Bezprozvanny *et al.*, 1991; Iino, 1991; Bezprozvanny & Ehrlich, 1993; Tu *et al.*, 2005). It was demonstrated that IP_3R activity is enhanced or potentiated by cytosolic ATP in a hydrolysis-independent manner in smooth muscle (Iino, 1991) and cerebellar preparation (Bezprozvanny & Ehrlich, 1993). Supporting evidence comes from using non-hydrolysable ATP analogues in the presence of IP_3, which produced similar potentiating effect (Ehrlich & Watras, 1988; Bezprozvanny & Ehrlich, 1993). Isoforms of IP_3R differ in their ATP dependence of Ca^{2+} release with IP_3R1 channel gating been the most sensitive to ATP and IP_3R3 channel gating was less sensitive, whereas IP_3R2 channel gating was insensitive to ATP (Miyakawa *et al.*, 1999; Tu *et al.*, 2005). Tu et al. (2005) hypothesised that under optimal conditions (i.e. in the presence of maximal IP_3) required for channel activity IP_3R2 was insensitive to ATP. This was later demonstrated to be correct. IP_3R2 channel gating was indeed sensitive to ATP but only in the presence of sub-saturating $[IP_3]$, and in contrast to findings at saturating $[IP_3]$, IP_3R2 activity was strikingly the most

sensitive of all isoforms under this condition (Betzenhauser *et al.*, 2008; Betzenhauser *et al.*, 2009; Wagner & Yule, 2012; Vervloessem *et al.*, 2014).

Post-translational modifications i.e. phosphorylation/dephosphorylation of IP_3Rs have also been linked to the fine-tuning of Ca^{2+} release activity and efficient Ca^{2+} signals, which in turn are essential for numerous cellular processes ranging from oocyte maturation to cell death (Pieper *et al.*, 2001; Vanderheyden *et al.*, 2009). From the primary sequence of IP_3R isoforms, there are multiple phosphorylation consensus sites and numerous docking sites for protein kinases and phosphatases such as protein kinase A (PKA) and protein phosphatase (PP1), respectively. Currently, at least 12 different protein kinases are believed to directly phosphorylate the IP_3Rs. Adding to the complexity of the modulation of IP_3R activity by regulatory proteins such as IRBIT and Bcl-2 that associate with IP_3Rs are themselves regulated by phosphorylation and/or dephosphorylation (Vanderheyden *et al.*, 2009). Collectively, numerous intracellular factors co-operatively contribute to the regulation of IP_3R gating and IICR.

1.1.4 Subcellular localisation of IP_3Rs

IP_3Rs are intracellular Ca^{2+} release channels primarily located in the membranes of the ER (Vermassen *et al.*, 2004). The three isoforms of IP_3Rs share common similarities in structure (Mignery & Sudhof, 1990; Miyawaki *et al.*, 1991) but they differ in many respects with regards to their subcellular localisation and cellular abundance, regulation by small intracellular molecules (IP_3, free Ca^{2+} and ATP), post-translational modifications (i.e. phosphorylation), degradation by proteases during prolonged agonist stimulation and protein-protein interactions (Wojcikiewicz, 1995; Miyakawa *et al.*, 1999; Tu *et al.*, 2005; Vanderheyden *et al.*, 2009; Decuypere

et al., 2011; Pantazaka & Taylor, 2011). Vermassen et al. (2004) postulated that the exact subcellular localisation of IP_3Rs is an important determinant for the correct initiation, propagation of Ca^{2+} signals and the physiological consequences of IP_3-induced Ca^{2+} release. Unregulated Ca^{2+} signalling is implicated in a vast number of pathological conditions including cancer, cardiovascular and neurodegenerative diseases (Berridge *et al.*, 2000; Decuypere *et al.*, 2011; Vervloessem *et al.*, 2014). It is therefore essential to appreciate the significance of the expression and distribution of IP_3R Ca^{2+} release channels in the context of many physiological functions. In most cell and tissue types, isoforms of IP_3R are differentially expressed (Wojcikiewicz, 1995) and with the availability of good isoform-specific antibodies and the use of fluorescently labelled IP_3Rs, the subcellular localisation and distribution of IP_3R isoforms have been determined and shown not to be uniformly distributed within the ER (Vermassen *et al.*, 2004). It is a general consensus among researchers in the field that the relative expression levels and the subcellular localisation of IP_3Rs varies widely, for example, within a particular cell type (COS cells) and in different cell types depending on the isoform expressed (Wojcikiewicz, 1995; Vermassen *et al.*, 2004; Pantazaka & Taylor, 2011).

In the brain, IP_3R1 is highly expressed (~ 96% of total IP_3Rs) and IP_3R2 is expressed in trace amount (~ 4% of total IP_3Rs) with no apparent detection of IP_3R3 expression (Wojcikiewicz, 1995). However, some IP_3R3 was detected in neuronal terminals (Sharp *et al.*, 1999). IP_3R1, the first of the three isoforms to be identified was purified and cloned from rat/mouse cerebellum because of its high abundance in this tissue (Supattapone *et al.*, 1988; Furuichi *et al.*, 1989). It was later confirmed and currently accepted that neuronal cells in the central nervous system mainly express IP_3R1 (Furuichi *et al.*, 1993; Vermassen *et al.*, 2004). For example, in mouse cerebellum

there are five distinct neuronal cell types, one of which is the Purkinje cell, which plays a key role in information processing expresses high density of IP_3R1 (Furuichi *et al.*, 1989; Wojcikiewicz, 1995). Using immunohistochemical technique, the distribution of IP_3R1 has been shown to localise throughout the cell including the axon, dendrites and cell bodies (Maeda *et al.*, 1989). This uniformly observed distribution could perhaps account for the total IP_3R1 present in the cerebellar cells without distinguishing between the differential subcellular localisation of post-translationally modified IP_3R1 and unmodified IP_3R1. More than a decade later, Pieper et al. (2001) showed that in cerebellar Purkinje neurons of the brain, protein kinase A (PKA)-phosphorylated IP_3R1 was selectively enriched in dendrites while the unphosphorylated version of the receptor was most prominent in cell bodies. Besides the ER being uniformly distributed within the cell (Finch & Augustine, 1998; Takechi *et al.*, 1998), IP_3-induced Ca^{2+} release (IICR) evoked by synaptic stimuli is predominantly restricted to the spines of Purkinje cells (Fukatsu *et al.*, 2010) and is important for the induction of long-term depression (LTD) (Inoue *et al.*, 1998). This perhaps suggest that post-translational modification i.e. phosphorylation could play a role in the differential activity and functional properties of IP_3R1 in the brain.

Ca^{2+} signalling and the differential localisation of IP_3R isoforms have also been studied in epithelial cells because of their polarised nature and vectorial transport functions, which requires specialised signalling microdomains (Vermassen *et al.*, 2004). Early work by Wojcikiewicz (1995) in AR4-2J rat pancreatoma cells and in rat pancreas showed that these cells expressed all three isoforms but their relative abundance varied widely. In rat pancreas tissue, IP_3R2 and IP_3R3 were mainly expressed with relative abundance of 53% and 44%, respectively, while IP_3R1 accounted for 3% of total IP_3Rs expression. In AR4-2J cells, IP_3R2 was

predominantly expressed with a relative abundance of 86% and to a much lesser extent followed by that of IP_3R1 and IP_3R3 (Wojcikiewicz, 1995). In COS cells (COS-1) IP_3R isoforms are expressed in the relative abundance order of IP_3R3 (62%)>IP_3R2 (37%)>IP_3R1 (1%) (Wojcikiewicz, 1995). With the use of isoform-specific antibodies, it has been shown that all three isoforms localise to the apical part of pancreatic acinar cells (Lee *et al.*, 1997; Yule *et al.*, 1997; Lur *et al.*, 2009; Lur *et al.*, 2011). Differential distribution of IP_3Rs has also been reported in some epithelial cells expressing at least two isoforms. For example, in non-pigmented epithelial cells, IP_3R1 was localised at the basal pole whereas IP_3R3 was concentrated at the apical part of the cell (Hirata *et al.*, 1999). In cholangiocytes, IP_3R1 and IP_3R2 were shown to be uniformly distributed throughout the cytoplasm whereas IP_3R3 was mostly localised to the apical part (Hirata *et al.*, 2002a). Also in hepatocytes, the distribution of apical-localised IP_3R2 was different from IP_3R1, which was uniformly distributed (Hirata *et al.*, 2002b). In addition, it's become apparent that the subcellular localisation of IP_3Rs is dynamic and most likely depends on the physiological status of a cell (Vermassen *et al.*, 2004). For example, the maturation/oogenesis of oocytes is accompanied by the re-localisation of the predominant isoform IP_3R1 from a uniformly cytoplasmic distribution to a more polarised localisation in the cortical regions (Kume *et al.*, 1997). During the course of Madin-Darby canine kidney (MDCK) cell polarity development i.e. transition from subconfluence phase to a polarised phase, IP_3Rs underwent an apparent change in their subcellular localisation from a distribution throughout the cytoplasm and in the perinuclear region (like other ER markers) to a concentrated localisation near the lateral membranes and in close vicinity of the tight junctions (Colosetti *et al.*, 2003; Zhang *et al.*, 2003; Hours & Mery, 2010; Dingli *et al.*, 2012).

In smooth muscle cells, the subcellular distribution of IP_3R isoforms differ in that IP_3R1 was primarily distributed throughout the cytoplasm, IP_3R3 was mainly found in the perinuclear region whereas a heterogeneous distribution of IP_3R2 was observed in different cellular areas including near the plasma membrane (called plasmerosome – close associations between plasma membrane and the junctional components of ER) (Blaustein & Golovina, 2001) and in the perinuclear region (Tasker *et al.*, 2000). IP_3R1 expression is relatively high in smooth muscle cells but to lesser degree compared to that in the cerebellum. Its subcellular distribution varies widely depending on the muscle cell type (Vermassen *et al.*, 2004). IP_3R1 was found in the peripheral smooth ER in vas deferens, an example of phasic smooth muscle (Nixon *et al.*, 1994), whereas in tonic smooth muscle (aorta) IP_3R1 was centrally localised because for the most part, its ER is centrally located (Nixon *et al.*, 1994). Much lesser IP_3R density is expressed in skeletal and cardiac muscles, where IP_3R2 is the predominant isoform (Vermassen *et al.*, 2004). In addition, the redistribution of IP_3R1 was observed in vascular smooth muscle cell line A7r5 from a perinuclear-localised region to a more cytoplasmic localisation upon vasopressin stimulation (Vermassen *et al.*, 2003).

The importance of the subcellular localisation and redistribution of IP_3Rs in shaping the physiological consequences of IP_3-induced Ca^{2+} release signals are thought to be essential for many physiological functions and is increasingly becoming more appreciated. However, the molecular determinants and/or mechanisms underlying the redistribution and discrete subcellular localisation are currently not well elucidated. Moreover, in recent times, some advances have been made to elucidate the potential participating molecular determinants. Cytoskeletal proteins (Rossier *et al.*, 1991; Fukatsu *et al.*, 2004; Fukatsu *et al.*, 2010), adaptor and scaffolding

proteins (Dingli *et al.*, 2012), phospholipids – PI(4,5,)P_2 (Lupu *et al.*, 1998), post-translational modifications (i.e. phosphorylation) (Pieper *et al.*, 2001; Vanderheyden *et al.*, 2009), and microtubule dynamics and/or diffusion (Aihara *et al.*, 2001; Vermassen *et al.*, 2003) have all been implicated in the control of IP_3Rs localisation (Vermassen *et al.*, 2004). Actin cytoskeleton has been reported to play a crucial role in the localisation and positioning of IP_3Rs and IP_3-sensitive Ca^{2+} stores in close vicinity of the plasma membrane (Rossier *et al.*, 1991; Delmas *et al.*, 2002; Johenning & Ehrlich, 2002). The ER is a relatively dynamic structure and this is thought to be dependent on the status of the cytoskeleton (Aihara *et al.*, 2001; Berridge, 2002; Vermassen *et al.*, 2004). Since the primary location of IP_3Rs is the ER membrane, one would perhaps suggest that the subcellular localisation of IP_3Rs should be dependent on the ER morphology within a cell. In addition, a direct interaction between IP_3Rs and actin has been demonstrated through co-immunoprecipitation experiment (Sugiyama *et al.*, 2000). In hippocampal neurons, actin-dependent regulation of IP_3R1 lateral diffusion is mediated by a linker protein 4.1N, which binds to actin-spectrin filaments and to the IP_3R1 C-terminal (Fukatsu *et al.*, 2004). In Purkinje cells, Fukatsu et al. (2010) showed that actin filaments play a part in the regulation of IP_3R1 diffusion in the spines upon glutamate receptor activation; however, adaptor protein 4.1N is unlikely to be involved. Recently, in polarised MDCK cells, the coupling domain of IP_3Rs has been identified to be essential for targeting the receptor to the tight junction vicinity via an interaction with adaptor protein K-Ras-induced actin-binding protein (KRAP)-vimentin/keratin complexes (Dingli *et al.*, 2012). Collectively, these reported observations suggest that different molecular determinants are likely to be involved in the subcellular localisation of IP_3Rs through different domains within the IP_3Rs in different cell types.

1.2 Endoplasmic reticulum-Plasma membrane (ER-PM) junctions

1.2.1 ER-PM junctions

ER-PM junctions are specialised regions of close contact between the two organelles usually with an inter-membrane space of 7 to 25 nm (Wu *et al.*, 2006; Varnai *et al.*, 2007; Lur *et al.*, 2009; Orci *et al.*, 2009; Carrasco & Meyer, 2011; Chang *et al.*, 2013; Wu *et al.*, 2014). More than half a century ago, the existence of ER-PM junctions was observed in electrically excitable cells – first in striated muscles (Porter & Palade, 1957) and then later in neurons (Rosenbluth, 1962) using electron microscopy (EM) studies. These specialised contacts are formed between the ribosome-free terminals of the ER and the PM (Lur *et al.*, 2009; Orci *et al.*, 2009). Other key remarkable characteristics of the ER-PM junctions is that these specialised regions/platforms are: 1) a restricted protein-rich cytosolic microdomain, 2) the identity of both membranes are conserved due to the lack of any observable evidence of fusion between the two membranes (i.e. inter-membrane space of >0 and ≤25 nm) and 3) can be both stable and dynamic (Wu *et al.*, 2006; Lur *et al.*, 2009; Carrasco & Meyer, 2011; Dingsdale *et al.*, 2013). Therefore, this specialised platform must house complexes important for bridging the two membranes. A number of proteins including ER luminal proteins, cytosolic proteins and integral ER membrane proteins especially junctate (Treves *et al.*, 2004) and junctophilin (Takeshima *et al.*, 2000) have been reported to have a role in ER-PM junction bridge formation (Carrasco & Meyer, 2011). Recently, a number of elegant studies performed in yeast (Manford *et al.*, 2012) and mammalian cells (Chang *et al.*, 2013) have identified additional key proteins involved in tethering and maintaining the integrity of ER-PM junctions. In yeast cells, in order of importance – Scs2 and Scs22 (vesicle-associated membrane protein-associated proteins), Ist2 (related to

mammalian TMEM16 ion channels) and the tricalbins (Tcb1/2/3, orthologs of the extended synaptotagmins) were all identified to be essential for tethering ER-PM junctions using quantitative proteomic approach (Manford *et al.*, 2012). In mammalian cells (HeLa), using genetically encoded ER-PM marker membrane-attached peripheral ER (MAPPER), it was shown that cell surface receptor stimulation-mediated elevation of cytosolic Ca^{2+} enhanced the ER-PM connection via the recruitment and translocation of extended synaptotagmin (E-Syt1) (Chang *et al.*, 2013).

ER-PM junctions provide a platform for direct signal transduction between the ER and the PM in eukaryotes (Carrasco & Meyer, 2011). Currently, this platform has been demonstrated to serve as signalling hubs for Ca^{2+} signalling (Wu *et al.*, 2006; Varnai *et al.*, 2007; Lur *et al.*, 2009; Chang *et al.*, 2013; Wu *et al.*, 2014), phosphatidylinositol transfer, turnover and signalling (Carrasco & Meyer, 2011; Manford *et al.*, 2012; Chang *et al.*, 2013) and cAMP signalling (Lefkimmiatis *et al.*, 2009; Willoughby *et al.*, 2012). ER-PM junctions have been unequivocally shown to be important in bidirectional Ca^{2+} signalling i.e. in striated muscle excitation-contraction coupling "outside-in" Ca^{2+} signalling, and store operated Ca^{2+} entry-mediated "inside-out" Ca^{2+} signalling predominantly in non-excitable cells (Carrasco & Meyer, 2011). From here on in, the present study focuses on the roles of ER-PM junctions in store operated Ca^{2+} entry-mediated "inside-out" Ca^{2+} signalling.

1.2.2 Store operated Ca^{2+} entry (SOCE)

The "inside-out" Ca^{2+} signalling transduction pathway begins with the classic PM-localised G-protein coupled receptors (GPCRs) and/or receptor tyrosine kinases (RTKs) activation of phospholipase C (PLC) β/γ. In turn, PLC catalyses the

hydrolysis of phosphatidylinositol 4,5-bisphosphate ($PI(4,5)P_2$) to yield inositol 1,4,5-trisphosphate (IP_3) and diacylglycerol (DAG). IP_3 binds to IP_3Rs in the ER to mediate Ca^{2+} release (Berridge *et al.*, 2000; Carrasco & Meyer, 2011). Following ER Ca^{2+} store emptying through IP_3R Ca^{2+}-release channels in the ER, restoring of the ER Ca^{2+} concentration ($[Ca^{2+}]_{ER}$) involves Ca^{2+} influx across the PM through store operated Ca^{2+} entry (SOCE) process (Putney, 1986; Berridge *et al.*, 1998; Berridge *et al.*, 2000; Putney, 2005; Carrasco & Meyer, 2011). This process of Ca^{2+} replenishment is particularly prominent in non-excitable cells (Berridge *et al.*, 1998; Schindl *et al.*, 2009).

Intracellular Ca^{2+} store depletion triggers Ca^{2+} influx through SOCE mechanism, which is mediated by the dynamic interplay and coupling of ER Ca^{2+} sensor stromal interaction molecule (STIM) protein and PM Ca^{2+} release-activated Ca^{2+} (CRAC) channels Orai, which were both discovered by genome-wide RNA interference screens (Liou *et al.*, 2005; Roos *et al.*, 2005; Zhang *et al.*, 2005; Feske *et al.*, 2006; Vig *et al.*, 2006; Zhang *et al.*, 2006). STIM proteins are predominantly ER resident proteins that contain a single-pass transmembrane domain with an N terminal containing dual EF-hand Ca^{2+}-binding motif that faces into the ER lumen (which senses ER luminal Ca^{2+} content) and a C terminus facing into the cytosol. Two structurally similar isoforms of STIM – STIM1 and STIM2 are expressed in vertebrates, albeit both isoforms only differ structurally at the extreme N and C termini (Liou *et al.*, 2005; Deng *et al.*, 2009). An additional population of STIM1 was reported to also localise in the PM (Zhang *et al.*, 2005). Three closely related isoforms of Orai proteins have been identified, namely Orai1, Orai2 and Orai3 (Feske *et al.*, 2006; Vig *et al.*, 2006). Orai is characterised by four transmembrane domains with both N and C termini facing into the cytosol and it is a highly selective

pore-forming subunit of the plasma membrane-localised CRAC channel (Feske *et al.*, 2006). In its functional Ca^{2+} current conducting state, it exists as a tetramer (Deng *et al.*, 2009; Muik *et al.*, 2012). At resting state or before cell surface receptor-stimulated IP_3R-mediated ER Ca^{2+} store depletion, STIM1 exist as monomers and is normally distributed uniformly within the ER membrane in a reticular manner as observed using confocal microscopy (Liou *et al.*, 2005; Liou *et al.*, 2007). Upon ER Ca^{2+} store depletion, Ca^{2+} dissociates from STIM1 EF hand motif, enabling STIM1 to undergo profound oligomerisation and redistribution into discrete junctional ER sub-regions closely juxtaposed with the plasma membrane, a region called the ER-PM junctions. At these junctions STIM1 molecules aggregate, interact with and activate PM-localised Orai1 channels to induce Ca^{2+} entry (Liou *et al.*, 2007; Deng *et al.*, 2009). The coupling of STIM1 oligomers to tetrameric pore-forming Orai1 channels has been shown to involve the interaction between the Orai coupling site located within the cytoplasmic domain of STIM1 and the C terminus of Orai1 (Muik *et al.*, 2008; Deng *et al.*, 2009; Park *et al.*, 2009; Muik *et al.*, 2012). Meanwhile, the N-terminus of Orai1 is essential for Orai1 channel gating and current activation (Feske *et al.*, 2006; Muik *et al.*, 2008; Park *et al.*, 2009). In addition, Lewis and colleague postulated that the binding of 8 STIM1s to each tetrametric channel is required for peak CRAC channel activity by showing that the stoichiometric requirements for peak Ca^{2+} influx current was observed at a ratio of ~2 STIM1:Orai1 (Hoover & Lewis, 2011).

These ER-PM junctions are normally visualised as punctate structures using confocal microscopy (Liou *et al.*, 2007; Varnai *et al.*, 2007; Carrasco & Meyer, 2011; Chang *et al.*, 2013; Dingsdale *et al.*, 2013). Multiple molecular approaches have been developed to visualise pre-existing and newly formed ER-PM junctions prior to

and following ER-Ca^{2+} store depletion, respectively. These include: fluorescent/HRP-tagged STIM1 (Liou *et al.*, 2005; Wu *et al.*, 2006; Varnai *et al.*, 2007), rapamycin-inducible membrane linker technique (see Figure 2.1) (Varnai *et al.*, 2007), and the recently developed, elegantly designed and non-invasive membrane-attached peripheral ER (MAPPER) construct (Chang *et al.*, 2013).

1.3 Cell migration and its regulation by Ca^{2+} signalling

1.3.1 Cell migration and the polarity of migrating cells

Cell migration is a highly co-ordinated cellular behaviour integral to numerous physiological processes including embryogenesis, organ development, immune surveillance, wound healing and tissue regeneration after damage (Valeyev *et al.*, 2006; Ridley, 2011; Roussos *et al.*, 2011; Lamouille *et al.*, 2014). To date, it has been documented that most cell types undergo two distinct modes of migration: single cell migration and collective/cohort migration (Roussos *et al.*, 2011). These modes of cell migration also play critical roles in the development and progression of various pathological conditions including cancer and inflammatory diseases (Hanahan & Weinberg, 2000; Friedl & Gilmour, 2009; Hanahan & Weinberg, 2011; Roussos *et al.*, 2011). Cells can undergo both random and directional migration (Roussos *et al.*, 2011; Burdyga *et al.*, 2013). Cell migration in a directed fashion involves the co-ordination and sequential events of chemosensing, polarisation and locomotion (Iijima *et al.*, 2002; Iglesias & Devreotes, 2008). Cell migration is thought to be most efficient when cells move in a directed fashion (Hanahan & Weinberg, 2011; Roussos *et al.*, 2011) in response to soluble extracellular cues (chemotaxis) (Yang *et al.*, 2009; Burdyga *et al.*, 2013), mechanical cues (mechanotaxis/durotaxis) (Provenzano *et al.*, 2010; Roussos *et al.*, 2011) and substrate-bound cues (haptotaxis) (Roussos *et al.*, 2011). Directed cell migration in addition to cell adhesion and invasion are critical processes essential for the formation of metastasis and the development of chemotherapy-resistance phenotype of numerous cancer/tumour types including pancreatic ductal adenocarcinoma (PDAC) (Hanahan & Weinberg, 2000; Stathis & Moore, 2010; Hanahan & Weinberg, 2011; Roussos *et*

al., 2011; Chang *et al.*, 2012; Siegel *et al.*, 2013; Lamouille *et al.*, 2014). PDAC is the 4th leading cause of cancer-related mortalities worldwide (Siegel *et al.*, 2011) and it is characterised by disseminated metastasis at diagnosis and poor prognosis with median survival period of less than 12 months (Siegel *et al.*, 2013).

Cells move forward by net protrusion/extension of their plasma membrane at the front leading edge, which is closely accompanied by the movement of the cell body (Ridley *et al.*, 2003; Tsai & Meyer, 2012). Extension of the membrane at the leading edge requires the co-ordinated actions of structural components of specialised network of actin modules such as lamellipodia, filopodia and lamella (Burnette *et al.*, 2011; Ridley, 2011). Filopodia are actin-rich components involved in exploring the cell's environment (Ridley, 2011). They are characterised by long, thin protrusions that extend from the plasma membrane which are composed of unbranched and parallel actin filaments/filamentous actin (F-actin) (Ridley *et al.*, 2003; Mejillano *et al.*, 2004; Ridley, 2011). A number of regulatory proteins including Fascin and formins (primarily the mDia proteins) have been shown to localise to filopodia where they contribute to actin polymerisation and bundling in filopodia and filopodium stability (Campellone & Welch, 2010; Machesky & Li, 2010; Mellor, 2010; Ridley, 2011). Filopodia are thought to emerge, in part from the lamellipodial F-actin network (Ridley, 2011). Lamellipodia was first described to consist predominantly of F-actin and devoid of microtubules as observed in cultures of migrating fibroblasts by Michael Abercrombie over 40 years ago (Abercrombie *et al.*, 1970, 1971). Lamellipodia region of the leading edge is usually defined by an area of ~3-5 μm from the extreme front edge and is characterised by dynamic and branched/criss-crossed polymerised F-actin (Burnette *et al.*, 2011). Actin polymerisation within the lamellipodia is known to drive forward protrusion of the membrane during cell

migration (Ridley *et al.*, 2003). A network of key mediators such as actin related protein 2/3 (Arp2/3) complex and its stimulating factors the Wiskott-Aldrich syndrome protein (WASP) family regulates lamellipodia F-actin network (Campellone & Welch, 2010). Arp2/3 complex has been reported to localise throughout the lamellipodium but it is only integrated into the network at the front edge of the lamellipodium (Lai *et al.*, 2008). WASP (WAVE) proteins localise to the leading edge where it stimulates Arp2/3 complex to mediate nucleation and branching of actin filament networks (Mullins *et al.*, 1998) critical for lamellipodia extension (Campellone & Welch, 2010). The activation of Arp2/3 complex by WASP proteins might be the key regulatory step for the incorporation of Arp2/3 complex into the network at the front leading edge of the lamellipodium. Other regulators including formins and cofilins have also been implicated in lamellipodia extension (Bernard, 2007; Paul & Pollard, 2009; van Rheenen *et al.*, 2009; Chesarone *et al.*, 2010; Ridley, 2011). Immediately behind the highly dynamic lamellipodia, is the more stable/less dynamic region known as the lamella. This region is also wider than the lamellipodia spanning ~10 μm or more in width, and is composed of bundled antiparallel F-actin and enriched with myosin II (Ponti *et al.*, 2004; Giannone *et al.*, 2007; Burnette *et al.*, 2011; Tsai & Meyer, 2012). This region contributes to cell migration by coupling actomyosin contractile network with substrate adhesion for traction (Giannone *et al.*, 2004; Ponti *et al.*, 2004; Gupton & Waterman-Storer, 2006; Giannone *et al.*, 2007; Burnette *et al.*, 2011; Ridley, 2011).

In addition to membrane protrusion, cell migration also requires the formation of cell adhesion (Ridley *et al.*, 2003). The dynamics and turnover (i.e. the assembly and disassembly) of focal adhesions is critical for cell migration (Webb *et al.*, 2002; Ridley *et al.*, 2003; Yang *et al.*, 2009; Tsai & Meyer, 2012). Focal adhesions are

functional and structural signal transducers that link intracellular cytoskeletal structures with the extracellular matrix via integral membrane spanning proteins (Webb *et al.*, 2002). Key regulatory proteins of focal adhesions include vinculin, paxillin and focal adhesion kinase (FAK); these proteins are also used experimentally as markers for focal adhesion (Ziegler *et al.*, 2006; Deakin & Turner, 2008; Mierke, 2009; Carisey & Ballestrem, 2011; Vicente-Manzanares & Horwitz, 2011; Wehrle-Haller, 2012; Kim & Wirtz, 2013).

Migrating cells are polarised and exhibit front-rear polarity, which is characterised by broad and ruffling lamellipodia, and filopodia-like protrusions at the front leading edge while at the cell rear is the trailing tail (Burnette *et al.*, 2011; Ridley, 2011; Dingsdale *et al.*, 2013). Multiple signalling cues converge to co-ordinate the regulation of the aforementioned components of specialised network of actin modules during cell migration through actions of critical signalling molecules including Rho GTPases, phospholipids such as $PI(4,5)P_2$ and kinases such as LIM kinase (LIMK) (Ridley, 2011). Rho GTPases are important signal effectors that relay signals from cell surface receptors to the actin cytoskeleton (Ridley, 2011). Briefly, Rho family of GTPases are small monomeric G-proteins that switch from inactive guanosine diphosphate (GDP)-bound conformation to an active guanosine triphosphate (GTP)-bound conformation that activates downstream targets. GDP to GTP exchange is facilitated by guanine nucleotide exchange factors (GEFs). GTP hydrolysis to GDP, which confers Rho GTPases to an inactive form, is accelerated and catalysed by GTPase-activating proteins (GAPs) (Bishop & Hall, 2000). The major regulatory Rho GTPases are Rac, Cdc42 and RhoA, which acts cooperatively or distinctively on different actin modules to control forward membrane extension and exploratory protrusions, cell body contraction and tail retraction during cell migration

(Ridley *et al.*, 2003). All three Rho GTPases have been shown to localise in the lamellipodia during membrane protrusion (Machacek *et al.*, 2009). RhoA has also been shown to localise at the cell rear, where it is essential for tail retraction during cell migration (Ridley *et al.*, 2003). Rac primarily regulates lamellipodia extension through the activation of WAVE-Arp2/3 complexes. RhoA promotes stress fibre formation by mediating the phosphorylation and regulation of myosin II activity. Cdc42 regulates filopodia extension and chemosensing (Kaverina *et al.*, 2002; Ridley, 2011). These Rho GTPases, in particular Rac and RhoA have been reported to undergo activation upon microtubule polymerisation and depolymerisation, respectively (Kaverina *et al.*, 2002). Rac- and Cdc42-mediated PAK and LIMK phosphorylation and deactivation of cofilin (actin-severing protein) have also been reported to be important for actin polymerisation and lamellipodia protrusion (Bernard, 2007; Delorme *et al.*, 2007; van Rheenen *et al.*, 2009). In addition, both Rac and Cdc42 also regulate the formation of focal adhesion complexes, whereas RhoA regulates the maturation of focal adhesions (Kaverina *et al.*, 2002).

1.3.2 Regulation of cell migration by Ca^{2+} signalling

Ca^{2+} is another critical regulator of cell migration in many if not all cell types (Brundage *et al.*, 1991; Berridge *et al.*, 1998; Pettit & Fay, 1998; Berridge *et al.*, 2000; Wei *et al.*, 2009; Yang *et al.*, 2009; Middelbeek *et al.*, 2012; Tsai *et al.*, 2014). Ca^{2+} signals control cell migration in a multifunctional fashion by regulating directional sensing, polarisation, forward movement, cell adhesion and speed (Wei *et al.*, 2009; Yang *et al.*, 2009; Middelbeek *et al.*, 2012; Tsai & Meyer, 2012; Tsai *et al.*, 2014). Just as migrating cells are polarised exhibiting front-rear polarity (Wei *et al.*, 2009; Dingsdale *et al.*, 2013), both global and local intracellular Ca^{2+} signals also exhibit rear-front and front-rear polarities, respectively (Brundage *et al.*, 1991; Wei *et*

al., 2009; Tsai *et al.*, 2014). In particular, the polarity of local Ca^{2+} pulses (calcium flickers or high-calcium microdomains) with higher frequency in the front than in the back of cells control cyclic local lamellipodia membrane protrusion, focal adhesion dynamics and turning which are all critical for cell migration (Wei *et al.*, 2009; Tsai & Meyer, 2012). Ca^{2+} signals produced by both IP_3R-mediated Ca^{2+} release from intracellular stores and Ca^{2+} influx across the PM via SOCE channels Orai1 and TRP (TRPM7) channels have all been shown to be critical for the process of migration in a number of cell types (Wei *et al.*, 2009; Yang *et al.*, 2009; Middelbeek *et al.*, 2012; Schafer *et al.*, 2012; Tsai & Meyer, 2012; Tsai *et al.*, 2014). Interestingly, the inhibition of ryanodine receptors (another major intracellular Ca^{2+} release channels) had no effect on regulatory components critical for the migration of human embryonic lung fibroblasts (Wei *et al.*, 2009). In addition to a higher frequency of Ca^{2+} flickers (high Ca^{2+} microdomains) in the front leading edge than in the rear of migrating cells (Wei *et al.*, 2009; Tsai *et al.*, 2014) other signalling mechanisms and processes including RTK, PLC, DAG, $PI(4,5)P_2$, $PI(3,4,5)P_3$, STIM1 and Orai1 signalling together with PM Ca^{2+} pumps (PMCA) and protein kinase C (PKCβ) signalling have all been shown to exhibit front-rear polarisation with preferential localisation to the leading edge (Brzeska *et al.*, 2012; Dingsdale *et al.*, 2013; Tsai *et al.*, 2014). Collectively, this integrated Ca^{2+} control system with polarised Ca^{2+} signalling proteins and signalling messengers have been shown to be critical for cell migration (Tsai *et al.*, 2014). However and surprisingly, the localisation of IP_3Rs in migrating cells is not clear; the spatial relationship of IP_3Rs and SOCE-competent ER-PM junctions has not been characterised; and the spatial and functional relationship between IP_3Rs and migratory machinery in migrating cells (in particular PDAC) has not been determined.

1.4 Aims

The aims of the present study were: 1) To characterise the redistribution of IP_3Rs and SOCE-competent ER-PM junctions in PDAC cells during EMT; 2) To examine the role of IP_3R-mediated Ca^{2+} release and SOCE-mediated Ca^{2+} influx in PDAC cell migration; and 3) To examine the spatial and functional relationships between IP_3Rs/ IP_3R-mediated Ca^{2+} release and the components of migratory apparatus in PDAC cells.

Chapter 2: Materials and Methods

Chapter 2: Materials and Methods

2.1 Materials

2.1.1 Reagents and equipment for pancreatic ductal adenocarcinoma cell line (PANC-1) culture and transfection

Cell culture Dulbecco's modified Eagle's medium (DMEM) and supplements including heat-inactivated foetal bovine serum (FBS) and PenStrep Glutamine (PSG; 100x), were all purchased from Life technologies (Paisley, UK). Also 0.05% trypsin ethylenediaminetetraacetic acid (EDTA) was purchased from Life technologies (Paisley, UK). Phosphate buffered saline (PBS) with no Ca^{2+} and Mg^{2+} was purchased from Lonza (Verviers, Belgium). Cell culture flasks (25 cm^2 and 75 cm^2) and the cell culture incubator were purchased from Corning (Buckinghamshire, UK) and Wolf Laboratories (York, UK), respectively. Transfection reagents including PromoFectin and Lipofectamine 2000 were purchased from Promokine (Heidelberg, Germany) and Life technologies (Paisley, UK), respectively.

2.1.2 Chemicals

Xestospongin-B (inhibitor of IP_3-induced Ca^{2+} release from intracellular Ca^{2+} stores) was a gift from Dr J. Molgo (Institute of Neurobiology Alfred Fessard, Gif-sur-Yvette cédex, France) and GSK-7975A (inhibitor of SOCE (store operated Ca^{2+} entry)) was a gift from Dr Malcolm Begg (GlaxoSmithKline, Stevenage, UK). Cyclopiazonic acid (CPA) was purchased from Tocris (Bristol, UK), thapsigargin (TG) and rapamycin were purchased from Calbiochem (San Diego, CA, USA). UV-photoactivatable and membrane permeant Ins(1,4,5) IP_3 (cag-iso-2-145) was purchased from Sichem (Bremen, Germany), and paraformaldehyde (PFA) was purchased from Agar

Scientific (Essex, UK). Fluorescent Ca^{2+} indicators Fura-2 and Fluo-4, and Ca^{2+} chelator BAPTA were all purchased from Life technologies (Paisley, UK). RIPA lysis and extraction buffer, Halt protease inhibitor cocktail and EDTA supplements were purchased from Pierce-Thermo scientific (Rockford, Illinois, USA). Goat serum, bovine serum albumin (BSA), RNAse A and Triton X-100 were all purchased from Sigma Aldrich (St. Louis, Missouri, USA). Acetylated BSA was purchased from Aurion (Netherlands). Hoechst 33342, Sytox orange and propidium iodide were all purchased from Life technologies (Paisley, UK). Small interfering RNA (siRNA) oligomers directed against human IP_3R1, IP_3R2, IP_3R3, and STIM1 were all purchased from Life technologies (Paisley, UK). In-house designed IP_3R1-, IP_3R2- and IP_3R3-isoform specific primers were purchased from Eurofins Genomics (Germany).

2.1.3 Reagents and materials for Immunofluorescence and Immunoblotting

Primary antibodies used were: anti-IP_3R1 (rabbit polyclonal raised against C-terminal amino acids 2735-2749 (Dingli *et al.*, 2012), a gift from Prof. J. Parys (Catholic University of Leuven, Leuven, Belgium)); anti-IP_3R1 [D53A5 (rabbit)] was purchased from Cell Signalling Technologies (Danvers, MA, USA); anti-IP_3R1 (mouse monoclonal, fusion protein corresponding to amino acids 2680-2749 C-terminus of rat IP_3R1) was purchased from RayBiotech, Inc. (Norcross, GA, USA); anti-IP_3R2 (rabbit polyclonal raised against C-terminal amino acids 2686-2702, a gift from Prof. D. Yule (University of Rochester, Rochester, NY, USA)); anti-IP_3R3 (mouse) was purchased from BD Transduction Laboratories; and anti-PAN IP_3Rs rabbit polyclonal raised against C-terminal epitope common to all 3 isoforms was purchased from Millipore (CA, USA). Anti-green fluorescent protein (GFP) (rabbit and chicken) was purchased from Life technologies (Paisley, UK), and anti-occludin (rabbit and

mouse) was purchased from Zymed Laboratories (Carlsbad, CA, USA). Anti-vinculin (mouse), anti-calnexin (rabbit), and anti-β-actin (mouse) were all purchased from Sigma Aldrich (St. Louis, Missouri, USA). Anti-E-cadherin (mouse) was purchased from Santa-Cruz Biotechnology (Dallas, Texas, USA). Anti-PI(4,5)P_2 (mouse) antibody was purchased from Abcam (Cambridge, UK). Anti-human Orai1 extracellular (rabbit) antibody was purchased from Alomone labs (Israel). Anti-STIM1 (rabbit) antibody was purchased from both Prosci (CA, U.S.A.) and Proteintech-Europe, and anti-STIM1 (mouse) antibody was purchased from BD Transduction Laboratories. Alexa Fluor 647 phalloidin and species-specific fluorophore-conjugated secondary antibodies: Alexa Fluor 488, Alexa Fluor 568 and Alexa Fluor 647 were all purchased from Life technologies (Paisley, UK). HRP-conjugated secondary antibodies (anti-rabbit and anti-mouse species) were purchased from Sigma Aldrich (St. Louis, Missouri, USA).

MOPS running buffer and 4-12% NuPAGE Bis-Tris gradient gel were purchased from Life technologies (Paisley, UK). Nitrocellulose membrane was purchased from LI-COR Biosciences (Cullman, Alabama, USA).

2.1.4 Equipment for super-resolution imaging, Boyden chamber migration and wound-healing/scratch migration assay

Oxygen scavenging system for super-resolution dSTORM microscopy – glucose oxidase, catalase, cysteamine (mercaptoethylamine) were all purchased from Sigma Aldrich (St. Louis, Missouri, USA). Lab-Tek chambered coverglass 8-well ♯ 1.0 with low thickness variation was purchased from Thermo Scientific (Runcorn, UK).

BD Falcon 24-well Boyden chamber PET (polyethylene terephthalate; transparent) and Fluoroblok inserts with 8 µm pore size and BD Falcon cell culture companion

plates were purchased from Corning (FALCON/Corning, Durham, NC, USA). Cotton buds (Johnson's cotton buds) were purchased from Sainsbury's local (Liverpool, UK).

µ-Dish 35 mm high glass bottom dishes and cell culture inserts used for wound-healing/scratch migration assay were purchased form ibidi (Martinsried, Germany).

2.2 Methods

2.2.1 Cell culture

Pancreatic ductal adenocarcinoma (PDAC) cell line PANC-1 was obtained from the American Type Culture Collection (ATCC; ATCC number CRL-1469) and cultured in DMEM (Dulbecco's modified Eagle's medium) supplemented with 10% FBS (foetal bovine serum), 100 units/ml penicillin, 100 µg/ml streptomycin and 292 µg/ml glutamine. Cultured cells were maintained in a humidified incubator (Wolf Laboratories) at 37°C and 5% CO_2.

2.2.2 Constructs, cell transfection and siRNA knockdown

DNA constructs including YFP-STIM1 with a TK (thymidine kinase) promoter, and the rapamycin-inducible constructs with longer helical (LL) linkers were a gift from Dr T. Balla (National Institute of Child Health and Human Development, Bethesda, MD, USA). YFP-STIM1 with TK promoter was used to reveal endoplasmic reticulum-plasma membrane (ER-PM) junctions in cells following ER Ca^{2+} stores depletion. Alternatively, rapamycin-inducible linker constructs were used to reveal ER-PM junctions in cells with unemptied/unmodified ER Ca^{2+} stores. The application of the rapamycin-inducible linker system has been described before (Varnai *et al.*, 2007). Briefly, the rapamycin-inducible linker components include PM-targeted LL-FKBP-

mRFP (a plasma membrane-targeted FK506-binding protein coupled to mRFP) and ER-targeted CFP-FRB-LL (an endoplasmic reticulum-targeted fragment of mammalian target of rapamycin (mTOR) that binds FKBP). The rapamycin-inducible linker system is used to reveal the ER-PM junctions via a molecular bridge formed between the juxtaposed membranes as a result of the heterodimerisation of the FKBP and FRB modules, which can only be established in the presence of rapamycin and at sites where the distance between the ER membrane and the PM is less than 14 nm (Varnai *et al.*, 2007) as illustrated in Figure 2.1.

Figure 2.1. Rapamycin induces the heterodimerisation of two distinct membrane-targeted modules.

The formation of FKBP-FRB complex is induced only in the presence of rapamycin, and at sites where the gap between the juxtaposed membranes is less than 14 nm. The FKBP-FRB complex can be revealed as the site of co-localisation of the two membrane-targeted fluorophores depicted by red circles (mRFP; monomeric red fluorescence protein) and blue circles (CFP; cyan fluorescence protein).

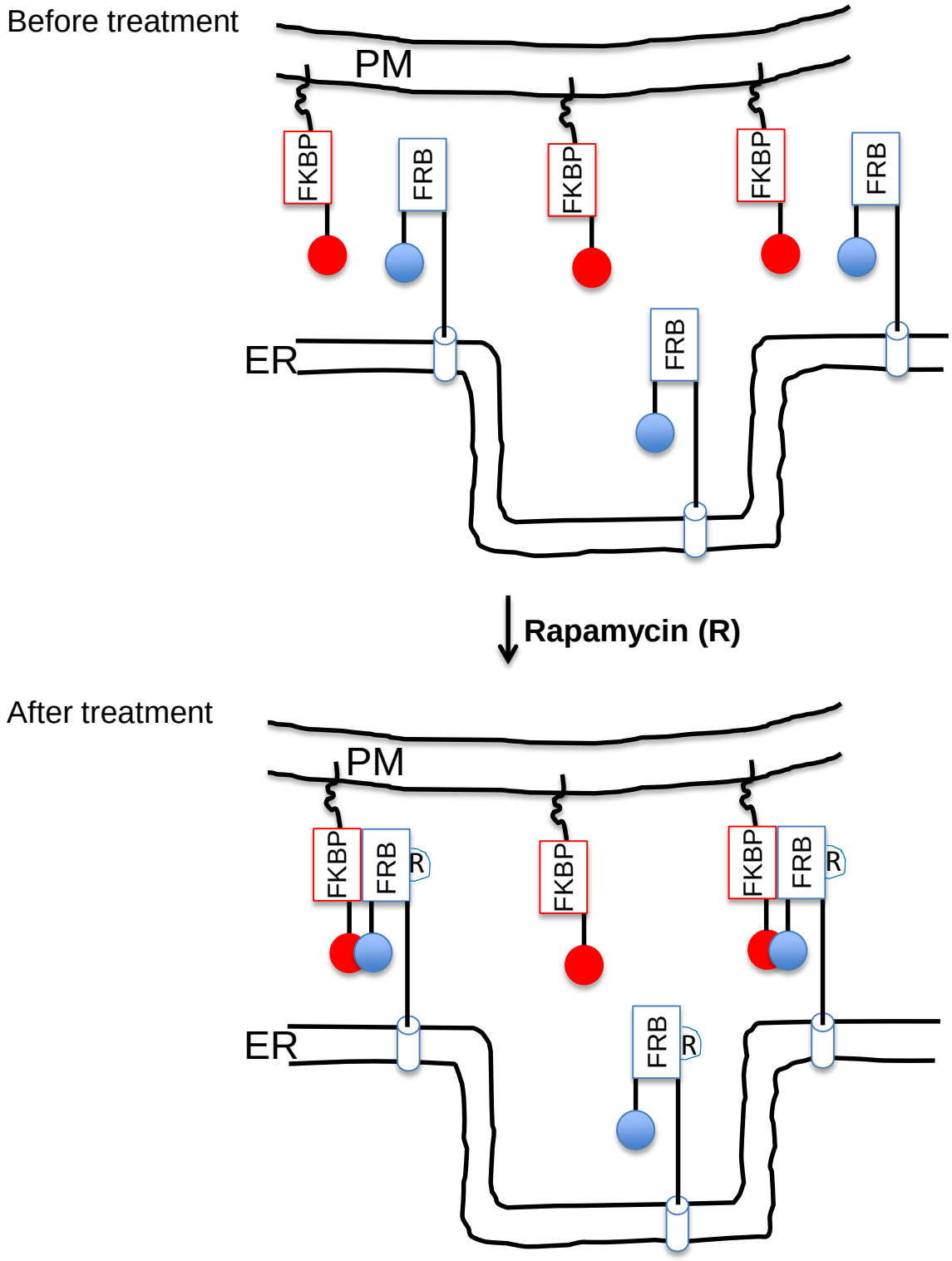
Before treatment
PM
FKBP
FRB
FKBP
FKBP
FRB
ER
FRB
Rapamycin (R)
After treatment
PM
FKBP
FRB
R
FKBP
FKBP
FRB
R
ER
FRB
R

Figure 2.1

In our study we utilised mCherry-labelled paxillin (Pax-mCh) and paxillin labelled with Ca^{2+} sensor GCaMP5 (Pax-GCaMP5). The coding sequence for GCaMP5 was obtained from Addgene (plasmid 31788, originally generated by Douglas Kim and Loren Looger (Akerboom *et al.*, 2012)). The GCaMP5 coding sequence was PCR amplified using the following primer pair containing restriction endonuclease sites (underlined) to permit sub-cloning into the pcDNA3.1(+) backbone (Life technologies, Paisley, UK) generating a new 'pcDNA-GCaMP5-CT' C-terminally tagging expression vector: Sense (NotI) 5'-ATATGCGGCCGCATGACTGGTGGACAGCAAATG-3'; Antisense (ApaI) 5'-ATATGGGCCCTCACTTCGCTGTCATCATTTGTAC-3'. Paxillin-GCaMP5 was created by PCR amplification of the chicken Paxillin sequence obtained from Addgene (plasmid 15233, originally deposited by Rick Horwitz (Laukaitis *et al.*, 2001)) using the following primer pair containing restriction endonuclease sites (underlined) to permit sub-cloning into pcDNA-GCaMP5-CT: Sense (EcoRI) 5'-ATATGAATTCACCATGGACGACCTCGATGCC-3'; Antisense (NotI) 5'-ATATGCGGCCGCTACAGAAGAGTTTGAGAAAGC-3'. Paxillin-mCherry was created by PCR amplification of the chicken paxillin sequence using the following primer pair containing restriction endonuclease sites (underlined) for sub-cloning into the mCherry-N1 vector (Clontech): Sense (XhoI) 5'-ATATCTCGAGACCATGGACGACCTCGATGCC-3'; Antisense (EcoRI) 5'-ATATGAATTCGACAGAAGAGTTTGAGAAAGCA-3'. All constructs were verified by automated sequencing (The Sequencing Service, University of Dundee, UK). These constructs were designed and produced by Dr Lee Haynes (University of Liverpool, UK).

To exogenously express proteins of interest, cells were transfected at approximately 60-70% confluence with 1 – 2 µg of DNA per plasmid construct for 24 hours using PromoFectin transfection reagent according to the manufacturer's instructions. Briefly, 2 – 4 µl of Promofectin, which was diluted in 100 µl of pre-warmed serum- and antibiotic-free medium was added to 1 - 2 µg of DNA diluted in 100 µl of pre-warmed serum- and antibiotic-free medium, and the DNA-PromoFectin mixture was allowed to stand for at least 20 min at room temperature (RT, approximately 18-22°C) before it was added in a drop-wise manner to PANC-1 cells seeded into 35 mm dishes (Mattek, Ashland, USA).

For the knockdown of cellular proteins of interest, siRNA oligomers directed against human IP_3R1, IP_3R2, IP_3R3, and STIM1 were used. siRNA sequences targeting each of the proteins of interest are: IP_3R1 silencer select siRNA sense 5'-GCACGACAGUGAAAACGCAtt-3', antisense 5'-UGCGUUUUCACUGUCGUGCct-3'; IP_3R2 silencer select siRNA sense 5'-GGUGUCUAAUCAAGACGUAtt-3', antisense 5'-UACGUCUUGAUUAGACACCag-3'; IP_3R3 silencer select siRNA sense 5'-GCAUGGAGCAGAUCGUGUUtt-3', antisense 5'-AACACGAUCUGCUCCAUGCtg-3'; and STIM1 silencer select siRNA sense 5'-GCCUAUAUCCAGAACCGUUtt-3', antisense 5'-AACGGUUCUGGAUAUAGGCaa-3'. Cells were transfected at approximately 30-40% confluence with 30 or 50 nM per siRNA oligomer for 72 hours using Lipofectamine 2000 transfection reagent according to the manufacturer's instructions. Briefly, 10 µl of Lipofectamine 2000 was diluted in 500 µl of pre-warmed Opti-MEM medium and was allowed to incubate for 5 min at RT prior to its addition to (12.5 or 15) µl of siRNA oligomer that was diluted in 500 µl of pre-warmed Opti-MEM medium. The siRNA oligomer-Lipofectamine 2000 mixture was then allowed to incubate for a further 20 min at RT before it was added in a drop-wise manner to

PANC-1 cells seeded in antibiotic-free DMEM medium in 25 cm^2 cell culture flasks. Approximately 6 hours after siRNA transfection of PANC-1 cells, antibiotic-free medium was replaced with full DMEM cell culture medium (supplemented with 10% FBS, 100 units/ml penicillin, 100 µg/ml streptomycin and 292 µg/ml glutamine) for an additional 66 hours before cells were harvested for subsequent experiments.

2.2.3 Quantitative real-time PCR

Isoform-specific PCR primers for human IP_3R1 (NM_001168272.1), IP_3R2 (NM_002223.2) and IP_3R3 (NM_002224.3) isoforms were designed in-house based on mRNA sequences obtained from both NCBI-PubMed and Uniprot databases. Sequences for all 3 isoforms were aligned using Clustal Omega multiple sequence alignment online program. Regions of distinct nucleotide sequences for both forward and reverse primers of approximately 20–22 bases in length for each IP_3R isoform with the desired nucleotide base ratio (G-C:A-T) were mapped using Clustal Omega multiple sequence alignment and following Netprimer sequence design recommendation guide. Selected forward and reverse primer sequences for each IP_3R isoform were run through an NCBI-BLAST system to be certain that they are specific to the individual IP_3R isoforms. Forward primers are 22 nucleotides long, whereas reverse primers are 20 nucleotides long. Amplicons in other words PCR amplified products were 120-200 base pairs (bp) in length based on primers' complimentary binding sites on IP_3R mRNA sequences, which can be detected and verified on a DNA gel electrophoresis (see Figure 3.2). Primer sequences are: IP_3R1 forward primer 5'-AGAGTTTGGCAAGCGAGTTCCT-3' and reverse 5'-CGTGACTCAGCACAGTGACA-3', amplicon is 171 bp (residues 7783-7953, spanning over 2 exon regions); IP_3R2 forward primer 5'-TGATGACATCTGGTCCACGAAT-3' and reverse 5'-CGGATTTTTCCTCAGTGTTT-

3', amplicon is 189 bp (residues 5945-6133, spanning over 2 exon regions); IP_3R3 forward primer 5'-AAGAGCGTGAGAACTCGGAGGT-3' and reverse 5'-GCTGAGGACTTGAGCATCTG-3', amplicon is 201 bp (residues 6334-6535, spanning over 3 exon regions); and β-actin (ACTB) forward primer 5'-CACCTTCTACAATGAGCTGCGTGTG-3' and reverse5'-ATAGCACAGCCTGGATAGCAACGTAC-3' (Faronato *et al.*, 2013), which was used as a transcript normaliser. Primers were synthesised by Eurofins Genomics (Germany).

PANC-1 cells seeded to full confluence were lysed, and RNA extracted using a QIAGEN RNA Preparation (RNeasy) mini columns extraction kit following the manufacturer's instructions. Following RNA extraction, a Nanodrop reader was used to determine the concentration of RNA in µg/µl and RNA purity (a ratio between absorbance at 260 nm and 280 nm = ~2.00 arbitrary units). Next, approximately 4 µl of RNA sample diluted in 5x loading buffer was run on a 1.2% agarose gel electrophoresis at 140 V for 1 hour to verify RNA extraction quality using a Syngene Bio-imaging camera system. The presence of two clear bands – the 28S and 18S rRNA (ribosomal RNA) subunits on the gel indicated high quality RNA extraction (see Figure 3.1).

Since RNA is relatively unstable, the next step was to reverse transcribe cDNA (complementary DNA) from RNA using RevertAid H-minus M-MuLV reverse transcriptase enzyme. Briefly, a reaction mixture was prepared in the following way: 1 µg of RNA, 1 µl Oligo dt (deoxy-thymine nucleotides) primer, 1 µl reverse transcriptase and ddH_2O (double-distilled H_2O) to a total volume of 12 µl, plus 8 µl of reaction mix containing 4 µl 5xRT Buffer, 2 µl PCR Nucleotide mix, 0.5 µl RNAsin and 1.5 µl ddH_2O. The reactions were set up in thin-walled PCR reaction tubes.

Using a PCR machine the reactions underwent the polymerase chain reaction. The cycling parameters were as follows:

Segment	Cycles	Temperature (°C)	Time (min)
1 RNA + dt primer + ddH_2O	1	70	5
2 5xRT Buffer + PCR Nucleotide mix + RNAsin + ddH_2O	1	37	5
3 Reverse transcriptase enzyme	n	42 70	60 10

After completion of the cDNA synthesis reaction, a further PCR reaction was performed using the synthesised cDNA, and IP_3R-isoforms specific forward and reverse primers. The product of the PCR reaction was run on a 2% agarose gel at 120 V for 1 hour to detect and validate the PCR amplified products of each IP_3R isoform based on the predicted amplicon or PCR amplified product size calculated during primer design.

After the predicted amplicon sizes for each isoform were confirmed on a DNA gel (see Figure 3.2), quantitative real-time PCR (qRT-PCR) was performed in triplicate to determine the transcript levels of each IP_3R isoforms using cDNA, IP_3R-isoforms specific primers, SYBR Green supermix and an IQ5 real-time PCR detection system (Bio-Rad). SYBR Green is a fluorescent dye that binds double-stranded DNA (dsDNA). Samples underwent two-step amplification phases at 94°C (0.5 min) and 60°C (1 min), and melting curves were analysed after 40 cycles. The cycle threshold

(C_T) values for each IP_3R isoform was determined, and C_T value is a measure of the amount of DNA in a sample. The C_T values for each IP_3R isoform transcript was normalised to β-actin (ACTB) and relative expression represented as ΔC_T.

2.2.4 Immunoblotting

After trypsin treatment, detached cells were collected by centrifugation and lysed for 30 min at 4°C on a rocking mixer using RIPA lysis and extraction buffer supplemented with Halt protease inhibitor cocktail and EDTA, which were both used at a final concentration of 1:100. After cell lysis, collected supernatant samples were diluted with 4% SDS (Sodium dodecyl sulfate) buffer at a ratio of 1:1 and boiled at 95°C for 5 min to denature or unravel proteins from their native state (i.e. disrupt secondary, tertiary and quaternary bonds) into a linearised state. Approximately 30 µl of samples were separated on a 4-12% NuPAGE Bis-Tris gradient gel for 1 to 2.5 hours depending on the molecular weight of the protein of interest at 125 V and transferred overnight onto nitrocellulose membranes in transfer buffer (2.5 litres of ddH_2O plus 7.6 g Tris base, 36 g Glycine and 500 ml 100% Methanol). Nitrocellulose membranes were blocked in 3% (w/v) non-fat dry skimmed milk powder dissolved in PBS (phosphate buffered saline) for 1 hour at RT (room temperature; approximately 18-22°C), and probed with primary antibodies including anti-IP_3R1 (1:500), anti-IP_3R2 (1:1000), anti-IP_3R3 (1:500), anti-STIM1 (1:500), anti-ORAI1 (1:200) and anti-β-actin (1:1000) at 4°C overnight. After overnight incubation, nitrocellulose membranes were incubated with appropriate species-specific HRP-conjugated secondary antibodies (1:400) for 1 hour at RT. After both primary and secondary antibody incubations, nitrocellulose membranes were subjected to a 0.05% Tween-PBS wash and 3 PBS washes (each wash lasting for 5 min). Both primary and secondary antibodies were diluted in 3% (w/v) non-fat dry skimmed milk powder

PBS-based solution. Prior to visualising blots, nitrocellulose membranes were subjected to a further wash in 0.5 M NaCl-PBS solution for at least 15 min at RT to remove residual non-specific binding. For siRNA knockdown experiments, blotting for β-actin was used as a loading control. Bands were visualised using ECL (enhanced chemiluminescence) Western blotting substrate in a Bio-Rad Quantity One imaging system. Band intensities were quantified and analysed using Image J software.

2.2.5 Immunofluorescence and confocal microscopy imaging

Cells seeded into 35 mm glass-bottom dishes (Mattek, Ashland, USA) or µ-Dish 35 mm high glass bottom dishes (ibidi, Martinsried, Germany) were either non-transfected or transfected with constructs, and followed with or without drug treatment. Briefly, to visualise ER-PM junctions, PANC-1 cells were transfected with TK-YFP-STIM1 for 24 hours prior to treatment with 30 µM cyclopiazonic acid (CPA, a reversible ER Ca^{2+}-ATPase pump inhibitor) for 1 hour at 37°C / 5% CO_2. Alternatively, PANC-1 cells were transfected with both PM-targeted LL-FKBP-mRFP and ER-targeted CFP-FRB-LL linker constructs (Varnai *et al.*, 2007; Dingsdale *et al.*, 2013) for 24 hours before treatment with 100 nM rapamycin for 4-5 min at 37°C / 5% CO_2. Drugs used were diluted to their respective final concentrations in Na^+-HEPES (4-(2-hydroxyethyl)-1-piperazineethanesulphonic acid)-based extracellular solution containing (in mM): 140 NaCl, 4.7 KCl, 10 HEPES, 1 $MgCl_2$, 10 glucose, 0.8 – 1.8 $CaCl_2$ (depending on the nature of experiment), and adjusted to pH 7.3-7.4 using NaOH. For example, rapamycin was used in Na^+-HEPES-based solution with 1.8 mM $CaCl_2$, whereas CPA was used in Na^+-HEPES-based solution with 0.8 mM $CaCl_2$. Cells were fixed using 4% (v/v; diluted in PBS) paraformaldehyde (PFA) for 10-15 min at RT followed by 3 PBS washes (each wash lasting between 3 to 5 min),

and subsequently permeabilised using 0.2% Triton X-100 (v/v; diluted in PBS) for 5 min at RT, before an additional 3 PBS washes. Non-specific antibody binding sites were blocked for 1 hour at RT in PBS containing 10% (v/v) goat serum and 1% (w/v) BSA prior to incubation with primary antibodies in PBS containing 5% (v/v) goat serum and 0.1% (v/v) acetylated BSA for 1 hour at RT or overnight at 4°C. Primary antibodies were used at the following dilutions: anti-IP_3R1, 1:200; anti-IP_3R2, 1:100; anti-IP_3R3, 1:100; anti-PAN IP_3Rs, 1:20; anti-vinculin, 1:200; anti-GFP, 1:200; anti-PIP_2, 1:100; anti-occludin, 1:100; anti-E-cadherin, 1:50; and anti-calnexin, 1:100. In specified experiments Alexa Fluor 647 phalloidin was used at a dilution of 1:50. Post-primary antibody incubation, cells were PBS washed 3 times followed by the addition of appropriate species-specific fluorophore-conjugated secondary antibodies for 30 min at RT at dilutions of 1:500–1:1000 in PBS. Additional 3 PBS washes were carried out prior to imaging in PBS or PBS-0.02% azide. All fluorescently conjugated secondary antibodies used in the present study were tested on PFA-fixed PANC-1 cells without the use of a primary antibody (also known as “no primary antibody control”). None of these fluorescently conjugated secondary antibodies produced any staining in PANC-1 cells.

Two different confocal microscopes were used in the present study to visualise fixed and immuno-stained cells. A Leica acousto-optical beam splitter (AOBS) TCS SP2 confocal microscope with HCX PL APO lbd.BL 63x OIL immersion objective, numerical aperture = 1.4. The other was a Zeiss Laser Scanning Microscope LSM 710 confocal microscope with Plan-Apochromat 63x oil objective (63x/1.4oil DIC M27) with a numerical aperture of 1.4. The pinhole was set between 1-2 airy units, and optical Z-sections were spaced by 0.25-0.5 µm. Images were recorded at 512 by

512 pixels per frame unless otherwise stated. Scale bars represent 10 µm unless otherwise stated.

2.2.6 Live-cell imaging, Ca^{2+} imaging and uncaging

Ca^{2+} imaging experiments were performed on live cells. PANC-1 cells seeded to approximately 60-70% confluence in glass bottom dishes were loaded with either 5 µM Fura2-AM or 5 µM Fluo4-AM Ca^{2+} indicators.

To investigate IP_3-induced Ca^{2+} responses in PANC-1 cells, cells were dual-loaded with 1 µM UV-photoactivatable and membrane permeant Ins(1,4,5)P_3 (caged Ins(1,4,5)P_3/PM) and 5 µM fluo4-AM in Na^+-HEPES-based extracellular solution containing 1.8 mM Ca^{2+} in the absence or presence of Xestospongin B (inhibitor of IP_3-induced Ca^{2+} release) at RT for 1 hour. Then followed by 2 washes in Na^+-HEPES-based 1.8 mM Ca^{2+} extracellular solution, before an additional 30 min incubation in Na^+-HEPES-based 1.8 mM Ca^{2+} extracellular solution at RT to allow for the adaptation and de-esterification phase of fluorophore fluo4-AM to occur. Prior to imaging, Na^+-HEPES-based 1.8 mM Ca^{2+} extracellular solution was replaced with Na^+-HEPES-based nominally Ca^{2+} free extracellular solution to be certain that the cytosolic Ca^{2+} responses observed following un-caging of caged Ins(1,4,5)P_3 originated only from intracellular Ca^{2+} stores. Recordings were acquired on a Zeiss Laser Scanning Microscope LSM 510 confocal microscope with maximally opened pinhole (corresponding to 7.94 airy units) using a 63x Water objective with a numerical aperture of 1.2; 4% power of UV laser- (351 and 364 nm) and 0.7% power of 488 nm laser-lines were used. Uncaging of caged Ins(1,4,5)P_3 was performed at several uncaging iterations i.e. the duration of uncaging, which ranged from 3 to 20 seconds. Images were recorded at 256 by 256 pixels per frame.

2.2.7 Boyden Chamber Migration assay

Untransfected or transfected PANC-1 cells were subjected to both symmetric (1% FBS in both upper and lower chambers) and asymmetric (chemotactic; 0% FBS in upper chamber and 5% FBS in lower chamber) Boyden chamber cell migration assay for 6 hours in a humidified environment at 37°C / 5% CO_2 in the presence or absence of the inhibitors of specific Ca^{2+} signalling complexes. Inhibitors used were the inhibitor of SOCE (store operated Ca^{2+} entry) GSK-7975A and the inhibitor of IP_3-induced Ca^{2+} release from intracellular Ca^{2+} stores Xestospongin-B. No FBS (0% FBS)-treated group was employed as a negative control for the Boyden chamber cell migration assay. In addition, chemotactic Boyden chamber cell migration assay (0% FBS in upper chambers and 5% FBS in lower chambers) was also performed on PANC-1 cells after 72-hour siRNA knockdown of IP_3R1, IP_3R2, IP_3R3, or STIM1 proteins.

Briefly, for both symmetrical and asymmetrical FBS distribution cell migration experiments, approximately 50,000 cells were seeded into each of the upper chambers of Boyden chamber PET or Fluoroblok inserts with 8 µm pore size, and were allowed to migrate through the porous membrane for 6 hours. After 6 hours incubation, Boyden chamber inserts were fixed using 100% methanol for 10 min. Boyden chamber inserts were then washed in PBS for 10 min and non-migrated cells were removed from the top-side of the chamber inserts using cotton buds and rinsed 2 times in PBS. Boyden chamber inserts were incubated in PBS solution, which contained 10 µg/ml RNAse A for 30 min prior to incubation in PBS solution containing 100 µg/ml propidium iodide for 10 min. Once more, after propidium iodide staining, any residual non-migrated cells were removed from the top-side of the chamber inserts with cotton buds and rinsed 2 times in PBS, and the under-side of

the Boyden chamber inserts were imaged on a Leica AOBS TCS SP2 confocal microscope using a HC PL FLUOTAR 10x DRY objective with a numerical aperture of 0.3 (Burdyga *et al.*, 2013). Five regions of interest were imaged per Boyden chamber insert and these regions collectively represent the majority (~70%) of the total surface area of each chamber membrane that was analysed. Fluorescently-stained migrated cells were counted using a CellProfiler cell counting algorithm software.

2.2.8 Wound-healing/Scratch migration assay

Ibidi µ-Dish 35 mm high glass bottom or 35 mm glass bottom dishes (Mattek) were used. Ibidi cell culture inserts were placed into the above-mentioned glass bottom dishes before non-transfected PANC-1 cells were seeded into either side of the inserts. Approximately 24 hours after cell seeding, the cells reached full confluence and the inserts were then carefully removed with a tweezers creating a defined open gap or 'wound' of approximately 500 µm. The defined open gap or 'wound' area was imaged at time=0 immediately after cells were incubated in 0% FBS medium or in 1% FBS medium supplemented with or without the inhibitors of specific Ca^{2+} signalling complexes. Cells were then allowed to migrate for 18 hours into the open space of 'wound' area in a humidified environment at 37°C / 5% CO_2; and at the end of experiment at time=18 hours, the corresponding 'wound' area containing migrated cells was imaged. This experiment was performed on a Leica AOBS TCS SP2 confocal microscope using a HC PL FLUOTAR 10x DRY objective (numerical aperture of 0.3) with a PH1 or PH2 DIC (Differential Interference Contrast) settings.

2.2.9 Testing effects of Xestospongin-B and GSK-7975A on cell viability

To investigate the effect of the Ca^{2+} signalling inhibitors (Xestospongin-B and GSK-7975A) on cell viability, PANC-1 cells seeded into 35 mm glass bottom dishes were treated with / without 50 µM Xestospongin-B or 30 µM GSK-7975A for 6 hours at 37°C / 5% CO_2 to mimic the condition employed for the Boyden chamber migration assays. Incubation conditions were grouped into 0% FBS DMEM, 1% FBS-supplemented DMEM (control), 1% FBS-supplemented DMEM with 50 µM Xestospongin-B and 1% FBS-supplemented DMEM with 30 µM GSK-7975A. Following the initial 6h incubation, PANC-1 cells were briefly co-incubated for 20 min with 10 µg/ml Hoechst 33342 to stain cellular nuclei for total cell count and 0.5 µM Sytox orange to stain cellular nuclei of cells with compromised plasma membrane at 37°C / 5% CO_2 prior to live-cell imaging. Hoechst 33342 and Sytox orange were prepared in 1.8 mM Ca^{2+}-containing Na^{+}-HEPES-based extracellular solution. Live images were acquired on a Leica AOBS TCS SP2 confocal microscope with pinhole corresponding to 2 airy units. HC PL FLUOTAR 20x DRY objective with a numerical aperture of 0.5 was used in these experiments. The number of live cells was calculated by subtracting Sytox orange-stained positive cells (dead cells) from Hoechst-stained positive cells (total cell count). Mean ± SEM was obtained from at least 3 independent experiments.

2.2.10 Super-resolution imaging

For super-resolution imaging, PANC-1 cells were seeded into Lab-Tek chambered coverglass 8-well ♯ 1.0 with low thickness variation (Thermo Scientific, Runcorn, UK). To visualise IP_3R1 at super-resolution level, PANC-1 cells were fixed with 4% PFA for 10-15 min at RT and subsequently immunostained with anti-IP_3R1 antibody,

followed by the use of an appropriate species-specific Alexa Fluor 647 secondary antibody. To visualise ER-PM junctions at super-resolution level, PANC-1 cells were co-transfected with PM-targeted LL-FKBP-mRFP and ER-targeted CFP-FRB-LL linker constructs and incubated for 24 hours. The cells were then fixed using 4% PFA for 10-15 min at RT after treatment with 100 nM rapamycin for 4-5 min at 37°C / 5% CO_2 to reveal the pre-existing ER-PM junctions without ER Ca^{2+} store depletion. Briefly, the heterodimerisation of both ER- and PM-targeted constructs reveal the ER-PM junctions as punctate structures in both CFP and RFP fluorescence channels. To reveal the ER-FRB-LL-CFP counterpart of the ER-PM junctions' puncta at super-resolution level, ER-FRB-LL-CFP counterpart of the ER-PM linker construct was immunostained using anti-GFP antibody (which also recognizes CFP), and followed by appropriate species-specific Alexa Fluor 647 secondary antibody. Better quality super-resolution images are best acquired in the red-absorbing part of the visible light spectrum (Dempsey *et al.*, 2011), and hence an Alexa Fluor 647 secondary antibody was used to amplify anti-GFP primary antibody staining, which was used to highlight ER-FRB-LL-CFP accumulated in ER-PM junctions.

After immunostaining of IP_3R1 or ER-PM junctions, samples were immersed and imaged in a dSTORM buffer containing 100 U/ml glucose oxidase, 2000 U/ml catalase, 50 mM mercaptoethylamine-HCl and 50 mg/ml glucose in PBS (Metcalf *et al.*, 2013). Wells were filled and sealed with a cover slip to exclude oxygen. Briefly, super-resolution microscopy was performed using a custom-built instrument, as described previously (Metcalf *et al.*, 2013; Ferraro *et al.*, 2014). An Olympus IX71 formed the basis of an inverted TIRF instrument with a UAPON 100XOTIRF, NA=1.49 objective. Laser illumination was provided by a 640 nm, 150mW, diode laser (Toptica Photonic AG) and a 561 nm, 200 mW optically pumped semiconductor

laser (Coherent Europe B.V.). Additionally, a 405 nm laser diode (Mitsubishi Electronics Corp.) was available for re-activation of fluorophores if required. Laser power on the diode lasers was controlled directly, whereas a rotating quarter-wave plate was used to alter the power of the 561 nm laser. Lower powers (1-10%) were used for field of view selection, context and conventional fluorescence images. High powers (50-100%) were used for dSTORM imaging. Fluorescence and excitation light were spectrally separated by the dichroic mirror and emission filter from a multi-edge filter set (LF405/488/561/635-A-000, Semrock (Rochester, NY, USA)), and an additional band pass filter was used to remove cross-talk in each channel (FF01-676/37 with 640 nm excitation and FF01-600/37 with 561 nm excitation, both from Semrock (Rochester, NY, USA)).

Images were acquired using an EMCCD camera (Andor iXon 897, Belfast, UK) using software written in LabVIEW (National Instruments). Typically dSTORM image "stacks" was composed of 10000 frames, with 10 ms exposure time per frame. Super-resolution images were reconstructed from these image stacks using the open-source rainSTORM package (Metcalf *et al.*, 2013). The super-resolution microscopy experiments were performed in collaboration with Dr Alex Knight and Dr Daniel Metcalf at the National Physical Laboratory (Middlesex, London, UK).

2.2.11 Image, data and statistical analyses

Image acquisition and preliminary analysis was performed using either Leica LAS or Zeiss LSM 510 or Zeiss Zen software. Further analysis was performed using Image J software. Linear adjustments of contrast and brightness were applied if necessary using Image J. The 'mask' images (labelled ER&PM linkers) used for illustrating the co-localisation of the rapamycin-inducible linker components were created using the

Co-localise RGB Image J plugin as described before (Dingsdale *et al.*, 2013). Briefly, this Image J plugin determines the presence of co-localised pixels between ER- and PM-linker images after threshold values were adjusted for each image of interest.

For statistical analysis of two groups of measurements unpaired t-test with a two-tailed distribution and unequal variance was applied. For experiments involving more than two groups, one-way ANOVA with Bonferroni test was applied. $p<0.05$ was considered statistically significant and indicated by symbol * on the graphs. All individual experiments were repeated at least 3 times (i.e. from at least 3 separate cell cultures; indicated by N numbers).

Chapter 3: The expression and distribution of IP_3Rs and ER-PM junctions in pancreatic ductal adenocarcinoma cells

Chapter 3: The expression and distribution of IP_3Rs and ER-PM junctions in pancreatic ductal adenocarcinoma cells

3.1 Epithelial phenotype and monolayer

Epithelial cells are known for their organisation into adherent groups established as single cell layers or multilayer tissues with several vital functions including secretory and protective roles (Rodriguez-Boulan & Nelson, 1989; Huang *et al.*, 2012). Epithelial cells have to be polarised to execute these specialised functions and thus exhibit apical-basal polarity and communicate with each other via specialised cell-cell or intercellular junctions known collectively as epithelial intercellular junctional complexes (IJCs) (Nelson, 2009). IJCs maintain and stabilise epithelial integrity and are sub-grouped into tight junctions (TJs), adherens junctions (AJs) and desmosomes (Farquhar & Palade, 1963; Steed *et al.*, 2010; Terry *et al.*, 2010). TJs are localised at the subapical end of the lateral membrane and are composed of integral membrane spanning proteins including occludin, junction adhesion molecules (JAMs) and claudins, and the cytoplasmic auxiliary proteins zonula occludens (ZO-1, ZO-2, and ZO-3). TJs function as bi-directional signalling transducers as well as dynamic barriers to regulate paracellular permeability and as a molecular fence to maintain epithelial integrity and polarity by restricting the intermixing of apical and basolateral membrane components (Steed *et al.*, 2010; Terry *et al.*, 2010). AJs and desmosomes contribute to maintaining cell-cell adhesion and are located predominantly within the lateral membrane and are composed of integral membrane spanning proteins such as epithelial cadherin (E-cadherin) and desmosomal cadherin, respectively (Yap *et al.*, 2007; Terry *et al.*, 2010; Lamouille *et al.*, 2014). Interestingly, these epithelial intercellular junctional complexes, in

particular E-cadherin are Ca^{2+} binding proteins (Shapiro & Weis, 2009), and the polarity and integrity of epithelial intercellular junctions have been shown in MDCK cells by Mauger and colleagues to be dependent on Ca^{2+} signalling (Colosetti *et al.*, 2003). Ca^{2+} signals are known to be regulated by Ca^{2+} signalling complexes, which prominently involve the interplay of Ca^{2+} release from intracellular stores primarily via IP_3Rs and RyRs, and Ca^{2+} replenishment via store operated Ca^{2+} entry (SOCE) channels localised at the ER-PM junctions (Carrasco & Meyer, 2011). In this part of the study, the subcellular distribution of Ca^{2+} signalling complexes (IP_3Rs and STIM1-competent ER-PM junctions) in monolayers of pancreatic ductal adenocarcinoma cells (PDAC; specifically PANC-1) was examined.

3.2 Expression of endogenous IP_3Rs in PANC-1 cells

The aim of this part of the study was to determine the expression profiles and define the distribution(s) of Ca^{2+} signalling complexes (IP_3Rs and STIM1-competent ER-PM junctions) in PDAC cells. Pancreatic ductal cells are epithelial cells lining the pancreatic duct, which functions as secretory exocrine cells of the pancreas and specifically recognised for their role in fluid and electrolyte secretion (Steward *et al.*, 2005; Pandol, 2010). PDAC probably arises from pancreatic acinar cells (PAC), which assume ductal phenotype (Rooman & Real, 2012). PANC-1 cells are established from pancreatic carcinoma of ductal origin and were used as a model cell line to examine the expressions and distributions of Ca^{2+} signalling complexes. Preliminary experiments were carried out to determine whether IP_3Rs are endogenously expressed in PANC-1 cells at both mRNA (messenger RNA) and protein levels. To probe the expression of IP_3Rs at mRNA level, total RNA was extracted from PANC-1 cells and the quality of extraction was analysed by gel

electrophoresis. The presence of two clear bands – the 28S and 18S rRNA (ribosomal RNA) subunits indicated high quality RNA extraction (Figure 3.1). In quantitative real time PCR (qRT-PCR) analysis, it was observed that PANC-1 cells endogenously express all 3 isoforms (subtypes) of IP_3R at mRNA level (Figures 3.2 and 3.3). The relative expression of all 3 isoforms of IP_3R at mRNA level varies with IP_3R3 (36.6%) greater than both IP_3R1 (32.2%) and IP_3R2 (31.2%) (Figure 3.3). Next, the expression of all 3 isoforms of IP_3R at the protein level was examined, and it was convincingly established from the Western blot profiles that all 3 isoforms are endogenously expressed at detectable levels in PANC-1 cells using isoform specific antibodies (Figure 3.4). All 3 isoforms of IP_3R migrate with similar electrophoretic mobilities, and hence exhibit similar apparent molecular weights (Figure 3.4).

The experimental data shows that PDAC cells endogenously express all 3 isoforms of IP_3R albeit with differing expression profiles.

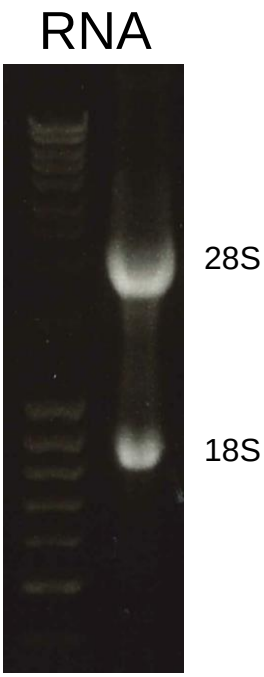

Figure 3.1. Total RNA isolated from pancreatic ductal adenocarcinoma (PANC-1) cells.

PANC-1 cells were lysed, RNA contents extracted and analysed by gel electrophoresis. The quality of RNA extraction is detected as two strong clear bands – the 28S rRNA and 18S rRNA, which are visible on the gel.

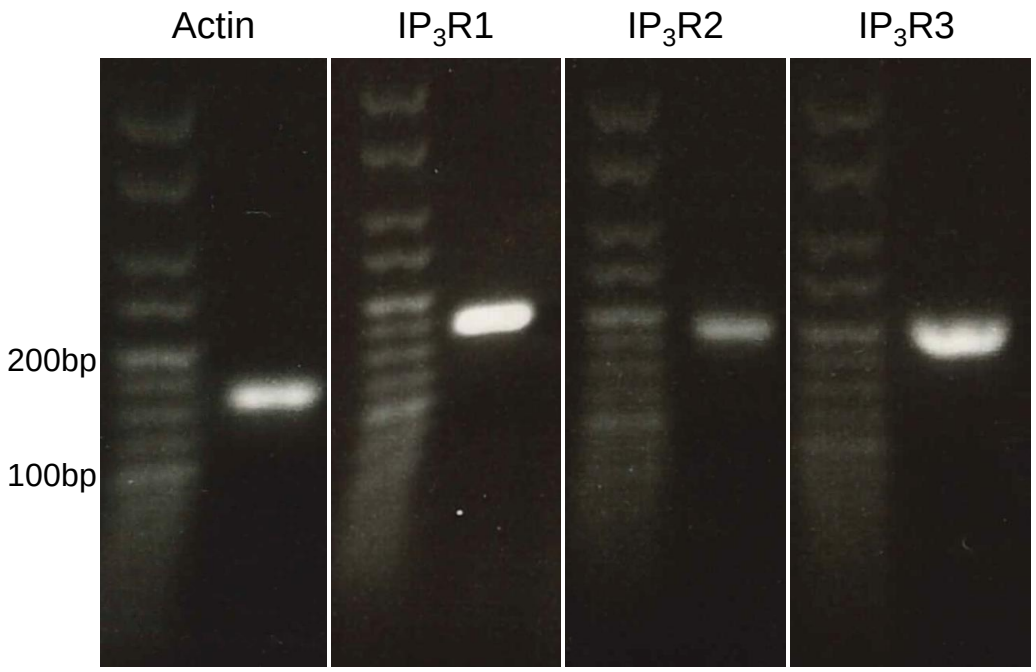

Figure 3.2. mRNA transcripts of IP_3R isoforms in pancreatic ductal adenocarcinoma cells.

PANC-1 cells were lysed, RNA contents extracted and processed into cDNA using reverse transcriptase enzyme. Amplicons are PCR amplified products based on targeting primers, and are typically between 120-200 base pairs in length. Shown are the representative gel profiles for actin and each IP_3R isoform. Note - these gel profiles are indication of the presence of each isoform of IP_3R rather than the expression levels or amounts of each isoform of IP_3R present in PANC-1 cells.

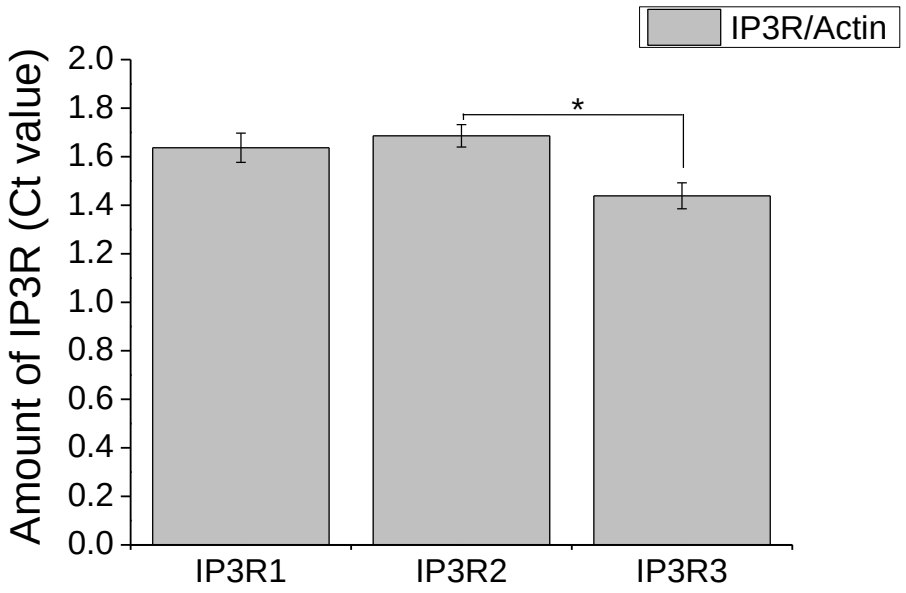

Figure 3.3. Relative amount of IP_3Rs mRNA levels in pancreatic ductal adenocarcinoma cells.

PANC-1 cells were lysed, RNA contents extracted and processed into cDNA. The amount of IP_3Rs mRNA levels was determined by quantitative real time RT-PCR using IP_3R-isoform specific primers, cDNA and SYBR DNA-binding fluorescent dye. The cycle threshold (C_T) value for each IP_3R isoform was determined and C_T value is a measure of the amount of DNA in a sample (note that smaller C_T values correspond to larger DNA content). The C_T value for each IP_3R isoform transcript was normalised to β-actin (ACTB) and relative expression represented as ΔC_T.

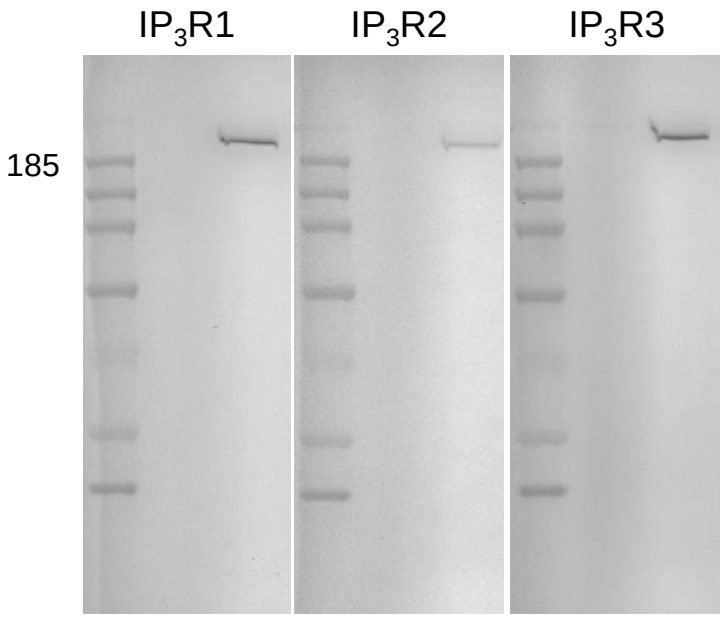

Figure 3.4. Expression of IP_3R proteins in pancreatic ductal adenocarcinoma cells.

PANC-1 cells were lysed, contents collected by centrifugation, separated on SDS-PAGE, and immunoblotted using anti-IP_3R1, anti-IP_3R2 and anti-IP_3R3 antibodies. The molecular weights of all IP_3R isoforms are approximately similar.

3.3 IP_3Rs expressed in PANC-1 cells are functional Ca^{2+} release channels

After the expression profiles of IP_3R isoforms were established in our model cell line PANC-1, the next step was to determine whether or not these IP_3Rs were functional Ca^{2+} release channels. To test the Ca^{2+} releasing function of endogenously expressed IP_3Rs in PANC-1 cells, UV-photoactivatable and membrane permeant Ins(1,4,5) IP_3 (caged IP_3) was utilised. PANC-1 cells were co-loaded with both caged IP_3 and Ca^{2+} indicator Fluo-4, and pulses of UV light used to induce IP_3 uncaging and subsequent release of Ca^{2+} from intracellular stores into the cytosol. In these experiments nominally Ca^{2+} free extracellular solution was used to reveal cytosolic Ca^{2+} responses occurring specifically due to Ca^{2+} release from IP_3-sensitive intracellular stores. Figure 3.5 shows that UV-uncaged IP_3 induced Ca^{2+} release from intracellular stores (red trace; red arrows on the image fragments show the fluorescence of Fluo-4 before, during and after uncaging). No detectable Ca^{2+} response (black trace; blue arrows on the image fragments) was observed in control cells that were not UV illuminated. Furthermore, to demonstrate that the Ca^{2+} responses observed after pulses of UV light induced uncaging were released primarily through IP_3Rs in PANC-1 cells, a selective IP_3R inhibitor Xestospongin-B (Jaimovich *et al.*, 2005; Criollo *et al.*, 2007) was utilised. Xestospongin-B strongly inhibited IP_3-induced Ca^{2+} release from intracellular stores of PANC-1 cells (Figure 3.6).

These experimental findings convincingly demonstrate that the Ca^{2+} fluxes following pulses of UV light-induced uncaging were mediated primarily through IP_3Rs, and

therefore the IP_3Rs expressed in PDAC cells are indeed functional IP_3-induced Ca^{2+} release channels.

Figure 3.5. IP_3 induces Ca^{2+} release from intracellular Ca^{2+} stores in pancreatic ductal adenocarcinoma cells.

Ca^{2+} release from intracellular stores were measured in cells loaded with caged IP_3 and Fluo-4. Caged IP_3 can only be activated in the presence of UV illumination in pancreatic ductal adenocarcinoma cells. Pulse of UV light induced uncaging (i.e. release of IP_3 from its caged precursor) and subsequent release of Ca^{2+} from intracellular stores into the cytosol. These are representative traces composed from normalised values for individual time points of Fluo-4 fluorescence measurements. Red trace depicts UV-illuminated cell (indicated by red arrows on the image fragments), whereas black trace depicts the cell, which was not exposed to UV light (indicated by blue arrows on the image fragments). Red arrows on the image fragments outline fluorescence of Fluo-4 before, during and after uncaging. The black arrow indicates the duration of uncaging (~8s). In these experiments nominally Ca^{2+} free extracellular solution was used to reveal cytosolic Ca^{2+} responses occurring specifically due to Ca^{2+} release from the intracellular stores.

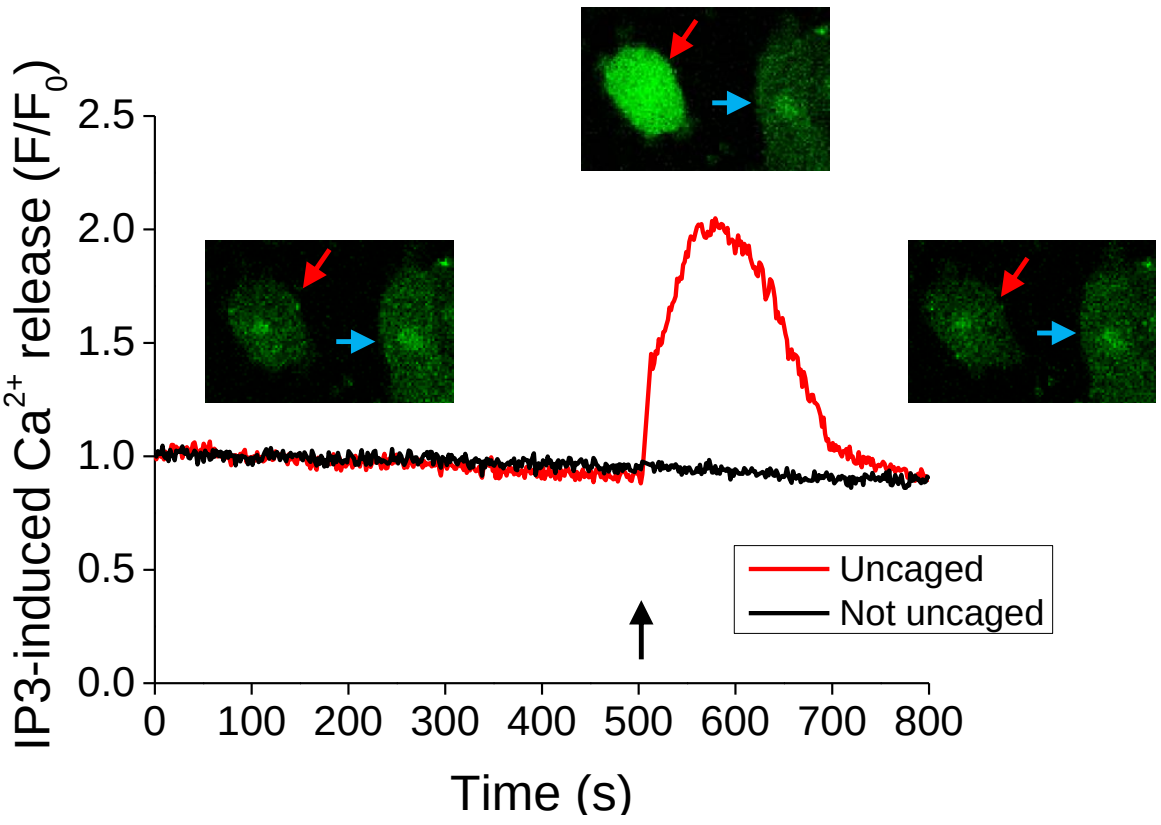
IP3-induced Ca2+ release (F/F0)
2.5
2.0
1.5
1.0
0.5
0.0
0
100
200
300
400
500
600
700
800
Time (s)
Uncaged
Not uncaged

Figure 3.5

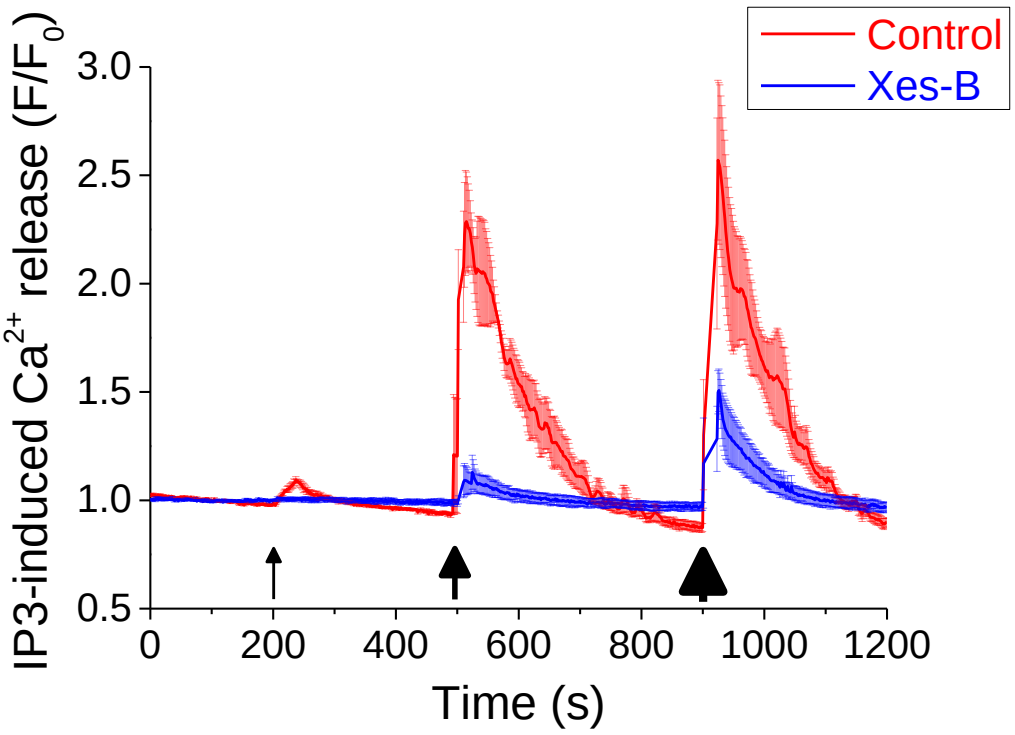

Figure 3.6. Xestospongin-B blocks IP_3-induced Ca^{2+} release in pancreatic ductal adenocarcinoma cells.

Ca^{2+} release from intracellular stores were measured in cells loaded with caged IP_3 in the absence (control; red trace, 28 cells) or presence of 50 µM Xestospongin-B (blue trace, 29 cells). The traces were composed from normalised mean values ± SEM for individual time points of Fluo-4 fluorescence measurements. Pulses of UV light induced uncaging (i.e. release of IP_3 from its caged precursor) and subsequent releases of Ca^{2+} from intracellular stores into the cytosol. The intensities of the black arrows indicate the durations of uncaging (3s, 8s and 20s). In these experiments nominally Ca^{2+} free extracellular solution was used to reveal cytosolic Ca^{2+} responses occurring specifically due to Ca^{2+} release from the intracellular stores.

3.4 Distribution of IP_3Rs in connected PANC-1 cells

After successfully demonstrating that PANC-1 cells endogenously express all 3 isoforms of IP_3R, and these IP_3Rs are functional IP_3-induced Ca^{2+} release channels, we sought to examine the subcellular distribution and localisation of each isoform of IP_3R in PANC-1 cells. Cultured PANC-1 cells usually grow in a monolayer fashion after reaching full confluence in any defined space (i.e. standard culture vessels), and exhibit an epithelial phenotype. Using immunofluorescence and confocal microscopy applications, E-cadherin (adherens junction marker) and occludin (tight junction marker) staining were used to reveal and validate the establishment of the epithelial phenotype of PANC-1 cells in monolayer cultures (Figures 3.7 and 3.8). The fluorescence profile of E-cadherin localisation measured along the line spanning the cell-cell contacts region demonstrate approximately 40-times increase in the density of E-cadherin staining at the cell-cell contact region in comparison with the adjacent regions of the cytoplasm (Figure 3.7, lower panel) in connected PANC-1 cells, and this observation resembles the fluorescence profile of occludin localisation in connected PANC-1 cells (Figures 3.8, lower panel). After the epithelial phenotype of PANC-1 cells in monolayer culture was established, the distribution of IP_3R isoforms was visualised. IP_3R1 shows a polarised distribution and appears to be primarily localised at the cell-cell contacts region in PANC-1 cell monolayer (Figure 3.9). A similar polarised distribution of IP_3R1 at cell-cell contacts was observed in smaller PANC-1 cell clusters (Figure 3.10). Fluorescence profiles measured along the line spanning the cell-cell contacts region demonstrate 4-7 times increase in the density of IP_3R1 at the cell-cell contacts region in comparison with the neighbouring regions of the cytoplasm (Figures 3.9 and 3.10). In contrast to the subcellular

localisation of IP_3R1, both IP_3R2 and IP_3R3 exhibit perinuclear localisation in clusters of PANC-1 cells (Figures 3.11 and 3.12; see also Figures 3.15 and 3.16).

These experimental findings demonstrate that isoforms of IP_3R exhibit differential subcellular localisations and distributions in clusters and monolayers of PDAC cells.

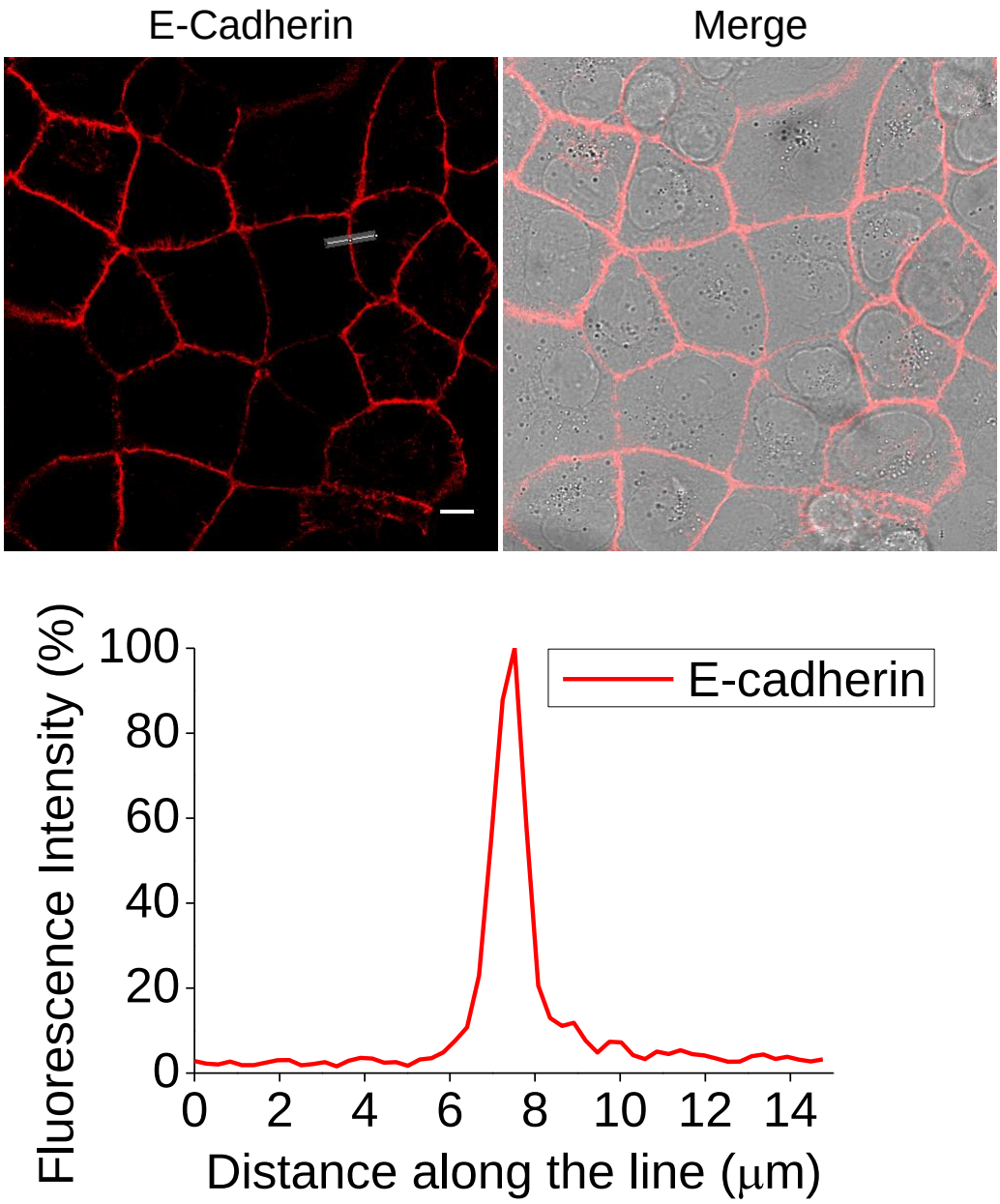

Figure 3.7. The polarised distribution of E-cadherin (adherens junction marker) in connected pancreatic ductal adenocarcinoma cells.

E-cadherin is localised at the cell-cell contact sites of PANC-1 cells forming a confluent monolayer. PANC-1 cells were fixed and immunostained using anti-E-cadherin antibody. Fluorescence profile (bottom panel) was measured along the line spanning the cell-cell contact region. Scale bar represents 10 μm. Merge - indicates the overlay of fluorescence and DIC images.

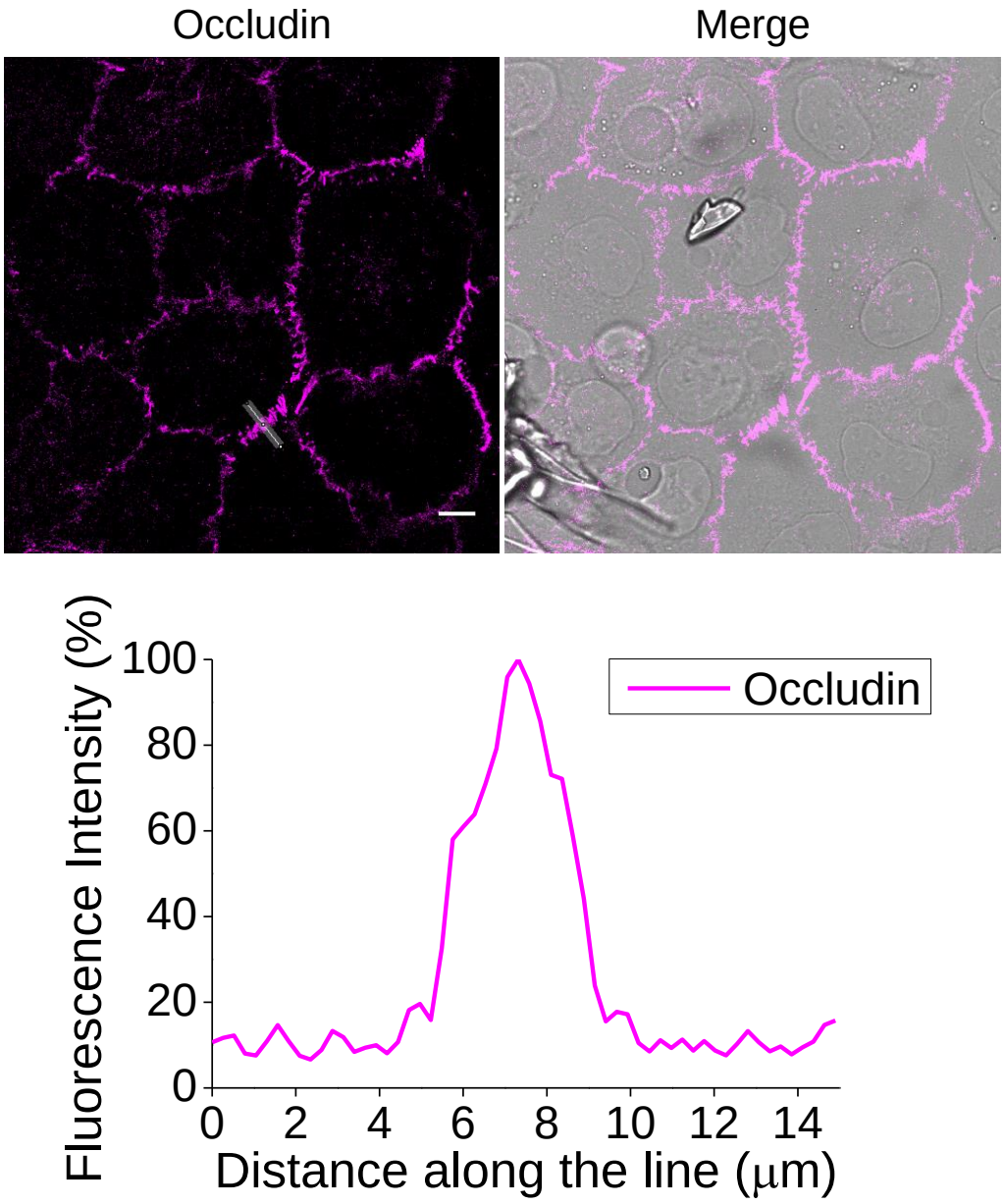

Figure 3.8. The polarised distribution of occludin (tight junction marker) in connected pancreatic ductal adenocarcinoma cells.

Occludin is localised at the cell-cell contact sites of PANC-1 cells forming a confluent monolayer. PANC-1 cells were fixed and immunostained using anti-occludin antibody. Fluorescence profile (bottom panel) was measured along the line spanning the cell-cell contact region. Scale bar represents 10 μm. Merge - indicates the overlay of fluorescence and DIC images.

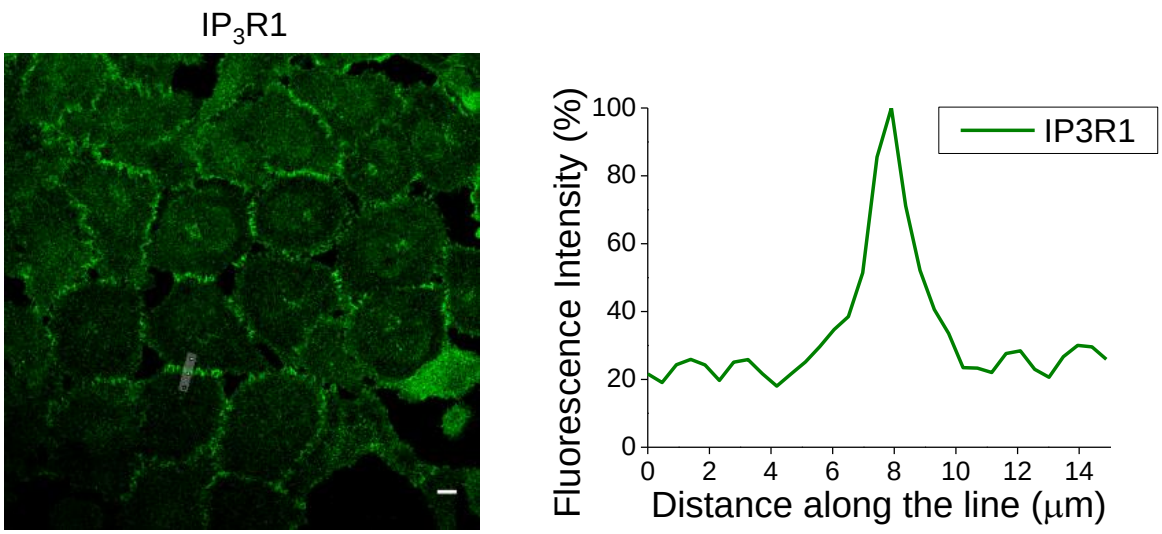

Figure 3.9. The polarised distribution of IP_3R1 in connected pancreatic ductal adenocarcinoma cells.

IP_3R1 are localised at the cell-cell contact sites of PANC-1 cells forming a confluent monolayer. PANC-1 cells were fixed and immunostained using anti-IP_3R1 antibody. Fluorescence profile (right panel) was measured along the line spanning the cell-cell contact region. Scale bar represents 10 μm.

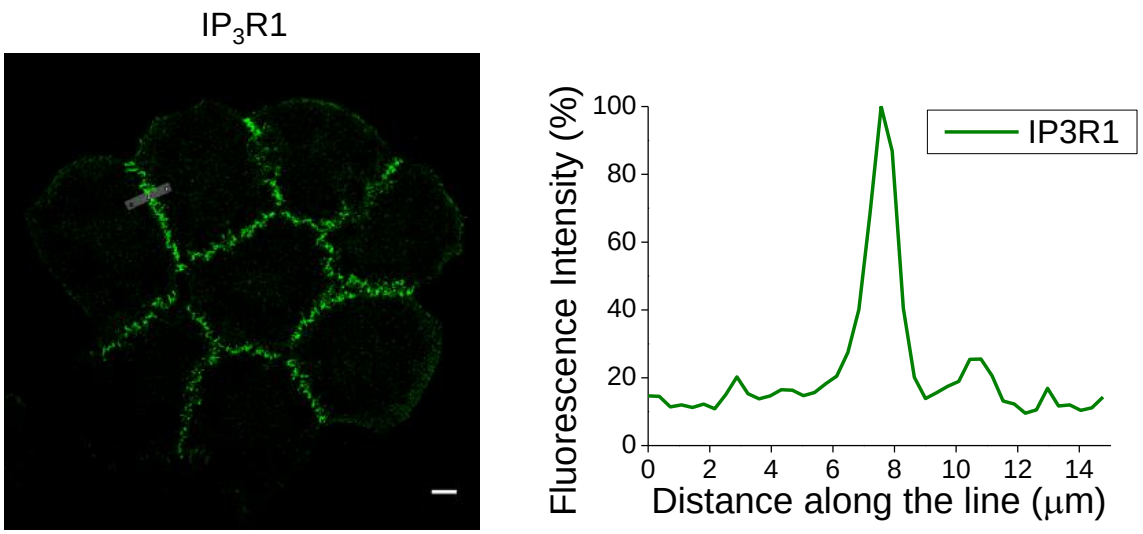

Figure 3.10. The polarised distribution of IP_3R1 in connected pancreatic ductal adenocarcinoma cells.

IP_3R1 are localised at the cell-cell contact sites in cluster of PANC-1 cells. PANC-1 cells were fixed and immunostained using anti-IP_3R1 antibody. Fluorescence profile (right panel) was measured along the line spanning the cell-cell contact region. Scale bar represents 10 μm.

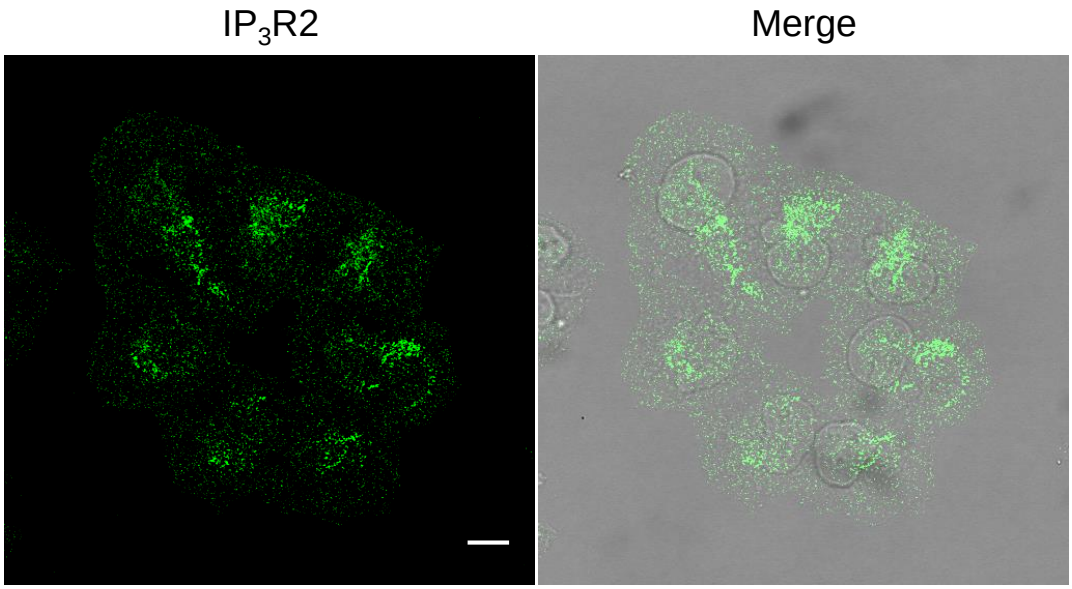

Figure 3.11. Distribution of IP_3R2 in connected pancreatic ductal adenocarcinoma cells.

IP_3R2 are preferentially localised to the perinuclear region in PANC-1 cell cluster. PANC-1 cells were fixed and immunostained using anti-IP_3R2 antibody. Scale bar represents 10 μm. Merge - indicates the overlay of fluorescence and DIC images.

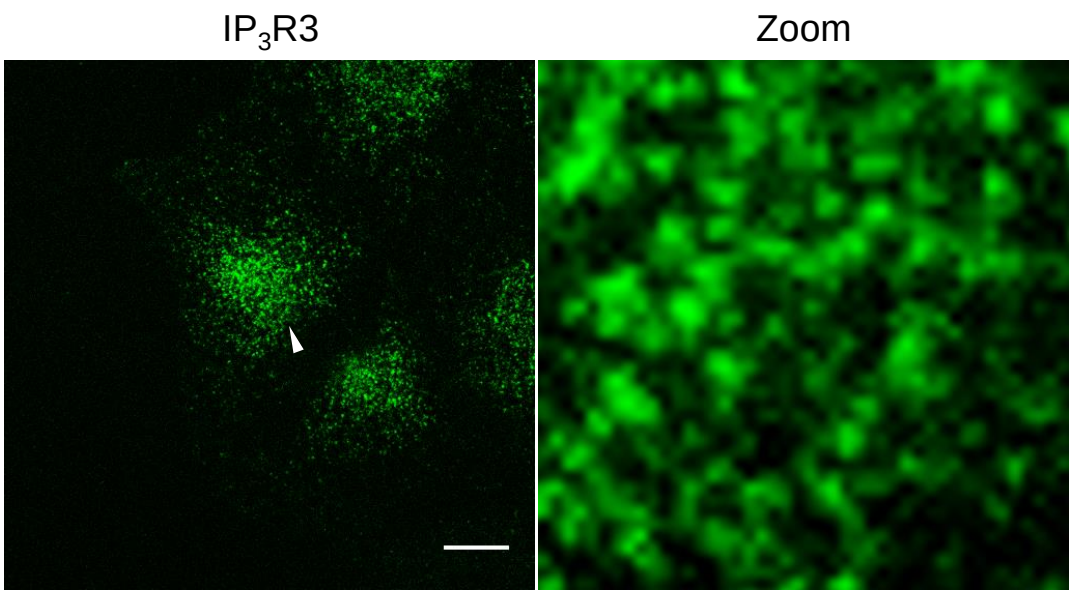

Figure 3.12. Distribution of IP_3R3 in connected pancreatic ductal adenocarcinoma cells.

IP_3R3 is enriched in the perinuclear region in cluster of PANC-1 cells. Right panel shows the fragment indicated by the white arrowhead on the left panel. PANC-1 cells were fixed and immunostained using anti-IP_3R3 antibody. Scale bar represents 10 μm.

3.5 IP_3R1 localises to cell-cell contact sites in PANC-1 cell monolayer and clusters

Following the interesting observation that IP_3R1 appears to be localised at the cell-cell contact region in connected PANC-1 cells, I sought to establish that the regions of IP_3R1 accumulation were indeed the cell-cell contact junctions. Dual immunostaining using anti-IP_3R1 and anti-E-cadherin antibodies showed that IP_3R1s co-localised with E-cadherin at the cell-cell contact region in connected PANC-1 cells (Figure 3.13). Note the yellow colour on the 'Merge' image of Figure 3.13, indicating that in contact regions, IP_3R1 and E-cadherin are so closely positioned that the distance between the proteins is below the resolution of a confocal microscope (i.e. <300 nm). Dual immunostaining with anti-IP_3R1 and anti-occludin antibodies similarly highlighted that IP_3R1s co-localise with occludin at the cell-cell contact region in connected PANC-1 cells (Figure 3.14). Fluorescence profiles measured along the lines spanning cell-cell contacts also shows the close positioning of IP_3R1 and occludin in cellular contact regions (Figure 3.14, lower panel). Note the white colour on the 'Merge' image of Figure 3.14, indicating that in the cellular contact regions, the distance between IP_3R1 and occludin is below the resolution of a confocal microscope. In contrast to IP_3R1, IP_3R2 and IP_3R3 are not preferentially localised to the cellular contact regions revealed by occludin staining in connected PANC-1 cells (Figures 3.15 and 3.16).

Our experimental findings strongly suggested that IP_3R1 was localised at cell-cell contacts and co-localised or closely co-positioned with adherens and tight junction markers in connected PDAC cells, whereas both IP_3R2 and IP_3R3 are perinuclear-localised and spatially segregated from the cellular contact regions. This perhaps

suggests that the isoforms of IP_3R could exhibit different structural and functional roles in monolayer or clusters of PDAC cells depending on their subcellular localisations.

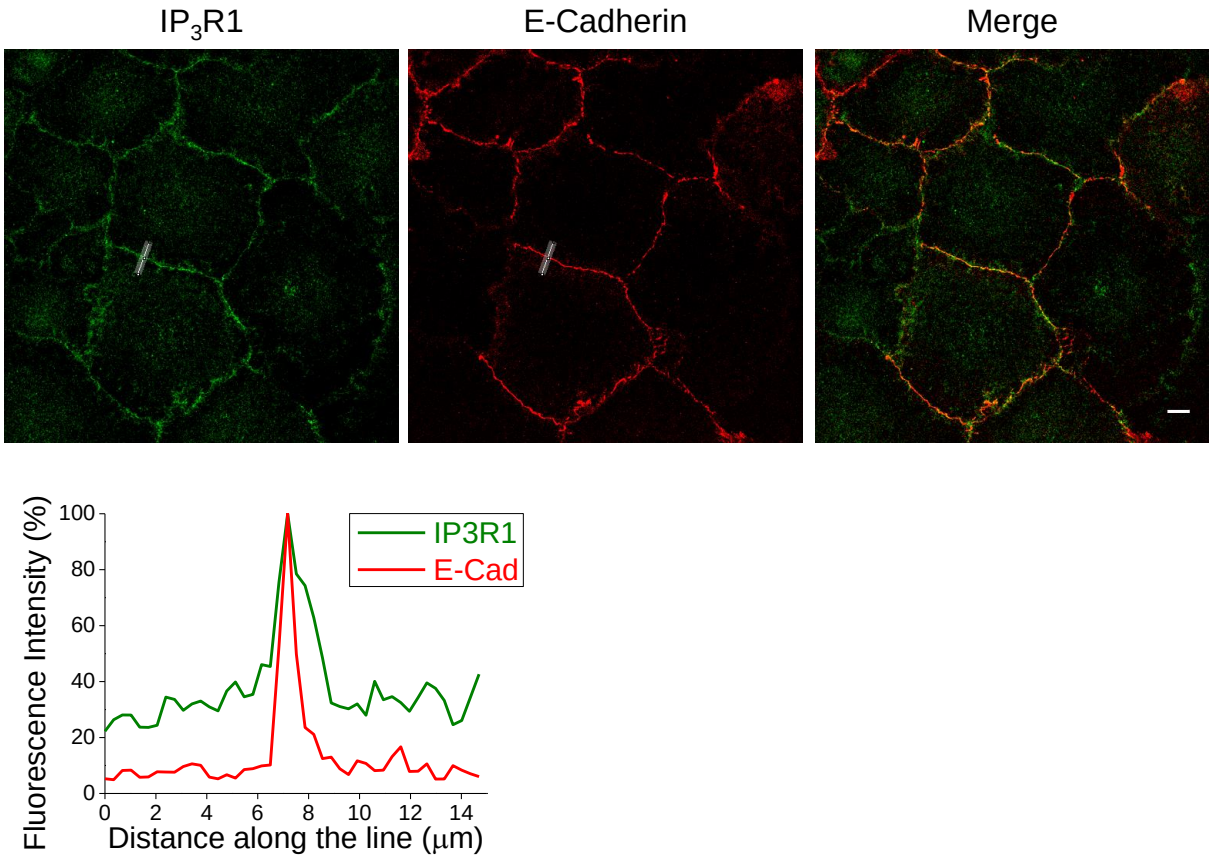

Figure 3.13. IP_3R1 co-localise with E-cadherin (adherens junction marker) at the cell-cell contact sites in cluster of pancreatic ductal adenocarcinoma cells.

PANC-1 cells were fixed and co-immunostained using anti-IP_3R1 and anti-E-cadherin antibodies. Scale bar represents 10 μm. Fluorescence profile (bottom panel) that illustrates juxtaposition of the proteins was measured along the line spanning the cell-cell contact region. Fluorescence intensity shown was normalised to the maximum fluorescence for each individual staining.

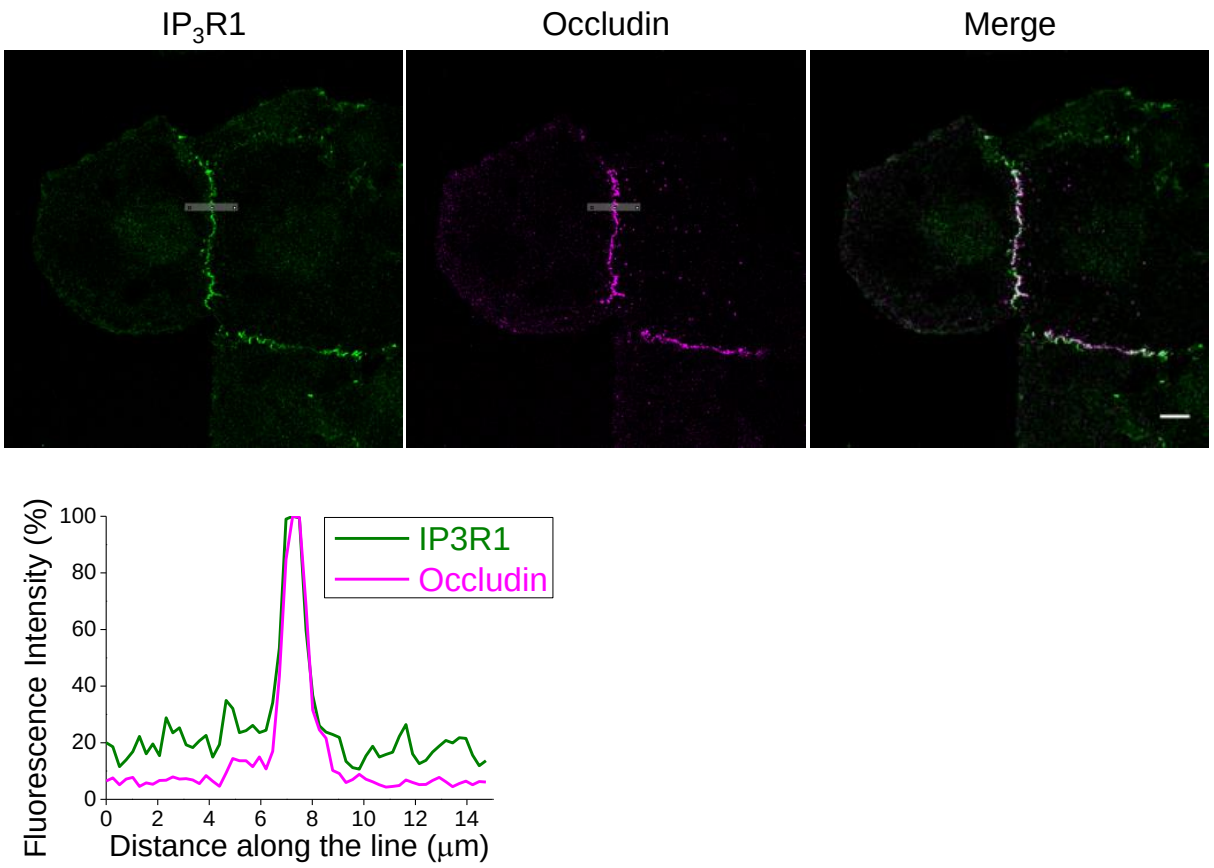

Figure 3.14. IP_3R1 co-localise with Occludin (tight junction marker) at the cell-cell contact sites in cluster of pancreatic ductal adenocarcinoma cells.

PANC-1 cells were fixed and co-immunostained using anti-IP_3R1 and anti-occludin antibodies. Scale bar represents 10 μm. Fluorescence profile (bottom panel) that illustrates juxtaposition of the proteins was measured along the line spanning the cell-cell contact region. Fluorescence intensity shown was normalised to the maximum fluorescence for each individual staining.

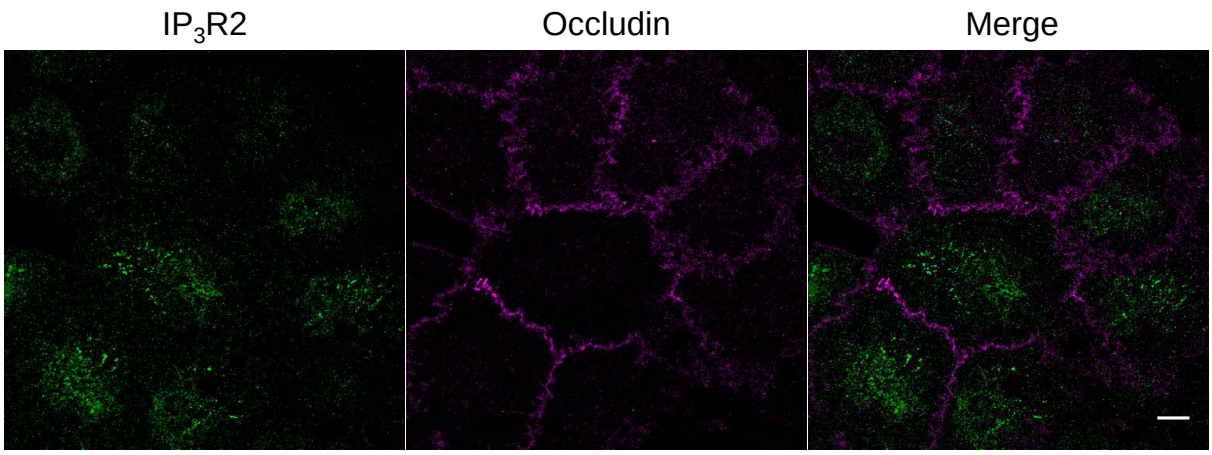

Figure 3.15. Distribution of IP_3R2 and occludin in connected pancreatic ductal adenocarcinoma cells.

IP_3R2 is preferentially localised to the perinuclear region and does not co-localise with occludin (tight junction marker) in PANC-1 cell cluster. PANC-1 cells were fixed and co-immunostained using anti-IP_3R2 and anti-occludin antibodies. Scale bar represents 10 μm.

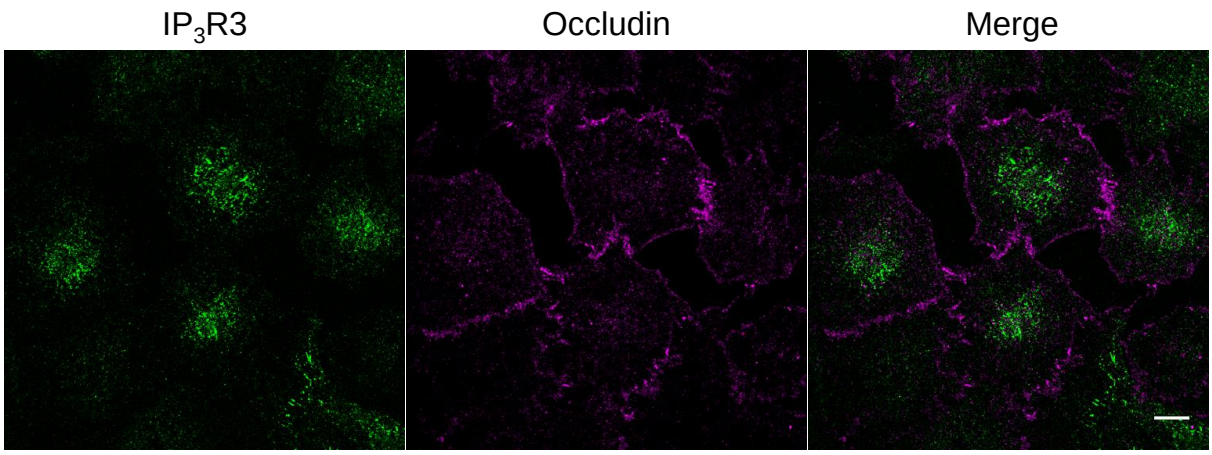

Figure 3.16. Distribution of IP_3R3 and occludin in connected pancreatic ductal adenocarcinoma cells.

IP_3R3 is predominantly enriched in the perinuclear region and does not co-localise with occludin (tight junction marker) in PANC-1 cell cluster. PANC-1 cells were fixed and co-immunostained using anti-IP_3R3 and anti-occludin antibodies. Scale bar represents 10 μm.

3.6 Expression of endogenous STIM1 and Orai1 in PANC-1 cells

Following plasma membrane receptor-stimulated phosphatidylinositol 4,5-bisphosphate ($PI(4,5)P_2$) hydrolysis, inositol 1,4,5-trisphosphate (IP_3) production, stimulation of IP_3Rs, and subsequent Ca^{2+} release through IP_3Rs in the endoplasmic reticulum (ER), ER Ca^{2+} concentration ($[Ca^{2+}]_{ER}$) can become depleted; restoring ($[Ca^{2+}]_{ER}$) after such Ca^{2+} release events involve store operated Ca^{2+} entry (SOCE) mediated by stromal interaction molecule (STIM), which activates plasma membrane (PM) ion channel Orai to permit influx of Ca^{2+}. This process of activation takes place in specialised ER-PM junctions (Wu *et al.*, 2006; Lur *et al.*, 2009; Carrasco & Meyer, 2011). This process of Ca^{2+} replenishment is particularly important for non-excitable cells, which do not possess voltage-gated Ca^{2+} channels (VGCCs) (Berridge *et al.*, 1998; Schindl *et al.*, 2009). In the non-excitable PDAC cell line PANC-1, I sought to determine whether or not the key components of SOCE – STIM1 and Orai1 proteins are endogenously expressed. From the Western blot profiles, it could be demonstrated that both STIM1 and Orai1 were endogenously expressed in PANC-1 cells at protein level (Figure 3.17). Furthermore, a selective small molecule inhibitor (GSK-7975A) of Orai1 channels (Derler *et al.*, 2013) was used to demonstrate that these endogenously expressed key players of SOCE are functional in mediating Ca^{2+} influx following ER Ca^{2+} store depletion in PANC-1 cells (unpublished results obtained by T. Parker in our laboratory, data not shown).

Collectively, these experimental findings show that PDAC cells endogenously express STIM1 and Orai1 proteins, and that these proteins are capable of mediating functional Ca^{2+} influx after ER Ca^{2+} store depletion.

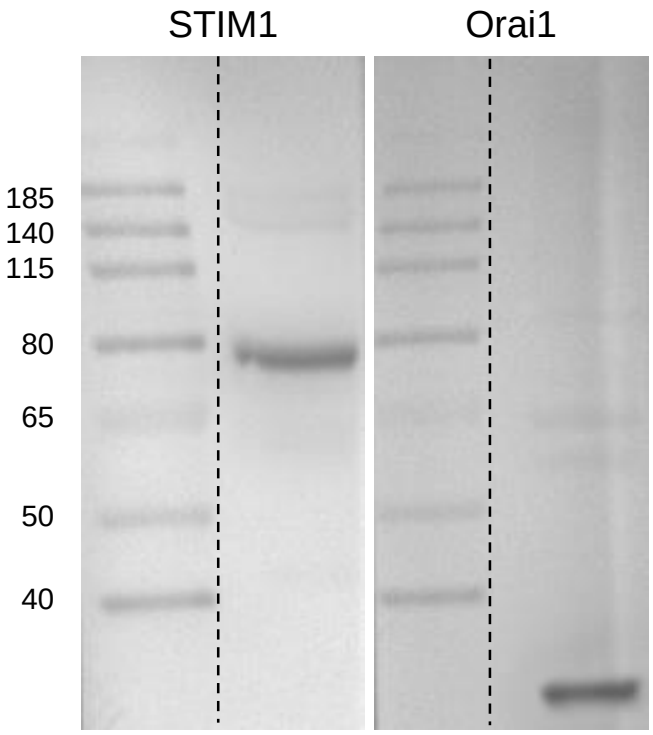

Figure 3.17. Expression of the key components of store operated Ca^{2+} entry (SOCE) process: STIM1 and Orai1 proteins in pancreatic ductal adenocarcinoma cells.

PANC-1 cells were lysed, contents collected by centrifugation, separated on SDS-PAGE, and immunoblotted using anti-STIM1 and anti-Orai1 antibodies. The molecular weights of STIM1 and Orai1 proteins are estimated at approximately 80 kDa and 30 kDa, respectively.

3.7 Localisation of IP_3R1 and ER-PM junctions in connected PANC-1 cells

Following the determination that PANC-1 cells endogenously express functionally competent IP_3R Ca^{2+} release channels and STIM1-Orai1 complexes, I next sought to examine simultaneously the subcellular localisations and distributions of IP_3Rs and SOCE-competent ER-PM junctions in connected PANC-1 cells by immunofluorescence and confocal microscopy. To visualise SOCE-competent ER-PM junctions, PANC-1 cells were transfected with TK-YFP-STIM1 for 24 hours prior to treatment with 30 μM CPA for 1 hour at 37°C / 5% CO_2. Alternatively, PANC-1 cells were transfected with both PM-targeted LL-FKBP-mRFP and ER-targeted CFP-FRB-LL linker constructs (Varnai *et al.*, 2007; Dingsdale *et al.*, 2013) for 24 hours before treatment with 100 nM rapamycin for 4-5 min at 37°C / 5% CO_2. After revealing ER-PM junctions by these methods, cells were fixed and immunostained with anti-IP_3R1 antibody.

In connected PANC-1 cells, IP_3R1 was, as previously localised in cell-cell contacts whilst ER-PM junctions revealed by STIM1 puncta formation following ER Ca^{2+} store depletion with CPA (Figure 3.18) or by co-localised ER and PM linkers without ER Ca^{2+} store depletion (Figure 3.19), could be found in the closely adjacent cytosolic region. As I had previously demonstrated IP_3R1 co-localisation with the tight junction marker occludin in connected PANC-1 cells (Figure 3.14), the relative positioning of occludin and STIM1-competent ER-PM junctions was next examined in connected PANC-1 cells. Similar to the observed relative positioning of IP_3R1 and ER-PM junctions, STIM1-competent ER-PM junctions were found in a closely adjacent region next to tight junctions (i.e. tight junctions are spatially segregated from the adjacently positioned ER-PM junctions) in connected cells (Figure 3.20). Further to

this observation, the relative positioning of tight junctions (occludin) and ER bulk/strands (revealed by calnexin staining) was visualised. It was found that ER strands decrease in density towards the cell periphery and project as far as the area that is closely adjacent to tight junctions (Figure 3.21). This observation could perhaps explain why STIM1-competent ER-PM junctions do not co-localise with tight junctions but instead are positioned in close proximity to cell-cell contacts.

These experimental findings show that both IP_3R1 and ER-PM junctions are localised at the cell periphery with IP_3R1 localised at cell-cell contacts spatially segregated from the adjacently positioned ER-PM junctions in connected PDAC cells.

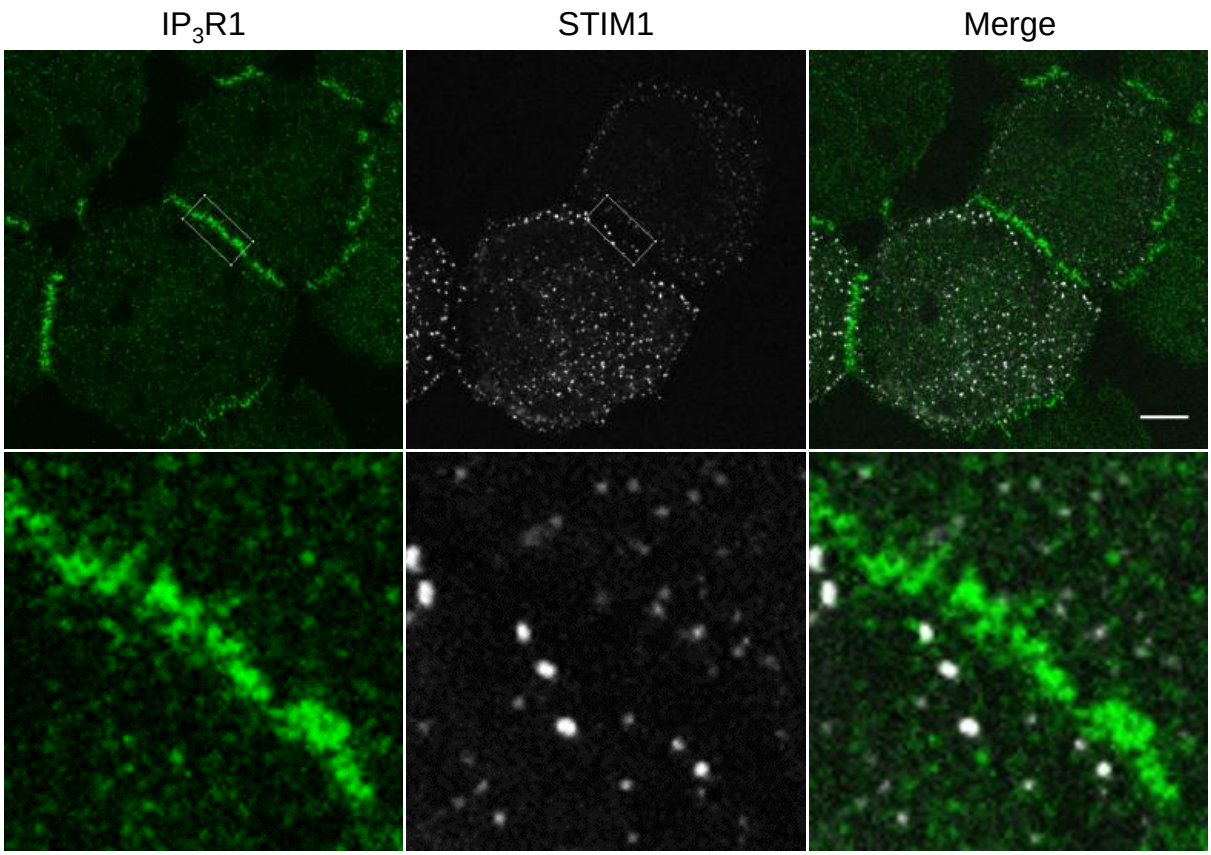

Figure 3.18. Relative positioning of IP_3R1 and STIM1 puncta in connected pancreatic ductal adenocarcinoma cells.

In connected PANC-1 cells IP_3R1 are localised in cell-cell contacts region whilst ER-PM junctions revealed by STIM1 puncta formation following ER Ca^{2+} store depletion with cyclopiazonic acid (CPA), can be found in closely adjacent region. Upper panels show the distribution of IP_3R1 and STIM1 in connected cells. Confocal images were taken from the cellular regions adjacent to the coverslip. Scale bar represents 10 μm. Lower panel show the fragment outlined by the rectangle in left and central upper panels.

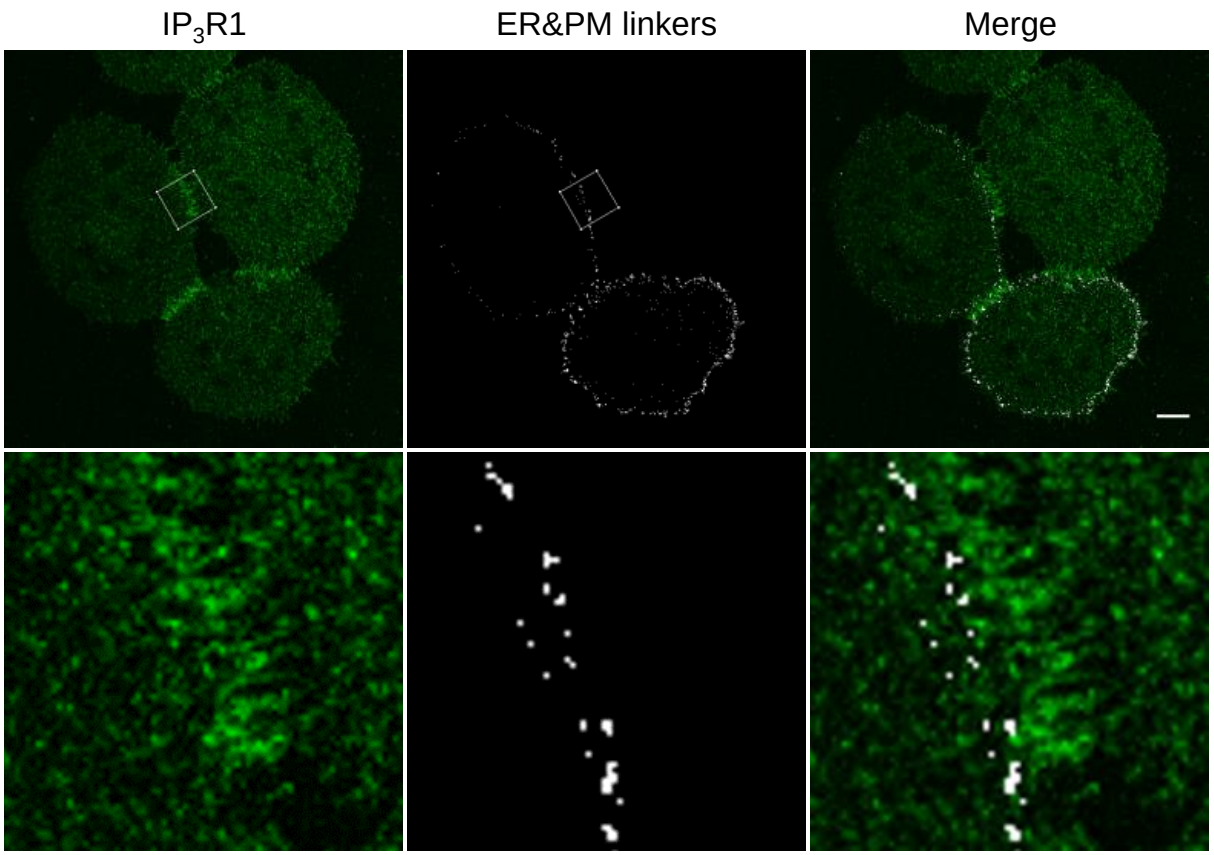

Figure 3.19. Relative positioning of IP_3R1 and ER-PM junctions in connected pancreatic ductal adenocarcinoma cells.

In connected PANC-1 cells IP_3R1 are localised in cell-cell contacts region whilst ER-PM junctions revealed by co-localised ER and PM linkers can be found in closely adjacent region. Upper panels show the distribution of IP_3R1 and ER-PM junctions in 3 connected cells. Confocal images were taken from the cellular regions adjacent to the coverslip. Scale bar represents 10 μm. Lower panel show the fragment outlined by the rectangle in left and central upper panels.

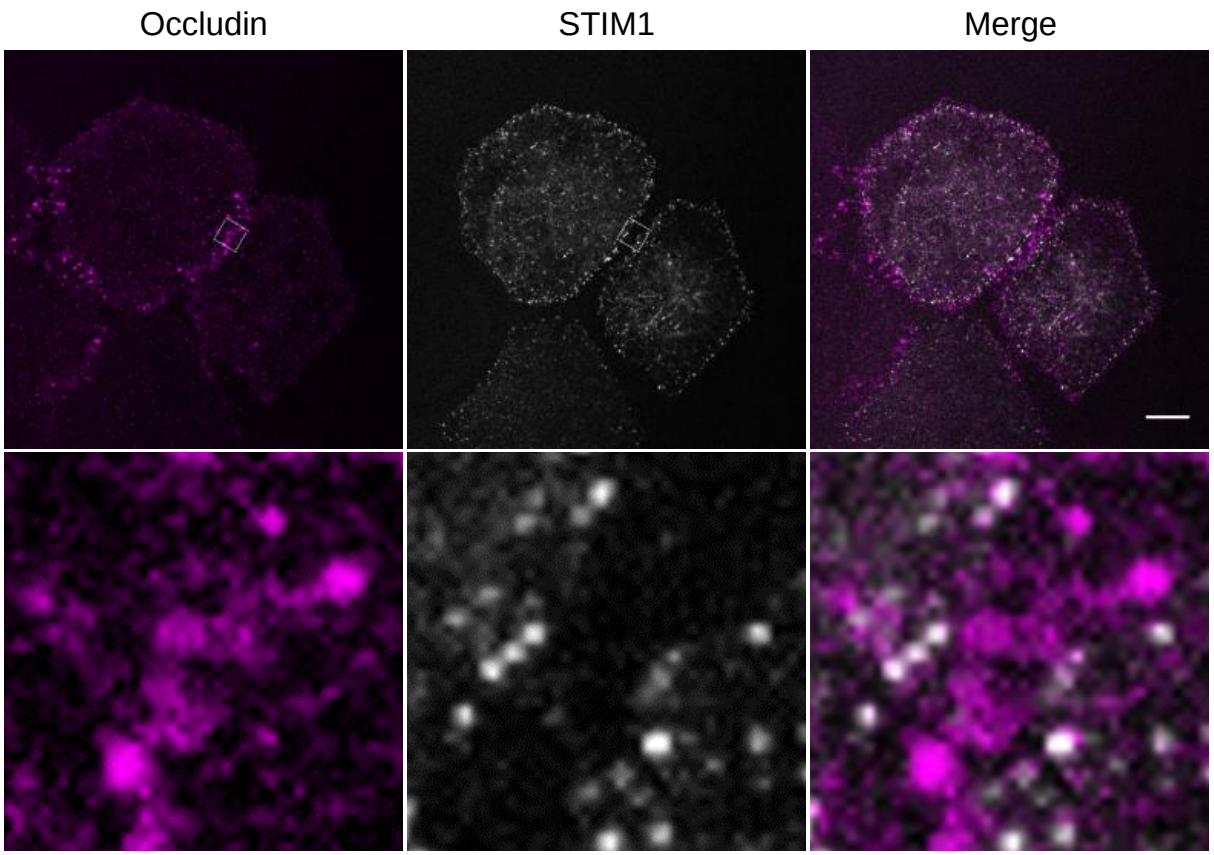

Figure 3.20. Relative positioning of occludin (tight junction marker) and STIM1 puncta in connected pancreatic ductal adenocarcinoma cells.

Tight junction marker occludin is spatially segregated from ER-PM junctions (revealed by STIM1 puncta formation) in PANC-1 cell cluster. TK-YFP-STIM1-transfected PANC-1 cells were fixed after treatment with CPA and immunostained with anti-occludin antibody. Scale bar represents 10 μm. Lower panel show the fragment outlined by the rectangle in left and central upper panels.

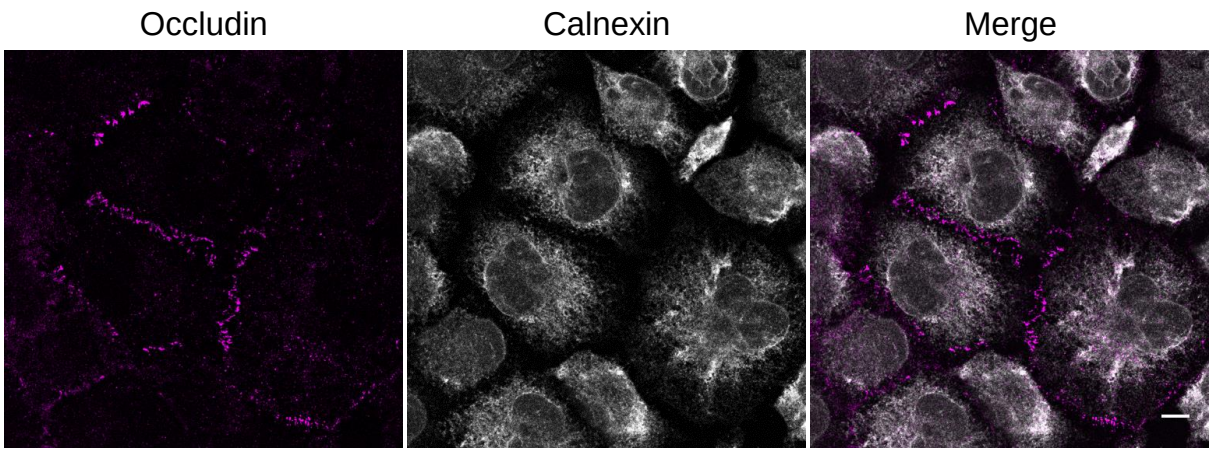

Figure 3.21. Relative positioning of occludin (tight junction marker) and calnexin (ER marker) in connected pancreatic ductal adenocarcinoma cells.

Tight junction marker occludin is spatially segregated from peripheral ER strands (revealed by calnexin staining) in PANC-1 cell cluster. PANC-1 cells were fixed and co-immunostained with anti-occludin and anti-calnexin antibodies. Scale bar represents 10 μm.

3.8 Discussion

This part of the present study has successfully shown that all 3 isoforms of IP_3R, and store operated Ca^{2+} entry (SOCE) components STIM1 and Orai1 proteins are endogenously expressed in PDAC cells (Figures 3.4 and 3.17). With the use of caged IP_3 and selective IP_3Rs inhibitor Xestospongin-B (Figure 3.6), it was successfully demonstrated that these IP_3Rs are functional Ca^{2+} channels capable of mediating IP_3-induced Ca^{2+} release from intracellular stores in PANC-1 cells. Furthermore, I also successfully characterised the subcellular distribution of all 3 isoforms of IP_3R, and the relative positioning of polarised IP_3Rs and STIM1-competent ER-PM junctions in connected polarised PANC-1 cells.

Ca^{2+} is a remarkable, versatile and universal signalling ion known for its crucial role in numerous cellular processes including proliferation, differentiation and secretion (Berridge *et al.*, 1998; Berridge *et al.*, 2000). Ca^{2+} is able to mediate a vast number of cellular processes. Its versatility is most likely due to the ability of this remarkable ion to form numerous specific complex spatial and temporal patterns (Berridge *et al.*, 2000). IP_3Rs are important platforms for Ca^{2+} signals, and it has been postulated by Vermassen et al. (2004) that the exact subcellular localisation of IP_3Rs determines the physiological consequences of IP_3-induced Ca^{2+} release, which is subsequently important for the correct initiation and propagation of Ca^{2+} signals.

To map the exact subcellular localisations of IP_3Rs in polarised connected PANC-1 cells, firstly, it was established that the 3 isoforms of IP_3R present in PANC-1 cells at mRNA level exhibited differential expression profiles with IP_3R3 been the most abundant isoform whereas IP_3R2 was the least abundant isoform. This data is in good agreement with a previous work by Wojcikiewicz (1995) showing that the

presence or abundance of each isoform of IP_3R is cell type dependent and IP_3R isoforms are expressed in different proportions in different cell and tissue types. I also established that these IP_3Rs are functional Ca^{2+} release channels in PANC-1 cells by using the most selective inhibitor of IP_3Rs channels available Xestospongin-B (Jaimovich *et al.*, 2005; Criollo *et al.*, 2007). Xestospongin-B is a member of the Xestospongins family; a macrocyclic bis-1-oxaquinolizidines isolated from the marine sponge *Xestospongia exigua* (Quirion *et al.*, 1992; Jaimovich *et al.*, 2005). Xestospongin-B has been demonstrated to be a potent membrane-permeable inhibitor of IP_3Rs (Gafni *et al.*, 1997; Jaimovich *et al.*, 2005; Criollo *et al.*, 2007). The selectivity and fidelity of Xestospongin-B acting specifically on IP_3Rs and inhibiting IP_3-induced Ca^{2+} release from intracellular Ca^{2+} stores (primarily the ER) has been demonstrated in HeLa cells and rat skeletal myotubes by the Molgo group, where they elegantly showed that Xestospongin-B had no effect on the following Ca^{2+} signalling events and Ca^{2+} regulatory processes: ER Ca^{2+} leak, $[Ca^{2+}]_{ER}$ and basal $[Ca^{2+}]_C$ level, Ca^{2+} ATPase pump activity or thapsigargin action, and store operated Ca^{2+} entry after ER Ca^{2+} store depletion with thapsigargin (Jaimovich *et al.*, 2005; Criollo *et al.*, 2007).

Interestingly, isoforms of IP_3R exhibit differential subcellular localisations in clusters and monolayers of polarised PANC-1 cells. IP_3R1 is predominantly localised at cell-cell contact junctions as demonstrated by its remarkable co-localisation with occludin and E-cadherin in connected PANC-1 cells. IP_3R2 and IP_3R3 are primarily localised at the perinuclear region in connected PANC-1 cells. In support of the differential subcellular distribution of isoforms of IP_3R we observed in PANC-1 cells, a number of previous reports have shown that isoforms of IP_3R exhibit diverse subcellular distributions within the same cell, and in different cell and tissue types. In some

epithelial cell types for example in pancreatic acinar cells (PACs), all 3 isoforms of IP_3R are predominantly concentrated near the apical membrane where they co-localised with tight junction markers ZO1 and occludin (Nathanson *et al.*, 1994; Lee *et al.*, 1997; Yule *et al.*, 1997; Lur *et al.*, 2009; Lur *et al.*, 2011). This region has been demonstrated to be functionally important as a trigger zone in which Ca^{2+} waves originate, and subsequently mediates a number of cellular processes including fluid secretion and exocytosis (Thorn *et al.*, 1993; Ito *et al.*, 1997; Lee *et al.*, 1997; Yule *et al.*, 1997). In cholangiocytes, both IP_3R1 and IP_3R2 were found uniformly distributed in the cytoplasm whereas IP_3R3 was primarily found near the apical membrane (Hirata *et al.*, 2002a). In liver hepatocytes where two isoforms of IP_3R are expressed, IP_3R2 can be found near the apical membrane (canalicular), while the other isoform (IP_3R1) was found uniformly distributed in the cytoplasm (Dufour *et al.*, 1999; Hirata *et al.*, 2002b). In vascular smooth muscle cells, IP_3R1 was localised throughout the cytoplasm, IP_3R2 was localised near the plasma membrane and also in the perinuclear region, and IP_3R3 was only found in the perinuclear region (Tasker *et al.*, 2000). In confluent, polarised and fully differentiated non-tumourigenic Madin-Darby canine kidney (MDCK) cells, exogenously expressed IP_3R1 in addition to the predominantly endogenously expressed isoform IP_3R3 have both been shown to primarily localise in the vicinity of tight junctions (Colosetti *et al.*, 2003; Dingli *et al.*, 2012). Interestingly, these IP_3Rs have been shown not to always co-localise with ER markers but instead with PM markers such as tight/adherens junction markers in MDCK and PACs (Colosetti *et al.*, 2003; Lur *et al.*, 2011; Dingli *et al.*, 2012). IP_3Rs in liver cells have also been shown not to co-purify or fractionate with ER markers but instead with PM markers e.g. alkaline phosphodiesterase 1 (Rossier *et al.*, 1991). Taken together the experimental observations described here and reported findings

from previous works, it is clear that the distribution of isoforms of IP_3R varies widely in epithelial cells, suggesting that the subcellular localisation of IP_3Rs and IP_3-induced Ca^{2+} release sites are important determinants of the spatial and temporal characteristics of Ca^{2+} signals. Such signals in turn likely regulate different epithelial functions including but not limited to the regulation of paracellular diffusion/tight junction permeability, fluid and electrolyte secretion, exocytosis, and cell proliferation/differentiation.

In the present study, the importance of tight junctions for IP_3Rs localisation was not investigated. However, from reviewing elegant work by Colosetti et al. (2003) and others, one could speculate on the possible relationship between the tight junctions and IP_3Rs localisation. In MDCK cells the most abundantly expressed isoform of IP_3R is IP_3R3 (Colosetti *et al.*, 2003; Dingli *et al.*, 2012). Monitoring the establishment of polarity by measuring trans-epithelial resistance (TER), it was shown that the concentration of IP_3R3 in the close vicinity of tight junctions is positively dependent on the cellular polarity state of MDCK cells (Colosetti *et al.*, 2003). Using a calcium switch experiment (i.e. polarised MDCK cells were placed in Ca^{2+} free medium for several hours and then replaced in Ca^{2+} supplemented medium), Colosetti et al. (2003) showed that polarity was dynamically lost and re-established, respectively. The former was accompanied by disruption of tight junctions and IP_3R3 was localised in the cytoplasm. During re-establishment of polarity, re-localisation of tight junction marker ZO-1 to intercellular junctions was rapid and preceded that of IP_3R3, the latter occurring only after intercellular junctions were well established (TER of ≥200 ohm cm2), suggesting that the localisation of IP_3Rs at intercellular junctions required fully constituted tight junctions, and that the recruitment of IP_3Rs to the

intercellular junctions is most likely a secondary event that is required for providing Ca^{2+} signals needed for functioning of epithelium.

In view of the remarkable polarised distribution of IP_3R1 at cell-cell contacts region in connected polarised PANC-1 cells, the studies presented in this chapter were focused on the distribution of IP_3R1. Following ER Ca^{2+} store emptying through IP_3R Ca^{2+}-release channels in the ER, restoring of the $[Ca^{2+}]_{ER}$ involves SOCE mediated by STIM1, which activates PM channels Orai1 to permit influx of Ca^{2+}, and this Ca^{2+} refilling process takes place in the ER-PM junctions (Wu *et al.*, 2006; Varnai *et al.*, 2007; Lur *et al.*, 2009; Carrasco & Meyer, 2011). ER-PM junctions are a specialised region of close contact with an inter-membrane space of 7 to 25 nm between the two organelles (Wu *et al.*, 2006; Varnai *et al.*, 2007; Lur *et al.*, 2009; Orci *et al.*, 2009; Carrasco & Meyer, 2011; Chang *et al.*, 2013; Wu *et al.*, 2014), which serves as signalling hubs for Ca^{2+} signalling (Wu *et al.*, 2006; Varnai *et al.*, 2007; Lur *et al.*, 2009; Chang *et al.*, 2013; Wu *et al.*, 2014), phosphatidylinositol transfer and signalling (Carrasco & Meyer, 2011; Manford *et al.*, 2012; Chang *et al.*, 2013) and cAMP signalling (Lefkimmiatis *et al.*, 2009; Willoughby *et al.*, 2012). In the present study, I successfully showed that SOCE components – STIM1 and Orai1 proteins are endogenously expressed in PANC-1 cells (Figure 3.17). I next examined the subcellular distribution of Ca^{2+} releasing sites in relation to that of Ca^{2+} replenishing/reloading sites in PANC-1 cells in greater detail. It was observed that both IP_3R1 and STIM1/SOCE-competent ER-PM junctions exhibit a polarised distribution and localise in the cell periphery area of connected PANC-1 cells. Notably, STIM1/SOCE-competent ER-PM junctions (Ca^{2+} replenishing platform) do not co-localise with IP_3R1 but are positioned in close proximity to these Ca^{2+} releasing platform.

Thus, it can be reasoned that Ca^{2+} releasing sites are strategically positioned with respect to Ca^{2+} replenishing sites, creating a stratified distribution of Ca^{2+} signalling complexes in the vicinity of intercellular junctions in connected PDAC cells. This further suggests that coordination of strategically positioned SOCE-competent ER-PM junctions and IP_3R1 mediated Ca^{2+} release platforms may cooperatively provide and sustain prolonged Ca^{2+} signalling. The functions of these Ca^{2+} signals have not been investigated in this study but one can speculate that these signals could play a role in establishing/maintaining epithelial phenotype or on the contrary in soliciting epithelial-mesenchymal transition (EMT). Ca^{2+} signalling in the proximity of tight junctions could be also important for epithelial functions like exocytotic and fluid secretion (Rodriguez-Boulan & Nelson, 1989; Ito *et al.*, 1997; Steward *et al.*, 2005; Pandol, 2010; Huang *et al.*, 2012).

Chapter 4: Redistribution of IP_3Rs and ER-PM junctions in pancreatic ductal adenocarcinoma cells during epithelial-mesenchymal transition

Chapter 4: Redistribution of IP_3Rs and ER-PM junctions in pancreatic ductal adenocarcinoma cells during epithelial-mesenchymal transition

4.1 Epithelial-mesenchymal transition

PDAC is the 4th leading cause of cancer-related mortalities worldwide (Siegel *et al.*, 2011), with poor prognosis and a median survival period of less than 12 months after diagnosis (Siegel *et al.*, 2013). The poor outcome of this cancer is characterised by its aggressive, disseminated, metastatic nature and strong resistance to chemotherapy (Stathis & Moore, 2010; Siegel *et al.*, 2013). The metastatic nature of PDAC and other cancer types is associated with epithelial-mesenchymal transition (EMT) (Chang *et al.*, 2012), migration and invasion (Hanahan & Weinberg, 2011; Lamouille *et al.*, 2014).

EMT is the conversion of epithelial cells into mesenchymal cells, and external cues such as growth factors e.g. epidermal growth factor (EGF), the transforming growth factor family e.g. TGFβ and extracellular matrix components e.g. fibronectin and collagen have been shown to be key mediators of this process (Nelson, 2009; Terry *et al.*, 2010; Lamouille *et al.*, 2014). EMT is characterised by the apparent change in cellular phenotypes after trans-differentiation from apical-basal polarity to front-rear polarity (Lamouille *et al.*, 2014). SNAIL, zinc-finger-E-box-binding (ZEB), and basic helix-loop-helix (bHLH) transcription factors have been reported to regulate the process of the EMT switch at a transcriptional level. In addition, regulatory factors of the EMT switch are also regulated at post-transcriptional, translational and post-translational levels (Chang *et al.*, 2012; Lamouille *et al.*, 2014). During EMT, epithelial cells disconnect from their neighbours following down-regulation of

epithelial signatures by disassembly of intercellular junctional complexes (IJCs) and loss of apical-basal polarity. There is a concomitant up-regulation of genes that define the formation of new front-rear cellular polarity permitting trans-differentiation into motile mesenchymal cells (Lamouille *et al.*, 2014). The loss of epithelial IJCs is accompanied by the dissolution of tight junction markers claudins, occludin and ZO-1 and adherens junction marker E-cadherin (Chang *et al.*, 2012). Desmosome markers as well as markers for polarity complexes (comprising of Crumbs complex, partitioning defective (PAR) and Scribble complex) are also lost from the intercellular junction area (Nelson, 2009; Lamouille *et al.*, 2014). Concomitantly, mesenchymal gene markers including N-cadherin, vimentin and fibronectin as well as genes that define the remodelling of the actin cytoskeleton are up-regulated leading to the formation of lamellipodia, filopodia and invadopodia to increase cell motility and invasive phenotypes of mesenchymal cells (Ridley *et al.*, 2003; Chang *et al.*, 2012; Lamouille *et al.*, 2014). A number of recent studies have reported the importance of Ca^{2+} signalling for EMT (Davis *et al.*, 2014), cell adhesion, cell motility and invasion in a number of different cell types (Wei *et al.*, 2009; Yang *et al.*, 2009; Middelbeek *et al.*, 2012; Tsai & Meyer, 2012; Tsai *et al.*, 2014). The efficient Ca^{2+} signalling mediated by IP_3Rs requires $[Ca^{2+}]_{ER}$ reloading mechanisms, which involve Ca^{2+} sensor STIM1 and PM Ca^{2+} channel Orai1 that are localised in the ER-PM junctions (Carrasco & Meyer, 2011), and some types of TRP channels are probably also involved (Worley *et al.*, 2007). In this part of the study, we induced transition from epithelial to mesenchymal phenotype and investigated the changes in the distribution of Ca^{2+} signalling mechanisms.

4.2 During EMT PANC-1 cells change cellular morphology

Having established that PANC-1 cells in a monolayer exhibit apical-basal polarity and cell-cell contact junctions, which are classic characteristic features of the epithelial phenotype, I next sought to examine any observable change(s) in PANC-1 cells' morphology and phenotype during EMT. 'Wounding' of cellular monolayers is known to induce EMT (Nelson, 2009; Lamouille *et al.*, 2014). Using wound-healing or scratch migration assay with ibidi cell culture inserts, I observed dramatic changes in the morphology of PANC-1 cells during EMT. The formation of new cellular (front-rear) polarity is characterised by thin and long (red and yellow arrows in Figure 4.1) or wide and short (white arrow in Figure 4.1) tails at the rear, while broad and ruffling lamellipodia and filopodia protrusions formed at the front leading edges of migrating PANC-1 cells (Figure 4.1). PANC-1 cells in migratory mode exhibit smooth-like lamellipodia (Figure 4.1, yellow arrowhead) or a complex of smooth-like lamellipodia and spiky protrusions at the leading edges (Figure 4.1, red and white arrowheads).

This experimental finding demonstrates that PDAC cells undergo profound morphological changes during EMT.

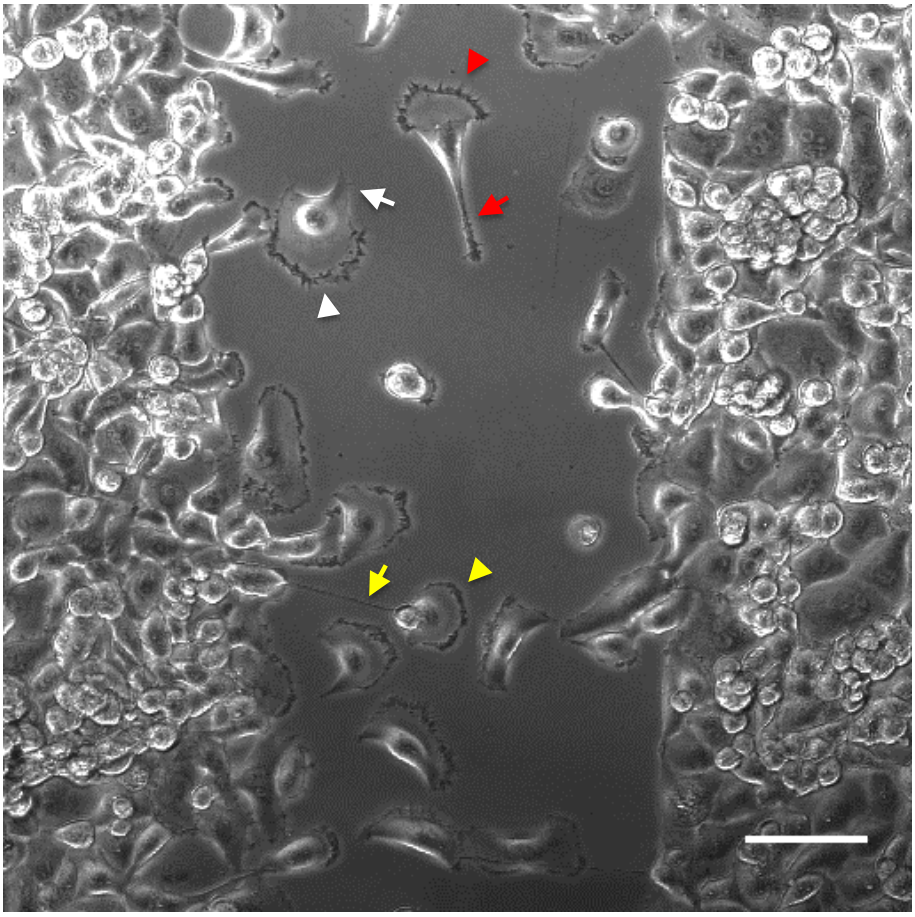

Figure 4.1. The differential phenotypes/morphologies of pancreatic ductal adenocarcinoma cells (PANC-1) in connected monolayer versus migration modes.

Significant changes in the morphology of PANC-1 cells were observed as these cells transit between connected monolayer and migration modes. PANC-1 cells in migration modes exhibit smooth-like lamellipodia leading edges (yellow arrowhead), or a complex of smooth-like lamellipodia and spiky protrusions at the leading edges (red and white arrowheads) with thin and long tails (red and yellow arrows) or with wide and short tails (white arrow). PANC-1 cells were seeded into either side of the ibidi cell culture inserts, and allowed to reach full confluence. The insert was carefully removed creating a defined open gap of approximately 500 µm, and PANC-1 cells were allowed to migrate for 6 hours at 37°C / 5% CO_2. Scale bar represents 100 µm.

4.3 IP_3Rs exhibit differential subcellular distribution in migrating PANC-1 cells

In light of the above findings I next sought to determine the fate and distribution of Ca^{2+} signalling complexes (i.e. IP_3Rs) during EMT in PDAC cells. Using wound-healing or scratch migration assays with ibidi cell culture inserts to induce EMT, and subsequent immunostaining for IP_3R1 (Figure 4.2), I observed profound changes in the subcellular localisation of IP_3R1. IP_3R1 underwent remarkable translocation from the cell-cell contact region in connected PANC-1 cells to preferentially localise at the leading edge of migrating PANC-1 cells (Figure 4.2A). Fluorescence profiles measured along the lines spanning the cell membrane of the leading edge regions show that IP_3R1 preferentially accumulated at the leading edge and in the spiky filopodia-like protrusions at the front of migrating PANC-1 cells (Figure 4.3, upper and lower panels). A similar polarised distribution of IP_3R1 with increased density at the leading edge of migrating PANC-1 cells was also observed using a second commercially obtained anti-IP_3R1 antibody, suggesting that the redistribution was a specific phenomenon (Figure 4.4). Immunostaining for IP_3R2 highlighted a similar polarised distribution in migrating PANC-1 cells (Figure 4.5). In contrast to the observed polarised distribution of IP_3R1 and IP_3R2, IP_3R3 maintained its enriched distribution in the perinuclear region after EMT (Figure 4.6) in spite of the dramatic morphological changes observed in PANC-1 cells during EMT. Fluorescence profile measured along the line spanning the cell membrane of the leading edge region show that the density of IP_3R3 distribution increased towards the perinuclear region (Figure 4.6, right panel). Consistent with this, the fluorescence profile of IP_3R3 showed an inverse relationship to those of IP_3R1 and IP_3R2 in migrating PANC-1 cells (Figure 4.6 compared to Figures 4.3 – 4.4 and 4.5). All images in figures 4.3 –

4.7a show confocal sections taken from ventral parts of the cells located in the immediate proximity to the coverslip. Pan-IP_3Rs antibodies (raised against a conserved region in the C terminal of all subtypes of IP_3R) also revealed a similar polarised distribution of IP_3Rs (most likely IP_3R1 and IP_3R2) with preferential localisation at the leading edge of individual migrating cells (Figure 4.7a). In addition, visualising IP_3R distribution at the ventral (bottom z-plane, in close proximity to the coverslip), middle and dorsal (top z-plane, furthest distance from the coverslip) parts of PANC-1 cells using the Pan-IP_3Rs antibody interestingly provided further evidence that IP_3Rs localise to different subcellular regions within migrating PANC-1 cells, with a population of receptors at the periphery (consistent with data obtained with type I and type II specific antibodies) and another population in a perinuclear region (consistent with data obtained with type III specific antibody and to a certain extent with type II specific antibody) (Figure 4.7b).

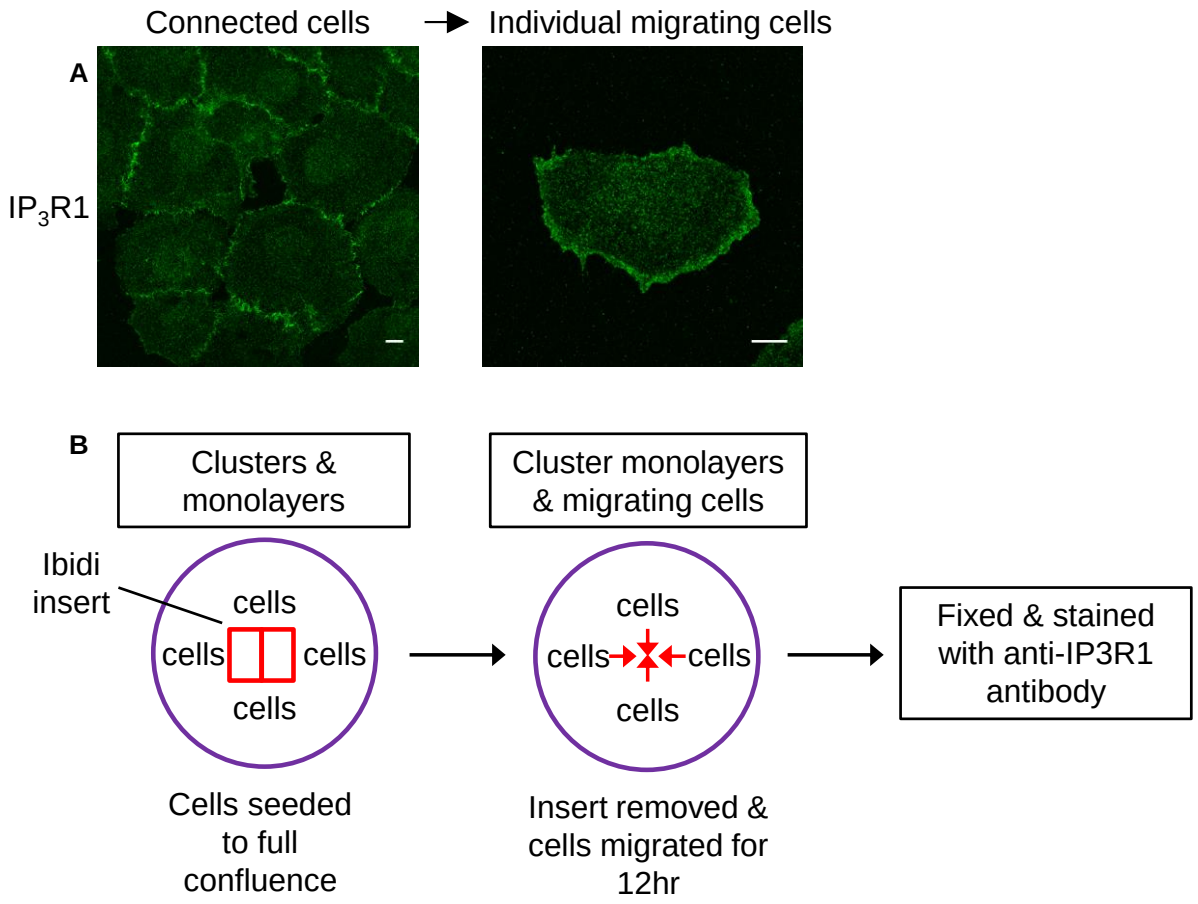

Figure 4.2. The polarised distribution of IP_3R1 in connected and migrating cells, and the procedure used to change the cellular phenotype.

(A). Illustrates the translocation of IP_3R1 from cell-cell contacts (upper left panel) to the leading edge (upper right panel) of PANC-1 cells. An example of preferential accumulation of IP_3R1 at the leading edge in a cell that was induced to migrate as a result of removal of the insert (see part B) is shown on the upper right panel. Scale bars represent 10 μm.

(B). Illustrates procedure utilised to induce migratory phenotype.

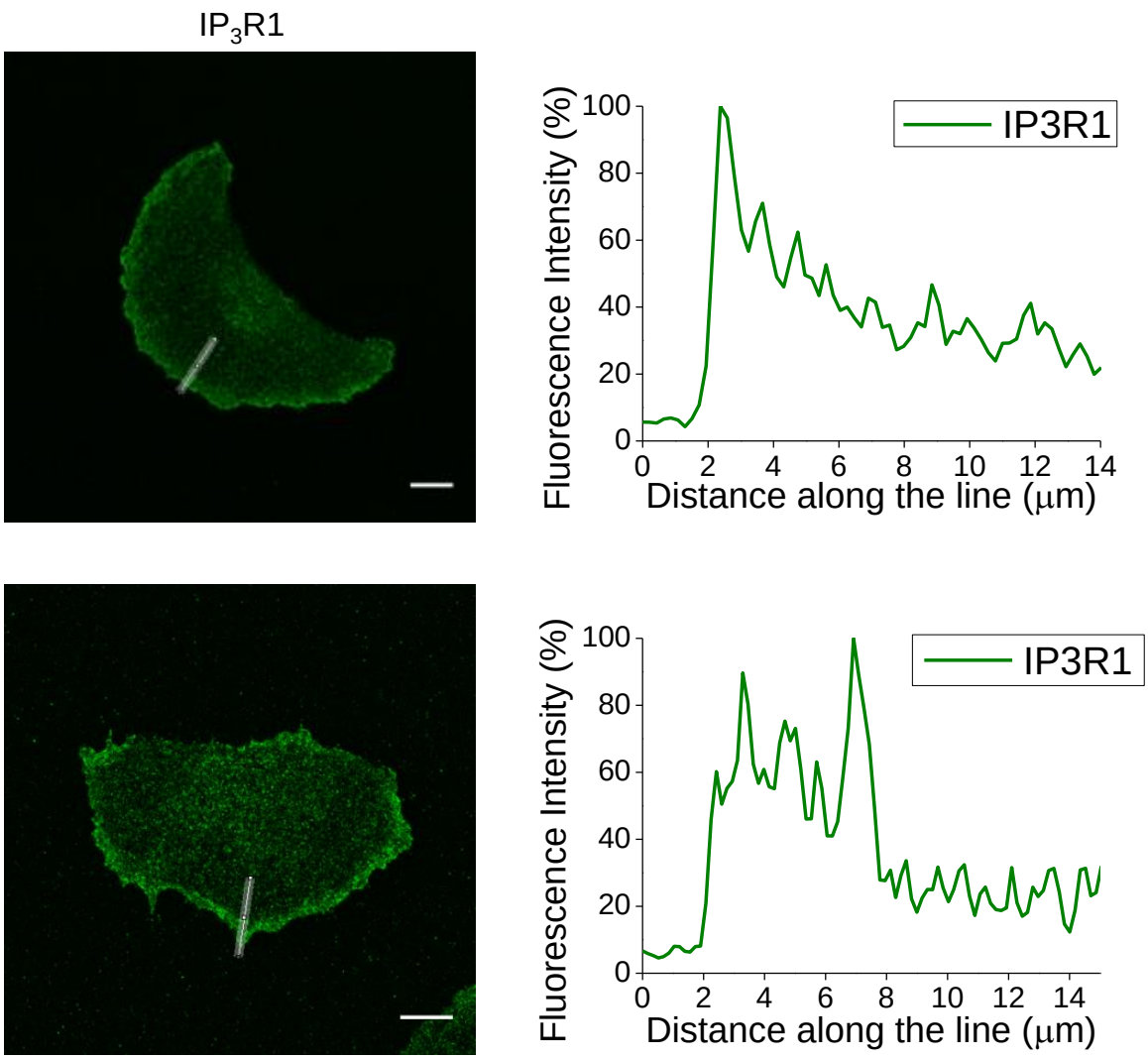

Figure 4.3. IP_3R1 predominantly decorates the leading edge of pancreatic ductal adenocarcinoma cells.

Polarised PANC-1 cells were fixed and immunostained using anti-IP_3R1 antibody. Migrating PANC-1 cells with a smooth-like lamellipodia leading edge (top panel), and with a combination of smooth-like lamellipodia and spiked protrusions at the leading edge (bottom panel). Fluorescence profiles (right panels) were measured along the line spanning the cell membrane of the leading edge regions. Scale bars represent 10 μm.

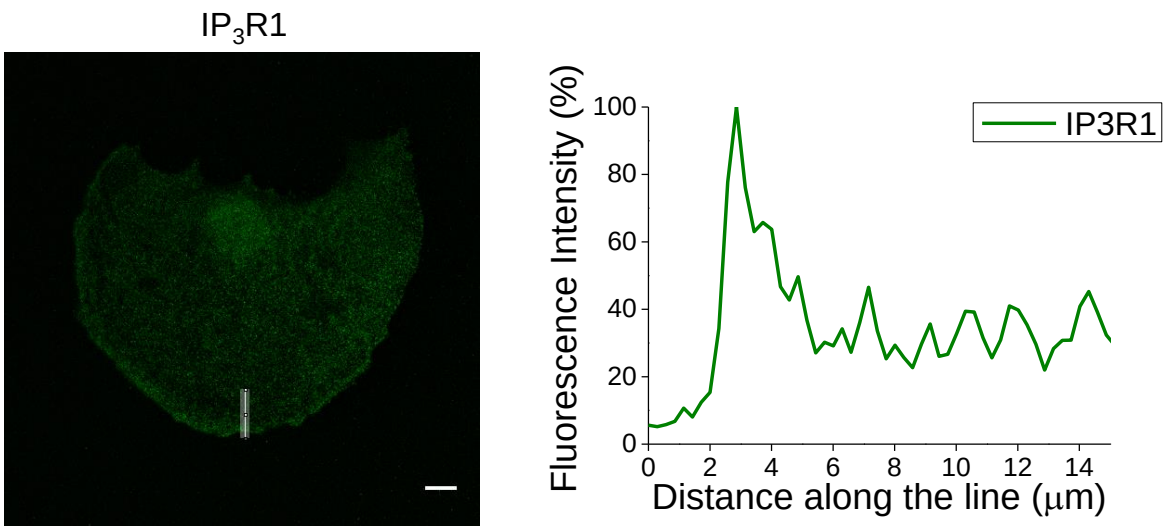

Figure 4.4. Distribution of IP_3R1 in individual migrating pancreatic ductal adenocarcinoma cells.

Polarised PANC-1 cells were fixed and immunostained using anti-IP_3R1 antibody (commercially obtained antibody). The right panel of the figure shows the fluorescence distribution along the line spanning the cell membrane of the leading edge regions on the left panel. Scale bar represents 10 μm.

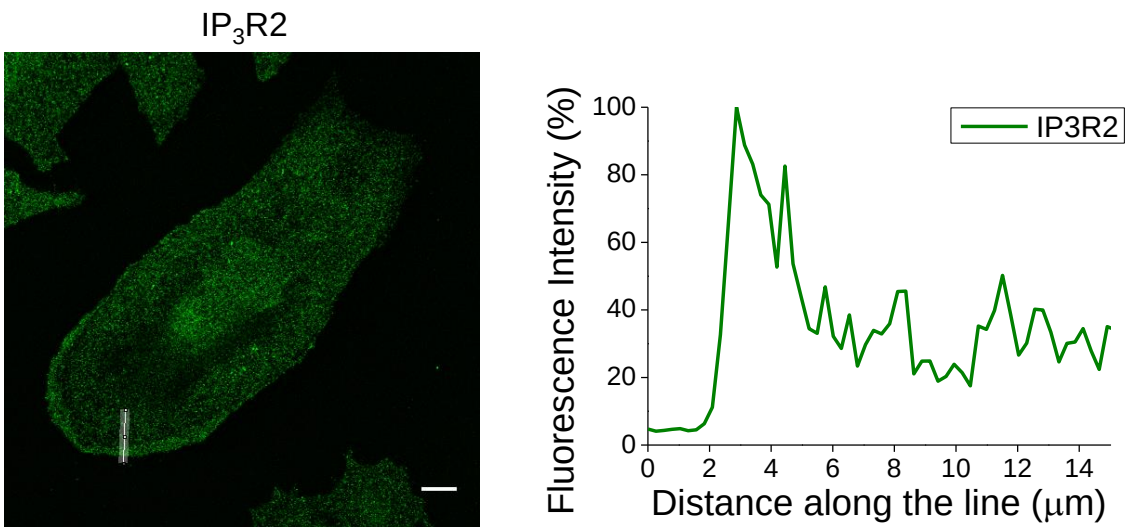

Figure 4.5. Distribution of IP_3R2 in individual migrating pancreatic ductal adenocarcinoma cells.

Polarised PANC-1 cells were fixed and immunostained using anti-IP_3R2 antibody. The right panel of the figure shows the fluorescence distribution along the line spanning the cell membrane of the leading edge region (shown on the left panel). Scale bar represents 10 μm.

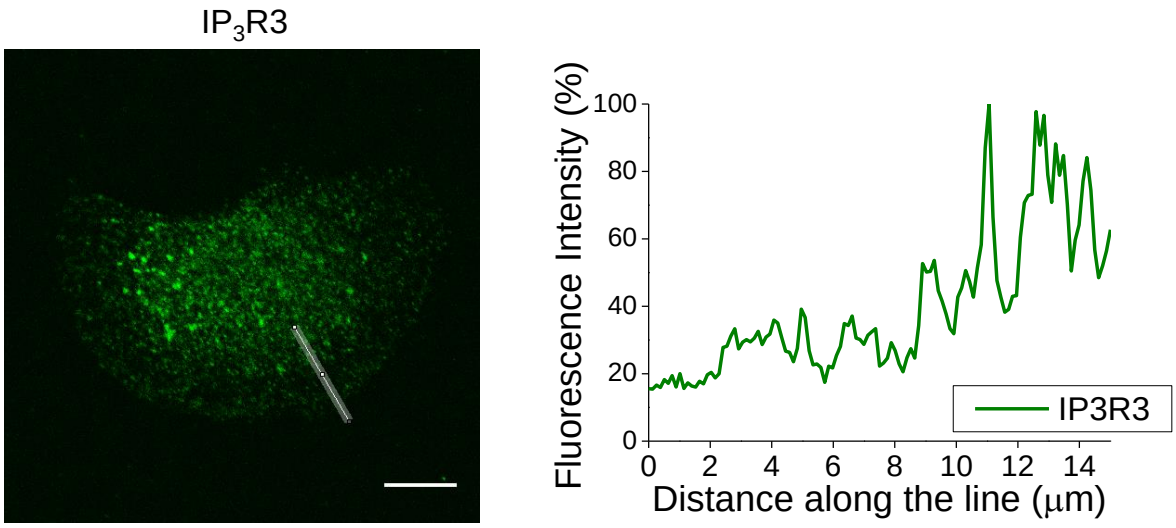

Figure 4.6. Distribution of IP_3R3 in individual migrating pancreatic ductal adenocarcinoma cells.

In polarised PANC-1 cells, IP_3R3 are richly localised to the perinuclear region and somewhat in the cytosolic region. Polarised PANC-1 cells were fixed and immunostained using anti-IP_3R3 antibody. The right panel of the figure shows the fluorescence distribution along the line spanning the cell membrane of the leading edge region (shown on the left panel). Scale bar represents 10 μm.

These experimental results show that profound morphological changes including the formation of new cellular polarity in PDAC cells were observed after EMT, and this was accompanied by the redistribution of IP_3Rs, with IP_3R1 and IP_3R2 undergoing redistribution from cell-cell contacts and perinuclear regions in connected PANC-1 cells, respectively, to preferentially localise at the leading edge region of migrating PANC-1 cells. In contrast, IP_3R3 retained its enriched perinuclear localisation after EMT. The observed redistribution of IP_3R1 and IP_3R2 in migrating cells suggest that

IP_3R1 and IP_3R2 (but less likely IP_3R3) could be important for the migration of pancreatic ductal adenocarcinoma cells (see chapter 5).

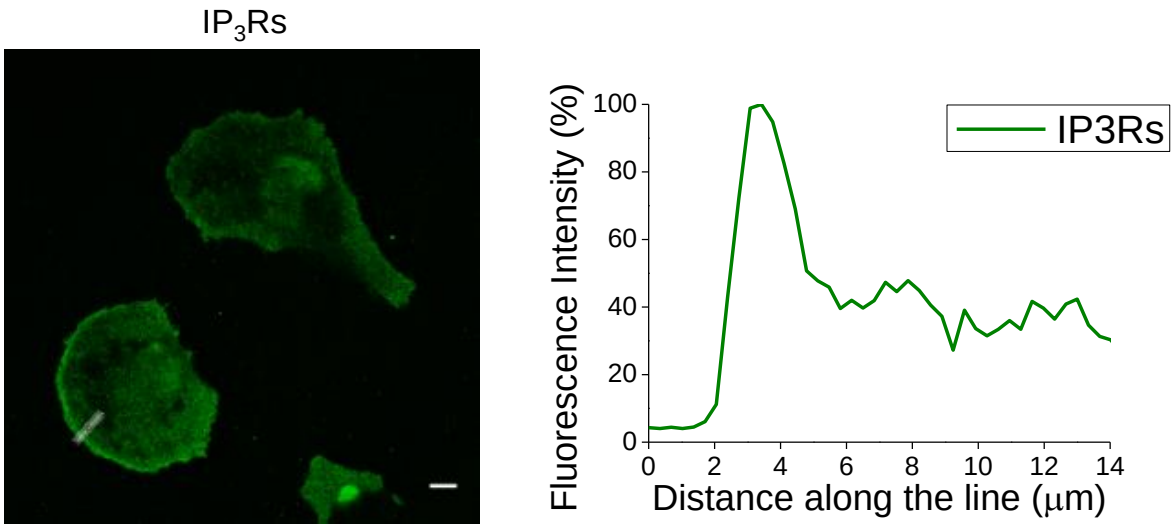

Figure 4.7a. IP_3Rs predominantly decorate the leading edge of pancreatic ductal adenocarcinoma cells.

Polarised PANC-1 cells were fixed and immunostained using anti pan-IP_3R antibody. Fluorescence profile (right panel) was measured along the line spanning the cell membrane of the leading edge region (shown on the left panel). Scale bar represents 10 μm.

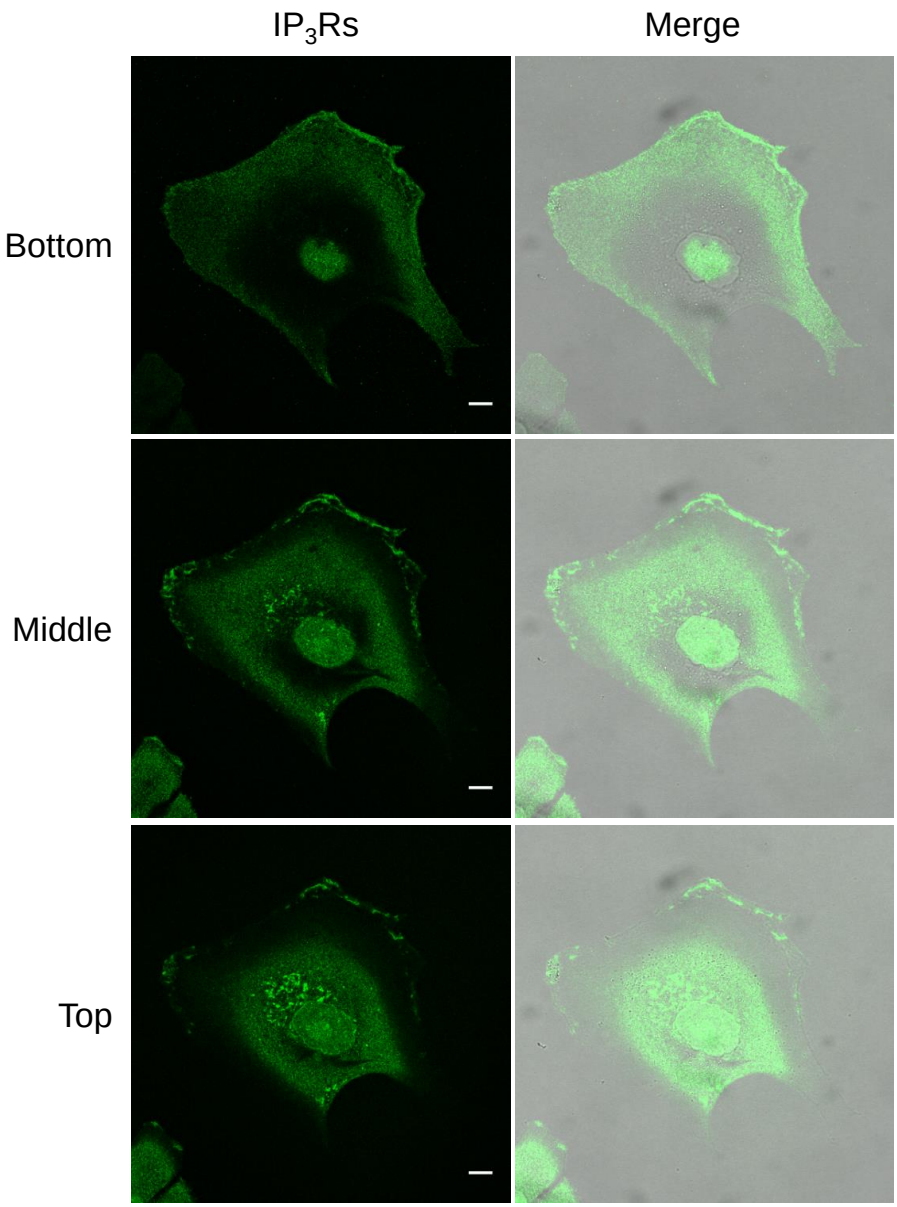

Figure 4.7b. Differential distribution of IP_3Rs in migrating pancreatic ductal adenocarcinoma cells.

Polarised PANC-1 cells were fixed and immunostained using anti pan-IP_3R antibody. Bottom, middle and top panels represent the Z-positions, with the bottom z-position being the nearest to the coverslip. Pan-IP_3Rs antibody interestingly provided further evidence that IP_3Rs localise to different subcellular regions within migrating PANC-1 cells. Scale bars represent 10 μm. Merge - indicates the overlay of fluorescence and DIC images.

4.4 Distribution of STIM1 / ER-PM junctions in migrating PANC-1 cells

Having established from previous experiments that EMT of PDAC cells is accompanied by the formation of new cellular polarity and profound changes in the distribution of cellular Ca^{2+} signalling components i.e. IP_3Rs, I sort to determine the distribution of STIM1-competent ER-PM junctions in actively migrating PANC-1 cells. After the exogenous expression of rapamycin-inducible ER and PM linker constructs in PANC-1 cells without ER Ca^{2+} store depletion or modification, we observed that ER-PM junctions preferentially accumulate at the leading edge of migrating PANC-1 cells (Figure 4.8, middle panel). ER & PM linker image (shown as white dotes, bottom panel of Figure 4.8) was created to highlight ER-PM junctions revealed by the regions of co-localisation of the ER and PM linker constructs using the Image J co-localise RGB plugin described previously (Dingsdale *et al.*, 2013). Alternatively, following the exogenous expression of TK-YFP-STIM1 in PANC-1 cells and ER Ca^{2+} store depletion using ER Ca^{2+}-ATPase inhibitor CPA, we observed that STIM1 puncta (highlighting ER-PM junctions) accumulated and decorated the leading edge of migrating PANC-1 cells (Figure 4.9). Similar observations have been reported by a number of studies including Dingsdale et al. (2013) and Tsai et al. (2014). Dingsdale et al. (2013) further demonstrated that STIM1-competent ER-PM junctions form at the leading edge of migrating PANC-1 cells in a saltatory manner.

Figure 4.8. Distribution of ER and PM linker constructs before and after treatment with rapamycin in live migrating pancreatic ductal adenocarcinoma cells.

PANC-1 cells co-transfected with PM-targeted LL-FKBP-mRFP and ER-targeted CFP-FRB-LL linker constructs were imaged live on a confocal microscope before and during the addition of 100 nM rapamycin. ER & PM linker images (bottom panel) were created to highlight ER-PM junctions revealed by the region of co-localisation of the two linker constructs using Image J Co-localise RGB plugin. Scale bar represents 10 μm.

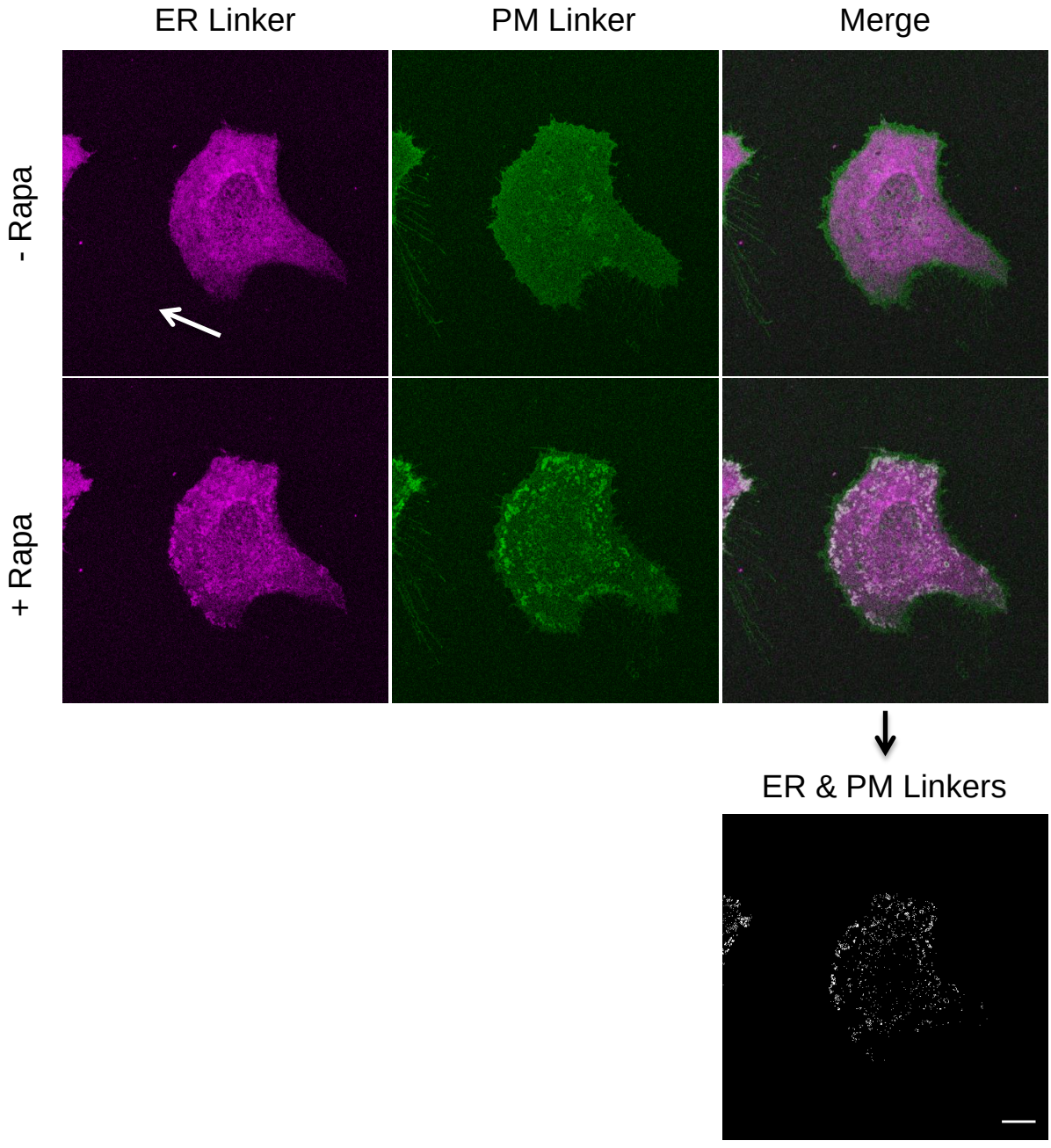

Figure 4.8

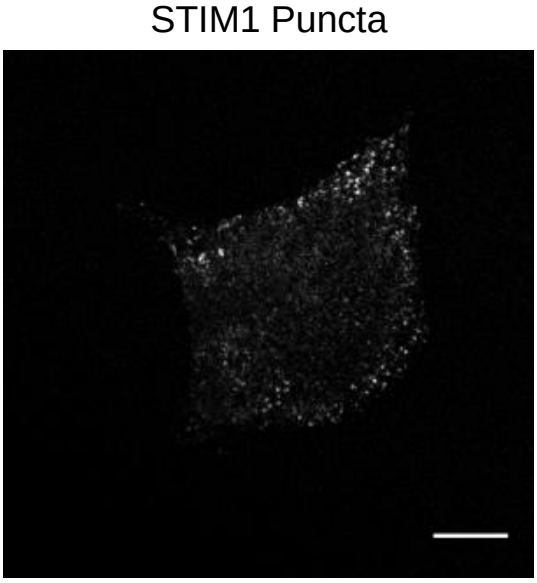

Figure 4.9. STIM1 puncta decorates the leading edge of migrating pancreatic ductal adenocarcinoma cells.

PANC-1 cells transfected with TK-YFP-STIM1 were treated with CPA and imaged on a confocal microscope. Scale bar represents 10 μm.

The increased density of STIM1-competent ER-PM junctions at the leading edge of migrating PANC-1 cells was a surprising observation. A possible explanation for this phenomenon is increased density of ER strands (and consequently higher probability of ER-PM junction formation). Therefore, I next examined the distribution of the ER network in migrating PANC-1 cells. We observed that the distribution of ER-density (revealed by calnexin staining) exhibited an inverse relationship to the distribution of ER-PM junctions (revealed by STIM1 puncta) i.e. the density of ER network decreased towards the cell periphery whilst the density of ER-PM junctions increased towards the cell periphery (Figures 4.10a and 4.10b).

These experimental findings show that STIM1-competent ER-PM junctions redistribute from sites closely adjacent to cell-cell contact junctions in connected PANC-1 cells to the leading edge of migrating PANC-1 cells. In addition, it was also observed that the distribution of ER-PM junctions (revealed by STIM1 puncta) exhibited an inverse relationship to the distribution of ER-density in migrating PANC-1 cells. The proximity of STIM1-competent ER-PM junctions to the leading edge suggests that these junctions could be important for PDAC cell migration (see chapter 5).

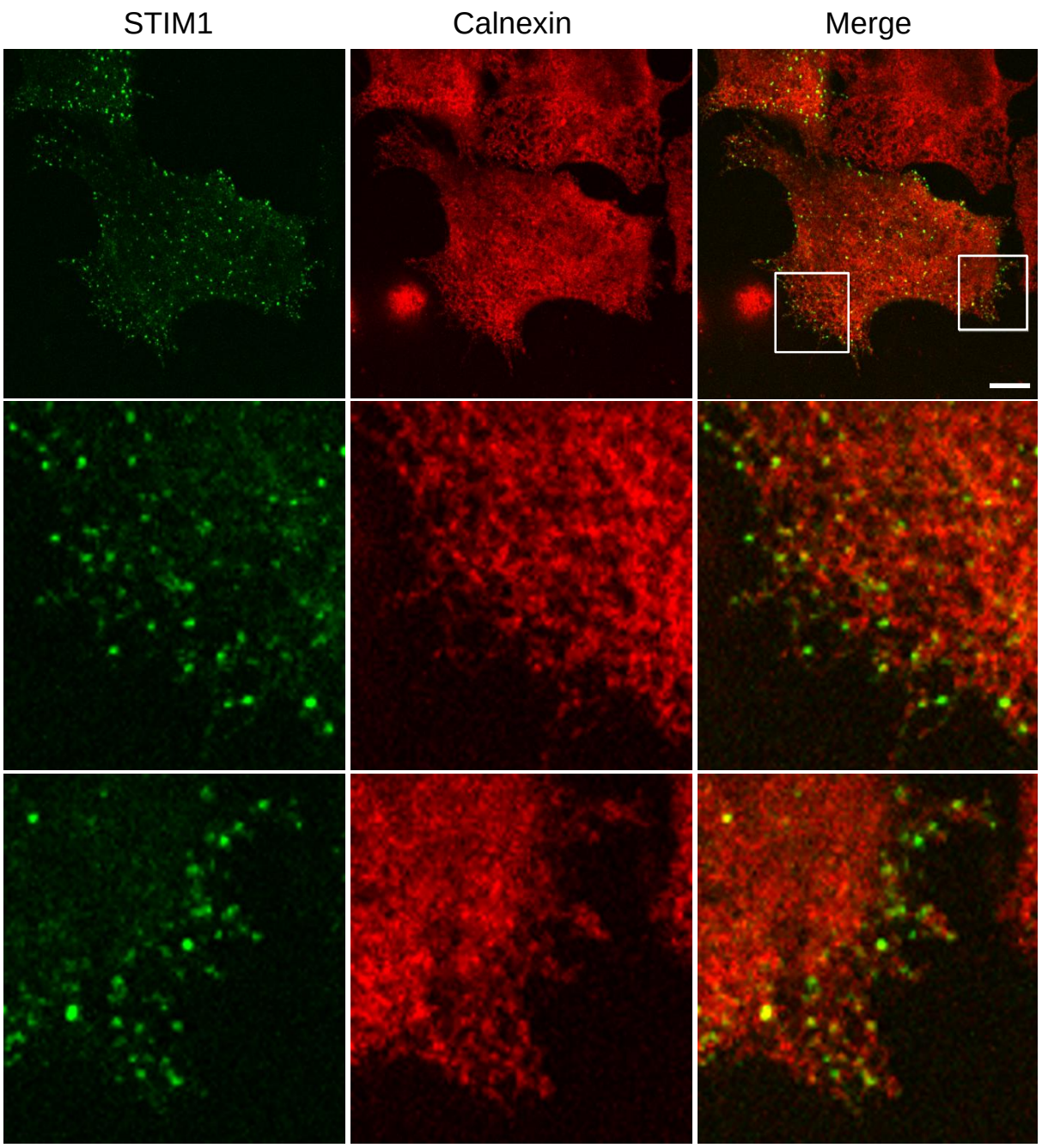

Figure 4.10a. Relative distribution of ER-PM junctions and ER-density in migrating pancreatic ductal adenocarcinoma cells.

PANC-1 cells transfected with TK-YFP-STIM1 were fixed and immunostained with anti-calnexin antibody following ER Ca^{2+} store depletion using CPA. Scale bar represents 10 μm. Middle and bottom panels show the fragments outlined by the rectangles in the upper panel (Merge).

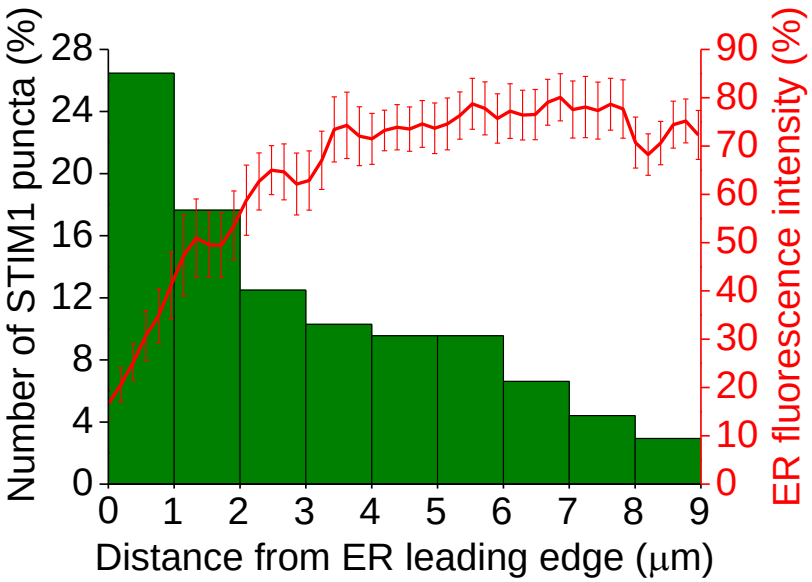

Figure 4.10b. STIM1 puncta gradient versus ER-density gradient in migrating pancreatic ductal adenocarcinoma cells.

The distribution of ER-PM junctions (revealed by STIM1 puncta) exhibits an inverse relationship to the distribution of ER-density in migrating PANC-1 cells. Measurements of average calnexin fluorescence ± SEM and STIM1 puncta were measured from the ER leading edge (resolvable peripheral ER strands) of 8 cells.

4.5 Localisation of IP_3R1 and ER-PM junctions in migrating PANC-1 cells

After observing the redistribution of Ca^{2+} signalling complexes (i.e. IP_3Rs and STIM1-competent ER-PM junctions) in PANC-1 cells following EMT, the distributions of both IP_3R1 and ER-PM junctions were simultaneously examined in migrating cells. PANC-1 cells were transfected with TK-YFP-STIM1 for 24 hours prior to treatment with 30 μM CPA for 1 hour at 37°C / 5% CO_2. Alternatively, PANC-1 cells were transfected with both PM-targeted LL-FKBP-mRFP and ER-targeted CFP-FRB-LL linker constructs (Varnai *et al.*, 2007; Dingsdale *et al.*, 2013) for 24 hours before treatment with 100 nM rapamycin for 4-5 min at 37°C / 5% CO_2. After revealing ER-PM junctions by these methods, cells were fixed and immunostained with anti-IP_3R1 antibody. In migrating PANC-1 cells IP_3R1 decorated the leading edge whilst STIM1 puncta/ER-PM junctions concentrated in a closely adjacent region (just behind the leading edge) (Figures 4.11 and 4.12). All images show confocal sections taken from ventral parts of the cells located in the immediate proximity to the coverslip.

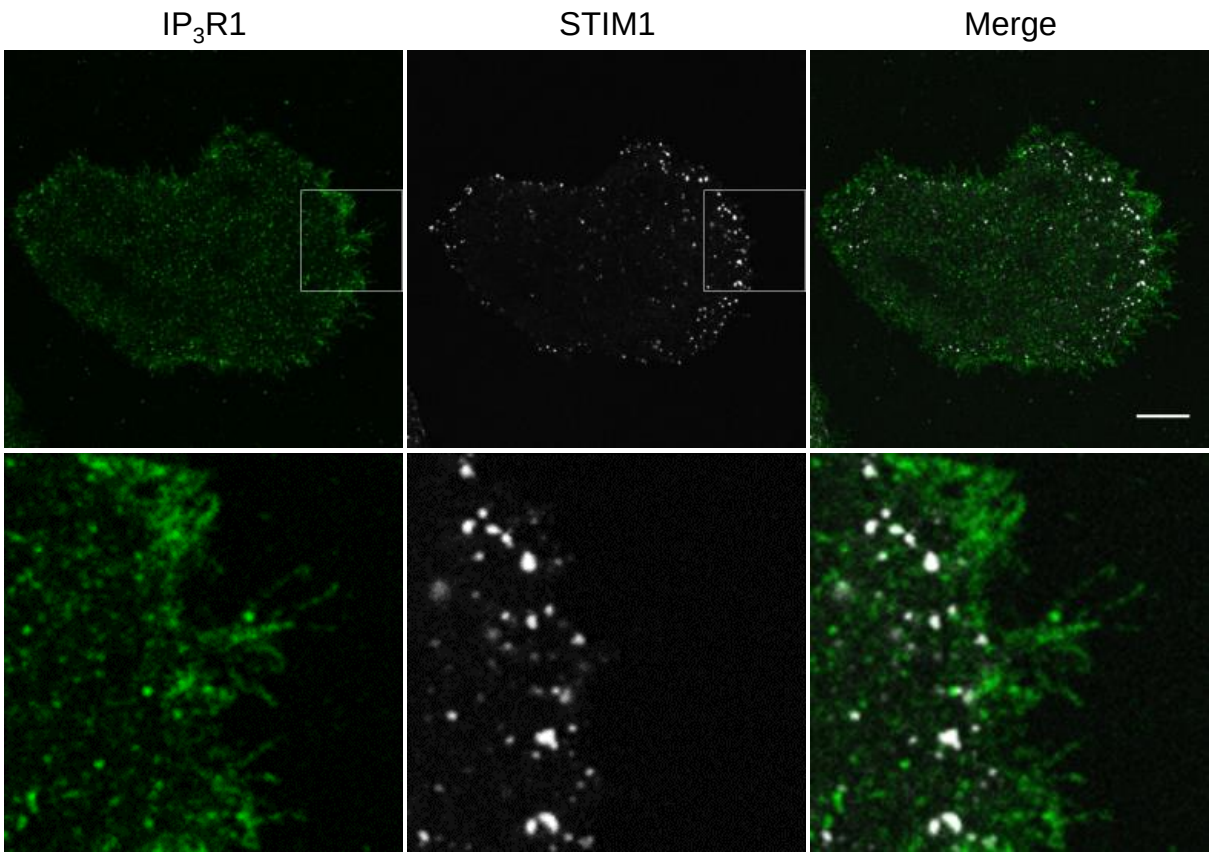

Figure 4.11. Relative positioning of IP_3R1 and STIM1 / ER-PM junctions in migrating pancreatic ductal adenocarcinoma cells.

In migrating PANC-1 cells IP_3R1 decorate the leading edge whilst STIM1 puncta concentrate in the adjacent region (just behind the leading edge). PANC-1 cells were transfected with TK-YFP-STIM1 and then treated with 30 μM CPA to reveal STIM1 puncta. Cells were then fixed and immunostained using anti-IP_3R1 antibody. All images show confocal sections taken from ventral parts of the cells located in the immediate proximity to the coverslip. Scale bar represents 10 μm. Bottom panel show the fragment outlined by the rectangle in left and central upper panels.

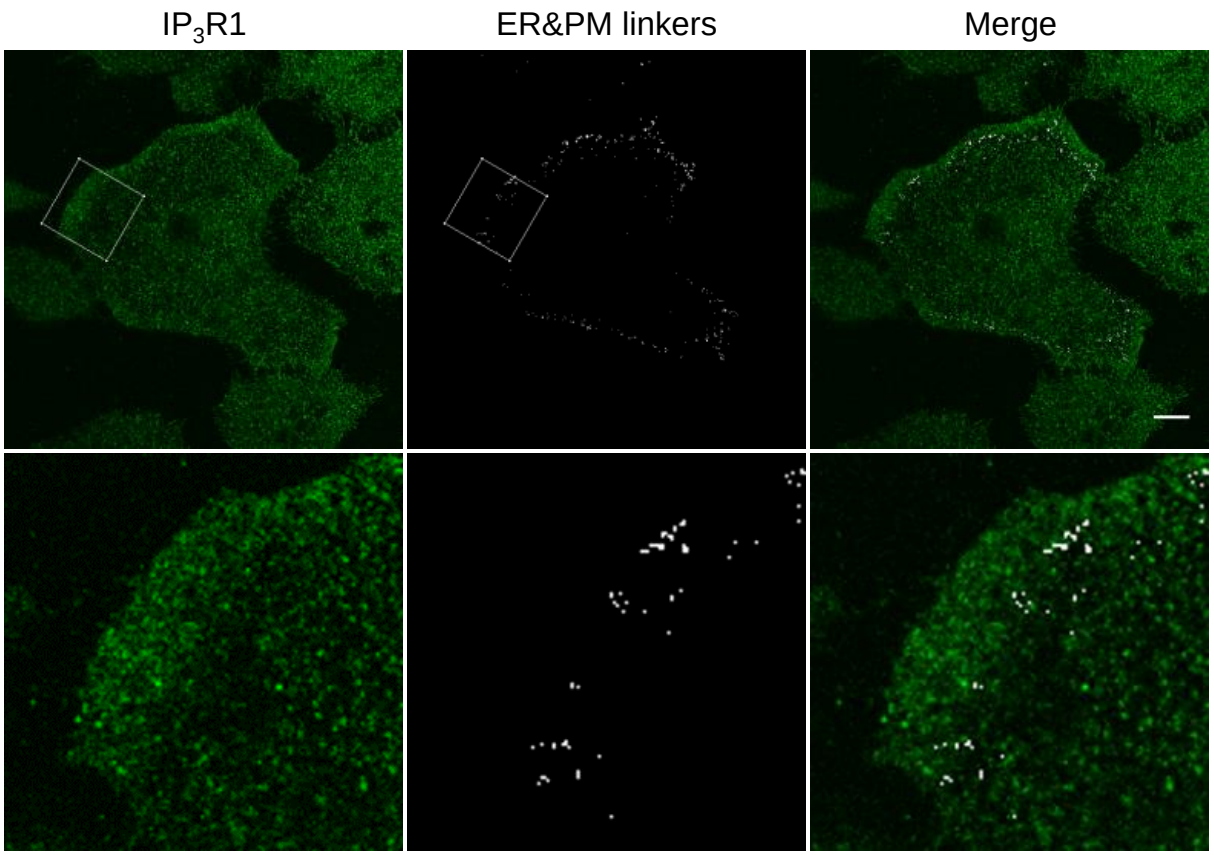

Figure 4.12. Relative positioning of IP_3R1 and ER-PM junctions (ER&PM linkers) in migrating pancreatic ductal adenocarcinoma cells.

In migrating PANC-1 cells IP_3R1 decorate the leading edge whilst ER-PM junctions concentrate in the adjacent region (just behind the leading edge). PANC-1 cells were transfected with both linker constructs ER-targeted CFP-FRB-LL and PM-targeted LL-FKBP-mRFP and then treated with 100 nM rapamycin to reveal ER-PM junctions. Cells were then fixed and immunostained using anti-IP_3R1 antibody. Scale bar represents 10 μm. Bottom panel show the fragment outlined by the rectangle in left and central upper panels.

Furthermore, the preferential localisation of IP_3R1 and ER-PM junctions at the front of migrating cells was also confirmed using super-resolution microscopy (Dempsey *et al.*, 2011; Metcalf *et al.*, 2013). In these experiments, employing dSTORM technique, we observed that the leading edge of migrating cells indeed had an increased density of IP_3R1 (Figure 4.13) and higher concentration of ER-PM junctions (Figure 4.14a). Note the increased resolution of dSTORM images (in x-y plane) in comparison to diffraction limited (in x-y plane) TIRF images taken from the same cellular regions (high magnification fragments in Figures 4.13, 4.14a and 4.14b). The actual size of both ER-PM junctions and clusters of IP_3R1 are significantly smaller than the limit of resolution of diffraction-limited microscopy but the preferential localisation at the leading edge was observed using all types of microscopy. dSTORM imaging, which has considerably improved axial and lateral resolution (60-70 nm) in comparison with conventional microscopy (~300 nm), confirmed that both IP_3R1 and ER-PM junctions can be observed close to the leading edge and in the immediate proximity to the ventral membrane of the migrating cells (i.e. portion of the membrane which is involved in forming contacts with the substratum and sliding along the substratum).

These experimental data show that STIM1-competent ER-PM junctions are positioned just behind IP_3R1s at the leading edge, creating a stratified distribution of Ca^{2+} signalling complexes at the front of migrating PDAC cells. In addition, the observed stratified distribution of Ca^{2+} signalling complexes at the leading edge suggests that these complexes could be important for the migration of PDAC cells (see chapter 5).

Figure 4.13. Positioning of IP_3R1 in migrating pancreatic ductal adenocarcinoma cells imaged at super-resolution level.

Super-resolution microscopy of IP_3R1 at the leading edge of a PANC-1 cell. Left panel shows the leading edge of a cell immunostained using antibody against IP_3R1 and imaged using a TIRF microscope ("diffraction-limited" refers to its lateral resolution). Scale bar corresponds to 1 μm. The fragment, highlighted as a square on the left panel, was then imaged using dSTORM and the result is shown on the central panel. Scale bar corresponds to 1 μm. Right panel (Merge) shows co-positioning of the two images. Expanded fragments on the middle and bottom panels are taken from the peripheral regions indicated by arrowheads on the 'Merge' (left arrowhead corresponds to the middle set of images). Note the improvement of resolution in comparison with diffraction limited images (left panels). Lateral dSTORM resolution in these experiments was approximately 60-70 nm.

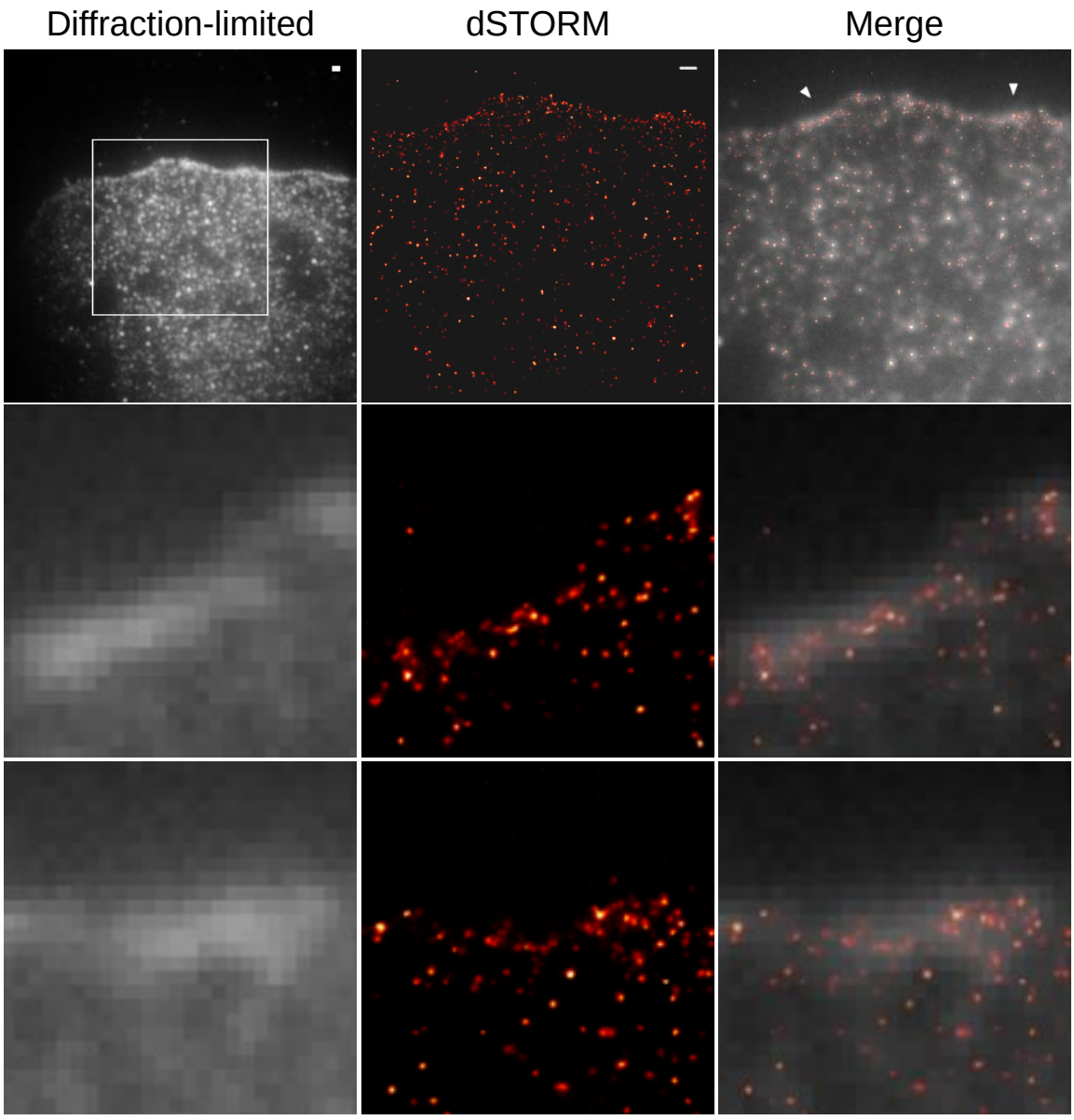

Figure 4.13

Figure 4.14a. Positioning of ER-PM junctions (ER&PM linkers) in migrating pancreatic ductal adenocarcinoma cells imaged at super-resolution level.

Super-resolution microscopy of ER-PM junctions near the leading edge of PANC-1 cells. PANC-1 cells transfected with both linker constructs (PM-targeted FBKP-LL-mRFP and ER-FRB-LL-CFP) were fixed after treatment with 100 nM rapamycin to highlight the pre-existing ER-PM junctions without ER Ca^{2+} store depletion. PANC-1 cells were then stained using anti-GFP antibody (which also recognizes CFP) to reveal ER-FRB-LL-CFP accumulated in ER-PM junctions. Left panel shows localisation of ER-PM junctions visualised using a TIRF mode ("diffraction-limited" refers to its lateral resolution). Scale bar corresponds to 1 μm. The plasma membrane border outline on this panel was generated using the Threshold and Wand (tracing) tool functions of Image J (see figure 4.15). The fragment, highlighted as a square on the left upper panel, was then imaged using dSTORM and the result is shown on the central panel. Scale bar corresponds to 1 μm. Right panel (Merge) shows co-positioning of the two images. Expanded fragments on the middle and bottom panels are taken from the peripheral regions highlighted on the Merge image by arrowheads (upper arrowhead corresponds to the middle set of images).

Note the improvement of resolution in comparison with diffraction-limited images (left panels). Lateral dSTORM resolution in these experiments was approximately 60-70 nm.

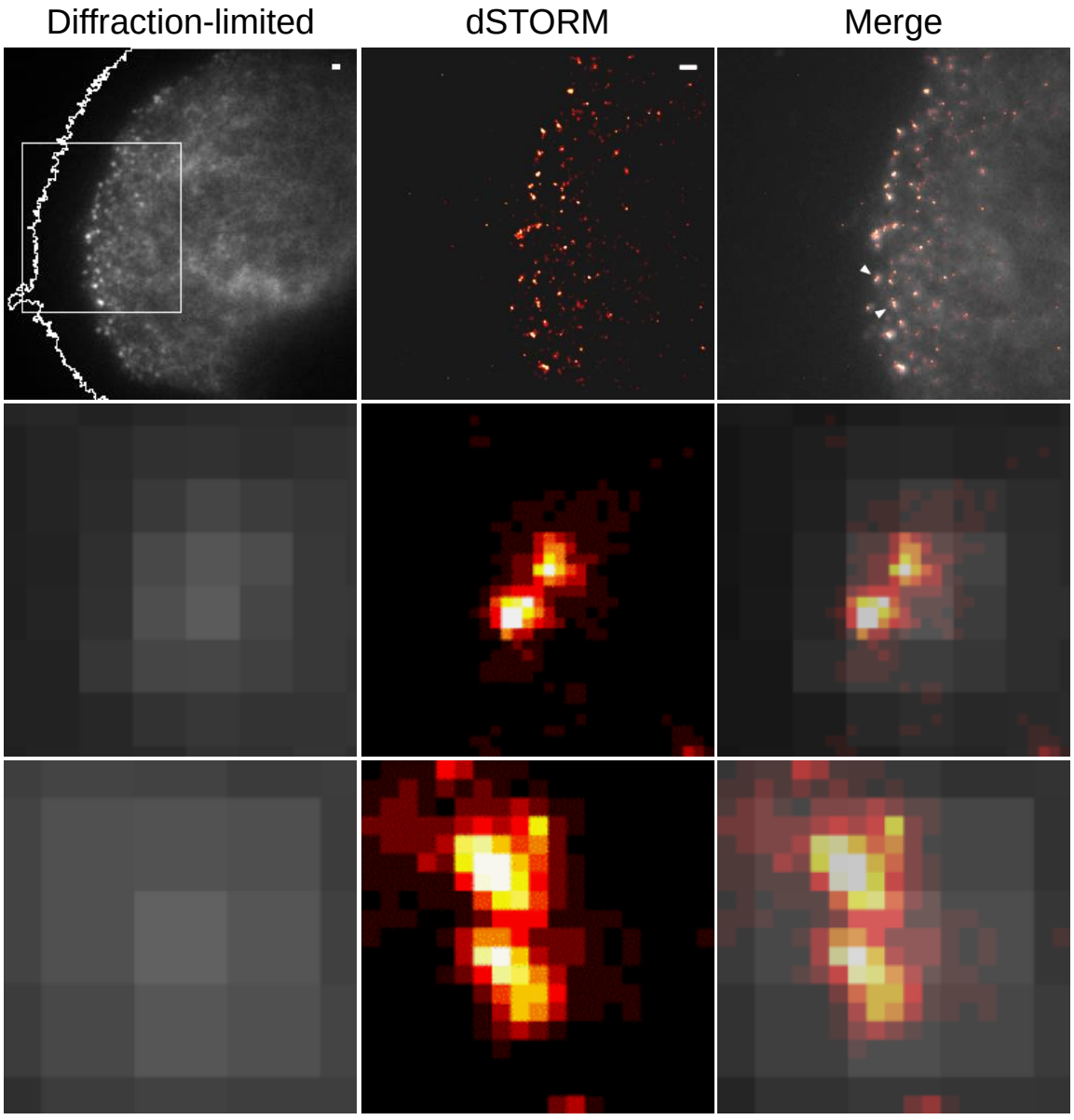

Figure 4.14a

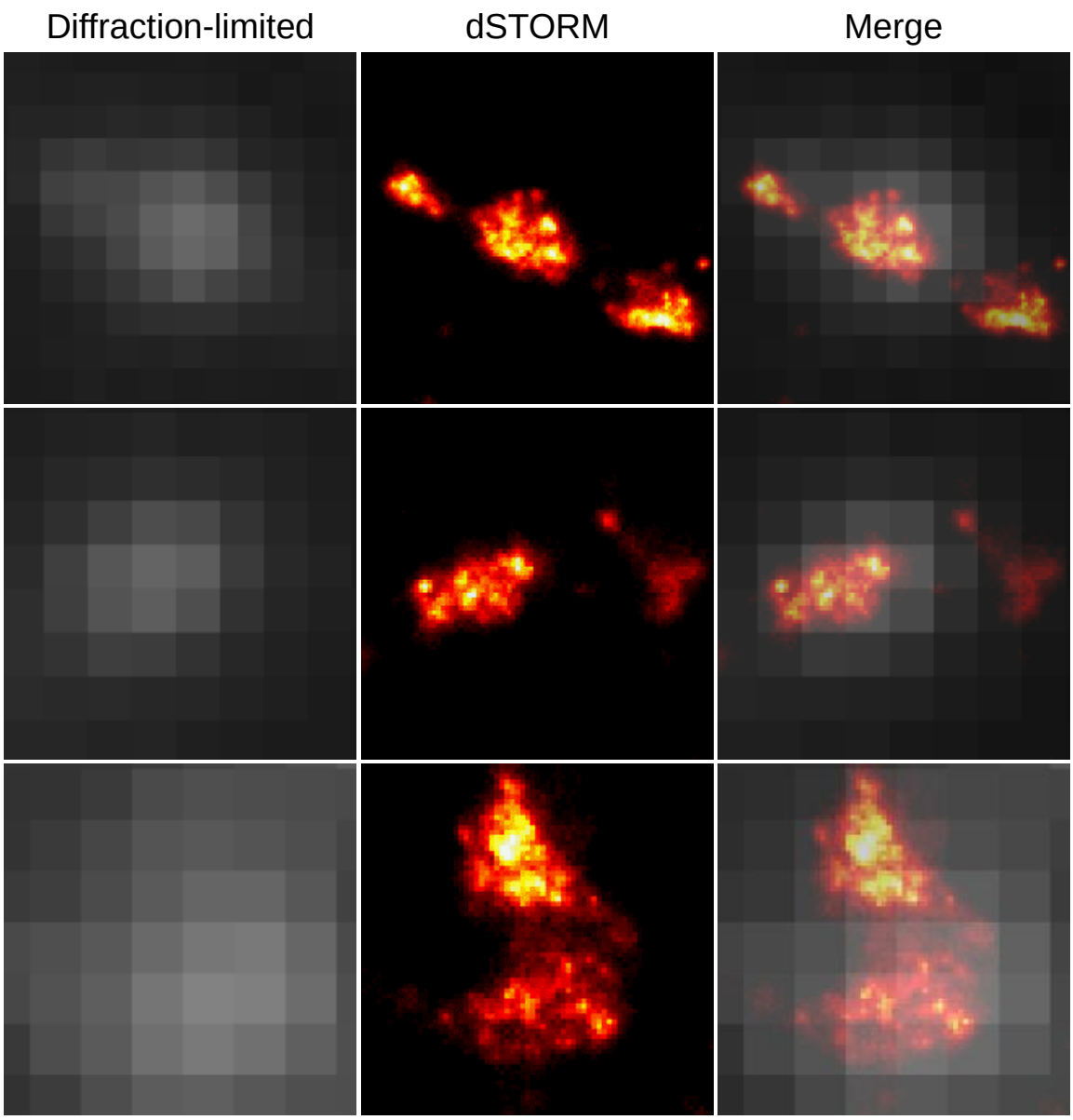

Figure 4.14b. ER-PM junctions (ER&PM linkers) in migrating pancreatic ductal adenocarcinoma cells imaged at super-resolution level.

Expanded fragments taken from the peripheral regions of other super-resolution images (not shown). Note the improvement of resolution in comparison with diffraction limited images (left panels). Lateral dSTORM resolution in these experiments was approximately 60-70 nm.

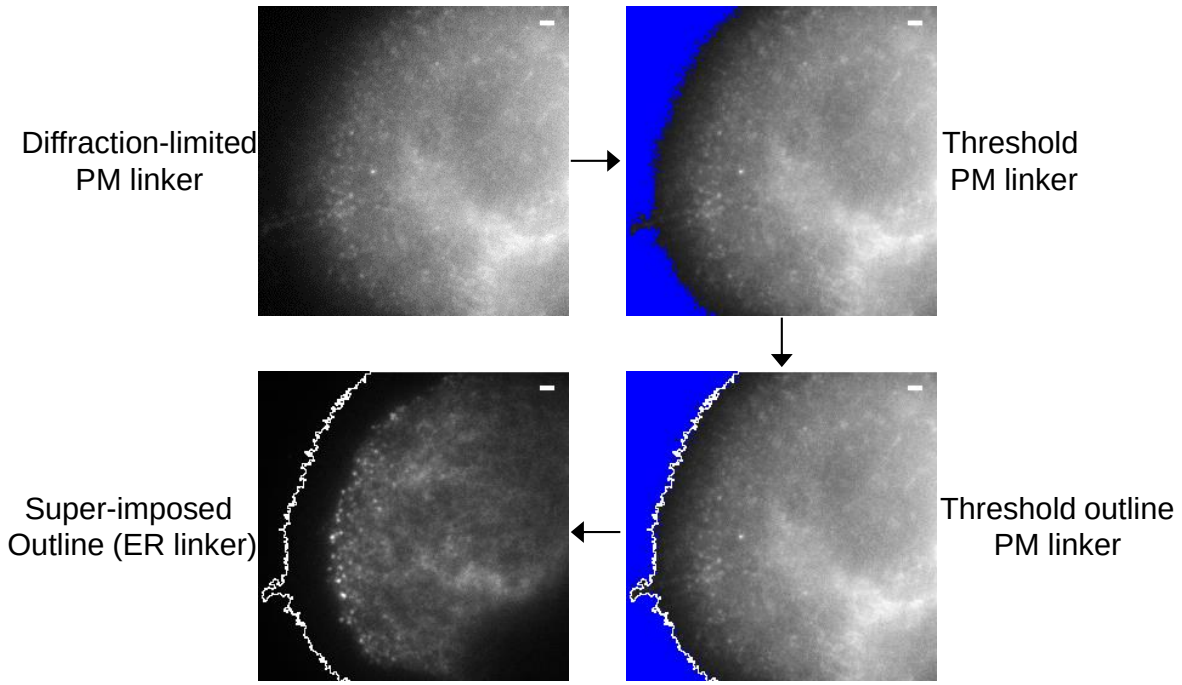

Figure 4.15. A procedure for determining the outline of the leading edge and superimposing it on image of ER-PM junctions.

This image set shows how the plasma membrane border outline on the diffraction-limited image of ER-PM junctions (figure 4.14a) was created by using the Threshold and Wand (tracing) tool functions in Image J software. Briefly, image of PM linker was adjusted to threshold points until the plasma membrane border can be distinguished (top right) and then the now-distinguishable border line was mapped using the Wand tracing tool (bottom right). Finally the mapped outline was super-imposed onto the ER linker image using ROI manager add tool in Image J (bottom left). Scale bars represent 2 μm.

4.6 Discussion

In this chapter I show that PANC-1 cells undergo dramatic morphological changes from apical-basal polarity to front-rear polarity upon EMT observed using light microscopy approach. The morphological changes we observed are phenotypic characteristic hallmarks of the EMT switch (Hanahan & Weinberg, 2011; Lamouille *et al.*, 2014). EMT is integral to a number of physiological processes including embryogenesis, organ development, and wound healing and tissue regeneration after damage (Lamouille *et al.*, 2014). Moreover, cancer cells have adopted the physiological process of EMT to enable the development of motile and invasive signatures in order to aid their metastatic nature, survival and progression. Reverse EMT also known as mesenchymal-epithelial transition (MET) cooperates with EMT to facilitate the formation of cancer metastases at distant sites from primary tumour sites (Thiery *et al.*, 2009; Hanahan & Weinberg, 2011; Chang *et al.*, 2012). A number of studies have reported the importance of EMT in cervical (Ricono *et al.*, 2009), ovarian (Ahmed *et al.*, 2006) and liver (Fuchs *et al.*, 2008) cancers as well as in the progression of pancreatic cancer (Li *et al.*, 2009; Cano *et al.*, 2010; Hotz *et al.*, 2011; Wang *et al.*, 2011; Chang *et al.*, 2012).

The formation of new cellular front-rear polarity is characterised by the formation of broad, ruffling lamellipodia, and filopodia-like protrusions at the front leading edge while at the cell rear is the trailing tail. We observed that the newly formed front-rear polarity in individual migrating PANC-1 cells upon EMT is accompanied by the redistribution of ER Ca^{2+} release channels IP_3Rs – specifically of IP_3R1 and IP_3R2 but not IP_3R3. IP_3R1 and IP_3R2 underwent redistribution from intercellular junctions and perinuclear regions in connected PANC-1 cells, respectively, to the specialised

front leading edge of individual migrating PANC-1 cells upon EMT (Figures 4.2 and 4.5). In addition to the observed redistribution of IP_3Rs, the distribution of SOCE-competent ER-PM junctions was monitored during EMT switch. Pre-existing ER-PM junctions as revealed by ER-PM linkers and the sum-total of pre-existing and newly formed ER-PM junctions as revealed by STIM1 puncta formation following ER Ca^{2+} store depletion also underwent redistribution from near-intercellular junctions to the leading edge of individual migrating PANC-1 cells. A recent study from our group also showed that SOCE-competent ER-PM junctions prominently decorate the leading edge of migrating PANC-1 cells, and ER density was not increased but instead decreased towards the cell periphery (Dingsdale *et al.*, 2013). Upon EMT and disconnection of individual cells from their neighbours, E-cadherin staining was not detectable in individual migrating PANC-1 cells with mesenchymal phenotype (N = ≥3, data not shown), supporting the loss of epithelial phenotype. This is consistent with previously reported findings of the down-regulation of 'epithelial' genes during EMT switch and thus epithelial intercellular junction complexes (tight junction components, adherens junction components and desmosomes components) are destabilised, deconstructed, trafficked away from the intercellular junctions and perhaps degraded (Chang *et al.*, 2012; Lamouille *et al.*, 2014). Particularly, Chang and colleagues showed that the cellular depletion of EFGR in PANC-1 cells suppressed EMT and to a significant extent reversed EMT (MET) by restoring apical-basal polarity and intercellular junctions as the epithelial phenotype marker E-cadherin was augmented. Concomitantly, the mesenchymal markers including N-cadherin, vimentin and fibronectin, and transcription factors SNAIL and SLUG were significantly decreased (Chang *et al.*, 2012). In addition, a number of other studies

have reported that EGF and EGFR induce EMT in cervical (Ricono *et al.*, 2009), ovarian (Ahmed *et al.*, 2006) and liver (Fuchs *et al.*, 2008) cancers.

It is widely reported and generally accepted that dramatic morphological changes from apical-basal to front-rear polarity observed at the cellular level upon EMT is also accompanied by remodelling of the actin cytoskeleton and other intracellular proteins and structures at the subcellular level (Nelson, 2009; Chang *et al.*, 2012; Lamouille *et al.*, 2014). This is in line with the observed redistribution of IP_3R1 and IP_3R2 during EMT switch. However, IP_3R3 failed to undergo redistribution and was retained in the perinuclear region of individual migrating PANC-1 cells. The distribution of ER network in polarised connected PANC-1 cells (epithelial phenotype) and in individual migrating PANC-1 cells (mesenchymal phenotype) was determined (compare Figure 4.10 from this chapter to Figure 3.21 from chapter 3) and surprisingly was similar i.e. the density of ER network is enriched in the perinuclear region and reduced towards the cell periphery in both cases. This suggests that bulk ER network is resistant to remodelling in PANC-1 cells upon EMT, and that IP_3R3 are not dynamic but rather somehow immobilised in the perinuclear bulk ER region where they are resistant to redistribution following EMT. On the other hand, perinuclear-localised IP_3R2 as well as intercellular junctional-localised IP_3R1 in connected PANC-1 cells underwent redistributions to concentrate at the leading edge of individual migrating PANC-1 cells, suggesting that IP_3R1 and IP_3R2 isoforms are significantly more mobile than IP_3R3s, and hence can be translocated to specialised regions (possibly that of cortical ER) in close proximity to the leading edge plasma membrane upon EMT through a currently unknown mechanism. Isoforms of IP_3R have been reported to exhibit different mobility within the ER membrane (Pantazaka & Taylor, 2011). A possible mechanism underlying the redistribution of IP_3R1 upon EMT could be

mediated via the polarity complexes (Crumbs, PAR and Scribble), as they have also been reported to redistribute from the intercellular junctional area to the leading edge of migrating cells following EMT (Nelson, 2009; Lamouille *et al.*, 2014). It is also possible that phospholipids such as phosphatidylinositol 4,5-bisphosphate (PIP_2) and phosphatidylinositol 3,4,5-bisphosphate (PIP_3), which have been shown to redistribute during EMT (Saarikangas *et al.*, 2010) could play a part in the redistribution of IP_3R1 upon EMT.

In view of the highly polarised distribution of IP_3R1 at intercellular junctions and at the leading edge in connected and migrating PANC-1 cells, respectively, I next examined the subcellular spatial relationship of IP_3R1 Ca^{2+} release platforms and SOCE-competent ER-PM junctions in individual migrating PANC-1 cells. Interestingly, it was observed that Ca^{2+} release platforms (IP_3R1) and Ca^{2+} replenishing platforms (ER-PM junctions) were both localised at the leading edge of migrating PANC-1 cells, where the ER-PM junctions were positioned just behind the IP_3R1 positive region at the leading edge. The positional relationship between Ca^{2+} release and Ca^{2+} replenishing signalling complexes has been demonstrated in non-motile polarised pancreatic acinar cell clusters, which showed that apically-localised IP_3Rs Ca^{2+} release channels are spatially segregated from the basolaterally-positioned SOCE/ER-PM junctions (Lur *et al.*, 2009). This is the first study to demonstrate the spatial relationship of Ca^{2+} release and Ca^{2+} replenishing signalling complexes at the leading edge of migrating cells, suggesting that a stratified distribution of Ca^{2+} signalling complexes might be a strategy employed by both normal and cancerous cells of the exocrine pancreas to achieve and maintain effective co-ordination of Ca^{2+} signals in proximity to migratory apparatus. The localisation of both IP_3R1 and ER-PM junctions was also observed at the leading

edge of individual migrating PANC-1 cells using dSTORM super-resolution imaging technique (see methods section), which has considerably improved axial and lateral resolution of ~60 nm in comparison to the conventional confocal microscope (~300 nm). dSTORM imaging also showed that both IP_3R1 and ER-PM junctions can be observed in the immediate proximity to the ventral membrane area of the leading edge in migrating PANC-1 cells (in other words, the region of the membrane involved in forming contacts with and sliding along the substratum). A number of recent studies have reported the importance of Ca^{2+} signalling for cell migration (Wei *et al.*, 2009; Yang *et al.*, 2009; Middelbeek *et al.*, 2012; Schafer *et al.*, 2012; Tsai & Meyer, 2012; Tsai *et al.*, 2014). Ca^{2+} responses have been shown to both potentiate (Wei *et al.*, 2009; Yang *et al.*, 2009; Middelbeek *et al.*, 2012; Schafer *et al.*, 2012; Tsai *et al.*, 2014) and suppress migration (Tsai *et al.*, 2014), depending on cell type and extracellular environment. Considering the observed prominent stratified localisation of IP_3Rs and STIM1-competent ER-PM junctions at the leading edge of migrating PANC-1 cells, I next tested the importance of IP_3Rs and SOCE for the migration of pancreatic ductal adenocarcinoma cells.

Chapter 5: IP_3Rs and ER-PM junctions regulate pancreatic ductal adenocarcinoma cell migration

Chapter 5: IP_3Rs and ER-PM junctions regulate pancreatic ductal adenocarcinoma cell migration

5.1 Cell migration and its regulation by IP_3Rs and SOCE

Cell migration is a highly co-ordinated cellular behaviour which is important for numerous physiological processes including embryogenesis, organ development, immune surveillance, wound healing and tissue regeneration (Valeyev *et al.*, 2006; Ridley, 2011; Roussos *et al.*, 2011; Lamouille *et al.*, 2014). The process of cell migration is also essential for the development, spreading and progression of cancer (Hanahan & Weinberg, 2000, 2011; Roussos *et al.*, 2011; Lamouille *et al.*, 2014). Ca^{2+} has been documented to be a critical regulator of cell migration in many cell types (Brundage *et al.*, 1991; Berridge *et al.*, 1998; Pettit & Fay, 1998; Berridge *et al.*, 2000; Wei *et al.*, 2009; Yang *et al.*, 2009; Middelbeek *et al.*, 2012; Tsai *et al.*, 2014). Ca^{2+} signals produced by both IP_3R-mediated Ca^{2+} release from intracellular stores and Ca^{2+} influx across the PM via STIM1-gated Orai1 channels and transient receptor potential (TRP, specifically TRPM7) channels have all been shown to be critical for migration in a number of cell types (Wei *et al.*, 2009; Yang *et al.*, 2009; Middelbeek *et al.*, 2012; Schafer *et al.*, 2012; Tsai & Meyer, 2012; Tsai *et al.*, 2014). In this part of the study, we investigated the significance of IP_3Rs and SOCE for the migration of PANC-1 cells using multiple cell migration assays, and studied how these Ca^{2+} signalling complexes regulate the migratory apparatus in order to control migration in this cancer cell type.

5.2 Inhibition of IP_3-induced Ca^{2+} release and store-operated Ca^{2+} entry (SOCE) suppresses PANC-1 cell migration

After characterising a remarkable redistribution and positioning of IP_3Rs and STIM1-competent ER-PM junctions at the leading edge of migrating PANC-1 cells, and considering their subcellular localisation I next sought to determine whether or not IP_3Rs and ER-PM junctions are essential for the migration of PDAC cells. Employing Xestospongin-B (selective inhibitor of IP_3Rs (Jaimovich *et al.*, 2005); see Figure 3.6) and GSK-7975A (selective inhibitor of store-operated Ca^{2+} channels Orai1 and Orai3 (Derler *et al.*, 2013)), and using Boyden chamber migration assay with symmetric Foetal Bovine Serum (FBS) distribution (1% (v/v) FBS in both upper and lower chambers), it was found that both Xestospongin-B and GSK-7975A significantly inhibit the migration of PANC-1 cells (Figure 5.1). Using asymmetric FBS distribution (0% (v/v) FBS in upper chamber and 5% (v/v) FBS in lower chamber) as a model of chemotactic migration, it was observed that both Xestospongin-B and GSK-7975A significantly inhibit the migration of PANC-1 cells (Figure 5.2). Note that inhibitory effects of Xestospongin-B and GSK-7975A on the migration of PANC-1 cells were stronger in experiments with asymmetric FBS distribution (Figure 5.2 compared to Figure 5.1). In the chemotactic condition, Xestospongin-B inhibited migration by 74 ± 9% (Mean ± SEM), and GSK-7975A inhibited migration by 84 ± 3%. Furthermore, both Xestospongin-B and GSK-7975A also inhibited PANC-1 cell migration as measured by wound-healing assay (Figure 5.3). A zero FBS condition (0% FBS in both chambers) was employed for comparison, and this effectively inhibits PANC-1 cell migration (Figures 5.1 – 5.3). Moreover, neither Xestospongin-B nor GSK-7975A induced substantial cellular toxicity (Figures 5.4 and 5.5).

Our experimental data showing strong inhibition of migration by Xestospongin-B and GSK-7975A suggest that the striking accumulation of IP_3Rs and STIM1/SOCE-competent ER-PM junctions at the leading edge of PDAC cells has a clear function, which is to provide Ca^{2+} signals important for the migration of this type of cancer cell.

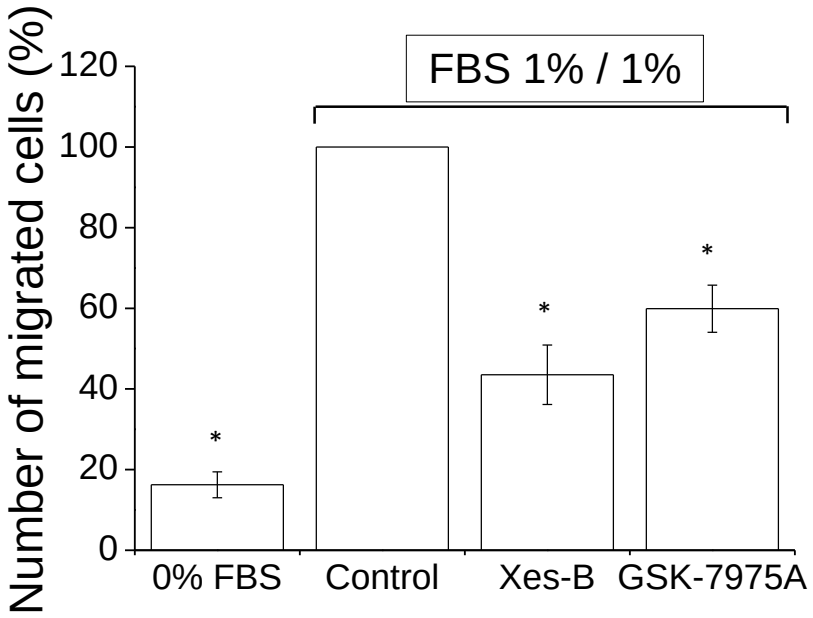

Figure 5.1. Inhibition of IP_3Rs and SOCE suppress pancreatic ductal adenocarcinoma cell migration.

Xestospongin-B and GSK-7975A suppress migration of PANC-1 cells. PANC-1 cells were subjected to symmetric (1% FBS in both chambers) Boyden chamber migration assay for 6 hours at 37°C in the absence (Control) or presence of the inhibitors. No FBS condition (0% FBS in both chambers) was employed for comparison (this effectively inhibits cell migration). The effects of the inhibitor-treated groups were obtained as a function of normalisation to the control group; normalisation was conducted for each individual experiment. Mean ± SEM was obtained from at least 3 independent experiments. In all cases the number of migrated cells in the presence of an inhibitor was statistically different from that in the control condition.

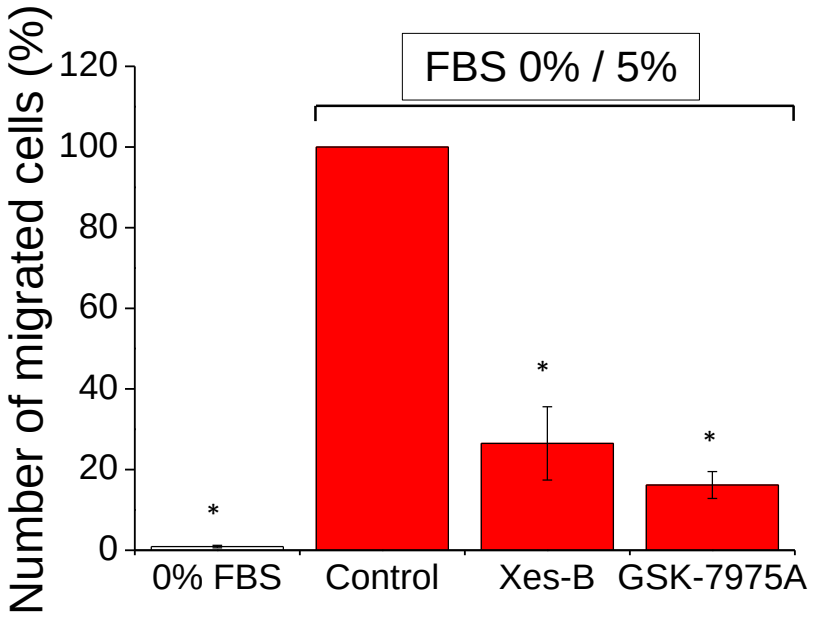

Figure 5.2. Inhibition of IP_3Rs and SOCE suppress pancreatic ductal adenocarcinoma cell migration.

Xestospongin-B and GSK-7975A suppress migration of PANC-1 cells. PANC-1 cells were subjected to asymmetric (0% FBS in upper chamber and 5% FBS in lower chamber) Boyden chamber migration assay for 6 hours at 37°C in the absence (Control) or presence of the inhibitors. No FBS condition (0% FBS in both chambers) was employed for comparison (this effectively inhibits cell migration). The effects of the inhibitor-treated groups were obtained as a function of normalisation to the control group; normalisation was conducted for each individual experiment. Mean ± SEM was obtained from at least 3 independent experiments. In all cases the number of migrated cells in the presence of an inhibitor was statistically different from that in the control condition.

Figure 5.3. Inhibition of IP_3Rs and SOCE suppress pancreatic ductal adenocarcinoma cell migration measured using wound-healing assay.

Xestospongin-B and GSK-7975A suppress migration of PANC-1 cells. PANC-1 cells seeded on uncoated glass-bottom dishes with ibidi cell culture inserts were subjected to a wound-healing assay for 18 hours at 37°C in the absence (Control) or presence of the inhibitors. No FBS condition (0% FBS) was employed for comparison (this effectively inhibits cell migration). Wound area was imaged at time 0 and 18 hours. Mean ± SEM was obtained from at least 3 independent experiments. In all cases the number of migrated cells in the presence of an inhibitor was statistically different from that in the control condition.

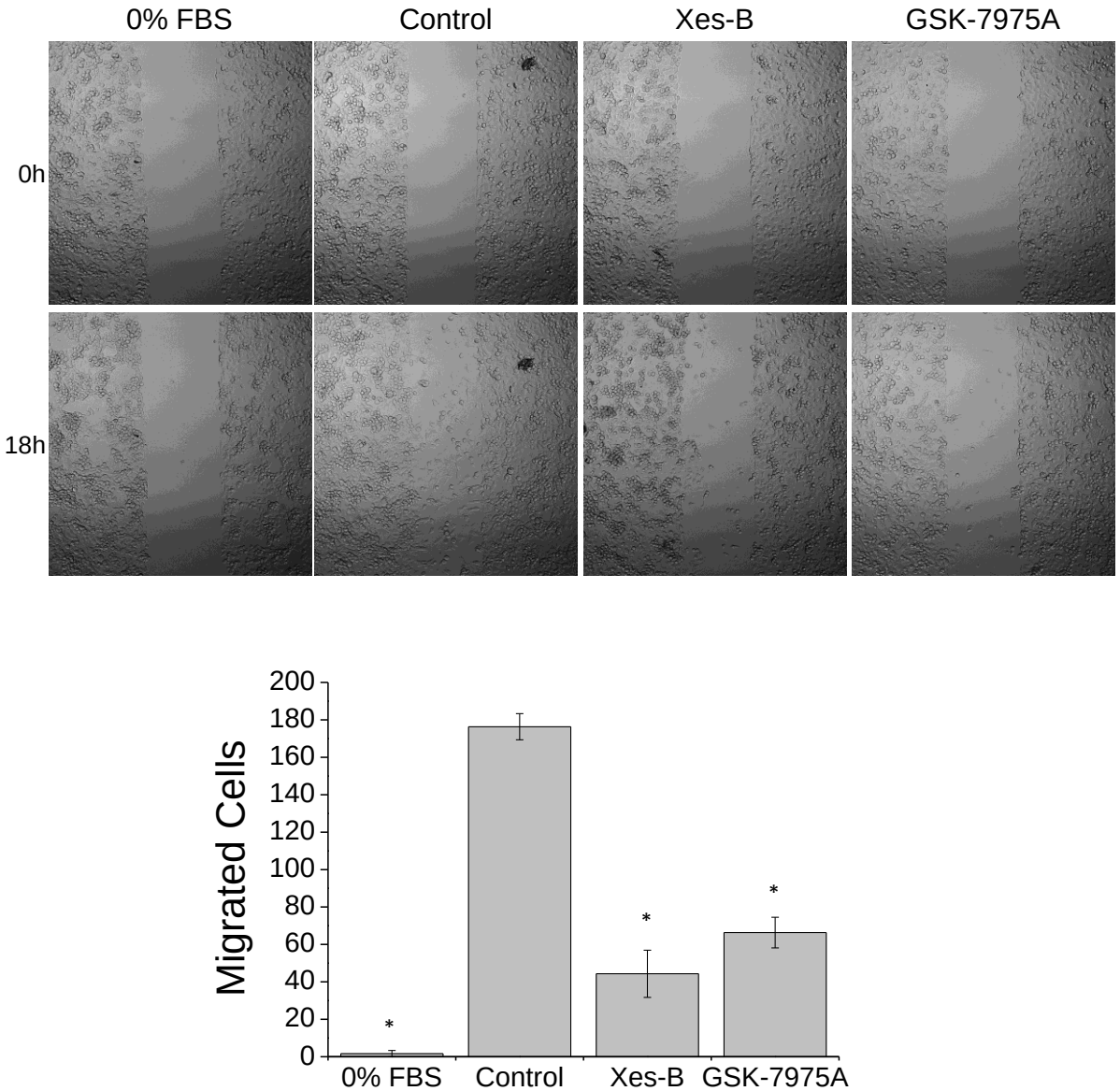
0% FBS
Control
Xes-B
GSK-7975A
0h
18h
Migrated Cells
200
180
160
140
120
100
80
60
40
20
0
*
*
*
0% FBS
Control
Xes-B
GSK-7975A

Figure 5.3

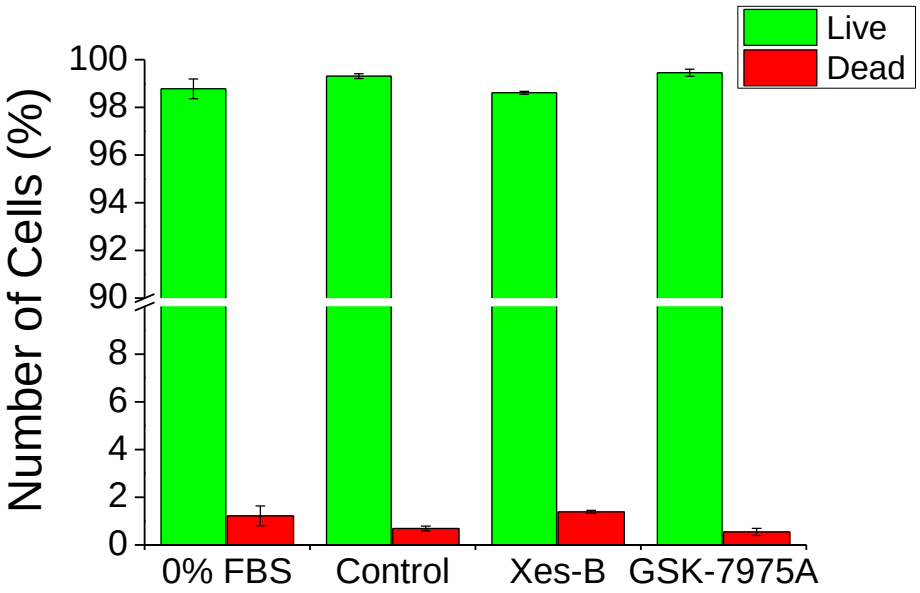

Figure 5.4. Xestospongin-B and GSK-7975A did not induce substantial cellular toxicity in pancreatic ductal adenocarcinoma cells.

PANC-1 cells were incubated without / with 50 μM Xestospongin-B or 30 μM GSK-7975A for 6 hours at 37°C / 5% CO_2 to mimic the condition employed in Boyden chamber and wound-healing migration assays. Post-incubation, PANC-1 cells were co-incubated with Hoechst-33342 (cellular nuclei marker for total cell count) and Sytox orange (red, cellular nuclei marker for cells with compromised plasma membrane i.e. dead cells) for 20 min at 37°C / 5% CO_2 prior to cell imaging. Green column indicates live cells and the number of live cells were calculated by subtracting Sytox orange-stained positive cells (red, dead cells) from Hoechst-stained positive cells (total cell count). Red column indicates dead cells. Mean ± SEM was obtained from at least 3 independent experiments. In all cases the number of live/dead cells in the presence of an inhibitor was not statistically different from that in the control condition.

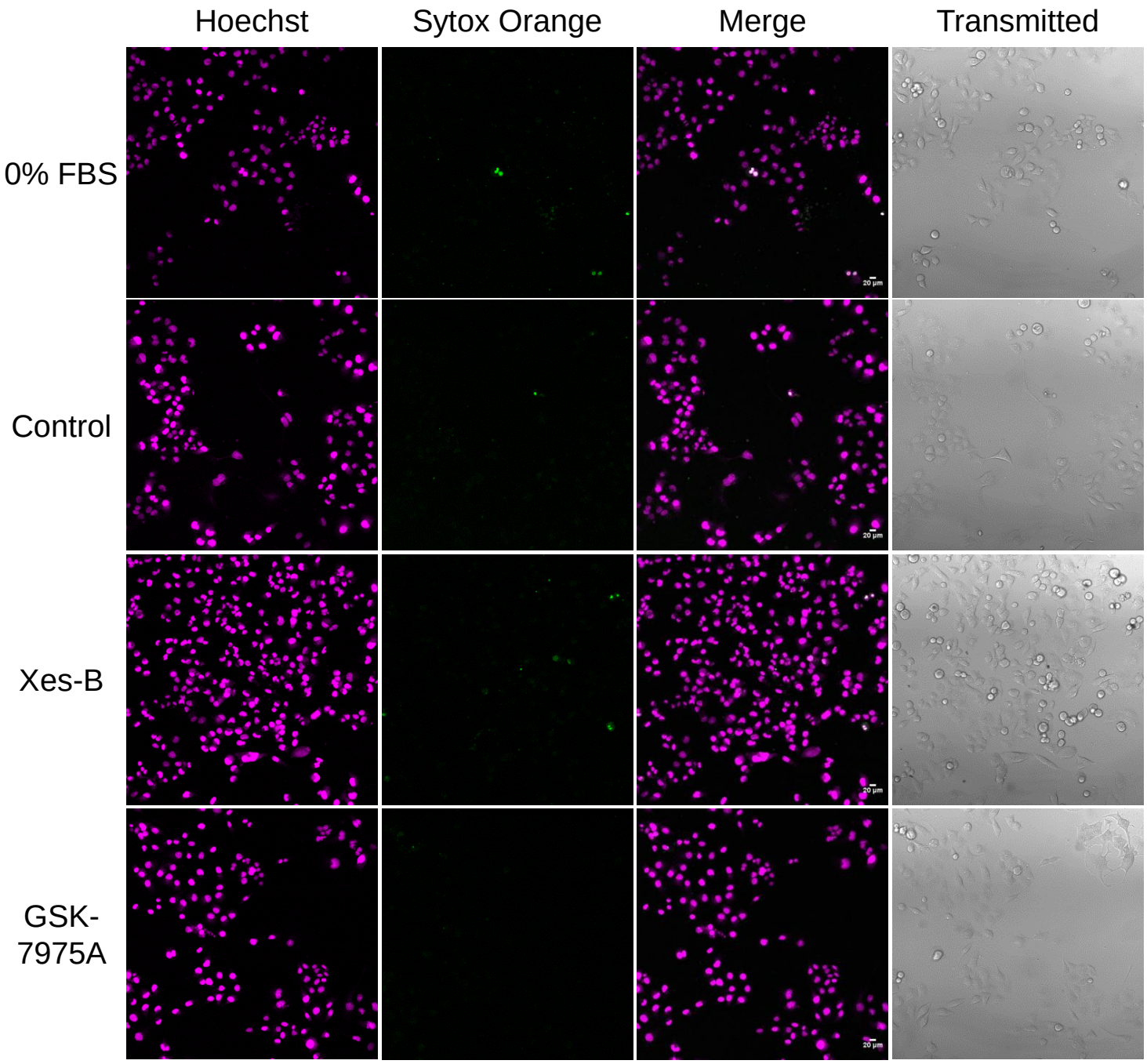

Figure 5.5. Xestospongin B and GSK-7975A did not induce cellular toxicity in pancreatic ductal adenocarcinoma cells.

Representative images showing Hoechst 33342- and Sytox orange-stained cells in the presence or absence of the inhibitors of specific Ca^{2+} signalling complexes employed in this experiment.

5.3 Cellular depletion of IP_3Rs suppresses PANC-1 cell migration

After using the specific pharmacological inhibitor Xestospongin-B to demonstrate that IP_3Rs are important for the migration of PDAC cells, it was necessary to determine whether all 3 isoforms or a particular isoform of IP_3R is responsible for providing the Ca^{2+} signals required for PDAC cell migration. To address this question, the effect of siRNA knockdown of each isoform of IP_3R on the chemotactic model of cell migration was examined. Cellular depletion of IP_3R1 significantly inhibited cell migration by 58 ± 6% (Figure 5.6, upper panel). Similar significant inhibitory effect on cell migration (by 36 ± 1%) was observed after siRNA knockdown of IP_3R2 (Figure 5.7, upper panel), although the magnitude of inhibition observed after IP_3R2 knockdown was less than that observed after IP_3R1 knockdown. siRNA knockdown of IP_3R3 had no effect on cell migration (Figure 5.8, upper panel). To confirm the cellular depletion of each isoform of IP_3R, the extent of knockdown of each isoform of IP_3R was analysed by Western blotting. Western blot profiles showed clear evidence for IP_3R1 (Figure 5.6, lower panels), IP_3R2 (Figure 5.7, lower panels) and IP_3R3 (Figure 5.8, lower panels) knockdown.

These experimental observations indicate that the cellular depletion of IP_3R1 and IP_3R2 suppressed the migration of PDAC cells, and that IP_3R1 and IP_3R2 but not IP_3R3 are the isoforms responsible for providing Ca^{2+} signals required for PDAC cell migration. This finding is in agreement with the previous observation of the formation of new cellular (front-rear) polarity after EMT, which was accompanied by the redistribution of IP_3R1 and IP_3R2 (but not IP_3R3) from cell-cell contacts and the perinuclear region in connected PDAC cells, respectively, to preferential localisation at the leading edge.

Figure 5.6. Cellular depletion of IP_3R1 suppresses pancreatic ductal adenocarcinoma cell migration.

siRNA knockdown of IP_3R1 inhibits the chemotactic migration of pancreatic ductal adenocarcinoma cells. PANC-1 cells were subjected to chemotactic (asymmetric; 0% FBS in upper chamber and 5% FBS in lower chamber) Boyden chamber migration assay for 6 hours at 37°C / 5% CO_2, 72 hours post-transfection with IP_3R1 siRNA (R1 siRNA) or non-targeting siRNA (NC siRNA) oligomer sequences. The effect of the targeting siRNA group was obtained as a function of normalisation to the non-targeting control group. Mean ± SEM was obtained from at least 3 independent experiments.

Western blot profile shows the evidence for IP_3R1 siRNA knockdown (lower panel). IP_3R1 and actin levels were quantified using Image J densitometry tool. The amount of IP_3R1 was obtained as a function of normalisation to the amount of actin protein. Actin blot was used as a loading control. Mean ± SEM was obtained from at least 3 independent experiments. Unpaired t-test with a two-tailed distribution and unequal variance was applied. In all cases, the number of migrated cells and the amount of IP_3R1 protein after IP_3R1 knockdown were statistically different from that in the control conditions

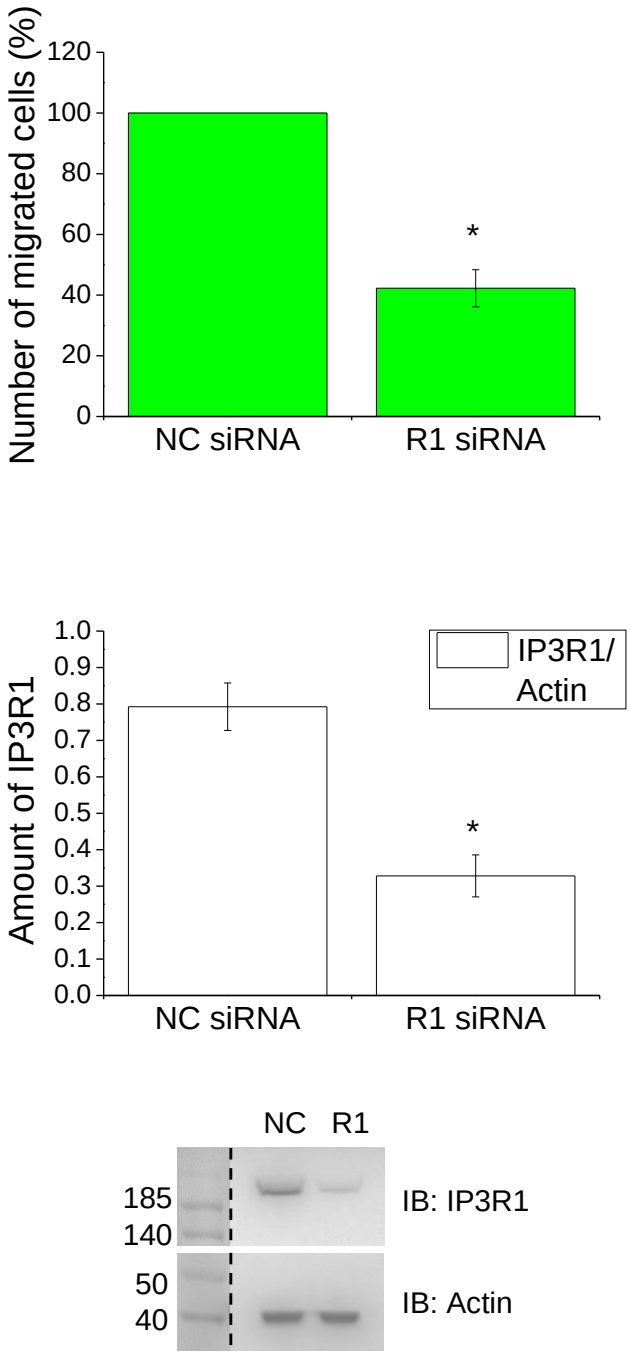
Number of migrated cells (%)
120
100
80
60
40
20
0
*
NC siRNA
R1 siRNA
Amount of IP3R1
1.0
0.9
0.8
0.7
0.6
0.5
0.4
0.3
0.2
0.1
0.0
IP3R1/
Actin
*
NC siRNA
R1 siRNA
NC
R1
185
140
IB: IP3R1
50
40
IB: Actin

Figure 5.6

Figure 5.7. Cellular depletion of IP_3R2 suppresses pancreatic ductal adenocarcinoma cell migration.

siRNA knockdown of IP_3R2 inhibits the chemotactic migration of pancreatic ductal adenocarcinoma cells. PANC-1 cells were subjected to chemotactic (asymmetric; 0% FBS in upper chamber and 5% FBS in lower chamber) Boyden chamber migration assay for 6 hours at 37°C / 5% CO_2, 72 hours post-transfection with IP_3R2 siRNA (R2 siRNA) or non-targeting siRNA (NC siRNA) oligomer sequences. The effect of the targeting siRNA group was obtained as a function of normalisation to the non-targeting control group. Mean ± SEM was obtained from at least 3 independent experiments.

Western blot profile shows the evidence for IP_3R2 siRNA knockdown (lower panel). IP_3R2 and actin levels were quantified using Image J densitometry tool. The amount of IP_3R2 was obtained as a function of normalisation to the amount of actin protein. Actin blot was used as a loading control. Mean ± SEM was obtained from at least 3 independent experiments. Unpaired t-test with a two-tailed distribution and unequal variance was applied. In all cases, the number of migrated cells and the amount of IP_3R2 protein after IP_3R2 knockdown were statistically different from that in the control conditions.

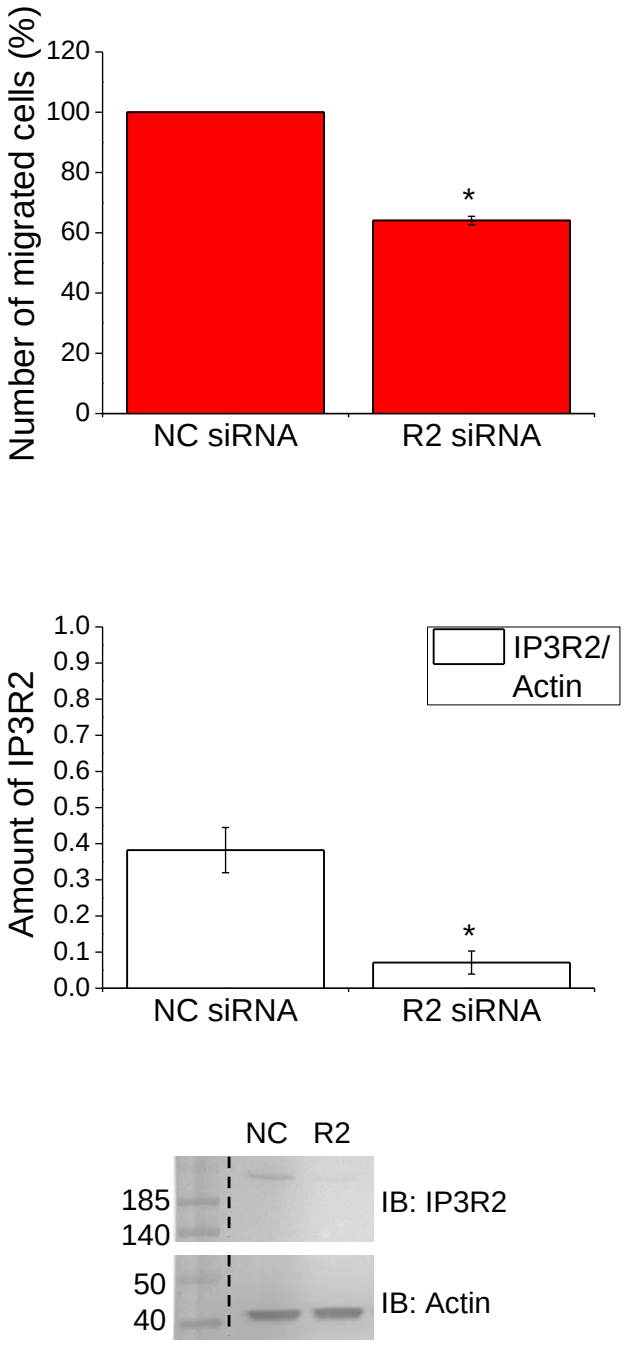
Number of migrated cells (%)
120
100
80
60
40
20
0
*
NC siRNA
R2 siRNA
Amount of IP3R2
1.0
0.9
0.8
0.7
0.6
0.5
0.4
0.3
0.2
0.1
0.0
IP3R2/
Actin
*
NC siRNA
R2 siRNA
NC
R2
185
140
IB: IP3R2
50
40
IB: Actin

Figure 5.7

Figure 5.8. Cellular depletion of IP_3R3 does not suppress pancreatic ductal adenocarcinoma cell migration.

siRNA knockdown of IP_3R3 fails to inhibit the chemotactic migration of pancreatic ductal adenocarcinoma cells. PANC-1 cells were subjected to chemotactic (asymmetric; 0% FBS in upper chamber and 5% FBS in lower chamber) Boyden chamber migration assay for 6 hours at 37°C / 5% CO_2, 72 hours post-transfection with IP_3R3 siRNA (R3 siRNA) or non-targeting siRNA (NC siRNA) oligomer sequences. The effect of the targeting siRNA group was obtained as a function of normalisation to the non-targeting control group. Mean ± SEM was obtained from at least 3 independent experiments.

Western blot profile shows the evidence for IP_3R3 siRNA knockdown (lower panel). IP_3R3 and actin levels were quantified using Image J densitometry tool. The amount of IP_3R3 was obtained as a function of normalisation to the amount of actin protein. Actin blot was used as a loading control. Mean ± SEM was obtained from at least 3 independent experiments. Unpaired t-test with a two-tailed distribution and unequal variance was applied. The amount of IP_3R3 protein after IP_3R3 knockdown was statistically different from that in the control condition but the number of migrated cells was not statistically different from that in the control condition.

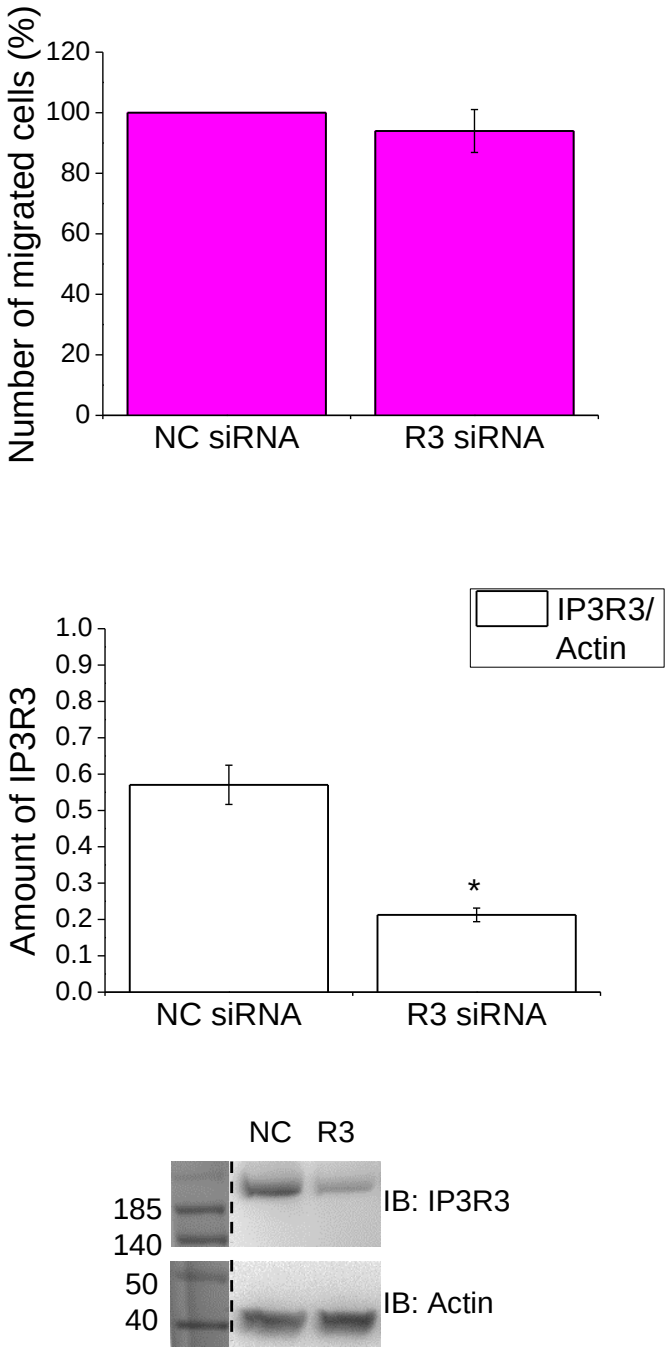
Number of migrated cells (%)
120
100
80
60
40
20
0
NC siRNA
R3 siRNA
IP3R3/
Actin
Amount of IP3R3
1.0
0.9
0.8
0.7
0.6
0.5
0.4
0.3
0.2
0.1
0.0
*
NC siRNA
R3 siRNA
NC
R3
185
140
IB: IP3R3
50
40
IB: Actin

Figure 5.8

5.4 Cellular depletion of STIM1 suppresses PANC-1 cell migration

After applying the pharmacological inhibitor GSK-7975A to demonstrate that store operated Ca^{2+} entry channels are important for the migration of PDAC cells, I further examined the effect of STIM1 depletion on the chemotactic model of cell migration. Briefly, SOCE is a Ca^{2+} influx mechanism triggered by ER Ca^{2+} store depletion, which involves oligomerisation of STIM1 (an EF-hand containing protein that serves as the ER Ca^{2+} sensor) and subsequent translocation of STIM1 oligomers to ER-PM junctions where they interact with and elicit opening of PM Orai-type Ca^{2+} channels (Liou *et al.*, 2005; Roos *et al.*, 2005; Feske *et al.*, 2006; Wu *et al.*, 2006; Park *et al.*, 2009). Following the siRNA knockdown of STIM1 proteins (primary activator of Orai channels), PANC-1 cell migration was significantly inhibited (Figure 5.9, upper panel). Cellular depletion of STIM1 was confirmed by Western blotting (Figure 5.19, lower panels).

This experimental finding shows that cellular depletion of STIM1 suppressed the migration of PDAC cells, and that STIM1-gated Orai1-mediated store operated Ca^{2+} entry is also involved in providing Ca^{2+} signals that drive PDAC cell migration.

Figure 5.9. Cellular depletion of STIM1 suppresses pancreatic ductal adenocarcinoma cell migration.

siRNA knockdown of STIM1 modestly inhibits the chemotactic migration of pancreatic ductal adenocarcinoma cells. PANC-1 cells were subjected to chemotactic (asymmetric; 0% FBS in upper chamber and 5% FBS in lower chamber) Boyden chamber migration assay for 6 hours at 37°C / 5% CO_2, 72 hours post-transfection with STIM1 siRNA (S1 siRNA) or non-targeting siRNA (NC siRNA) oligomer sequences. The effect of the targeting siRNA group was obtained as a function of normalisation to the non-targeting control group. Mean ± SEM was obtained from at least 3 independent experiments.

Western blot profile shows the evidence for STIM1 siRNA knockdown (lower panel). STIM1 and actin levels were quantified using Image J densitometry tool. The amount of STIM1 was obtained as a function of normalisation to the amount of actin protein. Actin blot was used as a loading control. Mean ± SEM was obtained from at least 3 independent experiments. Unpaired t-test with a two-tailed distribution and unequal variance was applied. In all cases, the number of migrated cells and the amount of STIM1 protein after STIM1 knockdown was statistically different from that in the control conditions.

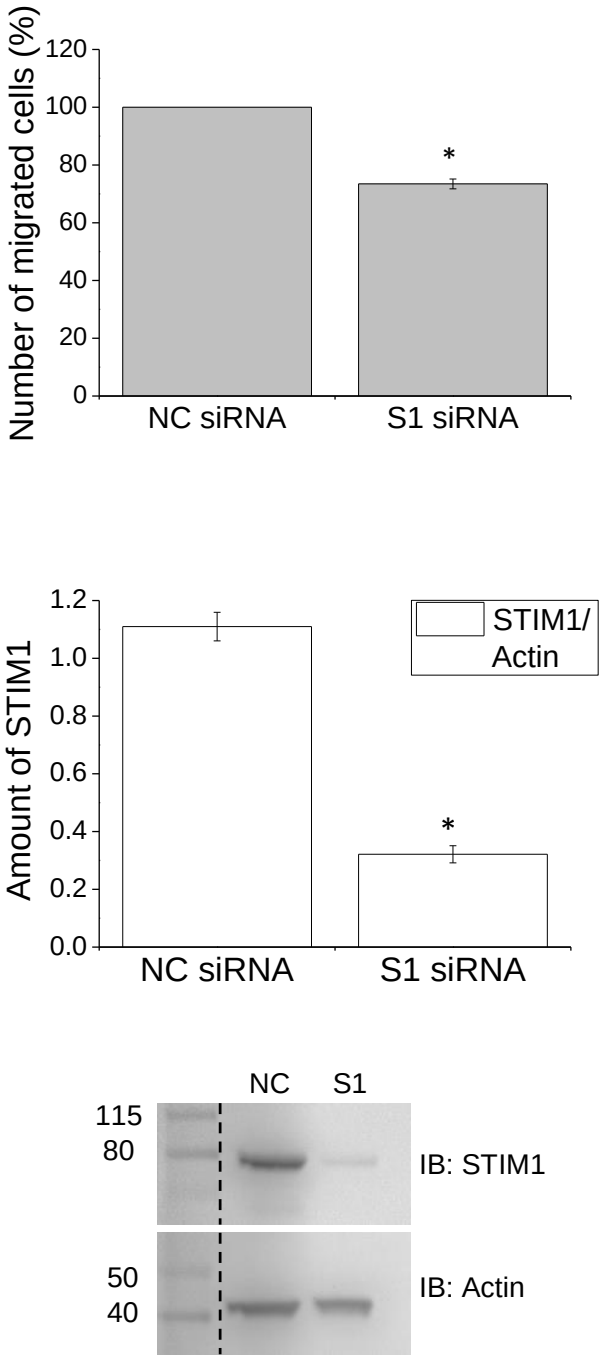
Number of migrated cells (%)
120
100
80
60
40
20
0
*
NC siRNA
S1 siRNA
Amount of STIM1
1.2
1.0
0.8
0.6
0.4
0.2
0.0
STIM1/
Actin
*
NC siRNA
S1 siRNA
NC
S1
115
80
IB: STIM1
50
40
IB: Actin

Figure 5.9

5.5 IP_3R1 co-positions with actin- and phospholipid-rich regions at the leading edge of migrating PANC-1 cells

Ca^{2+} is heavily buffered in the cytosol of most cell types (Zhou & Neher, 1993; Mogami *et al.*, 1999) and therefore the proximity of Ca^{2+} channels to their downstream targets is frequently crucial for the efficiency and specificity of signal transduction. This work convincingly establishes that IP_3Rs and STIM1-competent ER-PM junctions are positioned at the leading edge, and are responsible for providing Ca^{2+} signals that are required for the migration of PDAC cells. I therefore extended these analyses to examine the positioning of IP_3R1 with the effectors of the cellular migration machinery, which includes filamentous actin (F-actin) and phosphatidylinositols. The leading edge of migrating cells is characterised by a region of polymerised actin known as the actin-rich lamellipodia (Ridley, 2011). IP_3R1 co-positioned with actin-rich lamellipodia at the leading edge of migrating PANC-1 cells (Figure 5.10). In addition, a recent study by our laboratory demonstrated the close positioning of Ca^{2+} signalling complex – STIM1-competent ER-PM junctions to actin-rich lamellipodia at the leading edge of migrating PDAC cells (Dingsdale *et al.*, 2013). Furthermore, in addition to actin polymerisation, the importance of phosphatidylinositol signalling in cell migration has been reported (Tsai *et al.*, 2014), and phosphatidylinositol phosphates (specifically ($PI(4,5)P_2$ and $PI(3,4,5)P_3$) have been shown to display front-rear polarity during migration (Brzeska *et al.*, 2012; Tsai *et al.*, 2014). We found that IP_3R1 co-localised with PIP_2/PIP_3 rich regions at the leading edge of migrating PANC-1 cells (Figure 5.11).

Collectively these experimental findings illustrate a close co-positioning of IP_3R1 with components of the migratory apparatus (actin-rich lamellipodia and

phosphatidylinositol phosphates (PIP_2/PIP_3)) at the leading edge of actively migrating PDAC cells. This finding also supports the notion of the importance of close proximity of Ca^{2+} channels to their downstream targets for efficient and specific signalling.

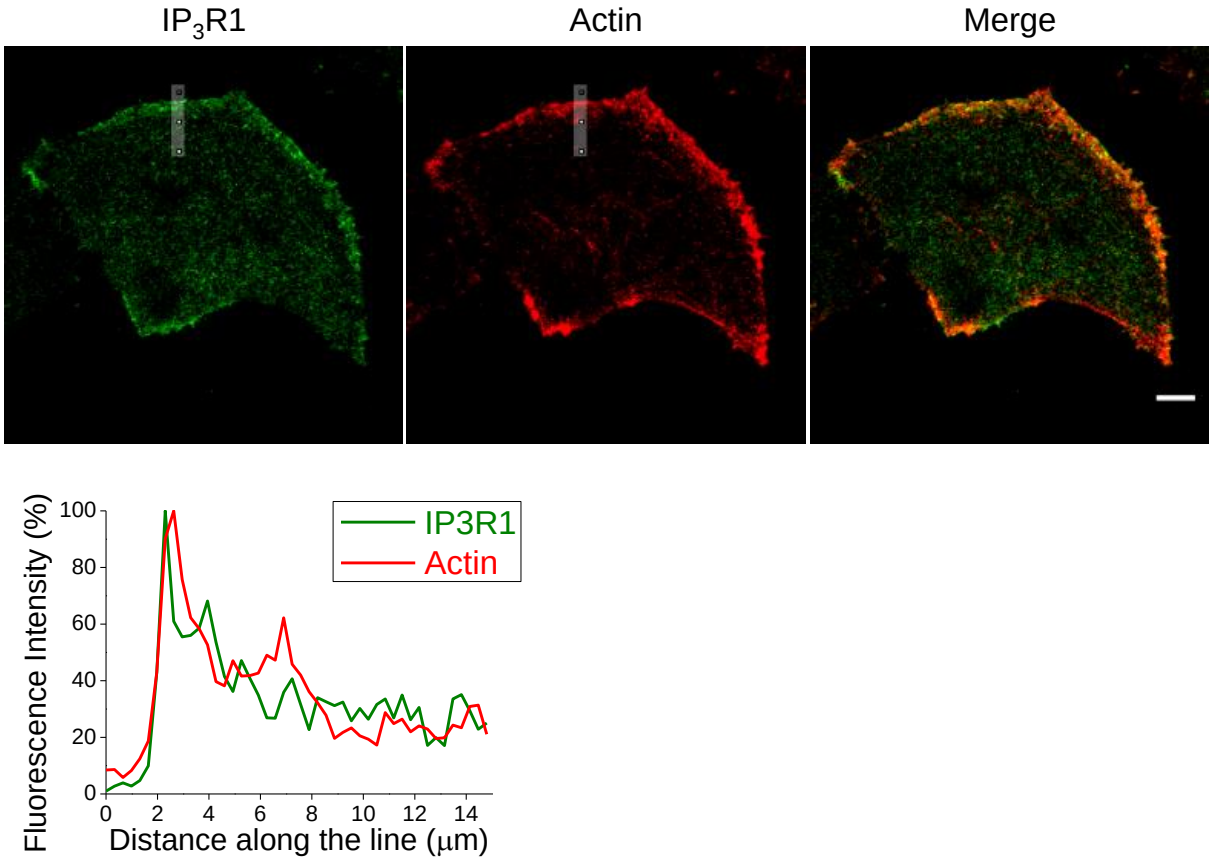

Figure 5.10. IP_3R1 co-positions with actin-rich lamellipodia at the leading edge of migrating pancreatic ductal adenocarcinoma cells.

Polarised PANC-1 cells were fixed and dual-stained using anti-IP_3R1 antibody and phalloidin conjugated Alexa Fluor 647. Scale bar represents 10 μm. Fluorescence profiles (bottom panel) are measured along the line spanning the cell membrane of the leading edge regions. Fluorescence intensity shown was normalised to the maximum fluorescence for each individual staining.

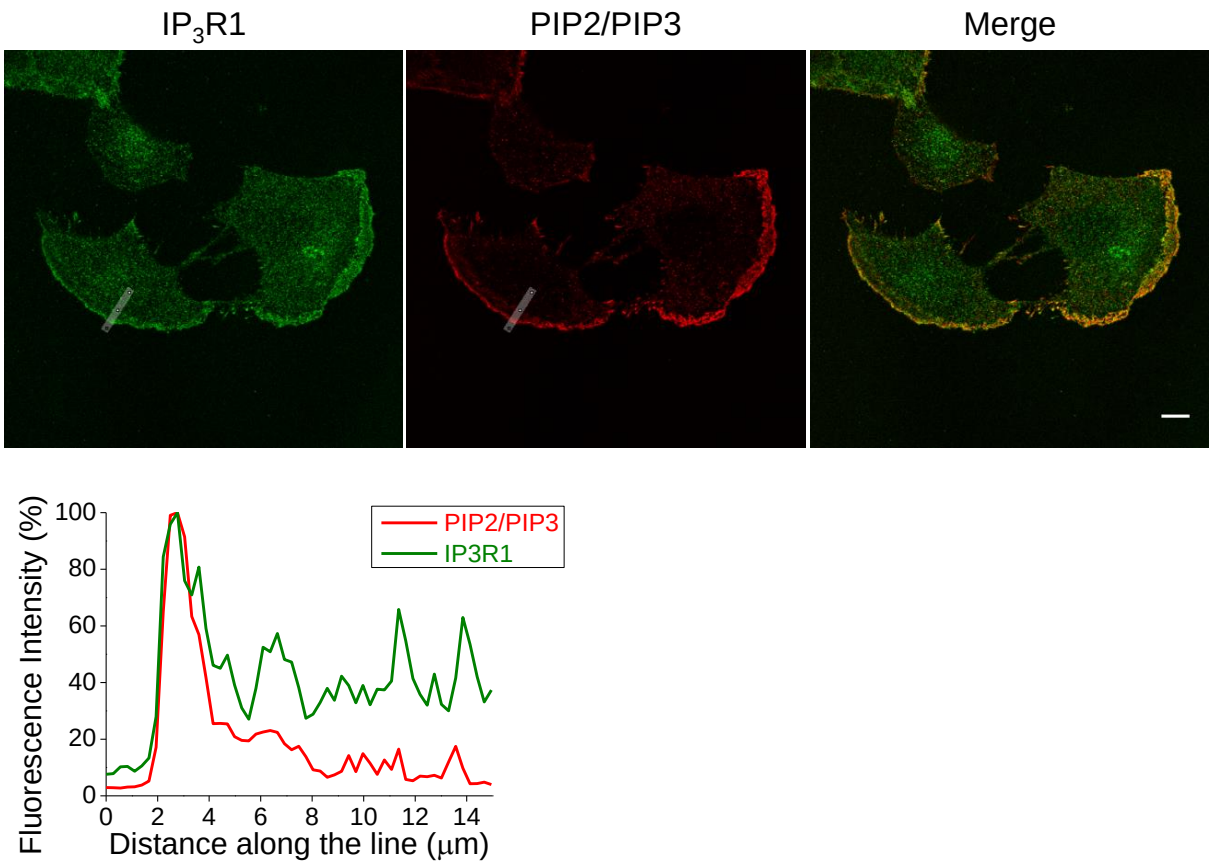

Figure 5.11. IP_3R1 co-localises with PIP_2/PIP_3 rich regions at the leading edge of migrating pancreatic ductal adenocarcinoma cells.

Polarised PANC-1 cells were fixed and dual-stained using anti-IP_3R1 and anti-PIP_2/PIP_3 antibodies. Scale bar represents 10 μm. Fluorescence profiles (bottom panel) are measured along the line spanning the cell membrane of the leading edge regions.

5.6 STIM1 / ER-PM junctions localise close to focal adhesions in migrating PANC-1 cells

It was earlier demonstrated that STIM1/SOCE contributes to the provision of Ca^{2+} signals required for the migration of PDAC cells (Figures 5.1-5.3 and 5.9). In addition to the formation of actin-rich lamellipodia at the leading edge, cell migration requires the formation of focal adhesions (structures responsible for interaction between the cell and the extracellular matrix) at the front of migrating cells. These observations were therefore extended to analyse the relative positioning of STIM1/SOCE-competent ER-PM junctions and focal adhesions. To visualise SOCE-competent ER-PM junctions, PANC-1 cells were transfected with TK-YFP-STIM1 for 24 hours prior to treatment with 30 μM CPA for 1 hour at 37°C / 5% CO_2. Alternatively, PANC-1 cells were transfected with both PM-targeted LL-FKBP-mRFP and ER-targeted CFP-FRB-LL linker constructs (Varnai *et al.*, 2007; Dingsdale *et al.*, 2013) for 24 hours before treatment with 100 nM rapamycin for 4-5 min at 37°C / 5% CO_2. After revealing ER-PM junctions by these methods, cells were fixed and immunostained with anti-vinculin specific antibody. ER-PM junctions were revealed by STIM1 puncta formation following ER Ca^{2+} store depletion with CPA or by co-localised ER and PM linkers without ER Ca^{2+} store depletion. The ER-PM junctions can be frequently found in close proximity to focal adhesions revealed by vinculin (a key regulatory component of focal adhesions) staining (Figures 5.12 and 5.13, see the fragment shown on the bottom panel). Furthermore, Dingsdale et al. (2013) showed that the majority of focal adhesions are positioned within 0.5 μm of nearest STIM1-competent ER-PM junctions in migrating PDAC cells.

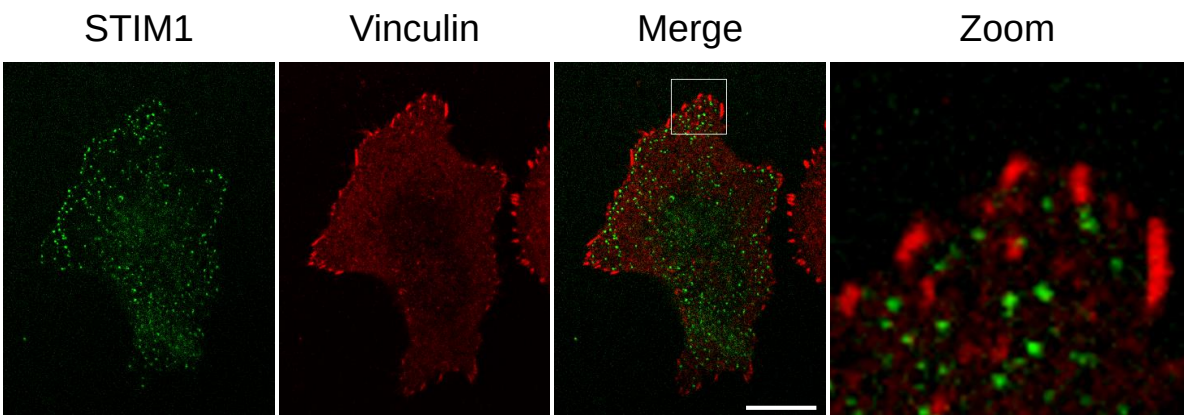

Figure 5.12. Relative positioning of STIM1 puncta and focal adhesions in migrating pancreatic ductal adenocarcinoma cells.

STIM1 puncta are in close proximity to focal adhesions in migrating PANC-1 cells. Polarised PANC-1 cells transfected with TK-YFP-STIM1 were fixed after treatment with CPA, and immunostained using anti-vinculin antibody (to visualise focal adhesions). Scale bar represents 10 μm. Zoom image (on the right) shows the fragment outlined by the rectangle in the 'Merge' image.

These data show that STIM1/SOCE-competent ER-PM junctions are strategically positioned close to focal adhesions in migrating PDAC cells. The close apposition between SOCE-competent ER-PM junctions and focal adhesions should make these structures particularly sensitive to Ca^{2+} signals provided through SOC channels at the leading edge of migrating cells and could explain the effect of SOCE on cell migration (see sub-chapters 5.2 and 5.4).

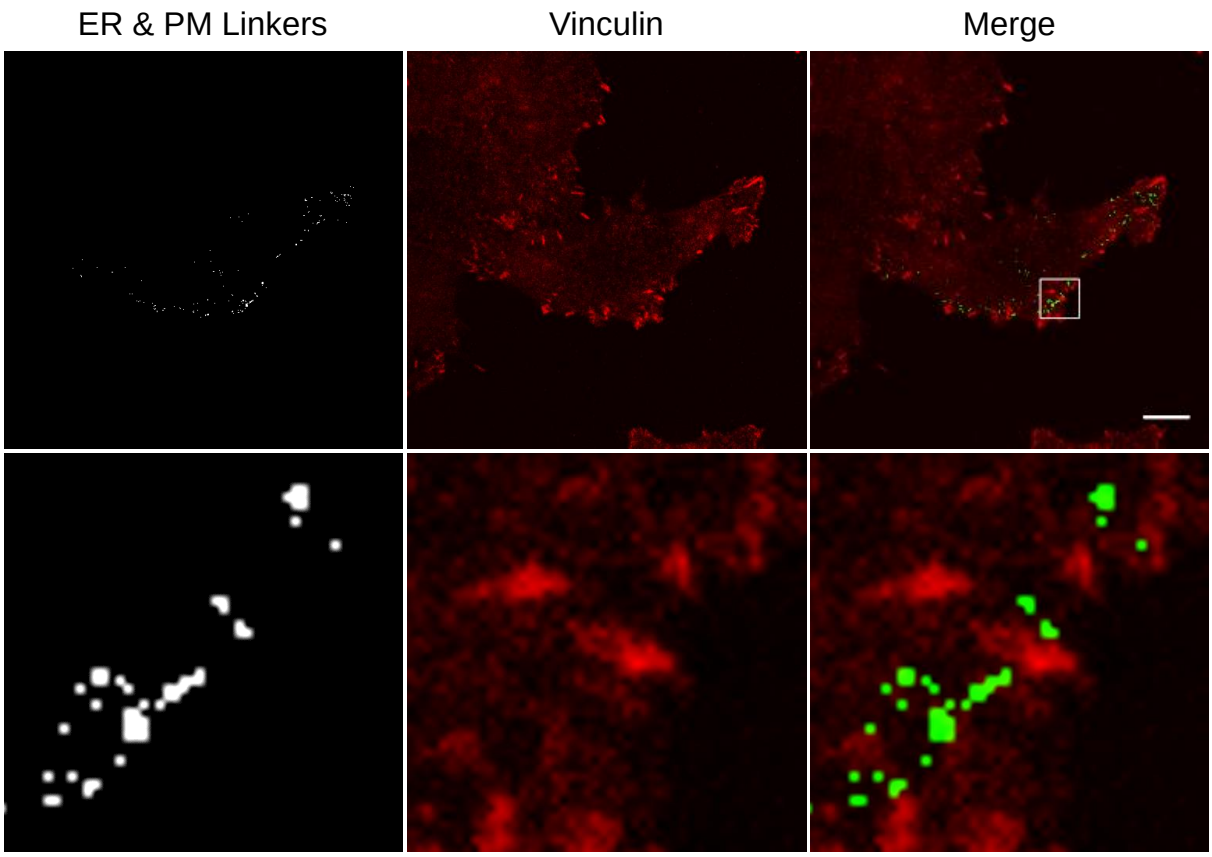

Figure 5.13. Relative positioning of ER-PM junctions (ER&PM linkers) and focal adhesions in migrating pancreatic ductal adenocarcinoma cells.

ER-PM junctions are in close proximity to focal adhesions in migrating PANC-1 cells. Polarised PANC-1 cells co-transfected with both PM-targeted FBKP-LL-mRFP and ER-FRB-LL-CFP linker constructs were fixed after treatment with 100 nM rapamycin, and immunostained using anti-vinculin antibody (to visualise focal adhesions). Scale bar represents 10 μm. Bottom panel shows the fragment outlined by the rectangle in the 'Merge' image.

5.7 IP_3R1 encompass focal adhesions and controls focal adhesion remodelling in migrating PANC-1 cells

Using Xestospongin-B or siRNA knockdown to inhibit/deplete IP_3R1 and IP_3R2 isoforms, I have demonstrated that IP_3Rs are important contributors to the provision of the Ca^{2+} signals required for the migration of PDAC cells. In addition to characterising the close co-positioning of IP_3R1 with actin-rich lamellipodia at the leading edge of migrating cells, it was logical to characterise the relative positioning of IP_3R1 with focal adhesions – another key effector of the migration machinery.

Dual immunostaining of focal adhesions (using antibody against vinculin, a key regulatory component of focal adhesions) and IP_3R1 revealed remarkable relative localisation of the adhesions and the receptors. As expected, focal adhesions were preferentially localised close to the front of the migrating cells; the front leading edge was also enriched with IP_3R1 (Figures 5.14 and 5.15). Importantly, focal adhesions were not co-localised but were instead closely surrounded by the receptors forming 'potholes' on the background of IP_3R1 immunostaining (see the fragments shown on the bottom panel of Figure 5.14 and the associated fluorescence profile). The preferential positioning of focal adhesions and IP_3R1 as well as 'potholes' were observed in the smooth-shaped lamellipodia regions of the leading edge (Figure 5.14 and the B row of Figure 5.15 with the associated fluorescence profile) as well as in spiky, filopodia-like protrusions at the leading edge (Figure 5.15 and specifically the C row and the associated fluorescence profile).

Figure 5.14. IP_3R1 encompass focal adhesions in migrating pancreatic ductal adenocarcinoma cells.

Non-transfected PANC-1 cells were fixed and dual-stained with anti-IP_3R1 and anti-vinculin antibodies. Scale bar represents 10 μm.

IP_3R1 encompass focal adhesions in migrating pancreatic ductal adenocarcinoma cells with a smooth-like leading edge. An expanded fragment of the cell is shown on the middle panels and arrowheads indicate focal adhesions encompassed by IP_3R1. Fluorescence profiles (bottom panel) were measured along the line (shown on the top left and top central images) spanning the cell membrane of the leading edge and crossing a focal adhesion (specifically the lowest of 3 focal adhesions indicated by the yellow arrowhead on the expanded fragment).

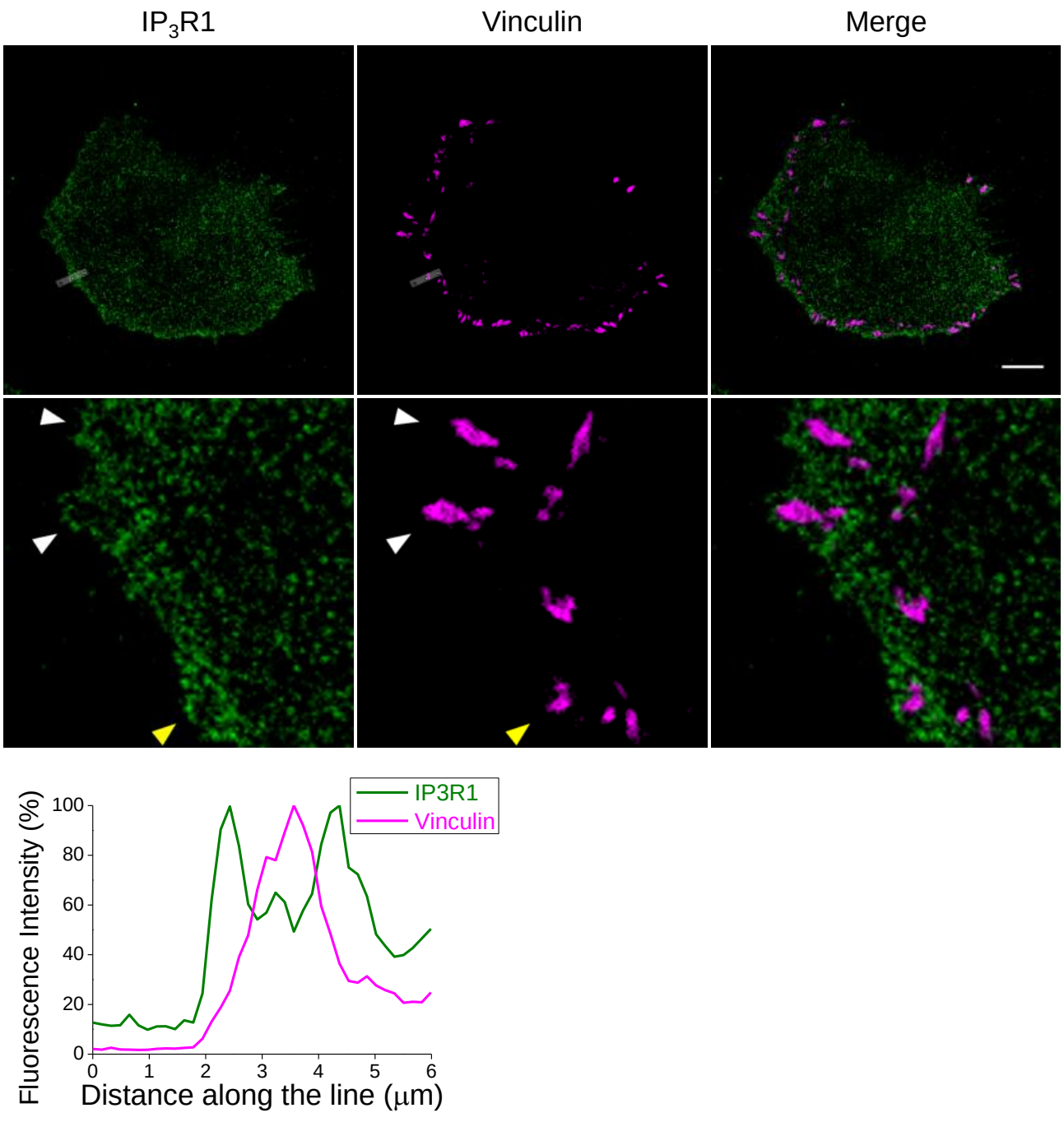
IP3R1
Vinculin
Merge
IP3R1
Vinculin
Fluorescence Intensity (%)
100
80
60
40
20
0
0
1
2
3
4
5
6
Distance along the line (μm)

Figure 5.14

Figure 5.15. IP_3R1 encompass focal adhesions in migrating pancreatic ductal adenocarcinoma cells.

(A) This figure illustrates the relationship between IP_3R1 and focal adhesions in a cell with a complex leading edge composed of smooth (lamellipodia-like) regions and some spiky protrusions. Scale bar represents 10 μm. (B) These panels and their associated fluorescence profiles (shown on the bottom left panel of row D) represent an expanded fragment of a smooth-like region (similar to figure 5.14). (C) These panels represent a spiky protrusion with its associated fluorescence profiles (shown on the bottom right panel of row D). In both cases the focal adhesions (indicated by arrowheads) are surrounded by IP_3R1. The associated fluorescence profiles were measured across the lines shown on the upper panels (A); the focal adhesions crossed by these lines are indicated by yellow arrowhead on B and C panels.

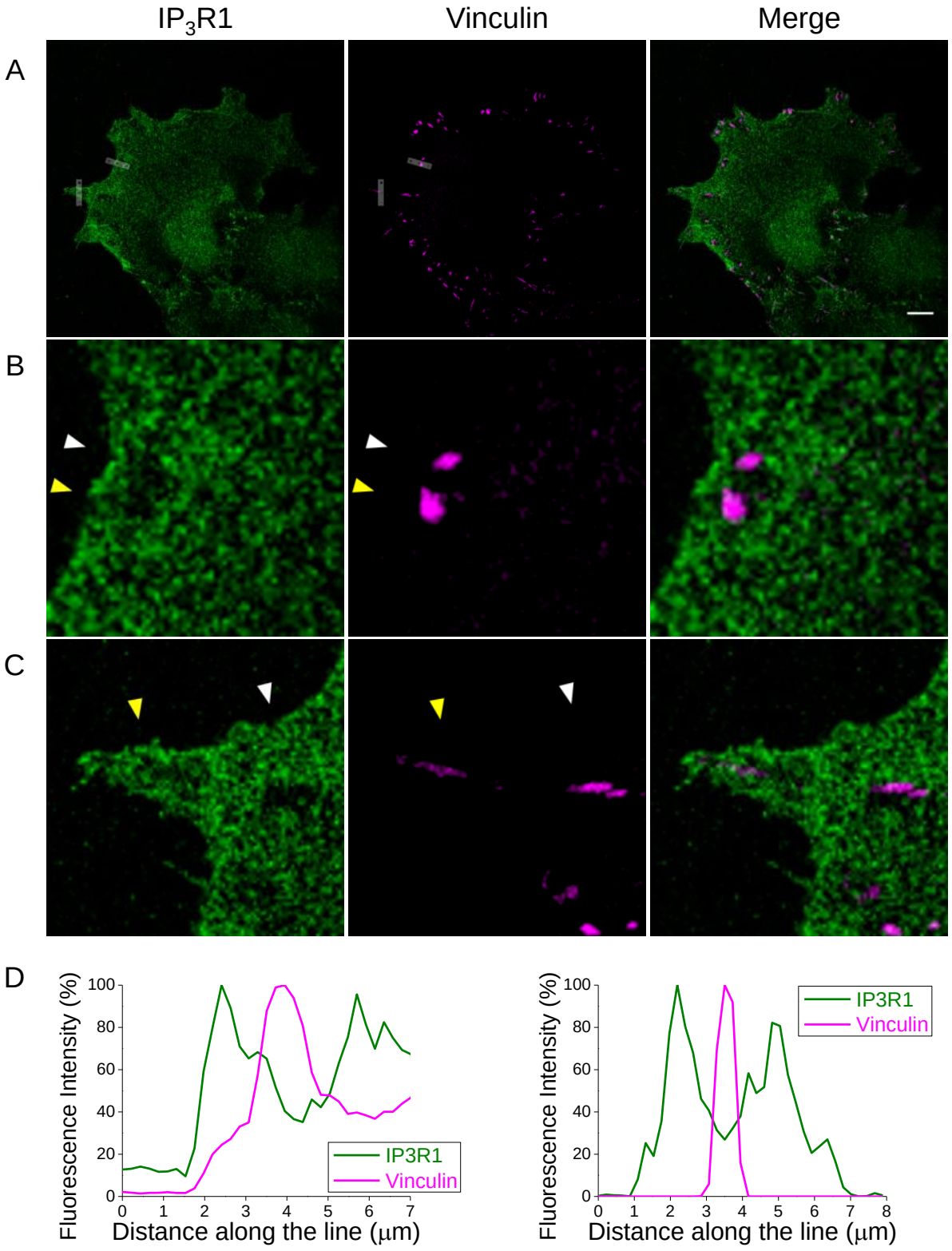
IP3R1
Vinculin
Merge
A
B
C
D
Fluorescence Intensity (%)
Distance along the line (μm)
IP3R1
Vinculin

Figure 5.15

The intimate spatial relationship between focal adhesions and IP_3R1 concentrated in this region should make these structures particularly sensitive to Ca^{2+} signals generated by IP_3Rs at the leading edge of migrating cells. Thus, it was of interest to further examine the sensitivity of focal adhesions to Ca^{2+} signals generated by IP_3Rs in PANC-1 cells. To address this, UV-photoactivatable and membrane permeant IP_3 (caged IP_3) was utilised. In these experiments PANC-1 cells expressing simultaneously mCherry-labelled paxillin (paxillin-mCherry) and paxillin labelled with the Ca^{2+} sensor GCaMP5 (paxillin-GCaMP5) were utilised. Paxillin was used in these experiments because it is an important regulatory component of focal adhesions (Deakin & Turner, 2008). Uncaging of IP_3 induced rapid accumulation of paxillin in focal adhesions and the loss of paxillin in the cytosol (Figure 5.16). These findings highlight the importance of IP_3Rs for focal adhesion remodelling – a process intimately related to migration (Deakin & Turner, 2008; Kim & Wirtz, 2013). Uncaging of IP_3 also induced Ca^{2+} rises resolvable both in the cytosol and at focal adhesions (Figure 5.16A). To convincingly demonstrate that the observed remodelling of focal adhesions was due to the Ca^{2+} signals released through IP_3Rs following the photorelease of IP_3 from its caged precursor (uncaging), PANC-1 cells co-expressing paxillin-mCherry and paxillin-GCaMP5 were UV-illuminated in the absence of caged IP_3. Figure 5.17 shows there were no observable changes in paxillin fluorescence in focal adhesions or in the cytosol (i.e. no remodelling of focal adhesions). Interestingly, after the photorelease of IP_3, the increase in the accumulation of paxillin in focal adhesions started approximately 20s after Ca^{2+} rise in focal adhesions (the increase in GCaMP5 fluorescence indicates Ca^{2+} rise) (Figure 5.16C), suggesting that Ca^{2+} rise precedes remodelling of focal adhesions.

These experimental findings show that focal adhesions are closely encompassed by IP_3R1, creating a novel stratified signalling microdomain i.e. potholes in excitable medium in which Ca^{2+} released through IP_3Rs affects the remodelling of focal adhesions necessary for the migration of PDAC cells.

Figure 5.16. IP_3-induced Ca^{2+} release mediates remodelling of focal adhesions in migrating pancreatic ductal adenocarcinoma cells.

IP_3 uncaging induces remodelling of focal adhesions. (A) Upper panels show the fluorescence of GCaMP5–labelled paxillin (Pax-GCaMP5) before (left) and after (right) uncaging. The increase of GCaMP5 fluorescence indicates Ca^{2+} rise; note the prominent fluorescence increase in focal adhesions. Scale bar represents 10 μm. The lower panels show the distribution of the fluorescence of mCherry-labelled paxillin (Pax-mCh) before (left) and after (right) IP_3 uncaging. Note the prominent increase of fluorescence in focal adhesions induced by the uncaging. (B) The graph shows the increase of fluorescence (i.e. Pax-mCh accumulation), recorded from the regions of interest containing focal adhesions (shown above the traces and indicated by arrowheads on A), and the decrease of the Pax-mCh fluorescence in the cytosol (the region of interest for this analysis included a large area of cytosol and did not include nucleus, not shown). The images on (B) are fragments of the cell shown on (A). (C) This panel shows the fluorescence of both GCaMP5–labelled paxillin (Pax-GCaMP5) and mCherry-labelled paxillin (Pax-mCh) before and after IP_3 uncaging as illustrated by the traces, which were recorded from the regions of interest containing focal adhesions (shown above the traces and indicated by arrowhead on the top left of A). The images on (C) are fragments of the cell shown on (A). Pax-mCh accumulation in focal adhesions starts ~ 20s after IP_3-induced Ca^{2+} releases. The arrows on the graphs indicate the period of uncaging.

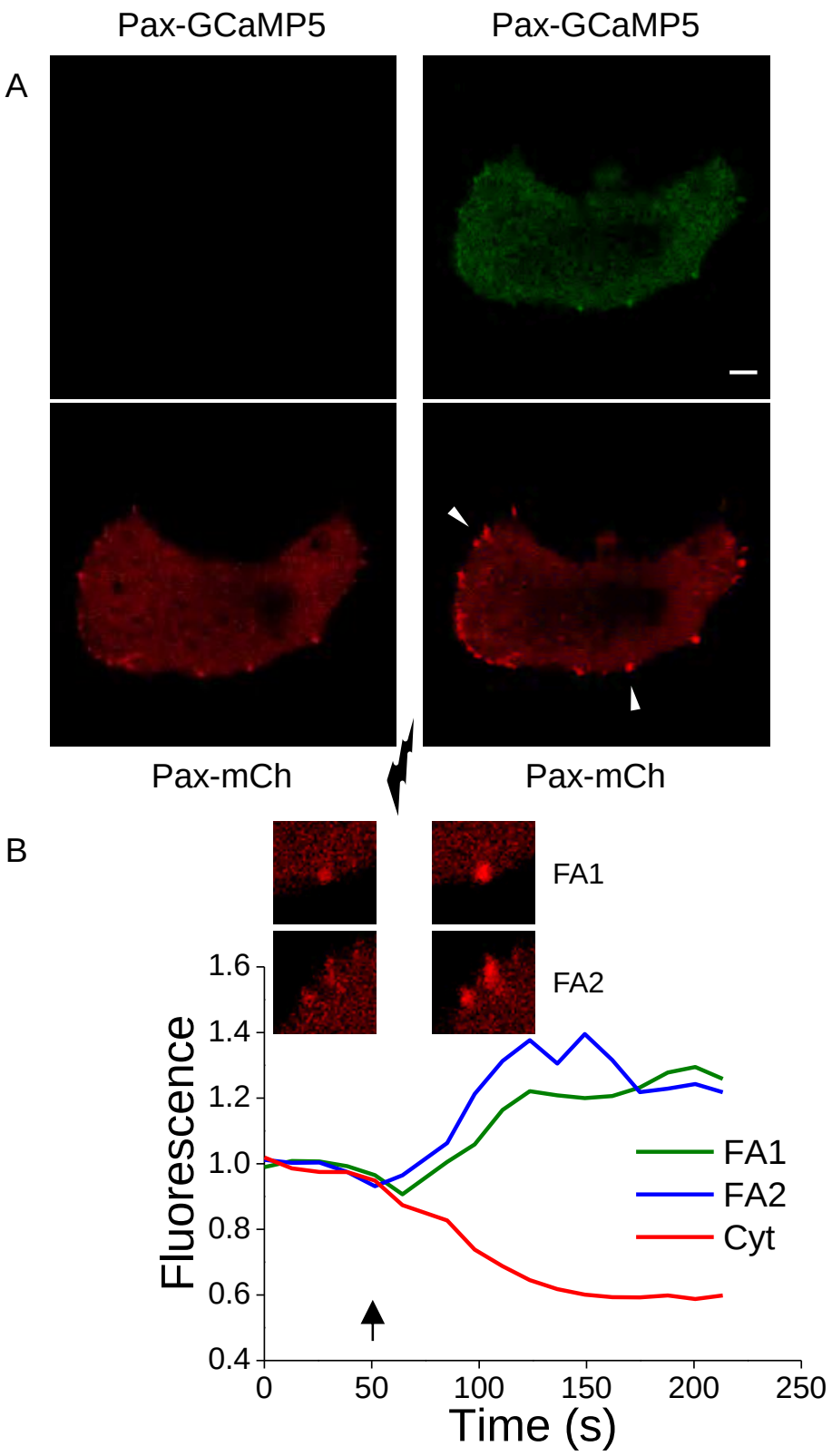
Pax-GCaMP5
Pax-GCaMP5
A
Pax-mCh
Pax-mCh
B
FA1
FA2
Fluorescence
1.6
1.4
1.2
1.0
0.8
0.6
0.4
0
50
100
150
200
250
Time (s)
FA1
FA2
Cyt

Figure 5.16

C

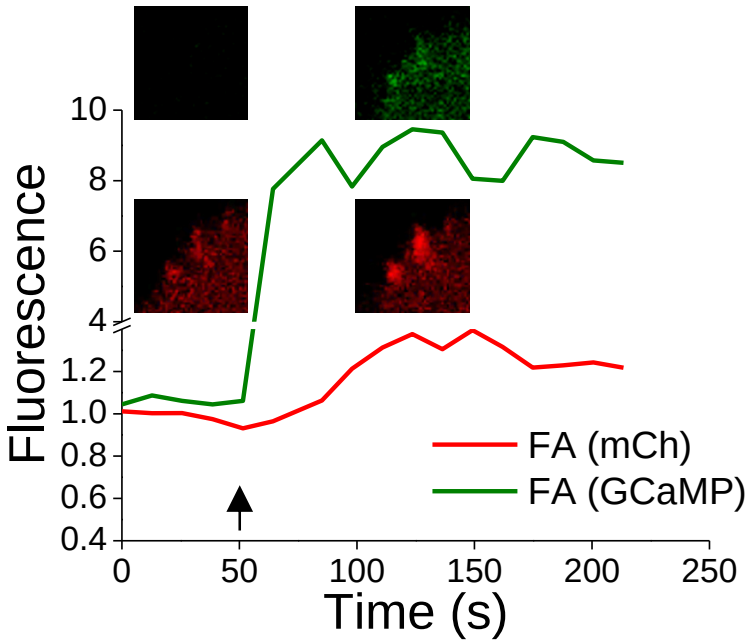
10
8
6
4
1.2
1.0
0.8
0.6
0.4
Fluorescence
0
50
100
150
200
250
Time (s)
FA (mCh)
FA (GCaMP)

Figure 5.16

Figure 5.17. UV illumination does not induce significant remodelling of focal adhesions in PANC-1 cells.

(A) Upper panels show the fluorescence of GCaMP5–labelled paxillin (Pax-GCaMP5) before (left) and after (right) UV illumination in the absence of caged-IP_3. Note that there is no detectable fluorescence increase in focal adhesions (see 5.16A for comparison). The lower panels show the distribution of the fluorescence of mCherry-labelled paxillin (Pax-mCh) before (left) and after (right) UV illumination in the absence of caged-IP_3. Note that there is no detectable change of fluorescence in focal adhesions (see 5.16B for comparison). Scale bars represent 10 μm. (B) The graph shows that there is no detectable change of fluorescence in both focal adhesions (i.e. Pax-mCh accumulation) and in the cytosol before and after UV illumination in the absence of caged-IP_3. The arrow on the graph indicates the period of uncaging. The images on (B) are fragments of the cell shown on (A) (the selected focal adhesions are indicated by arrowheads.

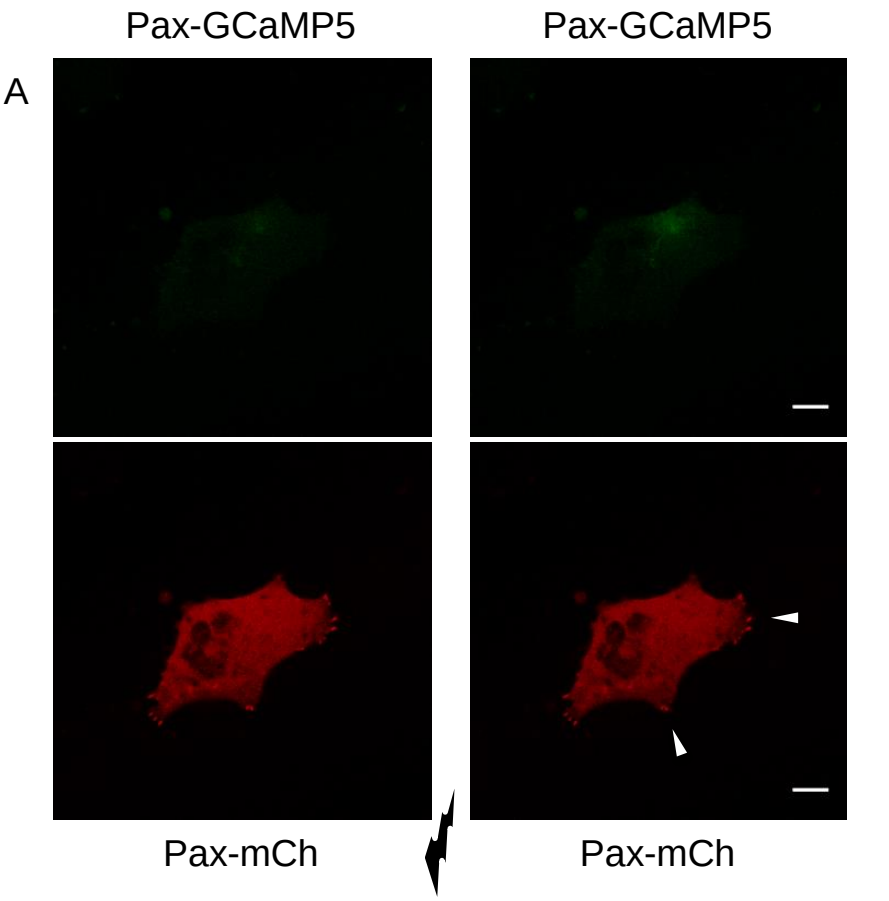
A
Pax-GCaMP5
Pax-GCaMP5
Pax-mCh
Pax-mCh

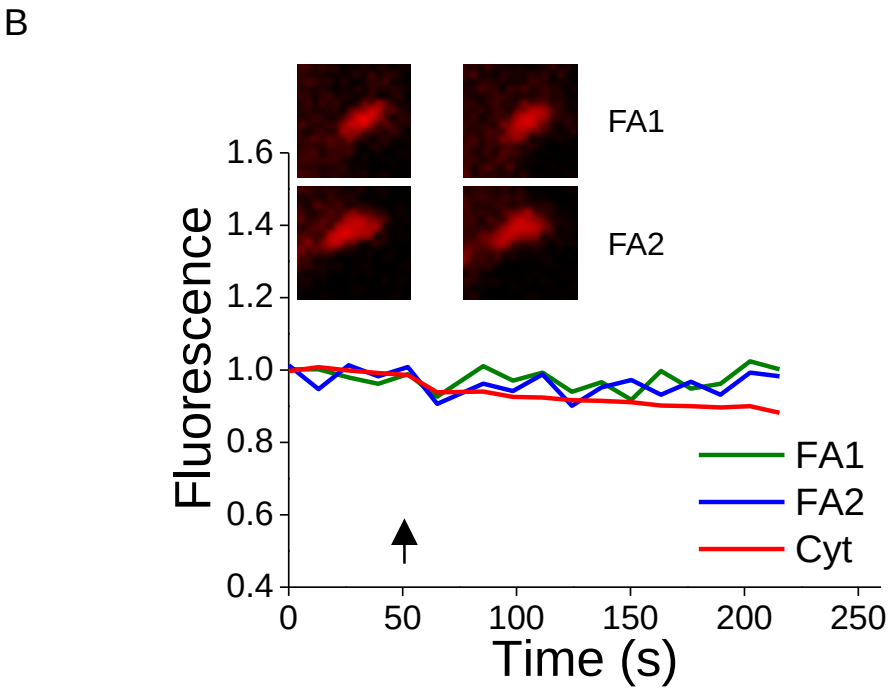
B
FA1
FA2
Fluorescence
1.6
1.4
1.2
1.0
0.8
0.6
0.4
0
50
100
150
200
250
Time (s)
FA1
FA2
Cyt

Figure 5.17

5.8 Discussion

PDAC is a lethal disease characterised by disseminated metastasis at diagnosis, and hence is accompanied with strong resistance to chemotherapy and poor prognosis with median survival period of less than 12 months (Stathis & Moore, 2010; Siegel *et al.*, 2013). To comprehensively address the pathophysiology and disseminated metastatic nature of PDAC, a better understanding of the processes integral to metastasis formation is imperative to aid the design of new and effective therapies with little or no off-target consequences. Epithelial-mesenchymal transition (EMT), cell adhesion, cell migration and invasion are processes essential for metastasis formation (Hanahan & Weinberg, 2011; Chang *et al.*, 2012; Lamouille *et al.*, 2014). The importance of Ca^{2+} signalling has been linked to the aforementioned processes relevant to the formation of metastases in other cancer cell types (Wei *et al.*, 2009; Yang *et al.*, 2009; Davis *et al.*, 2014); however, our understanding of the key participating Ca^{2+} signalling components in this cancer type is limited. Cell migration is a critical step in tumour spreading (Yang *et al.*, 2009), thus, the focus of the present study was to identify and characterise the role of Ca^{2+} signalling complexes in the migration of PDAC cells.

Initial observations detailed a remarkable stratified distribution of Ca^{2+} signalling complexes – IP_3Rs and STIM1-competent ER-PM junctions at the leading edge of migrating PANC-1 cells. The importance of Ca^{2+} signalling for cell migration in other cancer cell types has been documented (Wei *et al.*, 2009; Yang *et al.*, 2009; Middelbeek *et al.*, 2012; Schafer *et al.*, 2012; Tsai & Meyer, 2012; Tsai *et al.*, 2014) and led me to examine the importance of the observed Ca^{2+} signalling complexes in the migration of the model PDAC cell line, PANC-1. It was observed that the pharmacological inhibition of IP_3Rs and SOCE-competent Orai channels significantly

suppressed the migration of PANC-1 cells as measured using both Boyden chamber migration assay (with both symmetric and asymmetric (used as a model of chemotactic migration) FBS distribution), and wound-healing/scratch migration assay (figures 5.1-5.3); indicating that both IP_3Rs and SOCE components are functionally important for the migration of PANC-1 cells. In support of our finding, Ca^{2+} responses have been shown to potentiate cell migration (Wei *et al.*, 2009; Yang *et al.*, 2009; Middelbeek *et al.*, 2012; Schafer *et al.*, 2012; Tsai *et al.*, 2014); however, contrary to our observation, Ca^{2+} responses were also reported to suppress cell migration (Tsai *et al.*, 2014).

A small interference RNA (siRNA) approach was employed to assess specifically the contributory role of each isoform of IP_3R in the migration of PANC-1 cells. These experiments demonstrated that the cellular depletion of IP_3R1 and IP_3R2 but not IP_3R3 suppressed PANC-1 cell migration (Figures 5.6-5.8), with IP_3R1 knockdown producing the greatest inhibitory effect on cell migration. Interestingly, the remarkable redistribution of IP_3R1 and IP_3R2 (but not IP_3R3) from cell-cell contacts and perinuclear region in connected PANC-1 cells, respectively, to preferential localisation at the leading edge region of migrating PANC-1 cells upon the formation of new cellular (front-rear) polarity during EMT is consistent with the importance of IP_3R1- and IP_3R2-mediated Ca^{2+} release signals in the regulation of PANC-1 cell migration. In agreement with the finding that IP_3Rs are critical for the migration of PANC-1 cells, Cheng and colleagues also showed that IP_3R2 (but not IP_3R3) is important for the migration of lung fibroblasts that lack IP_3R1 (Wei *et al.*, 2009). This strengthens the evidence for a critical involvement of IP_3R-mediated Ca^{2+} release signals in the control of cell migration. It has been documented that the polarity of migrating cells is accompanied by the polarity of Ca^{2+} regulatory proteins and Ca^{2+}

signals, which are critical for the process of cell migration (Wei *et al.*, 2009; Tsai & Meyer, 2012; Dingsdale *et al.*, 2013; Tsai *et al.*, 2014). For example, receptor tyrosine kinase (RTK) signalling is polarised in migrating cells exhibiting front-rear polarity with high density at the front leading edge. PLC signalling which generates IP_3 to mediate Ca^{2+} release from ER, and DAG, which in turn activates PKCs (PKCβ) are also polarised in migrating cells (Tsai *et al.*, 2014). Also a higher frequency of local Ca^{2+} pulses (Ca^{2+} flickers (high Ca^{2+} microdomains) occur at the front leading edge compared to the rear of migrating cells (Wei *et al.*, 2009). Therefore, It is logical for one to speculate that high Ca^{2+} flicker activity at the front leading edge could be attributed to the enrichment of IP_3Rs in this region. Taken together, these observations suggest that the close proximity of RTK signalling, PLC activation, IP_3 and DAG signalling, Ca^{2+} flickers, and PKCβ activation in the front of migrating cells all function in a concerted fashion to mediate local, rapid and efficient Ca^{2+} signalling in close vicinity of downstream migratory effectors (e.g. focal adhesion complexes) to regulate cell migration.

In addition, the cellular depletion of STIM1 proteins (an activator of the PM Orai Ca^{2+} channels) also suppressed PANC-1 cell migration. Consistent with findings that STIM1 positively contributes to the migration of PANC-1 cells, other recent reports have also shown that STIM1, a key component of SOCE potentiates the migration of other cancer cell types including human breast tumour cells and lung cancer (H1299) cells (Yang *et al.*, 2009; Schafer *et al.*, 2012; Tsai *et al.*, 2014). Contrary to the observations detailed in the work presented here, Tsai et al. (2014) reported that STIM1 suppressed the migration of non-tumourigenic human umbilical vein endothelial (HUVECs) cells. Briefly, our and other groups (Wei *et al.*, 2009; Yang *et al.*, 2009; Middelbeek *et al.*, 2012) have observed that increased intracellular Ca^{2+}

signals potentiate cell migration, whereas Meyer and colleagues reported that increased intracellular Ca^{2+} signals suppressed cell migration (Tsai *et al.*, 2014). Possible reconciliations with the finding of Tsai et al. (2014) are, firstly, a difference in cell types: Human PANC-1 cells, human embryonic lung fibroblasts WI-38 (Wei *et al.*, 2009), and MEFs and breast tumour cells (Yang *et al.*, 2009) undergo single cell migration mode, whereas HUVEC cells employed by Tsai et al. (2014) undergo collective migration (with intact cell-cell adhesion). Finally, the findings of Tsai et al. (2014) are somewhat self-contradictory because they reported that inhibition of SOCE (decreased cytosolic Ca^{2+} signals) potentiated migration speed but the inhibition of PLC activity, which also decreased cytosolic Ca^{2+} signals, conversely suppressed migration speed of HUVEC cells; without describing the status of extracellular matrix (e.g. fibronectin) used in their study.

The data presented in this thesis chapter demonstrate that both IP_3Rs- and SOCE-mediated Ca^{2+} signals are critical for the migration of PANC-1 cells; however, the subcellular spatial relationship of these Ca^{2+} signalling complexes and effector proteins integral to the migration process has yet to be fully elucidated. Knowing that Ca^{2+} is heavily buffered in the cytosol of most cell types (Zhou & Neher, 1993; Mogami *et al.*, 1999), it is therefore often observed that the proximity of Ca^{2+} channels to their downstream targets is essential for the efficiency and fidelity of signal transduction. As a result, I addressed the subcellular organisation of these Ca^{2+} signalling complexes in relation to prominent components of the migration machinery in migrating PANC-1 cells. The ruffling region of the plasma membrane necessary for sustained forward movement of the plasma membrane with/without protrusions is termed the front leading edge of migrating cells, which is characterised by a specialised network of polymerised actin (Ridley, 2011). I observed that IP_3R1

closely co-positioned with actin-rich lamellipodia at the leading edge of migrating PANC-1 cells (Figure 5.10). Also, Tepikin and colleagues recently showed that STIM1-competent ER-PM junctions were found in close proximity to actin-rich lamellipodia in migrating PANC-1 cells (Dingsdale *et al.*, 2013).

The importance of phospholipid signalling in cell migration has been reported with $PI(4,5)P_2$/$PI(3,4,5)P_3$ exhibiting front-rear polarity in migrating cells (Brzeska *et al.*, 2012; Falke & Ziemba, 2014; Tsai *et al.*, 2014). I have been further able to demonstrate that IP_3R1 co-localises with $PI(4,5)P_2$/$PI(3,4,5)P_3$ phosphatidylinositol-rich regions at the leading edge of migrating PANC-1 cells (Figure 5.11). Interestingly, this suggests that IP_3Rs positioned in the immediate vicinity of plasma membrane region known as plasmerosome (Blaustein & Golovina, 2001) are potentially coupled to / in close proximity to $PI(4,5)P_2$. As a result, this could provide a platform for local, rapid and efficient coupling between PLC activation, PIP_2 hydrolysis, IP_3 and DAG synthesis and Ca^{2+} signalling. The significance of the functional coupling between IP_3Rs and $PI(4,5)P_2$ for efficient Ca^{2+} signalling has been previously described by Lupu et al. (1998). Phosphatidylinositol (particularly $PI(4,5)P_2$ and $PI(3,4,5)P_3$) has been reported to be essential for the regulation of actin cytoskeleton attachment to the plasma membrane and the dynamics of actin-lamellipodia (Raucher *et al.*, 2000; Saarikangas *et al.*, 2010; Falke & Ziemba, 2014). Specifically $PI(4,5)P_2$ has been shown to co-localise with filamentous actin (F-actin) at the leading edge protrusion of migrating cells (Brzeska *et al.*, 2012). Regarding the species of phosphatidylinositols with which IP_3Rs co-localise; I should note that anti-PIP_2 antibody used in the present study is not specific for $PI(4,5)P_2$ binding as revealed using a lipid strips binding test described by Brzeska et al. (2012). The binding affinity for phosphatidylinositol varies with $PI(3,4)P_2$>$PI(4,5)P_2$>$PI(3,4,5)P_3$

(Brzeska *et al.*, 2012). Nonetheless, since $PI(4,5)P_2$ is the most abundant phosphatidylinositol in the plasma membrane (Saarikangas *et al.*, 2010), phosphatidylinositol staining by the PIP_2 antibody should represent a significant amount of $PI(4,5)P_2$ staining.

Focal adhesions link intracellular cytoskeletal structures with the extracellular matrix via integral membrane spanning proteins (Webb *et al.*, 2002). Using vinculin as a marker for focal adhesions, it was observed that STIM1-competent ER-PM junctions (i.e. SOCE platforms) could be found in close proximity to focal adhesions at the leading edge, with the majority of focal adhesions positioned within 0.5 µm of nearest STIM1-competent ER-PM junctions in migrating PANC-1 cells (Dingsdale *et al.*, 2013). Interestingly, IP_3R1 remarkably encompassed focal adhesions i.e. by creating potholes of excitable local Ca^{2+} signalling medium that surrounds focal adhesions. The role of IP_3Rs as the fundamental building block of an excitable medium was previously documented in different cell types (Foskett *et al.*, 2007). Recently it has become widely accepted that focal adhesion size and turnover is critical for cell migration speed (Yang *et al.*, 2009; Kim & Wirtz, 2013) and tumour metastasis (Yang *et al.*, 2009).

Consistent with the findings of the present work, studies in breast cancer tumour cells (Yang *et al.*, 2009; Middelbeek *et al.*, 2012) and in other cell types (Schafer *et al.*, 2012; Tsai & Meyer, 2012; Tsai *et al.*, 2014) have shown that Ca^{2+} responses are important for cell migration by regulating focal adhesion dynamics and turnover. The mechanisms involved in these Ca^{2+} responses have yet to be fully elucidated. Recent reports have linked Ca^{2+} influx via Ca^{2+} release activated Ca^{2+} entry (CRAC) – STIM1 and Orai1 components (Yang *et al.*, 2009; Tsai *et al.*, 2014), and via transient receptor potential (TRP) channels in particular TRPM7 (a stretch-activated

Ca^{2+} channel (SACC)) (Middelbeek *et al.*, 2012) to focal adhesion turnover. Tsai and Meyer (2012) and Tsai et al. (2014) also suggested a link between IP_3R-mediated Ca^{2+} signals and focal adhesion remodelling but they were unable to provide experimental evidence directly connecting IP_3R-mediated Ca^{2+} signalling to focal adhesion remodelling. Therefore the present study sought to demonstrate a functional casual link between IP_3R-mediated Ca^{2+} release and focal adhesion remodelling in migrating PANC-1 cells. To address this, plasma membrane permeant and UV-photoactivatable IP_3, paxillin-mCherry and paxillin-GCaMP5 were utilised. Upon the photorelease of IP_3 and the subsequent opening of IP_3Rs, Ca^{2+} rises in cytosol and focal adhesions followed by the accumulation of paxillin in focal adhesions (Figure 5.16), suggesting that there is a casual relationship between IP_3R-mediated Ca^{2+} releases and focal adhesion remodelling. Interestingly after the photorelease of IP_3, a 20s latency period between Ca^{2+} releases and resolvable paxillin accumulation suggests that there may be additional regulatory steps involved in the remodelling of focal adhesions. In good agreement with this data, Meyer and colleague also reported a latency period of ~16s between local Ca^{2+} pulses and focal adhesion remodelling (Tsai & Meyer, 2012). Calpain and Rho family of small GTPases (mainly RhoA, Rac1 and CDC42) are potential candidate effectors downstream of Ca^{2+} responses which are thought to be involved in mediating focal adhesion remodelling and actin-lamellipodia-dependent forward movement (Ridley *et al.*, 2003; Yang *et al.*, 2009; Ridley, 2011). Calpain (μ-calpain) is a Ca^{2+} binding protease with five EF hand domains that is activated by elevation in cytosolic Ca^{2+} level and its activity has been reported to regulate focal adhesion disassembly and turnover (Valeyev *et al.*, 2006). This is another possible candidate for mediating the IP_3-induced focal adhesion remodelling observed in this study.

Collectively, these experimental data provides supporting evidence for the involvement of Ca^{2+} signalling complexes (IP_3Rs and SOCE – STIM1 & Orai1 components) in the regulation of PDAC cell migration. It was next discovered in the present work that these critical Ca^{2+} signalling complexes are localised at the leading edge of migrating PDAC cells and are strategically positioned in close proximity to prominent migratory machinery components including actin-rich lamellipodia, phospholipid-rich microdomains and focal adhesion complexes (vinculin and paxillin). Furthermore, it was demonstrated that focal adhesions were closely encompassed by IP_3Rs at the leading edge i.e. creating potholes in excitable medium in which Ca^{2+} released through IP_3Rs could affect the remodelling and turnover of focal adhesions, which in turn is critical for the migration of PDAC cells. Taken together, I successfully demonstrated that Ca^{2+} signalling complexes regulate focal adhesion turnover in order to control cell adhesion dynamics and forward movement of PANC-1 cells. The outcome of the present study suggests that interfering with the functional relationship between polarised Ca^{2+} responses and the migratory machinery could be an exciting therapeutic avenue to exploit in order to suppress the metastasis of pancreatic ductal adenocarcinoma.

Chapter 6: Concluding Remarks

Chapter 6: Concluding Remarks

6.1 Keynote

Firstly, the present study has demonstrated that Ca^{2+} signals (through IP_3Rs and SOCE) are essential for the migration of pancreatic ductal adenocarcinoma (PDAC, specifically PANC-1) cells. The molecular mechanism by which these Ca^{2+} signalling complexes control cell migration is likely to involve the regulation of focal adhesion remodelling, which in turn controls cell adhesion dynamics and forward movement of PANC-1 cells.

Secondly, based on our experimental findings which showed that IP_3Rs underwent redistribution upon EMT and a recent report that documented the model for PDAC tumour progression from pancreatic acinar cells (Rooman & Real, 2012), we postulate that the differential localisation of IP_3Rs could exhibit a binary ('good' or 'bad') role depending on the physiological and pathophysiological status of cells. For example, in non-cancerous epithelial cells (e.g. acinar cells) IP_3Rs could be critical for physiological functions including fluid and protein secretion, whereas following EMT switch in cancer cells (e.g. PDAC) redistribution of IP_3Rs to the leading edge is critical for the migration/invasion and formation of metastases.

6.2 IP_3Rs and SOCE during EMT and in cell migration

This study successfully showed that endogenously expressed isoforms of IP_3R exhibit differential subcellular localisation in clusters and monolayers of PANC-1 cells. Specifically, IP_3R1 was localised at intercellular contacts, whereas both IP_3R2 and IP_3R3 were preferentially localised to the perinuclear region. SOCE-competent ER-PM junctions were also found to concentrate in a region adjacent to the

intercellular junctions. The polarised distribution of IP_3Rs and SOCE suggests that these Ca^{2+} signalling complexes in the proximity of tight junctions could be important for epithelial functions e.g. exocytotic and fluid secretion (Rodriguez-Boulan & Nelson, 1989; Ito *et al.*, 1997; Steward *et al.*, 2005; Pandol, 2010; Huang *et al.*, 2012).

PDAC is a lethal disease characterised by disseminated metastasis at diagnosis, and as a result is accompanied with strong resistance to chemotherapy and poor prognosis with median survival period of less than 12 months (Stathis & Moore, 2010; Siegel *et al.*, 2013). Epithelial-mesenchymal transition (EMT) is an essential event in cancer development that is relevant to the process of metastasis (Hanahan & Weinberg, 2011; Chang *et al.*, 2012; Lamouille *et al.*, 2014). During EMT, epithelial cells disconnect from their neighbours following the down-regulation of epithelial signatures and concomitantly the up-regulation of genes that permit trans-differentiation into motile mesenchymal cells (Lamouille *et al.*, 2014). We observed profound morphological changes in PANC-1 cells after EMT and these includes the formation of new cellular (front-rear) polarity. This transition was accompanied by the redistribution of IP_3Rs – specifically IP_3R1 and IP_3R2 (but not IP_3R3) from cell-cell contacts and perinuclear region in connected PANC-1 cells, respectively, to the leading edge of migrating PANC-1 cells. Interestingly, these observations compliment the importance of IP_3R1 and IP_3R2 for PANC-1 cell migration because cellular depletions of IP_3R1 and IP_3R2 (but not IP_3R3) suppressed the migration of PANC-1 cells. In addition, SOCE-competent ER-PM junctions also underwent profound redistribution to concentrate at the leading edge following EMT. Pharmacological inhibition of SOCE and the knockdown of STIM1 (activator of PM SOC channels Orai1) also suppressed the migration of PANC-1 cells. Collectively,

these findings suggest that the striking accumulation of IP_3Rs and STIM1/SOCE-competent ER-PM junctions at the leading edge of PDAC cells has a clear function, which is to provide Ca^{2+} signals important for the migration of this type of cancer cell.

It is a widely acknowledged concept that the proximity of Ca^{2+} signals to their downstream targets is frequently crucial for the efficiency and specificity of signal transduction as Ca^{2+} is heavily buffered in the cytosol of most cell types (Zhou & Neher, 1993; Mogami *et al.*, 1999). We observed that IP_3R1 co-positioned with components of the migratory apparatus (actin-rich lamellipodia and phosphatidylinositols (PIP_2/PIP_3)) at the leading edge of migrating PANC-1 cells. STIM1/SOCE-competent ER-PM junctions were also found to be strategically positioned close to focal adhesions in migrating PANC-1 cells. The close apposition between these Ca^{2+} signalling complexes and migratory apparatus should make these structures particularly sensitive to Ca^{2+} signals provided through IP_3Rs and SOC channels at the leading edge of migrating cells and could explain the effect of IP_3R-mediated Ca^{2+} release and SOCE on cell migration. Furthermore, we demonstrated that focal adhesions were closely encompassed by IP_3R1, creating potholes in excitable medium in which Ca^{2+} released through IP_3Rs is linked to focal adhesion remodelling and turnover, which in turn is necessary for the migration of PANC-1 cells. This observation further supports the notion of the importance of close proximity of Ca^{2+} signals to their downstream targets (e.g. migratory apparatus) in order to mediate local, efficient and specific signalling.

Finally, the findings of the present study suggests that interfering with the functional relationship between polarised Ca^{2+} responses and the migratory apparatus could be exploited therapeutically to attenuate the metastatic capability of pancreatic ductal adenocarcinoma.

REFERENCES

Abercrombie M, Heaysman JE & Pegrum SM. (1970). The locomotion of fibroblasts in culture. II. "RRuffling". *Experimental cell research* **60,** 437-444.

Abercrombie M, Heaysman JE & Pegrum SM. (1971). The locomotion of fibroblasts in culture. IV. Electron microscopy of the leading lamella. *Experimental cell research* **67,** 359-367.

Ahmed N, Maines-Bandiera S, Quinn MA, Unger WG, Dedhar S & Auersperg N. (2006). Molecular pathways regulating EGF-induced epithelio-mesenchymal transition in human ovarian surface epithelium. *American journal of physiology Cell physiology* **290,** C1532-1542.

Aihara Y, Inoue T, Tashiro T, Okamoto K, Komiya Y & Mikoshiba K. (2001). Movement of endoplasmic reticulum in the living axon is distinct from other membranous vesicles in its rate, form, and sensitivity to microtubule inhibitors. *Journal of neuroscience research* **65,** 236-246.

Akerboom J, Chen TW, Wardill TJ, Tian L, Marvin JS, Mutlu S, Calderon NC, Esposti F, Borghuis BG, Sun XR, Gordus A, Orger MB, Portugues R, Engert F, Macklin JJ, Filosa A, Aggarwal A, Kerr RA, Takagi R, Kracun S, Shigetomi E, Khakh BS, Baier H, Lagnado L, Wang SS, Bargmann CI, Kimmel BE, Jayaraman V, Svoboda K, Kim DS, Schreiter ER & Looger LL. (2012). Optimization of a GCaMP calcium indicator for neural activity imaging. *The Journal of neuroscience : the official journal of the Society for Neuroscience* **32,** 13819-13840.

Ashby MC & Tepikin AV. (2001). ER calcium and the functions of intracellular organelles. *Seminars in cell & developmental biology* **12,** 11-17.

Baumann O & Walz B. (2001). Endoplasmic reticulum of animal cells and its organization into structural and functional domains. *International review of cytology* **205,** 149-214.

Bernard O. (2007). Lim kinases, regulators of actin dynamics. *The international journal of biochemistry & cell biology* **39,** 1071-1076.

Berridge MJ. (1983). Rapid accumulation of inositol trisphosphate reveals that agonists hydrolyse polyphosphoinositides instead of phosphatidylinositol. *The Biochemical journal* **212,** 849-858.

Berridge MJ. (1993). Cell signalling. A tale of two messengers. *Nature* **365,** 388-389.

Berridge MJ. (2002). The endoplasmic reticulum: a multifunctional signaling organelle. *Cell calcium* **32,** 235-249.

Berridge MJ, Bootman MD & Lipp P. (1998). Calcium--a life and death signal. *Nature* **395,** 645-648.

Berridge MJ, Lipp P & Bootman MD. (2000). The versatility and universality of calcium signalling. *Nature reviews Molecular cell biology* **1,** 11-21.

Betzenhauser MJ, Wagner LE, 2nd, Iwai M, Michikawa T, Mikoshiba K & Yule DI. (2008). ATP modulation of Ca2+ release by type-2 and type-3 inositol (1, 4, 5)-triphosphate receptors. Differing ATP sensitivities and molecular determinants of action. *The Journal of biological chemistry* **283,** 21579-21587.

Betzenhauser MJ, Wagner LE, 2nd, Park HS & Yule DI. (2009). ATP regulation of type-1 inositol 1,4,5-trisphosphate receptor activity does not require walker A-type ATP-binding motifs. *The Journal of biological chemistry* **284,** 16156-16163.

Bezprozvanny I & Ehrlich BE. (1993). ATP modulates the function of inositol 1,4,5-trisphosphate-gated channels at two sites. *Neuron* **10,** 1175-1184.

Bezprozvanny I, Watras J & Ehrlich BE. (1991). Bell-shaped calcium-response curves of Ins(1,4,5)P3- and calcium-gated channels from endoplasmic reticulum of cerebellum. *Nature* **351,** 751-754.

Bishop AL & Hall A. (2000). Rho GTPases and their effector proteins. *The Biochemical journal* **348 Pt 2,** 241-255.

Blaustein MP & Golovina VA. (2001). Structural complexity and functional diversity of endoplasmic reticulum Ca(2+) stores. *Trends in neurosciences* **24,** 602-608.

Bosanac I, Michikawa T, Mikoshiba K & Ikura M. (2004). Structural insights into the regulatory mechanism of IP3 receptor. *Biochimica et biophysica acta* **1742,** 89-102.

Brundage RA, Fogarty KE, Tuft RA & Fay FS. (1991). Calcium gradients underlying polarization and chemotaxis of eosinophils. *Science* **254,** 703-706.

Brzeska H, Guag J, Preston GM, Titus MA & Korn ED. (2012). Molecular basis of dynamic relocalization of Dictyostelium myosin IB. *The Journal of biological chemistry* **287,** 14923-14936.

Burdyga A, Conant A, Haynes L, Zhang J, Jalink K, Sutton R, Neoptolemos J, Costello E & Tepikin A. (2013). cAMP inhibits migration, ruffling and paxillin accumulation in focal adhesions of pancreatic ductal adenocarcinoma cells: effects of PKA and EPAC. *Biochimica et biophysica acta* **1833,** 2664-2672.

Burnette DT, Manley S, Sengupta P, Sougrat R, Davidson MW, Kachar B & Lippincott-Schwartz J. (2011). A role for actin arcs in the leading-edge advance of migrating cells. *Nature cell biology* **13,** 371-381.

Campellone KG & Welch MD. (2010). A nucleator arms race: cellular control of actin assembly. *Nature reviews Molecular cell biology* **11,** 237-251.

Cano CE, Motoo Y & Iovanna JL. (2010). Epithelial-to-mesenchymal transition in pancreatic adenocarcinoma. *TheScientificWorldJournal* **10,** 1947-1957.

Carisey A & Ballestrem C. (2011). Vinculin, an adapter protein in control of cell adhesion signalling. *European journal of cell biology* **90,** 157-163.

Carrasco S & Meyer T. (2011). STIM proteins and the endoplasmic reticulum-plasma membrane junctions. *Annual review of biochemistry* **80,** 973-1000.

Chang CL, Hsieh TS, Yang TT, Rothberg KG, Azizoglu DB, Volk E, Liao JC & Liou J. (2013). Feedback regulation of receptor-induced Ca2+ signaling mediated by E-Syt1 and Nir2 at endoplasmic reticulum-plasma membrane junctions. *Cell reports* **5,** 813-825.

Chang ZG, Wei JM, Qin CF, Hao K, Tian XD, Xie K, Xie XH & Yang YM. (2012). Suppression of the epidermal growth factor receptor inhibits epithelial-mesenchymal transition in human pancreatic cancer PANC-1 cells. *Digestive diseases and sciences* **57,** 1181-1189.

Chesarone MA, DuPage AG & Goode BL. (2010). Unleashing formins to remodel the actin and microtubule cytoskeletons. *Nature reviews Molecular cell biology* **11,** 62-74.

Colosetti P, Tunwell RE, Cruttwell C, Arsanto JP, Mauger JP & Cassio D. (2003). The type 3 inositol 1,4,5-trisphosphate receptor is concentrated at the tight

junction level in polarized MDCK cells. *Journal of cell science* **116,** 2791-2803.

Criollo A, Maiuri MC, Tasdemir E, Vitale I, Fiebig AA, Andrews D, Molgo J, Diaz J, Lavandero S, Harper F, Pierron G, di Stefano D, Rizzuto R, Szabadkai G & Kroemer G. (2007). Regulation of autophagy by the inositol trisphosphate receptor. *Cell death and differentiation* **14,** 1029-1039.

Davis FM, Azimi I, Faville RA, Peters AA, Jalink K, Putney JW, Jr., Goodhill GJ, Thompson EW, Roberts-Thomson SJ & Monteith GR. (2014). Induction of epithelial-mesenchymal transition (EMT) in breast cancer cells is calcium signal dependent. *Oncogene* **33,** 2307-2316.

Deakin NO & Turner CE. (2008). Paxillin comes of age. *Journal of Cell Science* **121,** 2435-2444.

Decuypere JP, Monaco G, Missiaen L, De Smedt H, Parys JB & Bultynck G. (2011). IP(3) Receptors, Mitochondria, and Ca Signaling: Implications for Aging. *Journal of aging research* **2011,** 920178.

Delmas P, Wanaverbecq N, Abogadie FC, Mistry M & Brown DA. (2002). Signaling microdomains define the specificity of receptor-mediated InsP(3) pathways in neurons. *Neuron* **34,** 209-220.

Delorme V, Machacek M, DerMardirossian C, Anderson KL, Wittmann T, Hanein D, Waterman-Storer C, Danuser G & Bokoch GM. (2007). Cofilin activity downstream of Pak1 regulates cell protrusion efficiency by organizing lamellipodium and lamella actin networks. *Developmental cell* **13,** 646-662.

Dempsey GT, Vaughan JC, Chen KH, Bates M & Zhuang X. (2011). Evaluation of fluorophores for optimal performance in localization-based super-resolution imaging. *Nature methods* **8,** 1027-1036.

Deng X, Wang Y, Zhou Y, Soboloff J & Gill DL. (2009). STIM and Orai: dynamic intermembrane coupling to control cellular calcium signals. *The Journal of biological chemistry* **284,** 22501-22505.

Derler I, Schindl R, Fritsch R, Heftberger P, Riedl MC, Begg M, House D & Romanin C. (2013). The action of selective CRAC channel blockers is affected by the Orai pore geometry. *Cell calcium* **53,** 139-151.

Dingli F, Parys JB, Loew D, Saule S & Mery L. (2012). Vimentin and the K-Ras-induced actin-binding protein control inositol-(1,4,5)-trisphosphate receptor

redistribution during MDCK cell differentiation. *Journal of cell science* **125,** 5428-5440.

Dingsdale H, Okeke E, Awais M, Haynes L, Criddle DN, Sutton R & Tepikin AV. (2013). Saltatory formation, sliding and dissolution of ER-PM junctions in migrating cancer cells. *The Biochemical journal* **451,** 25-32.

Dufour JF, Luthi M, Forestier M & Magnino F. (1999). Expression of inositol 1,4,5-trisphosphate receptor isoforms in rat cirrhosis. *Hepatology* **30,** 1018-1026.

Ehrlich BE & Watras J. (1988). Inositol 1,4,5-trisphosphate activates a channel from smooth muscle sarcoplasmic reticulum. *Nature* **336,** 583-586.

Falke JJ & Ziemba BP. (2014). Interplay between phosphoinositide lipids and calcium signals at the leading edge of chemotaxing ameboid cells. *Chemistry and physics of lipids* **182,** 73-79.

Faronato M, Patel V, Darling S, Dearden L, Clague MJ, Urbe S & Coulson JM. (2013). The deubiquitylase USP15 stabilizes newly synthesized REST and rescues its expression at mitotic exit. *Cell cycle* **12,** 1964-1977.

Farquhar MG & Palade GE. (1963). Junctional complexes in various epithelia. *The Journal of cell biology* **17,** 375-412.

Ferraro F, Kriston-Vizi J, Metcalf DJ, Martin-Martin B, Freeman J, Burden JJ, Westmoreland D, Dyer CE, Knight AE, Ketteler R & Cutler DF. (2014). A two-tier Golgi-based control of organelle size underpins the functional plasticity of endothelial cells. *Developmental cell* **29,** 292-304.

Feske S, Gwack Y, Prakriya M, Srikanth S, Puppel SH, Tanasa B, Hogan PG, Lewis RS, Daly M & Rao A. (2006). A mutation in Orai1 causes immune deficiency by abrogating CRAC channel function. *Nature* **441,** 179-185.

Finch EA & Augustine GJ. (1998). Local calcium signalling by inositol-1,4,5-trisphosphate in Purkinje cell dendrites. *Nature* **396,** 753-756.

Finch EA, Turner TJ & Goldin SM. (1991). Calcium as a coagonist of inositol 1,4,5-trisphosphate-induced calcium release. *Science* **252,** 443-446.

Foskett JK, White C, Cheung KH & Mak DO. (2007). Inositol trisphosphate receptor Ca2+ release channels. *Physiological reviews* **87,** 593-658.

Friedl P & Gilmour D. (2009). Collective cell migration in morphogenesis, regeneration and cancer. *Nature reviews Molecular cell biology* **10,** 445-457.

Fuchs BC, Fujii T, Dorfman JD, Goodwin JM, Zhu AX, Lanuti M & Tanabe KK. (2008). Epithelial-to-mesenchymal transition and integrin-linked kinase mediate sensitivity to epidermal growth factor receptor inhibition in human hepatoma cells. *Cancer research* **68,** 2391-2399.

Fukatsu K, Bannai H, Inoue T & Mikoshiba K. (2010). Lateral diffusion of inositol 1,4,5-trisphosphate receptor type 1 in Purkinje cells is regulated by calcium and actin filaments. *Journal of neurochemistry* **114,** 1720-1733.

Fukatsu K, Bannai H, Zhang S, Nakamura H, Inoue T & Mikoshiba K. (2004). Lateral diffusion of inositol 1,4,5-trisphosphate receptor type 1 is regulated by actin filaments and 4.1N in neuronal dendrites. *The Journal of biological chemistry* **279,** 48976-48982.

Furuichi T, Kohda K, Miyawaki A & Mikoshiba K. (1994). Intracellular channels. *Current opinion in neurobiology* **4,** 294-303.

Furuichi T & Mikoshiba K. (1995). Inositol 1, 4, 5-trisphosphate receptor-mediated Ca2+ signaling in the brain. *Journal of neurochemistry* **64,** 953-960.

Furuichi T, Simon-Chazottes D, Fujino I, Yamada N, Hasegawa M, Miyawaki A, Yoshikawa S, Guenet JL & Mikoshiba K. (1993). Widespread expression of inositol 1,4,5-trisphosphate receptor type 1 gene (Insp3r1) in the mouse central nervous system. *Receptors & channels* **1,** 11-24.

Furuichi T, Yoshikawa S, Miyawaki A, Wada K, Maeda N & Mikoshiba K. (1989). Primary structure and functional expression of the inositol 1,4,5-trisphosphate-binding protein P400. *Nature* **342,** 32-38.

Gafni J, Munsch JA, Lam TH, Catlin MC, Costa LG, Molinski TF & Pessah IN. (1997). Xestospongins: potent membrane permeable blockers of the inositol 1,4,5-trisphosphate receptor. *Neuron* **19,** 723-733.

Giannone G, Dubin-Thaler BJ, Dobereiner HG, Kieffer N, Bresnick AR & Sheetz MP. (2004). Periodic lamellipodial contractions correlate with rearward actin waves. *Cell* **116,** 431-443.

Giannone G, Dubin-Thaler BJ, Rossier O, Cai Y, Chaga O, Jiang G, Beaver W, Dobereiner HG, Freund Y, Borisy G & Sheetz MP. (2007). Lamellipodial actin

mechanically links myosin activity with adhesion-site formation. *Cell* **128,** 561-575.

Gnegy ME. (1993). Calmodulin in neurotransmitter and hormone action. *Annual review of pharmacology and toxicology* **33,** 45-70.

Gupton SL & Waterman-Storer CM. (2006). Spatiotemporal feedback between actomyosin and focal-adhesion systems optimizes rapid cell migration. *Cell* **125,** 1361-1374.

Hagar RE, Burgstahler AD, Nathanson MH & Ehrlich BE. (1998). Type III InsP3 receptor channel stays open in the presence of increased calcium. *Nature* **396,** 81-84.

Hanahan D & Weinberg RA. (2000). The hallmarks of cancer. *Cell* **100,** 57-70.

Hanahan D & Weinberg RA. (2011). Hallmarks of cancer: the next generation. *Cell* **144,** 646-674.

Hidaka H, Sasaki Y, Tanaka T, Endo T, Ohno S, Fujii Y & Nagata T. (1981). N-(6-aminohexyl)-5-chloro-1-naphthalenesulfonamide, a calmodulin antagonist, inhibits cell proliferation. *Proceedings of the National Academy of Sciences of the United States of America* **78,** 4354-4357.

Hirata K, Dufour JF, Shibao K, Knickelbein R, O'Neill AF, Bode HP, Cassio D, St-Pierre MV, Larusso NF, Leite MF & Nathanson MH. (2002a). Regulation of Ca(2+) signaling in rat bile duct epithelia by inositol 1,4,5-trisphosphate receptor isoforms. *Hepatology* **36,** 284-296.

Hirata K, Nathanson MH, Burgstahler AD, Okazaki K, Mattei E & Sears ML. (1999). Relationship between inositol 1,4,5-trisphosphate receptor isoforms and subcellular Ca2+ signaling patterns in nonpigmented ciliary epithelia. *Investigative ophthalmology & visual science* **40,** 2046-2053.

Hirata K, Pusl T, O'Neill AF, Dranoff JA & Nathanson MH. (2002b). The type II inositol 1,4,5-trisphosphate receptor can trigger Ca2+ waves in rat hepatocytes. *Gastroenterology* **122,** 1088-1100.

Hoover PJ & Lewis RS. (2011). Stoichiometric requirements for trapping and gating of Ca2+ release-activated Ca2+ (CRAC) channels by stromal interaction molecule 1 (STIM1). *Proceedings of the National Academy of Sciences of the United States of America* **108,** 13299-13304.

Hotz HG, Hotz B & Buhr HJ. (2011). Genes associated with epithelial-mesenchymal transition: possible therapeutic targets in ductal pancreatic adenocarcinoma? *Anti-cancer agents in medicinal chemistry* **11,** 448-454.

Hours MC & Mery L. (2010). The N-terminal domain of the type 1 Ins(1,4,5)P3 receptor stably expressed in MDCK cells interacts with myosin IIA and alters epithelial cell morphology. *Journal of cell science* **123,** 1449-1459.

Huang RY, Guilford P & Thiery JP. (2012). Early events in cell adhesion and polarity during epithelial-mesenchymal transition. *Journal of cell science* **125,** 4417-4422.

Iglesias PA & Devreotes PN. (2008). Navigating through models of chemotaxis. *Current opinion in cell biology* **20,** 35-40.

Iijima M, Huang YE & Devreotes P. (2002). Temporal and spatial regulation of chemotaxis. *Developmental cell* **3,** 469-478.

Iino M. (1990). Biphasic Ca2+ dependence of inositol 1,4,5-trisphosphate-induced Ca release in smooth muscle cells of the guinea pig taenia caeci. *The Journal of general physiology* **95,** 1103-1122.

Iino M. (1991). Effects of adenine nucleotides on inositol 1,4,5-trisphosphate-induced calcium release in vascular smooth muscle cells. *The Journal of general physiology* **98,** 681-698.

Inoue T, Kato K, Kohda K & Mikoshiba K. (1998). Type 1 inositol 1,4,5-trisphosphate receptor is required for induction of long-term depression in cerebellar Purkinje neurons. *The Journal of neuroscience : the official journal of the Society for Neuroscience* **18,** 5366-5373.

Ito K, Miyashita Y & Kasai H. (1997). Micromolar and submicromolar Ca2+ spikes regulating distinct cellular functions in pancreatic acinar cells. *The EMBO journal* **16,** 242-251.

Iwai M, Michikawa T, Bosanac I, Ikura M & Mikoshiba K. (2007). Molecular basis of the isoform-specific ligand-binding affinity of inositol 1,4,5-trisphosphate receptors. *The Journal of biological chemistry* **282,** 12755-12764.

Jaimovich E, Mattei C, Liberona JL, Cardenas C, Estrada M, Barbier J, Debitus C, Laurent D & Molgo J. (2005). Xestospongin B, a competitive inhibitor of IP3-

mediated Ca2+ signalling in cultured rat myotubes, isolated myonuclei, and neuroblastoma (NG108-15) cells. *FEBS letters* **579,** 2051-2057.

Johenning FW & Ehrlich BE. (2002). Signaling microdomains: InsP(3) receptor localization takes on new meaning. *Neuron* **34,** 173-175.

Joseph SK, Lin C, Pierson S, Thomas AP & Maranto AR. (1995). Heteroligomers of type-I and type-III inositol trisphosphate receptors in WB rat liver epithelial cells. *The Journal of biological chemistry* **270,** 23310-23316.

Kaverina I, Krylyshkina O & Small JV. (2002). Regulation of substrate adhesion dynamics during cell motility. *The international journal of biochemistry & cell biology* **34,** 746-761.

Kim DH & Wirtz D. (2013). Focal adhesion size uniquely predicts cell migration. *FASEB journal : official publication of the Federation of American Societies for Experimental Biology* **27,** 1351-1361.

Kume S, Yamamoto A, Inoue T, Muto A, Okano H & Mikoshiba K. (1997). Developmental expression of the inositol 1,4,5-trisphosphate receptor and structural changes in the endoplasmic reticulum during oogenesis and meiotic maturation of Xenopus laevis. *Developmental biology* **182,** 228-239.

Lai FP, Szczodrak M, Block J, Faix J, Breitsprecher D, Mannherz HG, Stradal TE, Dunn GA, Small JV & Rottner K. (2008). Arp2/3 complex interactions and actin network turnover in lamellipodia. *The EMBO journal* **27,** 982-992.

Lamouille S, Xu J & Derynck R. (2014). Molecular mechanisms of epithelial-mesenchymal transition. *Nature reviews Molecular cell biology* **15,** 178-196.

Laukaitis CM, Webb DJ, Donais K & Horwitz AF. (2001). Differential dynamics of alpha 5 integrin, paxillin, and alpha-actinin during formation and disassembly of adhesions in migrating cells. *The Journal of cell biology* **153,** 1427-1440.

Lee MG, Xu X, Zeng W, Diaz J, Kuo TH, Wuytack F, Racymaekers L & Muallem S. (1997). Polarized expression of Ca2+ pumps in pancreatic and salivary gland cells. Role in initiation and propagation of [Ca2+]i waves. *The Journal of biological chemistry* **272,** 15771-15776.

Lefkimmiatis K, Srikanthan M, Maiellaro I, Moyer MP, Curci S & Hofer AM. (2009). Store-operated cyclic AMP signalling mediated by STIM1. *Nature cell biology* **11,** 433-442.

Li Y, VandenBoom TG, 2nd, Kong D, Wang Z, Ali S, Philip PA & Sarkar FH. (2009). Up-regulation of miR-200 and let-7 by natural agents leads to the reversal of epithelial-to-mesenchymal transition in gemcitabine-resistant pancreatic cancer cells. *Cancer research* **69,** 6704-6712.

Liou J, Fivaz M, Inoue T & Meyer T. (2007). Live-cell imaging reveals sequential oligomerization and local plasma membrane targeting of stromal interaction molecule 1 after Ca2+ store depletion. *Proceedings of the National Academy of Sciences of the United States of America* **104,** 9301-9306.

Liou J, Kim ML, Heo WD, Jones JT, Myers JW, Ferrell JE, Jr. & Meyer T. (2005). STIM is a Ca2+ sensor essential for Ca2+-store-depletion-triggered Ca2+ influx. *Current biology : CB* **15,** 1235-1241.

Lupu VD, Kaznacheyeva E, Krishna UM, Falck JR & Bezprozvanny I. (1998). Functional coupling of phosphatidylinositol 4,5-bisphosphate to inositol 1,4,5-trisphosphate receptor. *The Journal of biological chemistry* **273,** 14067-14070.

Lur G, Haynes LP, Prior IA, Gerasimenko OV, Feske S, Petersen OH, Burgoyne RD & Tepikin AV. (2009). Ribosome-free terminals of rough ER allow formation of STIM1 puncta and segregation of STIM1 from IP(3) receptors. *Current biology : CB* **19,** 1648-1653.

Lur G, Sherwood MW, Ebisui E, Haynes L, Feske S, Sutton R, Burgoyne RD, Mikoshiba K, Petersen OH & Tepikin AV. (2011). InsP(3)receptors and Orai channels in pancreatic acinar cells: co-localization and its consequences. *The Biochemical journal* **436,** 231-239.

Machacek M, Hodgson L, Welch C, Elliott H, Pertz O, Nalbant P, Abell A, Johnson GL, Hahn KM & Danuser G. (2009). Coordination of Rho GTPase activities during cell protrusion. *Nature* **461,** 99-103.

Machesky LM & Li A. (2010). Fascin: Invasive filopodia promoting metastasis. *Communicative & integrative biology* **3,** 263-270.

Maeda N, Kawasaki T, Nakade S, Yokota N, Taguchi T, Kasai M & Mikoshiba K. (1991). Structural and functional characterization of inositol 1,4,5-trisphosphate receptor channel from mouse cerebellum. *The Journal of biological chemistry* **266,** 1109-1116.

Maeda N, Niinobe M, Inoue Y & Mikoshiba K. (1989). Developmental expression and intracellular location of P400 protein characteristic of Purkinje cells in the mouse cerebellum. *Developmental biology* **133,** 67-76.

Mak DO, McBride SM, Petrenko NB & Foskett JK. (2003). Novel regulation of calcium inhibition of the inositol 1,4,5-trisphosphate receptor calcium-release channel. *The Journal of general physiology* **122,** 569-581.

Manford AG, Stefan CJ, Yuan HL, Macgurn JA & Emr SD. (2012). ER-to-plasma membrane tethering proteins regulate cell signaling and ER morphology. *Developmental cell* **23,** 1129-1140.

Marshall IC & Taylor CW. (1994). Two calcium-binding sites mediate the interconversion of liver inositol 1,4,5-trisphosphate receptors between three conformational states. *The Biochemical journal* **301 (Pt 2),** 591-598.

Mejillano MR, Kojima S, Applewhite DA, Gertler FB, Svitkina TM & Borisy GG. (2004). Lamellipodial versus filopodial mode of the actin nanomachinery: pivotal role of the filament barbed end. *Cell* **118,** 363-373.

Meldolesi J & Pozzan T. (1998). The heterogeneity of ER Ca2+ stores has a key role in nonmuscle cell signaling and function. *The Journal of cell biology* **142,** 1395-1398.

Mellor H. (2010). The role of formins in filopodia formation. *Biochimica et biophysica acta* **1803,** 191-200.

Metcalf DJ, Edwards R, Kumarswami N & Knight AE. (2013). Test samples for optimizing STORM super-resolution microscopy. *Journal of visualized experiments : JoVE*.

Michikawa T, Hirota J, Kawano S, Hiraoka M, Yamada M, Furuichi T & Mikoshiba K. (1999). Calmodulin mediates calcium-dependent inactivation of the cerebellar type 1 inositol 1,4,5-trisphosphate receptor. *Neuron* **23,** 799-808.

Middelbeek J, Kuipers AJ, Henneman L, Visser D, Eidhof I, van Horssen R, Wieringa B, Canisius SV, Zwart W, Wessels LF, Sweep FC, Bult P, Span PN, van Leeuwen FN & Jalink K. (2012). TRPM7 is required for breast tumor cell metastasis. *Cancer research* **72,** 4250-4261.

Mierke CT. (2009). The role of vinculin in the regulation of the mechanical properties of cells. *Cell biochemistry and biophysics* **53,** 115-126.

Mignery GA & Sudhof TC. (1990). The ligand binding site and transduction mechanism in the inositol-1,4,5-triphosphate receptor. *The EMBO journal* **9,** 3893-3898.

Missiaen L, Parys JB, Weidema AF, Sipma H, Vanlingen S, De Smet P, Callewaert G & De Smedt H. (1999). The bell-shaped Ca2+ dependence of the inositol 1,4, 5-trisphosphate-induced Ca2+ release is modulated by Ca2+/calmodulin. *The Journal of biological chemistry* **274,** 13748-13751.

Miyakawa T, Maeda A, Yamazawa T, Hirose K, Kurosaki T & Iino M. (1999). Encoding of Ca2+ signals by differential expression of IP3 receptor subtypes. *The EMBO journal* **18,** 1303-1308.

Miyawaki A, Furuichi T, Ryou Y, Yoshikawa S, Nakagawa T, Saitoh T & Mikoshiba K. (1991). Structure-function relationships of the mouse inositol 1,4,5-trisphosphate receptor. *Proceedings of the National Academy of Sciences of the United States of America* **88,** 4911-4915.

Mogami H, Gardner J, Gerasimenko OV, Camello P, Petersen OH & Tepikin AV. (1999). Calcium binding capacity of the cytosol and endoplasmic reticulum of mouse pancreatic acinar cells. *The Journal of physiology* **518 (Pt 2),** 463-467.

Monkawa T, Miyawaki A, Sugiyama T, Yoneshima H, Yamamoto-Hino M, Furuichi T, Saruta T, Hasegawa M & Mikoshiba K. (1995). Heterotetrameric complex formation of inositol 1,4,5-trisphosphate receptor subunits. *The Journal of biological chemistry* **270,** 14700-14704.

Muik M, Frischauf I, Derler I, Fahrner M, Bergsmann J, Eder P, Schindl R, Hesch C, Polzinger B, Fritsch R, Kahr H, Madl J, Gruber H, Groschner K & Romanin C. (2008). Dynamic coupling of the putative coiled-coil domain of ORAI1 with STIM1 mediates ORAI1 channel activation. *The Journal of biological chemistry* **283,** 8014-8022.

Muik M, Schindl R, Fahrner M & Romanin C. (2012). Ca(2+) release-activated Ca(2+) (CRAC) current, structure, and function. *Cellular and molecular life sciences : CMLS* **69,** 4163-4176.

Mullins RD, Heuser JA & Pollard TD. (1998). The interaction of Arp2/3 complex with actin: nucleation, high affinity pointed end capping, and formation of branching networks of filaments. *Proceedings of the National Academy of Sciences of the United States of America* **95,** 6181-6186.

Nathanson MH, Fallon MB, Padfield PJ & Maranto AR. (1994). Localization of the type 3 inositol 1,4,5-trisphosphate receptor in the Ca2+ wave trigger zone of pancreatic acinar cells. *The Journal of biological chemistry* **269,** 4693-4696.

Nelson WJ. (2009). Remodeling epithelial cell organization: transitions between front-rear and apical-basal polarity. *Cold Spring Harbor perspectives in biology* **1,** a000513.

Nixon GF, Mignery GA & Somlyo AV. (1994). Immunogold localization of inositol 1,4,5-trisphosphate receptors and characterization of ultrastructural features of the sarcoplasmic reticulum in phasic and tonic smooth muscle. *Journal of muscle research and cell motility* **15,** 682-700.

Orci L, Ravazzola M, Le Coadic M, Shen WW, Demaurex N & Cosson P. (2009). From the Cover: STIM1-induced precortical and cortical subdomains of the endoplasmic reticulum. *Proceedings of the National Academy of Sciences of the United States of America* **106,** 19358-19362.

Pandol SJ. (2010). In *The Exocrine Pancreas*. San Rafael (CA).

Pantazaka E & Taylor CW. (2011). Differential distribution, clustering, and lateral diffusion of subtypes of the inositol 1,4,5-trisphosphate receptor. *The Journal of biological chemistry* **286,** 23378-23387.

Park CY, Hoover PJ, Mullins FM, Bachhawat P, Covington ED, Raunser S, Walz T, Garcia KC, Dolmetsch RE & Lewis RS. (2009). STIM1 clusters and activates CRAC channels via direct binding of a cytosolic domain to Orai1. *Cell* **136,** 876-890.

Patterson RL, Boehning D & Snyder SH. (2004). Inositol 1,4,5-trisphosphate receptors as signal integrators. *Annual review of biochemistry* **73,** 437-465.

Paul AS & Pollard TD. (2009). Review of the mechanism of processive actin filament elongation by formins. *Cell motility and the cytoskeleton* **66,** 606-617.

Petersen OH, Tepikin A & Park MK. (2001). The endoplasmic reticulum: one continuous or several separate Ca(2+) stores? *Trends in neurosciences* **24,** 271-276.

Pettit EJ & Fay FS. (1998). Cytosolic free calcium and the cytoskeleton in the control of leukocyte chemotaxis. *Physiological reviews* **78,** 949-967.

Pieper AA, Brat DJ, O'Hearn E, Krug DK, Kaplin AI, Takahashi K, Greenberg JH, Ginty D, Molliver ME & Snyder SH. (2001). Differential neuronal localizations and dynamics of phosphorylated and unphosphorylated type 1 inositol 1,4,5-trisphosphate receptors. *Neuroscience* **102,** 433-444.

Ponti A, Machacek M, Gupton SL, Waterman-Storer CM & Danuser G. (2004). Two distinct actin networks drive the protrusion of migrating cells. *Science* **305,** 1782-1786.

Porter KR, Claude A & Fullam EF. (1945). A Study of Tissue Culture Cells by Electron Microscopy : Methods and Preliminary Observations. *The Journal of experimental medicine* **81,** 233-246.

Porter KR & Palade GE. (1957). Studies on the endoplasmic reticulum. III. Its form and distribution in striated muscle cells. *The Journal of biophysical and biochemical cytology* **3,** 269-300.

Provenzano PP, Eliceiri KW, Inman DR & Keely PJ. (2010). Engineering three-dimensional collagen matrices to provide contact guidance during 3D cell migration. *Current protocols in cell biology / editorial board, Juan S Bonifacino [et al]* **Chapter 10,** Unit 10 17.

Putney JW, Jr. (1986). A model for receptor-regulated calcium entry. *Cell calcium* **7,** 1-12.

Putney JW, Jr. (2005). Capacitative calcium entry: sensing the calcium stores. *The Journal of cell biology* **169,** 381-382.

Quirion JC, Sevenet T, Husson HP, Weniger B & Debitus C. (1992). Two new alkaloids from Xestospongia sp., a New Caledonian sponge. *Journal of natural products* **55,** 1505-1508.

Ramos-Franco J, Fill M & Mignery GA. (1998). Isoform-specific function of single inositol 1,4,5-trisphosphate receptor channels. *Biophysical journal* **75,** 834-839.

Ramos-Franco J, Galvan D, Mignery GA & Fill M. (1999). Location of the permeation pathway in the recombinant type 1 inositol 1,4,5-trisphosphate receptor. *The Journal of general physiology* **114,** 243-250.

Raucher D, Stauffer T, Chen W, Shen K, Guo S, York JD, Sheetz MP & Meyer T. (2000). Phosphatidylinositol 4,5-bisphosphate functions as a second messenger that regulates cytoskeleton-plasma membrane adhesion. *Cell* **100,** 221-228.

Ricono JM, Huang M, Barnes LA, Lau SK, Weis SM, Schlaepfer DD, Hanks SK & Cheresh DA. (2009). Specific cross-talk between epidermal growth factor

receptor and integrin alphavbeta5 promotes carcinoma cell invasion and metastasis. *Cancer research* **69,** 1383-1391.

Ridley AJ. (2011). Life at the leading edge. *Cell* **145,** 1012-1022.

Ridley AJ, Schwartz MA, Burridge K, Firtel RA, Ginsberg MH, Borisy G, Parsons JT & Horwitz AR. (2003). Cell migration: integrating signals from front to back. *Science* **302,** 1704-1709.

Rodriguez-Boulan E & Nelson WJ. (1989). Morphogenesis of the polarized epithelial cell phenotype. *Science* **245,** 718-725.

Rooman I & Real FX. (2012). Pancreatic ductal adenocarcinoma and acinar cells: a matter of differentiation and development? *Gut* **61,** 449-458.

Roos J, DiGregorio PJ, Yeromin AV, Ohlsen K, Lioudyno M, Zhang S, Safrina O, Kozak JA, Wagner SL, Cahalan MD, Velicelebi G & Stauderman KA. (2005). STIM1, an essential and conserved component of store-operated Ca2+ channel function. *The Journal of cell biology* **169,** 435-445.

Rosenbluth J. (1962). Subsurface cisterns and their relationship to the neuronal plasma membrane. *The Journal of cell biology* **13,** 405-421.

Rossi AM, Riley AM, Tovey SC, Rahman T, Dellis O, Taylor EJ, Veresov VG, Potter BV & Taylor CW. (2009). Synthetic partial agonists reveal key steps in IP3 receptor activation. *Nature chemical biology* **5,** 631-639.

Rossier MF, Bird GS & Putney JW, Jr. (1991). Subcellular distribution of the calcium-storing inositol 1,4,5-trisphosphate-sensitive organelle in rat liver. Possible linkage to the plasma membrane through the actin microfilaments. *The Biochemical journal* **274 (Pt 3),** 643-650.

Roussos ET, Condeelis JS & Patsialou A. (2011). Chemotaxis in cancer. *Nature reviews Cancer* **11,** 573-587.

Saarikangas J, Zhao H & Lappalainen P. (2010). Regulation of the actin cytoskeleton-plasma membrane interplay by phosphoinositides. *Physiological reviews* **90,** 259-289.

Schafer C, Rymarczyk G, Ding L, Kirber MT & Bolotina VM. (2012). Role of molecular determinants of store-operated Ca(2+) entry (Orai1, phospholipase

A2 group 6, and STIM1) in focal adhesion formation and cell migration. *The Journal of biological chemistry* **287,** 40745-40757.

Schindl R, Muik M, Fahrner M, Derler I, Fritsch R, Bergsmann J & Romanin C. (2009). Recent progress on STIM1 domains controlling Orai activation. *Cell calcium* **46,** 227-232.

Shapiro L & Weis WI. (2009). Structure and biochemistry of cadherins and catenins. *Cold Spring Harbor perspectives in biology* **1,** a003053.

Sharp AH, Nucifora FC, Jr., Blondel O, Sheppard CA, Zhang C, Snyder SH, Russell JT, Ryugo DK & Ross CA. (1999). Differential cellular expression of isoforms of inositol 1,4,5-triphosphate receptors in neurons and glia in brain. *The Journal of comparative neurology* **406,** 207-220.

Siegel R, Naishadham D & Jemal A. (2013). Cancer statistics, 2013. *CA: a cancer journal for clinicians* **63,** 11-30.

Siegel R, Ward E, Brawley O & Jemal A. (2011). Cancer statistics, 2011: the impact of eliminating socioeconomic and racial disparities on premature cancer deaths. *CA: a cancer journal for clinicians* **61,** 212-236.

Sienaert I, Nadif Kasri N, Vanlingen S, Parys JB, Callewaert G, Missiaen L & de Smedt H. (2002). Localization and function of a calmodulin-apocalmodulin-binding domain in the N-terminal part of the type 1 inositol 1,4,5-trisphosphate receptor. *The Biochemical journal* **365,** 269-277.

Stathis A & Moore MJ. (2010). Advanced pancreatic carcinoma: current treatment and future challenges. *Nature reviews Clinical oncology* **7,** 163-172.

Steed E, Balda MS & Matter K. (2010). Dynamics and functions of tight junctions. *Trends in cell biology* **20,** 142-149.

Steward MC, Ishiguro H & Case RM. (2005). Mechanisms of bicarbonate secretion in the pancreatic duct. *Annual review of physiology* **67,** 377-409.

Striggow F & Ehrlich BE. (1996). The inositol 1,4,5-trisphosphate receptor of cerebellum. Mn2+ permeability and regulation by cytosolic Mn2+. *The Journal of general physiology* **108,** 115-124.

Sugiyama T, Matsuda Y & Mikoshiba K. (2000). Inositol 1,4,5-trisphosphate receptor associated with focal contact cytoskeletal proteins. *FEBS letters* **466,** 29-34.

Supattapone S, Worley PF, Baraban JM & Snyder SH. (1988). Solubilization, purification, and characterization of an inositol trisphosphate receptor. *The Journal of biological chemistry* **263,** 1530-1534.

Szlufcik K, Bultynck G, Callewaert G, Missiaen L, Parys JB & De Smedt H. (2006). The suppressor domain of inositol 1,4,5-trisphosphate receptor plays an essential role in the protection against apoptosis. *Cell calcium* **39,** 325-336.

Takechi H, Eilers J & Konnerth A. (1998). A new class of synaptic response involving calcium release in dendritic spines. *Nature* **396,** 757-760.

Takeshima H, Komazaki S, Nishi M, Iino M & Kangawa K. (2000). Junctophilins: a novel family of junctional membrane complex proteins. *Molecular cell* **6,** 11-22.

Tasker PN, Taylor CW & Nixon GF. (2000). Expression and distribution of InsP(3) receptor subtypes in proliferating vascular smooth muscle cells. *Biochemical and biophysical research communications* **273,** 907-912.

Tateishi Y, Hattori M, Nakayama T, Iwai M, Bannai H, Nakamura T, Michikawa T, Inoue T & Mikoshiba K. (2005). Cluster formation of inositol 1,4,5-trisphosphate receptor requires its transition to open state. *The Journal of biological chemistry* **280,** 6816-6822.

Taylor CW, Genazzani AA & Morris SA. (1999). Expression of inositol trisphosphate receptors. *Cell calcium* **26,** 237-251.

Taylor CW & Tovey SC. (2010). IP(3) receptors: toward understanding their activation. *Cold Spring Harbor perspectives in biology* **2,** a004010.

Terry S, Nie M, Matter K & Balda MS. (2010). Rho signaling and tight junction functions. *Physiology* **25,** 16-26.

Thiery JP, Acloque H, Huang RY & Nieto MA. (2009). Epithelial-mesenchymal transitions in development and disease. *Cell* **139,** 871-890.

Thorn P, Lawrie AM, Smith PM, Gallacher DV & Petersen OH. (1993). Local and global cytosolic Ca2+ oscillations in exocrine cells evoked by agonists and inositol trisphosphate. *Cell* **74,** 661-668.

Thrower EC, Lea EJ & Dawson AP. (1998). The effects of free [Ca2+] on the cytosolic face of the inositol (1,4,5)-trisphosphate receptor at the single channel level. *The Biochemical journal* **330 (Pt 1),** 559-564.

Treves S, Franzini-Armstrong C, Moccagatta L, Arnoult C, Grasso C, Schrum A, Ducreux S, Zhu MX, Mikoshiba K, Girard T, Smida-Rezgui S, Ronjat M & Zorzato F. (2004). Junctate is a key element in calcium entry induced by activation of InsP3 receptors and/or calcium store depletion. *The Journal of cell biology* **166,** 537-548.

Tsai FC & Meyer T. (2012). Ca2+ pulses control local cycles of lamellipodia retraction and adhesion along the front of migrating cells. *Current biology : CB* **22,** 837-842.

Tsai FC, Seki A, Yang HW, Hayer A, Carrasco S, Malmersjo S & Meyer T. (2014). A polarized Ca2+, diacylglycerol and STIM1 signalling system regulates directed cell migration. *Nature cell biology* **16,** 133-144.

Tu H, Wang Z, Nosyreva E, De Smedt H & Bezprozvanny I. (2005). Functional characterization of mammalian inositol 1,4,5-trisphosphate receptor isoforms. *Biophysical journal* **88,** 1046-1055.

Tu JC, Xiao B, Yuan JP, Lanahan AA, Leoffert K, Li M, Linden DJ & Worley PF. (1998). Homer binds a novel proline-rich motif and links group 1 metabotropic glutamate receptors with IP3 receptors. *Neuron* **21,** 717-726.

Uchida K, Miyauchi H, Furuichi T, Michikawa T & Mikoshiba K. (2003). Critical regions for activation gating of the inositol 1,4,5-trisphosphate receptor. *The Journal of biological chemistry* **278,** 16551-16560.

Valeyev NV, Downing AK, Skorinkin AI, Campbell ID & Kotov NV. (2006). A calcium dependent de-adhesion mechanism regulates the direction and rate of cell migration: a mathematical model. *In silico biology* **6,** 545-572.

van Rheenen J, Condeelis J & Glogauer M. (2009). A common cofilin activity cycle in invasive tumor cells and inflammatory cells. *Journal of cell science* **122,** 305-311.

Vanderheyden V, Devogelaere B, Missiaen L, De Smedt H, Bultynck G & Parys JB. (2009). Regulation of inositol 1,4,5-trisphosphate-induced Ca2+ release by reversible phosphorylation and dephosphorylation. *Biochimica et biophysica acta* **1793,** 959-970.

Varnai P, Toth B, Toth DJ, Hunyady L & Balla T. (2007). Visualization and manipulation of plasma membrane-endoplasmic reticulum contact sites indicates the presence of additional molecular components within the STIM1-Orai1 Complex. *The Journal of biological chemistry* **282,** 29678-29690.

Vermassen E, Parys JB & Mauger JP. (2004). Subcellular distribution of the inositol 1,4,5-trisphosphate receptors: functional relevance and molecular determinants. *Biology of the cell / under the auspices of the European Cell Biology Organization* **96,** 3-17.

Vermassen E, Van Acker K, Annaert WG, Himpens B, Callewaert G, Missiaen L, De Smedt H & Parys JB. (2003). Microtubule-dependent redistribution of the type-1 inositol 1,4,5-trisphosphate receptor in A7r5 smooth muscle cells. *Journal of cell science* **116,** 1269-1277.

Vervloessem T, Yule DI, Bultynck G & Parys JB. (2014). The type 2 inositol 1,4,5-trisphosphate receptor, emerging functions for an intriguing Ca-release channel. *Biochimica et biophysica acta*.

Vicente-Manzanares M & Horwitz AR. (2011). Adhesion dynamics at a glance. *Journal of cell science* **124,** 3923-3927.

Vig M, Peinelt C, Beck A, Koomoa DL, Rabah D, Koblan-Huberson M, Kraft S, Turner H, Fleig A, Penner R & Kinet JP. (2006). CRACM1 is a plasma membrane protein essential for store-operated Ca2+ entry. *Science* **312,** 1220-1223.

Voeltz GK, Rolls MM & Rapoport TA. (2002). Structural organization of the endoplasmic reticulum. *EMBO reports* **3,** 944-950.

Wagner LE, 2nd & Yule DI. (2012). Differential regulation of the InsP(3) receptor type-1 and -2 single channel properties by InsP(3), Ca(2)(+) and ATP. *The Journal of physiology* **590,** 3245-3259.

Wang Z, Li Y, Ahmad A, Banerjee S, Azmi AS, Kong D & Sarkar FH. (2011). Pancreatic cancer: understanding and overcoming chemoresistance. *Nature reviews Gastroenterology & hepatology* **8,** 27-33.

Webb DJ, Parsons JT & Horwitz AF. (2002). Adhesion assembly, disassembly and turnover in migrating cells -- over and over and over again. *Nature cell biology* **4,** E97-100.

Wehrle-Haller B. (2012). Structure and function of focal adhesions. *Current opinion in cell biology* **24,** 116-124.

Wei C, Wang X, Chen M, Ouyang K, Song LS & Cheng H. (2009). Calcium flickers steer cell migration. *Nature* **457,** 901-905.

Williams AJ, West DJ & Sitsapesan R. (2001). Light at the end of the Ca(2+)-release channel tunnel: structures and mechanisms involved in ion translocation in ryanodine receptor channels. *Quarterly reviews of biophysics* **34,** 61-104.

Willoughby D, Everett KL, Halls ML, Pacheco J, Skroblin P, Vaca L, Klussmann E & Cooper DM. (2012). Direct binding between Orai1 and AC8 mediates dynamic interplay between Ca2+ and cAMP signaling. *Science signaling* **5,** ra29.

Wojcikiewicz RJ. (1995). Type I, II, and III inositol 1,4,5-trisphosphate receptors are unequally susceptible to down-regulation and are expressed in markedly different proportions in different cell types. *The Journal of biological chemistry* **270,** 11678-11683.

Worley PF, Zeng W, Huang GN, Yuan JP, Kim JY, Lee MG & Muallem S. (2007). TRPC channels as STIM1-regulated store-operated channels. *Cell calcium* **42,** 205-211.

Wu MM, Buchanan J, Luik RM & Lewis RS. (2006). Ca2+ store depletion causes STIM1 to accumulate in ER regions closely associated with the plasma membrane. *The Journal of cell biology* **174,** 803-813.

Wu MM, Covington ED & Lewis RS. (2014). Single-molecule analysis of diffusion and trapping of STIM1 and Orai1 at endoplasmic reticulum-plasma membrane junctions. *Molecular biology of the cell* **25,** 3672-3685.

Yamada M, Miyawaki A, Saito K, Nakajima T, Yamamoto-Hino M, Ryo Y, Furuichi T & Mikoshiba K. (1995). The calmodulin-binding domain in the mouse type 1 inositol 1,4,5-trisphosphate receptor. *The Biochemical journal* **308 (Pt 1),** 83-88.

Yang S, Zhang JJ & Huang XY. (2009). Orai1 and STIM1 are critical for breast tumor cell migration and metastasis. *Cancer cell* **15,** 124-134.

Yap AS, Crampton MS & Hardin J. (2007). Making and breaking contacts: the cellular biology of cadherin regulation. *Current opinion in cell biology* **19,** 508-514.

Yoshikawa F, Morita M, Monkawa T, Michikawa T, Furuichi T & Mikoshiba K. (1996). Mutational analysis of the ligand binding site of the inositol 1,4,5-trisphosphate receptor. *The Journal of biological chemistry* **271,** 18277-18284.

Yule DI, Ernst SA, Ohnishi H & Wojcikiewicz RJ. (1997). Evidence that zymogen granules are not a physiologically relevant calcium pool. Defining the distribution of inositol 1,4,5-trisphosphate receptors in pancreatic acinar cells. *The Journal of biological chemistry* **272,** 9093-9098.

Zhang S, Mizutani A, Hisatsune C, Higo T, Bannai H, Nakayama T, Hattori M & Mikoshiba K. (2003). Protein 4.1N is required for translocation of inositol 1,4,5-trisphosphate receptor type 1 to the basolateral membrane domain in polarized Madin-Darby canine kidney cells. *The Journal of biological chemistry* **278,** 4048-4056.

Zhang SL, Yeromin AV, Zhang XH, Yu Y, Safrina O, Penna A, Roos J, Stauderman KA & Cahalan MD. (2006). Genome-wide RNAi screen of Ca(2+) influx identifies genes that regulate Ca(2+) release-activated Ca(2+) channel activity. *Proceedings of the National Academy of Sciences of the United States of America* **103,** 9357-9362.

Zhang SL, Yu Y, Roos J, Kozak JA, Deerinck TJ, Ellisman MH, Stauderman KA & Cahalan MD. (2005). STIM1 is a Ca2+ sensor that activates CRAC channels and migrates from the Ca2+ store to the plasma membrane. *Nature* **437,** 902-905.

Zhou Z & Neher E. (1993). Mobile and immobile calcium buffers in bovine adrenal chromaffin cells. *The Journal of physiology* **469,** 245-273.

Ziegler WH, Liddington RC & Critchley DR. (2006). The structure and regulation of vinculin. *Trends in cell biology* **16,** 453-460.